Design and Preparation of Solution Processable Hyperbranched Polymers for OLED Applications

The University Of Sheffield.

A thesis submitted in partial fulfilment of the requirements for the degree of Doctor of Philosophy

By

Saif Hussain Althagafi

Department of Chemistry

Jan 2024

Declaration

I hereby declare that this thesis is submitted for the degree of Doctorate of Philosophy (PhD) at the University of Sheffield, having been submitted for no other degrees. It records the research carried out at the University of Sheffield. It is entirely my original work, unless where referenced.

Signed Saif Althagafi

Date 14/01/2024

Acknowledgement

I would like to begin by expressing deep gratitude to Allah Almighty for granting me the ability to conduct this research study. This achievement would have been impossible without the blessing of him.

To the greatest mother, the most beautiful soul, what I did, what I am doing and what I am going to do, all because of you. You are my inspiration, my life and my light in the dark. Thanks, my lovely mother, for supporting me and encouraging me. I am nothing without you. May Allah reward you for your patience, your efforts and your tiredness with me and my siblings as well. I am so proud to have a mother like you, and I love you forever sweetheart.

I would like to extend my gratitude to Dr. Ahmed Iraqi for his assistance, patience, encouragement, and support during my PhD studies and research completion. Honestly, without him, I would not have been able to complete my PhD. He is a great advisor, and I am so grateful for the many ways in which he helped me to improve myself academically and personally.

I would like to express my sincere appreciation to all the incredibly valued individuals in the Department of Chemistry at the University of Sheffield. I am unable to provide a full list, but I would like also to express my profound gratitude to the great technical staff members: Dr. Khaled, Sharon, Luke, and Simon, who helped me in terms of training and characterisations

I would also like to express how thankful I am to all of my laboratory colleagues, Saif, Mohammed, Fatemah, Nujud, and Amal, for their invaluable assistance throughout the duration of my research. Furthermore, special thanks to Dr Bakhet, Dr Osama, Dr Yazeed and Dr Abdulelah for their help and support.

Of all things, I would like to convey my sincere thanks to my dear wife, Huda, for her constant encouragement, patience and love during my study journey. Since the birth of my little loved daughter, Maysam, our lives have become more blessed and gorgeous. There are no words to describe how thankful I am to have you both in my life. At last, I extend my profound appreciation to Al Baha University for giving me this opportunity to complete my PhD and for their financial support.

Abstract

The latest developments in organic light-emitting diodes (OLED) technology utilising thermally activated delayed fluorescence (TADF) materials are highly remarkable. The last generation of OLEDs based on TADF properties has the capability to convert triplet excitons into singlet excitons, achieving an exciton utilisation efficiency (EUE) of 100% without the inclusion of any heavy complex metal phosphorescent materials. Despite advancements in productivity, the evaporated deposition method for fabricating OLEDs presents disadvantages for producing large-scale devices, due to its strict structure requirements and significant challenges in achieving cost-effective mass production including high energy consumption, limited scalability and challenging control. As an alternative to other manufacturing processes, the solution processing method is a more straightforward, cost-effective, and easily controllable option for facilitating massive production. Nevertheless, most of the TADF dopants that have been described are mostly composed of small molecules (organic compounds with a molecular weight of 1000 daltons or less), making them unsuitable for solution deposition processes. Hence, there is a significant commercial motivation to create organic emissive materials that can be processed as solutions and possess TADF properties.

In comparison to linear polymers with one-dimensional (1D) architectures, electroluminescent hyperbranched polymers (HBPs) featuring three-dimensional (3D) architectures exhibit unique molecular shapes (dendritic and spherical architectures), branching patterns, reduced intrinsic viscosity (refers to the extent to which a solute affects the viscosity of a solution), enhanced solubility, improved processability, a more stable luminescent spectrum, and the capability to tune emission colours in the emissive layers of organic light-emitting diodes (OLEDs). In addition, the incorporation of hyperbranched polymers within the OLED emitting layer effectively disperses the TADF emitting material and inhibits aggregation-caused quenching (ACQ) and exciton annihilation effects.

Various strategies for the synthesis and design of solution-processable TADF hyperbranched polymers have been proposed in this study. Carbazole (Cbz) and Bis[2-(diphenylphosphino)phenyl] ether oxide (DPEPO) derivatives were employed as monomers in hyperbranched copolymers with minimal electronic conjugation for use as host materials due to their substantial triplet energies and their ability to facilitate the transport of holes and electrons, respectively.

Table of Contents

List of Figures

Figure 5.6 The CV analysis of P9 – P12. Polymer 9 (containing 0% of the TADF) exhibited only one oxidation and reduction peak. Polymers from P10-P12, which grafted with different molar ratios of the TADF (5%, 10% and 20% respectively) exhibited two peaks of oxidations; the first oxidation peak which corresponds to the polymer backbone, and the semi-oxidation peak which corresponds to the phenoxazine moiety (electron-donating molecule) of the TADF units. The intensity of this peak increases with increasing the molar ratio of TADF. The reduction peaks of all designed polymers could not be identified, therefore the LUMO values were calculated from the difference between the optical band gaps and the HOMO values.165

List of Schemes

List of Tables

List of Abbreviations

A	Anode
BDE	Bond dissociation energy
bm	Broad multiplet
br	Broad peak
bs	Broad singlet
C	Cathode
CT	Charge transfer
CV	Cyclic voltammetry
d	Doublet
D-A	Donor-Acceptor
DCM	Dichloromethane
dd	Doublet of doublet
DF	Delayed fluorescence
DMF	N,N-Dimethylformamide
DMSO	Dimethyl sulfoxide
DPEPO	Bis[2-(diphenylphosphino)phenyl] ether oxide
Eg (elec)	Electrochemical band gap
Eg (opt)	Optical band gap
EL	Electroluminescence
EML	Emitting layer
EQE	External quantum efficiency
ETL	Electron transport layer
eV	Electron volt

FWHM	Full Width at Half Maximum
HIL	Hole injection layer
HOMO	Highest Occupied Molecular Orbital
HTL	Hole transport layer
IC	Internal conversion
ICT	Intramolecular charge transfer
IQE	Internal quantum efficiency
ISC	Intersystem crossing
ITO	Indium tin oxide
J	Coupling constant (NMR)
LUMO	Lowest Occupied Molecular Orbital
Mn	Number-average molecular weight
MS	Mass spectrometry
Mw	Weight-average molecular weight
NMR	Nuclear Magnetic Resonance
OLEDs	Organic Light-Emitting Diodes
PDI	Polydispersity Index
PF	Promoted fluorescence
PL	Photoluminescence
PLQY	Photoluminescence quantum yields
ppm	Part per million
RISC	Reverse intersystem crossing
RT	Room temperature
S	Singlet

S_0	Singlet Ground State
S_1	Singlet Excited State
T	Triplet
T_1	Triplet Excited State
TADF	Thermally activated delayed fluorescence
TGA	Thermogravimetric analysis
THF	Tetrahydrofuran
TTA	Triplet-triplet annihilation
UV-vis	Ultra-Violet-visible spectroscopy
VR	Vibrational relaxation
ΔE_{ST}	Energy level difference between T_1 and S_1
λ	Wavelength

Chapter 1: Introduction

1.1 Organic Light Emitting Diodes (OLED)

1.1.1 Background

Electroluminescence is a physical phenomenon characterised by the emission of light from materials when subjected to an electric current.[1] The initial effort to provide illumination using electrical means occurred during the first decade of the nineteenth century, with the invention of the incandescent bulb by Thomas Edison.[1] The efficiency of the newly developed light bulb was found to be suboptimal, with a conversion rate of electrons to photons measuring below 6%. Subsequently, more efficient devices with enhanced performance (fluorescent tubes) were developed, marking the launch of the second generation of artificial lights.[1] The utilisation of enhanced fluorescence bulbs is prevalent in contemporary times. Despite these drawbacks, toxic mercury components for instance, the third version of synthetic lighting systems, was invented.[1] Researchers were attracted by organic light-emitting diodes (OLEDs) subsequent to the groundbreaking research and invention of these devices in 1987 by Tang and Van Slyke.[2] Subsequent to that time, their utilisation as lighting supplies and for full-colour displays has undergone increased advancements.[3]

OLEDs play an important role in contemporary lifestyle, finding applications in mobile phones, smartwatches, and other portable display devices. OLEDs are ideal for use in displays with flat panels because of their low power consumption, small size, and quick response time.[3] OLEDs convert electrical current into light, in contrast to solar cells, which convert light into electricity. The process of electron-hole pair recombination to excitons generates light. Layers such as emissive, hole transport, and electron transport are involved in the recombination process between the cathode and anode.[4] A 1:3 ratio of singlet to triplet excitons (25% of the excited singlet state to 75% of the excited triplet state) is produced by the recombination process, which happens when the charge transport layers inject the emissive layers with holes and electrons, respectively, taken from the anode and cathode.[4] In contrast to triplet excitons, which lose energy in the form of heat, singlet excitons emit light due to their radiative characteristics. The internal quantum efficiency (IQE) is consequently presented with a challenge. Simply because only 25% of the excitons produced are singlets, restricting the IQE of fluorescent OLEDs to 25%. Theoretically, however, the IQE of phosphorescent OLEDs could approach 100% through the intersystem crossing (ISC) harvesting of both singlet and triplet excitons (25% of the singlet and 75% of the triplet excitons).[5]

Phosphorescent OLEDs are constrained by their reliance on pricey heavy transition metals, including iridium and platinum. Due to their high cost, scarcity, and toxic effects, these substances are unsuitable for implementation on a large scale in OLED devices.[6] For incorporation into OLED devices, scientists have effectively identified substitutes for these hazardous metals. TADF, or thermally activated delayed fluorescence, is regarded as one of the most significant developments in OLEDs. Adachi and colleagues achieved an external quantum efficiency (EQE) of 20% by the effective utilisation of pure organic molecules such as polycarbazole derivatives (excluding any heavy metals and inorganic materials).[7] TADF-OLEDs employ a mechanism known as reverse intersystem crossing (RISC), which enables the efficient utilisation of both singlet (S) and triplet (T) excitons. This theoretical enhancement of the internal quantum efficiency (IQE) of the emissive molecules is achieved through the utilisation of these TADF mechanisms.[8, 9]

1.1.2 OLED device architecture

π-Conjugated materials are commonly categorised into two distinct groups, one of which is OLEDs. SMOLEDs refer to the category that involves small molecules such as biphenyl acetylene aryl derivatives; these derivatives are frequently employed in green and blue OLEDs due to their exceptional colour purity. Whereas POLEDs utilise larger molecules (polymers) such as Polyphenylenvinylene (PPV), this widely recognised conjugated polymer is commonly employed as an emissive material in OLEDs. It plays a role in producing different colours and has been thoroughly researched for its ability to emit light.[10]OLED-based devices are among the most promising due to the following characteristics of OLED materials: excellent adaptability, self-luminescence, powerful resolution, a wide viewing angle, low consumption of energy, and outstanding EL performance. Nevertheless, cold body radiation can induce luminescence when induced by external factors such as mechanical stress, photo-absorption, or electric fields.[11-13] When electrons and holes recombine, it produces light, a process known as electroluminescence.

OLED devices are made up of a single organic layer (active layer which is composed of a combination of organic compounds. An example of this would be a single-layer OLED that emits blue light and consists of a thermally activated delayed fluorescence emitter combined with a host material) that is positioned between two transporting electrodes.[14] This is the most fundamental type of OLED device. During the process of recombination between holes and electrons that takes place within the aforementioned layer, light is produced as a result. On

account of this, it is of the utmost importance that the organic layer possesses a transport capability (holes and electrons carrier ability) that is beneficial for both electrons and holes. These devices are mostly made up of two layers of organic construction. The cathode-connected layer possesses favourable electron-transporting characteristics, while the anode-connected layer operates favourably with regard to hole transport. When holes and electrons recombine at the interface, light is generated from the emissive layer which is in the middle of other transporting layers. Differences in the emissive organic layer materials' highest and lowest occupied molecular orbitals (HOMO and LUMO, respectively) control the different wavelengths of the emitted light. Additional layers are utilised to facilitate the efficient injection of holes and electrons from both cathode and anode with complicated OLED devices. By matching the work functions (the essential surface feature that governs the minimal energy required to remove an electron from a material's surface)of these layers to those of the electrodes, Schottky barriers are reduced, thereby enhancing carrier injection. Figure 1.1 shows the typical structure of OLED devices comprising multi-layers with respect to their functions.

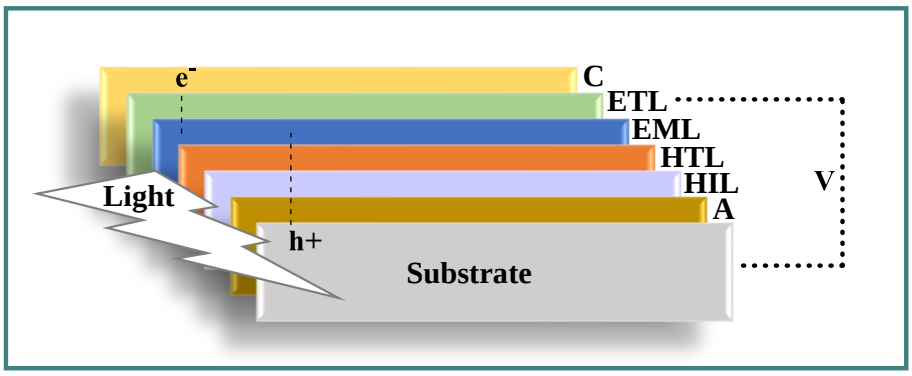

Figure 1.1 A typical structure of a multi-layer OLED device. Where C=cathode; ETL=electron transport layer; EML=emitting layer; HTL = hole transport layer; HIL = hole injection layer, A=anode (indium tin oxide); S =Substrate (glass).

1.1.3 Principle of Operation of OLED Devices

The anode is an electrode with high-performance characteristics, characterised by a high work function, and is mainly composed of indium tin oxide (ITO). This particular anode variant is well-known for its elevated work function, typically exceeding 4.8 (eV). The anode is primarily characterised as a transparent electrode with a high work function. The anode layer of the indium tin ITO exhibits excellent transparency and possesses a low plate resistance. Despite possessing remarkable characteristics, indium is a costly and scarce substance. Consequently,

continuous endeavours are being made to develop alternative anodes utilising nanotubes of carbon, polymeric materials, and graphene.[15-17]

The hole-injection layer (HIL), which is subsequently deposited on the anode, injects the holes that are present in the anode layer into the device.[18] The HIL's efficiency, operational voltage, stability of the device, and lifespan are all significantly impacted by its quality.[19] To reduce the obstacle to hole injection within this layer and to improve its ability to transport holes, various kinds of organic (made of organic materials) and inorganic (made of inorganic materials) semiconductor materials have been employed as the hole injection layer (HIL) in OLEDs.[19]Theseinclude transition metal oxides and metal halide substances, among others. Transition metal oxides such as molybdenum trioxide (MoO_3), which enable the effective transfer of electric charge from the electrode to the organic layer[20] andimprove the performance of OLEDs due to their favourable energy band structure and their proximity to the ITO anode Fermi level in terms of their conduction band.[19, 21] As a result of the distinctive characteristics that it possesses, copper iodide has been recognised as the most suitable metal halide for this particular sort of layer. In addition to having a high degree of conductivity, a matching work function, and low levels of temperature for thermal evaporation, it exhibits a very high level of transparency, particularly in the segment of the visible spectrum.[22, 23]

In the OLED structure, the hole-transporting layer (HTL) is the third layer. In addition to complying with the condition that this layer be transparent, the HOMO of this layer is required to be identical to the work function of the anode. Furthermore, it is imperative that the HTL exhibits excellent hole conductivity and the capability to obstruct electrons; this enhances the probability of electron-hole recombination within the emissive layer.[24]

In the core of OLEDs, the emissive layer is ideally positioned between the HTL and ETL. This layer is responsible for light generation and emission. The present layer is comprised of a substrate material that is doped with a chromophore to achieve colour emission. Substances such as polymers can be doped with chromophore using various techniques such as **Solution Blending (**The chromophore and polymer are combined in a solvent, then dispersion of chromophore molecules occurs within the polymer matrix), or by using **Vapor Phase Doping** (This can be done through introducing the chromophore vapour into the polymer matrix). The production of light occurs within this particular layer subsequent to its conversion from electrical energy.[23] This layer is where excitons are formed through the recombination of electrons and holes. (λ) is the light wavelength (emitted by the OLED device) which is

determined by the difference of energy between the LUMO and HOMO levels of this layer (energy band gap).

The primary function of the electron-transporting layer is to facilitate the transportation of electrons to the emissive layer. To maximise the OLED device's performance, it is crucial to minimise the Schottky barrier (describes the potential energy barrier that electrons may encounter when forming at a metal-semiconductor junction) in the OLED layers. A high Schottky barrier makes it difficult for charge carriers, such as electrons, to pass through a material. This has the potential to decrease the efficiency of charge transfer and the overall performance of the device. Improving the efficiency and brightness of OLED devices is possible by reducing the Schottky barrier, which in turn increases conductivity.[25] Furthermore, this particular layer must serve as an effective barrier against hole transport, keeping holes inside the emissive layer. This, in turn, enhances the chance of the recombination of electrons and holes and subsequent emission of light.[26, 27]

Electrons are injected into the organic emissive layer by the use of the cathode, which possesses a negative charge. Typically, the cathode is comprised of a metal material possessing a work function that is generally below 4 (eV). Magnesium (Mg) and calcium (Ca) are representative examples of metallic elements that are characterised by having low work functions. Despite possessing optimal work function values, these metals are unstable in ambient conditions such as (temperature, light, and humidity), rendering them unsuitable for application in OLED devices. Nevertheless, aluminium presents itself as an alternative option for these aforementioned metals. Aluminium has a work function of about 4.3 eV. So, the majority of OLEDs' cathodes made of aluminium.[24] The fundamental operational processes of OLEDs are depicted in Figure 1.2, commencing with the initial ground state of each molecule and resulting in the generation of excitons.

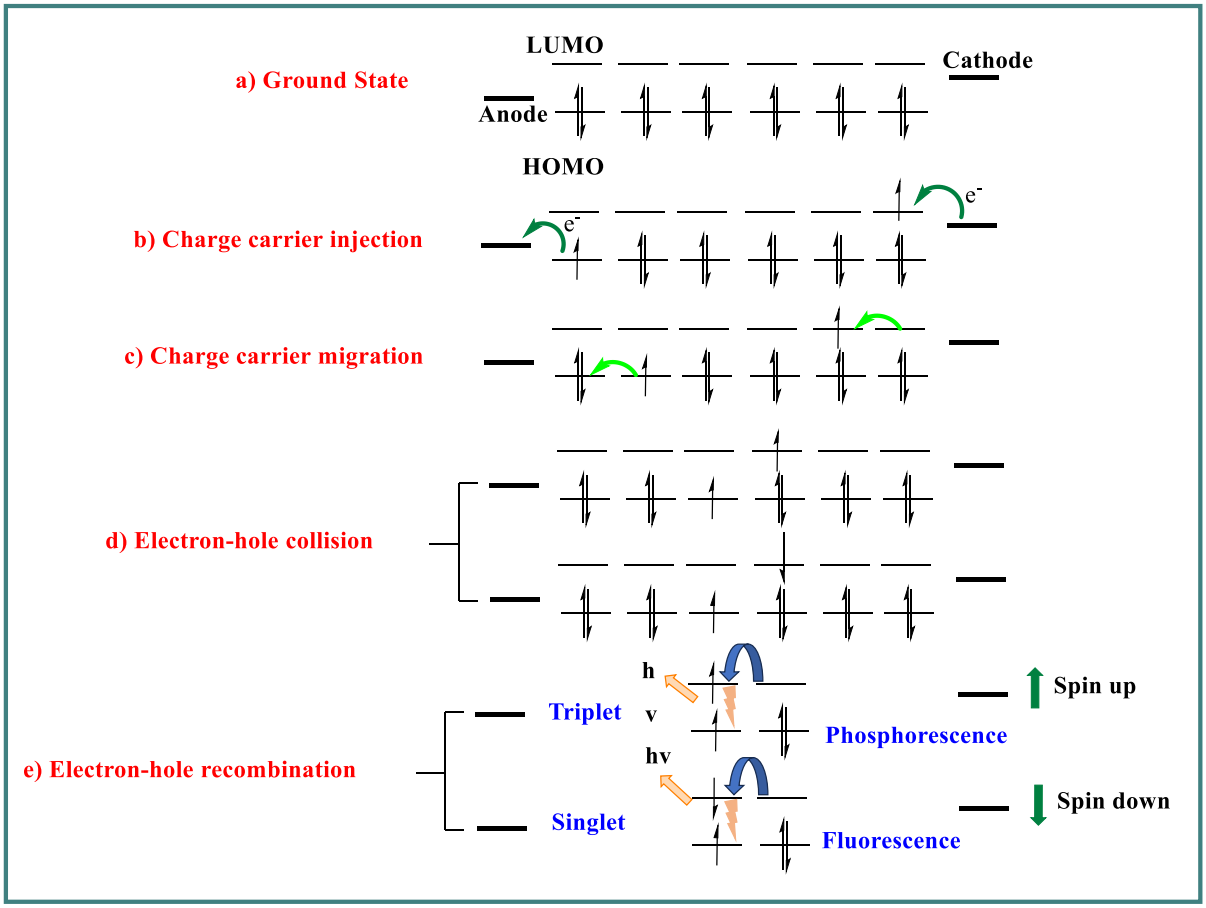

Figure 1.2 OLEDs working principle; it explains the basic steps for how polymeric OLEDs work, begin with all molecules (holes (positively charged) and electrons (negatively charged) being in the first ground state and completing with excitons being formed.[25]

1.1.4 OLEDs Applications

Ongoing investigations are being conducted to determine how to supply the commercial sector with more energy-efficient devices, such as fluorescent tubes, which represent the second generation of artificial lighting. Solid-state lighting technologies have been the subject of plenty of research in the early 2000 s.[28] QDLEDs, which originate light from quantum dots, and organic light-emitting diodes in particular, are two examples.[29] OLED devices are significant due to their substantial commercial demands. In addition, these substances demonstrate noteworthy attributes, including speed of response, simple preparation, and cost-effective and secure implementation. OLED devices are the most commonly found technology on the market as a result of their self-emitting characteristics, which facilitate their production with minimal weight, high efficiency, and quality. They have been applied and operated in a vast array of applications due to their adaptability.[30]

The commercial implementation of OLEDs is exemplified by the high performance (such as high brightness, accurate colour reproduction, and energy efficiency). Furthermore,high-quality displays found in contemporary mobile phones and televisions. In addition to exhibiting a broader viewing angle, self emission, and manufacturing thinner and lighter displays, OLED devices produce images of greater resolution in comparison to their predecessors which were produced using traditional LEDs.[26, 31] OLED displays have recently undergone numerous advancements that extend their operational lifespan. Commercial applications of OLED devices have steadily grown since their initial public introduction in early 2013. From smart watches to OLED wallpaper, the current selection of OLEDs available on the market is extensive. Furthermore, corporations engage in collaborative efforts with researchers to examine and improve OLED devices as well as the constituent materials. Nissan Chemical Industries, DuPont, and Merck are among the many corporations that are interested in OLEDs. A number of commercial lighting panels manufactured using OLED technology are depicted in Figure 1.3

Figure 1.3 OLEDs lighting panels for commercial purposes; including flat lighting panels for making TVs, Laptops and bulbs.[32]

1.2 OLEDs Generations

1.2.1 Emitters of Fluorescence (First Generation)

According to spin statistics, 25% of the excitons produced by an organic semiconductor in an electroluminescent device are in the singlet state (S_1). Although excitons are capable of being in excited states (Sn/Tn), their internal conversion will bring them down to a lower state. This is because the decay of the lowest excited state (S_1 or T_1) to the ground state, S_0, is when radiative emission is at its highest point. Additionally, 75% of T_1 excitons can be non-radiative, however this results in heat generation. The opposite is true for fluorescent materials; when an

excited state singlet radiatively decays to S_0, the result is a photon emission that is fluorescent. The only possible excited state in these materials that can emit light is a singlet state as a result of this. Transitions from triplet states to ground status are additionally hindered by the spin selection principles of quantum mechanics. This effectively reduces the amount of electrically excited excitons to a maximum 25%, which has a significant impact on efficiency.[33] As a result, the highest IQE yield that fluorescence-based devices can produce is 25%. Excitons from both singlet S_1 and triplet T_1 states must be gathered in order to reach the highest possible IQE. Figure 1.4 below illustrates number of fluorescent conjugated polymers.

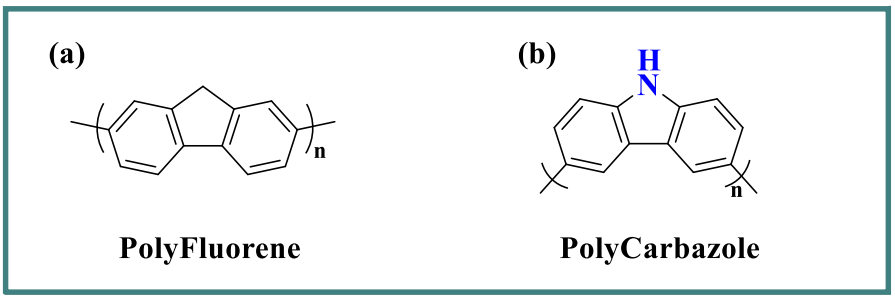

Figure 1.4 Examples of fluorescent conjugated polymers; including(a) Fluorescent conjugated polyfluorene is an interesting compound utilised in OLEDs, particularly for emitting light in the blue region. (b) Polymers based on carbazole with substitutions at positions 3 and 6 have attracted considerable attention because of their unique optical and electrical properties.

1.2.2 Emitters of Phosphorescence (Second Generation)

Baldo and his team have explored new ground in his study of spin-orbit coupling from heavy metal complexes to produce singlet and triplet states, which established the way for the development of high-efficiency organic light-emitting diodes (OLEDs).[34] A metal atom with a large orbital angular momentum, such as iridium or platinum, can be introduced into a molecule as reported by Baldo and his colleagues.[35, 36] This metal atom determines the rules for the transition between singlet and triplet excitons, allowing for singlet-triplet transitions *via* inter-system crossing (ISC). This facilitates the transition of excited S_1 excitons to T_1 excitons and emission from T_1 states through phosphorescence. Phosphorescence represents the highest IQE achievable, which is 100%. While this knowledge has definitely contributed to the development of highly effective OLEDs, drawbacks continue to exist. Even though fluorescent OLEDs have a lower efficiency than phosphorescent ones, the latter experiences a more noticeable decrease in terms of efficiency such as the lifespan of blue-emitting phosphorescent OLEDs is significantly decreased, and the formation of spin-orbit coupling relies on complexes composed of noble heavy metals.[7, 37, 38] OLEDs could only reach 100% IQE by

phosphorescence until the invention of materials with TADF properties. Advancements in engineering and material design using these new materials have made it possible to achieve 100% IQE straight from the fluorescent singlet states.

1.2.3 Emitters of TADF (Third Generation)

TADF OLED devices are the most recent innovation. Materials based on TADF emit light through the use of both singlet and triplet excitons, in the absence of heavy metals within the emissive molecules. Their application in the structure and molecular design of OLEDs has grown substantially over the past few years. Adachi and his colleagues achieved a comparable level of light production efficiency to phosphorescence-based devices using purely organic material.[7] The small energy gap between the singlet and triplet states ΔE_{ST} of TADF molecules enables the reverse intersystem crossing (RISC) to return the excitons from the excited triplet state (T_1) to the excited singlet state (S_1). The excited state lifespan in TADF is often measured in microseconds, whereas in conventional fluorescence it is typically measured in nanoseconds.[39-41] To prevent common triplet-triplet annihilation in PHOLED emitters, TADF emitters with these beneficial features have been introduced.[42] Because they do not contain any precious metals, TADF molecules and emitters are also more cost-effective. In addition, TADF materials are also thermally stable. However, TADF materials present certain constraints and difficulties, including degradation and a wide emission spectrum. A comparison of the three generations of OLEDs is illustrated in Figure 1.5 below.

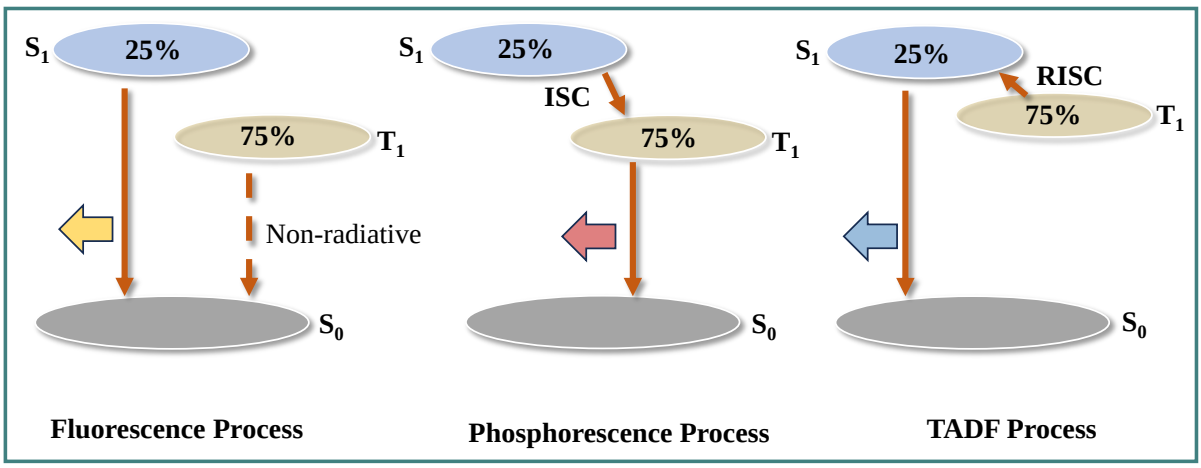

Figure 1.5 OLEDs generations and their developmental stages. In the fluorescence process, only 25% of singlet excitons can emit light while the triplet excitons (75%) are non-radiative. In the second generation (phosphorescence process), 100% of both singlet and triplet excitons can be harvested via ISC and emit light through the spin-orbit coupling from the heavy metal complex. The last generation (TADF process) can harvest 100% of both singlet and triplet excitons through the RISC.[39]

1.3 Thermally Activated Delayed Fluorescence (TADF)

1.3.1 Background

TADF substances represent the most recent development of materials designed for efficient OLEDs. They provide numerous advantages over the previous two generations, including the elimination of heavy metals and a notable increase in terms of internal quantum efficiency. Therefore, TADF-based materials are regarded as the most powerful materials for application in OLEDs. Moreover, some TADF-small molecule materials have demonstrated a high quantum yield and have the ability to cover the entire range of colours, ranging from blue to red. Nevertheless, there are still obstacles such as the low solubility behaviour of most small molecules in common organic solvents; making them unsuitable for solution processes. Moreover, they can be crystallised easily; making them more aggregated in the condensed state, which conflicts stability of the device. These must beovercome to optimise quantum efficiency and improve device manufacturing. Enhancing the previous two criteria can be achieved by directing attention towards the improvement techniques such as solution process and designs of the employed polymers such as selecting high triplet energy hosts that possess strong donor and acceptor to enable the efficient energy transfer between singlet and triplet states via RISC, and improves the TADF materials' overall performance respectively. Furthermore, more soluble in the common organic solvents and more thermal stability in terms of film morphology to enhance device stability. The development of precisely produced polymers yields cost-effective materials that are appropriate for solution processing.

The use of TADF has demonstrated remarkable efficacy in producing highly efficient fluorescence emitters. Consequently, the synthesis and development of materials that can function as the option of emitters or hosts in TADF systems has become a significant area of research in modern times. TADF molecules have been employed as a cost-effective alternative to organic phosphorescent materials in electroluminescent displays. These molecules offer greater display quality while being more affordable than phosphorescent materials.[43] Parker and Hatchard made the discovery of eosin dye in 1961, which demonstrates TADF (Thermally Activated Delayed Fluorescence) characteristics.[44] Blasse and his colleagues,[45] synthesised the initial TADF complex (Cu(I)-complex) after a period of nineteen years. Subsequent to that, additional TADF materials have been developed. Moreover, considerable progress has been made in the field of TADF utilised in OLEDs since 2009.

Following the discovery of Adachi et al. in 2012, interest in TADF applications for OLED devices reached its highest point.[7] With the development of newly effective TADF molecules, it is now practicable to fabricate OLED devices with an external quantum efficiency of 30%. Furthermore, it has been observed that the TADF emitter can cause an EQE increase of as high as thirty per cent in green emitting devices and almost twenty per cent in blue OLED devices.

1.3.2 Mechanism of TADF Luminescence

The OLED's basic architecture typically includes a metal anode, several different organic layers with different functionalities (such as transporting, injecting and emitting layers),and a cathode. Typically, there are four distinct kinds of OLEDs, distinguished by the number of layers they contain. Specifically, organic OLEDs have three, double, single, and multilayers. The most commonly used in OLEDs is the three-layer device.[46, 47] The composition of these organic layers consists of HT, ET, and EM layers, which play a crucial role in enhancing the performance of the device. Electron insertion occurs from the cathode, while hole injection occurs from the anode when a potential is applied. Within the organic emitting layer, they combine to generate excitons.[48] Both singlet S_1 and triplet excitons T_1 are generated as a result of their distinct spin states; according to quantum theory, the ratio of singlet to triplet excitons is 1:3 (The electrical excitation process in OLEDS, specifically the formation of excitons on the emitter, results in a singlet to triplet count ratio of 25:75. This ratio is determined by the spin-statistics of charge recombination.).[49, 50] Afterwards, the excitations are released into the ground state from the radiatively excited initial state of singlet or triplet excitons through the process of emission. All of the photons that are generated as a consequence of the above process are transmitted by the EML, which is the component that is accountable for the effectiveness of OLEDs.

Two types of methods are used to operate OLED devices. The first involves conventional fluorescence and phosphorescence, while the second is TADF, accomplished via two unimolecular mechanisms, as illustrated in Figure 1.6 below. The initial process is referred to as prompt fluorescence (PF), while the next step is widely recognised as delayed fluorescence (DF).[51, 52] In the process of promoting fluorescence, rapid emission occurs immediately following molecule excitation. Following the injection of charges into TADF materials, OLEDs produce both (S_1) and (T_1) in a ratio of 1:3 respectively. In contrast to conventional fluorescence, both the PF and DF mechanisms display differing fluorescence lifespans, in spite of their spectral distributions being comparable. TADF emission must also possess a number of critical

processes to function efficiently in OLEDs.The initial process includes the formation of singlet and triplet excitons, which are produced in a ratio of 1:3 by recombining both electrons and holes.[53] Secondly, by using rapid vibrational relaxation (VR), internal conversion (IC), and ISC, the high exciton states migrate to the lowest exciton levels, S_1 or T_1. Moreover, the third step of the TADF process is thermal activation, which helps the triplet excitons that have accumulated at T_1 return to S_1 during the RISC process. Ultimately, all excitons in the singlet-excited state, which consists of both the singlet excitons produced and the triplet excitons transferred, will eventually decay to the ground singlet state (S_0). This transition occurs with varying luminescence durations, depending on both PF and DF mechanisms.[54] Increased T_1 conversion leads to greater DF efficiency. The conversion rate of triplets relies on the RISC process. One method to enhance the RISC procedure is by minimising the gap in energy levels between T_1 and S_1. This indicates that there is a small energy gap (E_{ST}) between the first triplet excited state and the first singlet excited state.[43, 54]TADF molecules exhibit an energy level difference of less than 0.3 eV between the first singlet and first triplet states.

By converting all triplet excitons (75 %) to singlet excitons, which have extended lifetimes (microseconds), the RISC from T_1 to S_1 is accomplished through the utilisation of environmental heat. Furthermore, PF contributes to the production from the remaining 25% of excitons. Therefore, the internal quantum efficiency of TADF materials could attain 100 %. As both DF and PF are generated from S_1 emissions, their spectra are indistinguishable. The spatial separation of the LUMO and HOMO of excited state materials of charge transfer is commonly utilised to determine the emission of TADF molecules.[55] As a result of their molecular structure, which is typically bulky (strong donor and acceptor), TADF materials have a low (ΔE_{ST}). Thermal conditions may be utilised to implement the RISC. Therefore, upon conversion of every triplet exciton to S_1, the latter achieves an internal quantum efficiency of 100%.

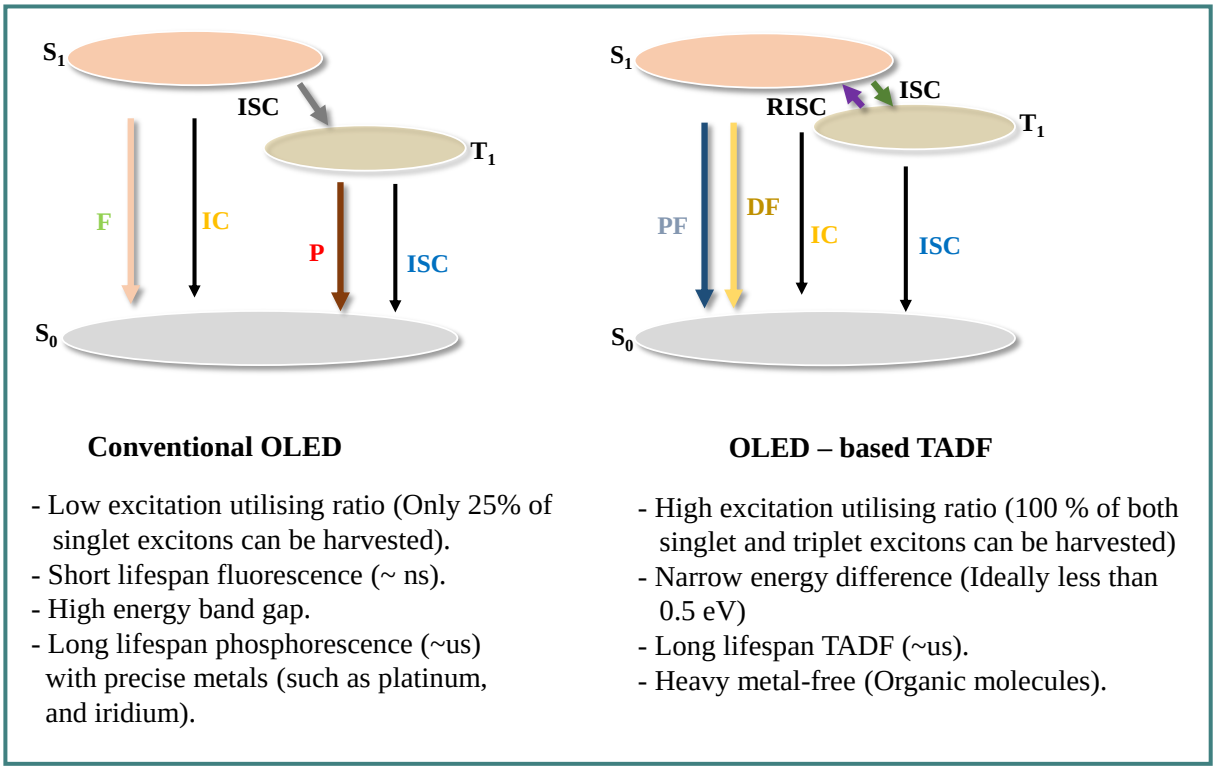

Figure 1.6 Schematic Diagram of Conventional and TADF OLEDs. Fluorescence, phosphorescence, prompt, delayed, thermally activated delayed, internal conversion, inter-system crossing and reverse inter-system crossing are represented by F, P, PF, DF, TADF, IC, ISC and RISC, respectively.[52]

1.3.3 Organic TADF Molecules Design Principles

Small ΔE_{ST} and high PLQY (photoluminescence quantum yields) are critical requirements for the fabrication of TADF emitters; these attributes are deeply linked to the characteristics of the light they emit. Additional factors that could significantly contribute to the advancement of the process include the stability of the molecules and the full width at half-maximum (FWHM) of the emission spectrum (Reduced FWHM values result in steady PL signals, minimising the occurrence of photobleaching and maintaining consistent data. In addition, a smaller FWHM) value implies a peak that is sharper and more precisely defined. Within the framework of PL, this signifies that the emission spectrum is highly concentrated around a particular wavelength).[56](see schematic diagram in figure 1.7). Considering the connection among the parameters, the objective in designing the TADF materials was to optimise the parameters; however, this approach may result in a minor reduction in the value of certain factors. According to a number of studies, the donor (D) -acceptor (A) molecular design is the most effective method for producing TADF molecules. In fact, current emitters are constructed in this manner, featuring large spatial separation between the HOMO and LUMO.[57-59] To be more

clear, Through the effective separation between electron-donating (D) and electron-withdrawing (A) units, it is possible to harvest triplet energy efficiently.[60]

In spite of the advantages associated with a donor-acceptor-based molecular design, the weaknesses become apparent across a wide range of light emission wavelengths. The charge transfer (CT) emissive state gives rise to this circumstance, and in certain instances, the device's lifespan (τ) is reduced due to the instability of its molecular structure. The lifespan of the devices is proportional to the instability of their chemical structures, while the wide emission spectrum is linked to their colour purity. Therefore, an effort has been made to eliminate these concerns by modifying the structure of the simple donor-acceptor design.

The properties of the device are linked to the aforementioned product parameters. The external quantum efficiency (EQE), which is regulated by PLQY, determines the colour purity (FWHM), while efficiency roll-off, which indicates that the effectiveness of OLED reduces with increasing brightness, is determined by the lifespan of delayed fluorescence controlled by ΔE_{ST}. In order to enable the utilisation of TADF emitters in display applications, it is imperative that the primary attributes of the devices be fulfilled: an extended operational lifetime, minimal efficiency roll-off, exceptional colour purity, and a high EQE. Notwithstanding this, excellent colour purity is not required for lighting applications. Therefore, the characteristics of both the emitter and the device will be included in the discussion of the molecular structural design strategies.[58]

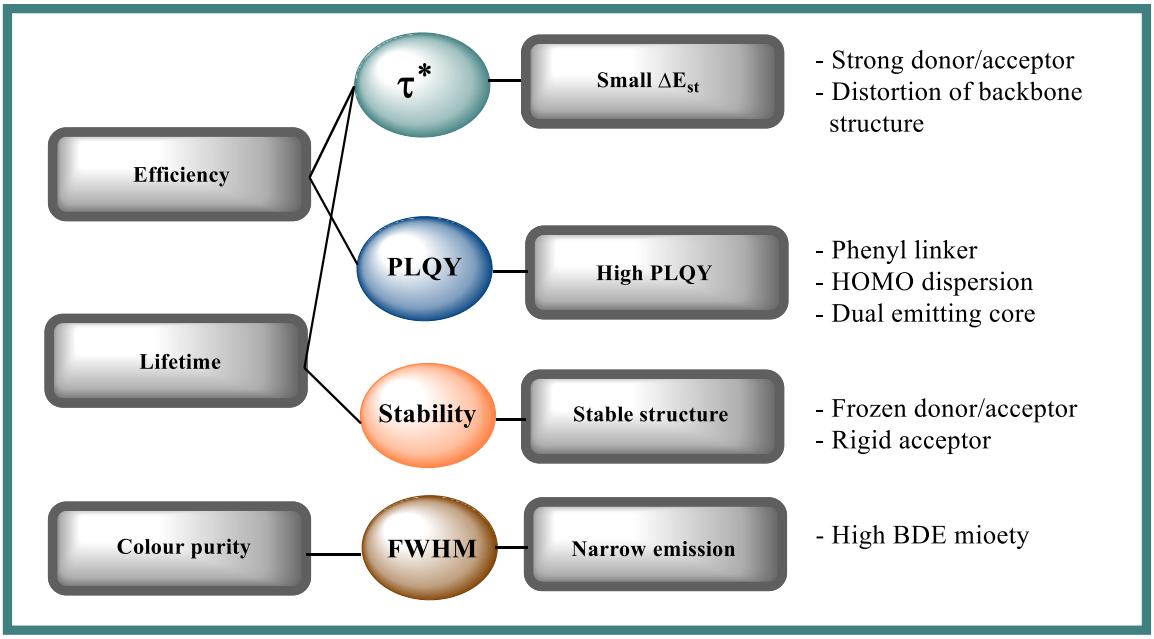

Figure 1.7 Schematic diagram of Material Design Methods, Device Performance, and Material Parameters. The key settings for achieving a small ΔEST and high PLQY are essential for obtaining desirable light-emitting features in TADF materials. Furthermore, crucial requirements involve the FWHM of the emission spectrum and the materials' stability.

1.3.3.1 TADF Emitters (Donors and Acceptors Moieties)

Effective selection of both the donor and the acceptor molecules is necessary to regulate the photophysical characteristics of TADF molecules. The localisation of HOMO and LUMO will take place on the donor and acceptor units, respectively, for strong donors and acceptors. This technique reduces the singlet energy of TADF emitters by creating a spatial separation between the HOMO and LUMO orbitals, with an insignificant effect on the triplet energy. When the HOMO and LUMO are located far apart from one other, their interaction becomes smaller. As a result, wider HOMO-LUMO gaps indicate higher stability and less reactivity. The spatial separation between the HOMO) and the LUMO can be estimated by measuring the relative strengths and weaknesses of both the donor and acceptor units. In contrast to strong donors; classified by the shallow HOMO value (Phenothiazine) and acceptors; classified by the deep LUMO value (CN heteroarmitics), weak donor; classified by the deep HOMO value (Carbazole) and acceptor; classified by the shallow LUMO value (Triphenyltriazines) molecules result in a small reduction in the singlet energy levels due to their capacity to localise the HOMO and LUMO energies less significantly. Subsequently, the energy transitions of TADF materials can be significantly reduced by strong donor and acceptor molecules in comparison to their weak counterparts. A wide range of donor and acceptor units have been recently used in the molecular design of TADF emitters, each with unique donor/acceptor strengths. Significantly, the HOMO

and LUMO levels of the emitter have a crucial role in determining the strengths of the donor and acceptor. Regarding the donor molecules, a deep HOMO signifies a weak electron donor strength, whereas a shallow HOMO indicates a high electron donor strength. In a comparable manner, a deep LUMO indicates a weak electron acceptor strength, while a shallow LUMO signifies a strong electron acceptor strength in relation to the acceptor molecules. The donor molecules are typically chosen from specific structures, such as amine, diamine, phenazine, phenothiazine, phenoxazine, acridine, carbazole, bicarbazole, and indolocarbazole. Alternatively, acceptor units commonly involve aromatic ketone, triazole, benzothiazole, oxadiazole, benzoxazole, thiadiazole, triazine, heptazine, phthalonitrile, anthraquinone, and quinoxaline. Phenazine, phenothiazine, phenoxazine and acridine are examples of powerful donor molecules with HOMO values of (-4.14 eV), (-4.67 eV), (-4.68 eV) and (-4.88 eV) respectively, (more shallower HOMO value refer to more strong donor moiety).While carbonitrile derivatives are considered powerful acceptor molecules.[58] Figure 1.8 below depicts distinct TADF acceptors and donors with respect to their structures.

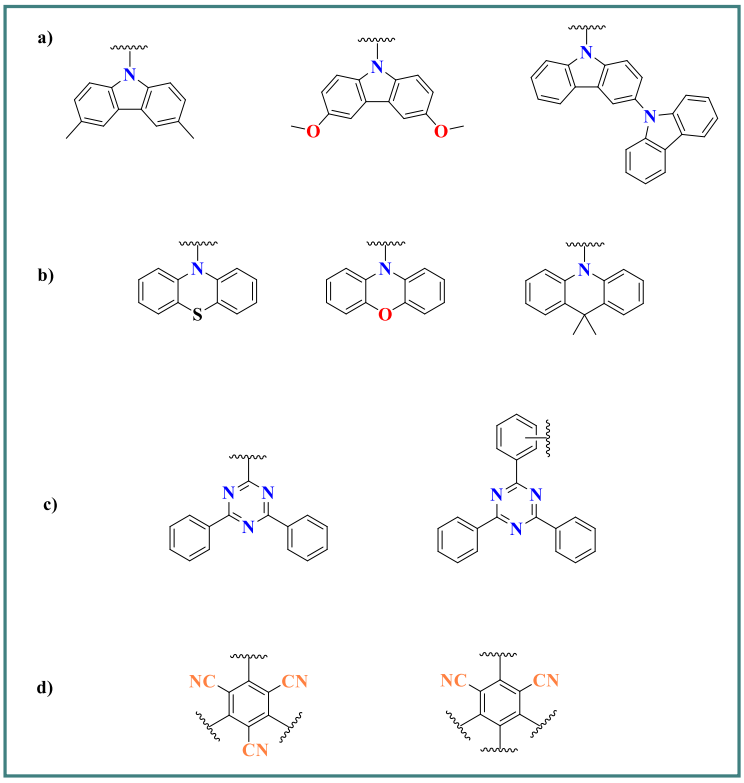

Figure 1.8 Variety of donors and acceptors used for TADF; (a) Carbazole donors; donor strength increase from the left to the right propotionally with increasing the donating ability (b) Arylamine donors;donor's strength decrease from the left to the right with decreasing the donating ability (phenothiazine > phenoxazine > acridan).(c) N-heterocyclic acceptors; diphenyltrizine more stronge acceptor than triphenyltrizine (acceptor's strength decrease from the left to the right). (d) Benzonitrile acceptors; classified as strong acceptors (high electron affinity).

1.3.3.2 Molecular Design for short-delayed Fluorescence Lifetime

TADF emitters exhibit light emission stage phenomena during which fluorescence and delayed fluorescence occur over time lengths of nanoseconds and microseconds, correspondingly. Reports indicate that the rapidly decaying fluorescence does not contribute to the non-radiative loss mechanism. On the contrary, the efficiency of non-radiation processes such as triplet-triplet annihilation (TTA) decreases in slow-decaying delayed fluorescence due to the fact that electrons remain in the T_1 level for an extended period of time on microsecond scales. In order to minimise the τ parameter, which represents delayed fluorescence resulting from a gradual transition from T_1 to S_1 to S_0 over the microsecond time scale, TADF emitters must be designed accordingly. ΔE_{ST} is decreased as a result of increasing the rate of the reverse intersystem crossing (k_{RISC}), which controls the lifetime by decreasing ΔE_{ST}, once the delayed fluorescence lifetime reduced by the molecular design method. Two primary strategies are necessary to address the ΔE_{ST} of TADF emitters: increasing the strength of the donor-acceptor interaction and deforming the linker that connects the donor and acceptor. Both methods were effective for decreasing ΔE_{ST} and therefore reducing the lifetime of delayed fluorescence.[58]

1.3.3.2.1 Donor and Acceptor Strengths Management

1.3.3.2.1.1 Management of Donor and Acceptor Molecules

An efficient approach to designing TADF emitters with reduced ΔE_{ST} entails the incorporation of strong donor and acceptor molecules, which enhance the CT properties of the materials and consequently stabilise the singlet energy. As strong donor moieties, acridan, phenothiazine, phenazine, and phenoxazine are the most widely used, whereas CN substituted heteroaromatics, heptazine, and CN are the most frequently employed acceptor moieties. The results of the study revealed that the delayed fluorescence in the TADF materials containing strong acceptors and donors had a photoluminescence lifespan of less than five microseconds. Numerous TADF emitters, which take advantage of acridan's strength as a strong donor , are capable of achieving a short lifespan of a few microseconds. Furthermore, it is noteworthy that 10,10′-(sulfonylbis(4,1-phenylene))bis(9,9-dimethyl-9,10-dihydroacridine) (DMAC-DPS) is widely utilised as a blue TADF emitter that possesses a reduced lifetime of 3.1 μs.[59, 61, 62] Notwithstanding the weak electron-accepting nature of diphenyl sulfone employed as an acceptor of DMAC-DPS, the presence of acridan, which is regarded as a strong electron donor (shallower HOMO value of acridan (-4.888 eV) refers to strong donor), effectively shortens the lifespan. There are multiple associated chemicals, such as 2,7-bis (9, 9-dimethylacridin-10

(9H)- yl)-9,9- dimethyl-9H-thioxanthene 10,10 -dioxide (DMTDAc) and 10-(4-((4-(9H-carbazol-9-yl)phenyl)-sulfonyl)phenyl)-9,9-dimethyl-9,10-dihydroacridine (CzAcSF), which have a short lifespan of 1.2 and 5.6 µs, respectively.[62-64] Although acridan is widely acknowledged as a donor molecule with a short lifespan, its electron-donating strength is not greater than that of phenoxazine, phenazine, and phenothiazine. Phenazine, phenothiazine, phenoxazine, and acridan were identified as the donor molecules in the order of strength due to their respective electron-donating capabilities of nitrogen, sulphur, oxygen, and carbon. The results indicate that with increasing donor strength, there was an accompanying decrease in the level of singlet-triplet energy difference (ΔE_{ST}), leading to a shortening of the lifespan. Strong donors effectively reduce the singlet-triplet gap by donating electrons to acceptors. As a result of this, a narrower ban gap leads to RISC being more effective (moving excitons from the T1 to S1 state within a shorter time and reducing the delayed fluorescence of excitons in the T1 state) which improves the efficiency of TADF. Furthermore, TADF emitters experience an identical impact regarding lifetime and ΔE_{ST} reduction when strong acceptors are employed. The utilisation of strong acceptors together with weak donors has been demonstrated to reduce both ΔE_{ST} and lifespan.[58]

1.3.3.2.1.2 Distortion between Donors and Acceptors

The advantage of strong CT characteristics for small ΔE_{ST} and τ is due to the presence of a twisted backbone structure between the donor and acceptor. An efficient approach to molecular design involving the distortion of the molecular structure includes linking the acceptor and donor *via* the ortho-position of a phenyl linker. The dihedral angle is increased due to steric hindrance between the donor and acceptor, which makes this strategy rational. Compounds such as 5-(2-(4,6-diphenyl-1,3,5-triazin-2-yl)-phenyl)-5H-benzofuro [3,2-c] carbazole (**o-BFCzTrz)**, 5-(3-(4,6-diphenyl-1, 3,5-triazin-2-yl)-phenyl)-5H-benzofuro[3,2-c]carbazole (**m-BFCzTrz)**, and 5-(4-(4, 6-diphenyl-1, 3,5-triazin-2-yl)-phenyl)-5H-benzofuro [3,2-c] carbazole (**p-BFCzTrz)**, each of the model compounds was utilised to assess the effectiveness of the ortho-linking approach in causing molecular distortion.[65] Based on the results, it was observed that **o-BFCzTrz** exhibited the highest efficacy in decreasing ΔE_{ST} and τ (with ΔE_{ST} decreasing from 0.19 eV for **m-BFCzTrz** and 0.30 eV for **p-BFCzTrz** to 0.002 eV for **o-BFCzTrz**). Simultaneously, the τ value of **o-BFCzTrz** was comparatively short, measuring 5.4 µs, in contrast to the 30 µs exhibited by the remaining emitters. Significantly, the reduced τ value made a substantial contribution to the enhancement of efficiency roll-off in TADF devices, resulting in a maximum 15% in EQE, even though the 1,000 cd/m^2 decrease from the

maximum values. The TADF emitters demonstrated that steric hindrance increases the CT character, as in molecule 1, 3, 6, 8-tetramethyl-9-(10-(2, 4, 6-triisopropylphenyl)-10H-dibenzo [b, e][1 ,4]-oxaborinin-3-yl)-9H-carbazole (7) in the presence of 1,3,6,8-tetramethylcarbazole as a donor.[65] The carbazole donor and a phenyl linker sterically hindered the two methyl groups located at positions 1 and 8 of the (7) emitter. The donor became vertically aligned with the phenyl linker as a consequence of this circumstance, leading to an enhanced CT character. As a result, the (7) emitter exhibited remarkably small ΔEST (0.01 eV) and short τ (3.49 μs) measurements. TADF emitters that incorporate phenoxazine, acridan, and phenothiazine-derived donor units typically exhibit small energy splitting (ΔE_{ST}) and short (τ) due to the distortion of the donor and the vertical position of the donor moieties to the phenyl linker. Within each design method classification, Figure 1.9 provides a summary of the molecular design approaches that are utilised for short τ and emitters.[58]

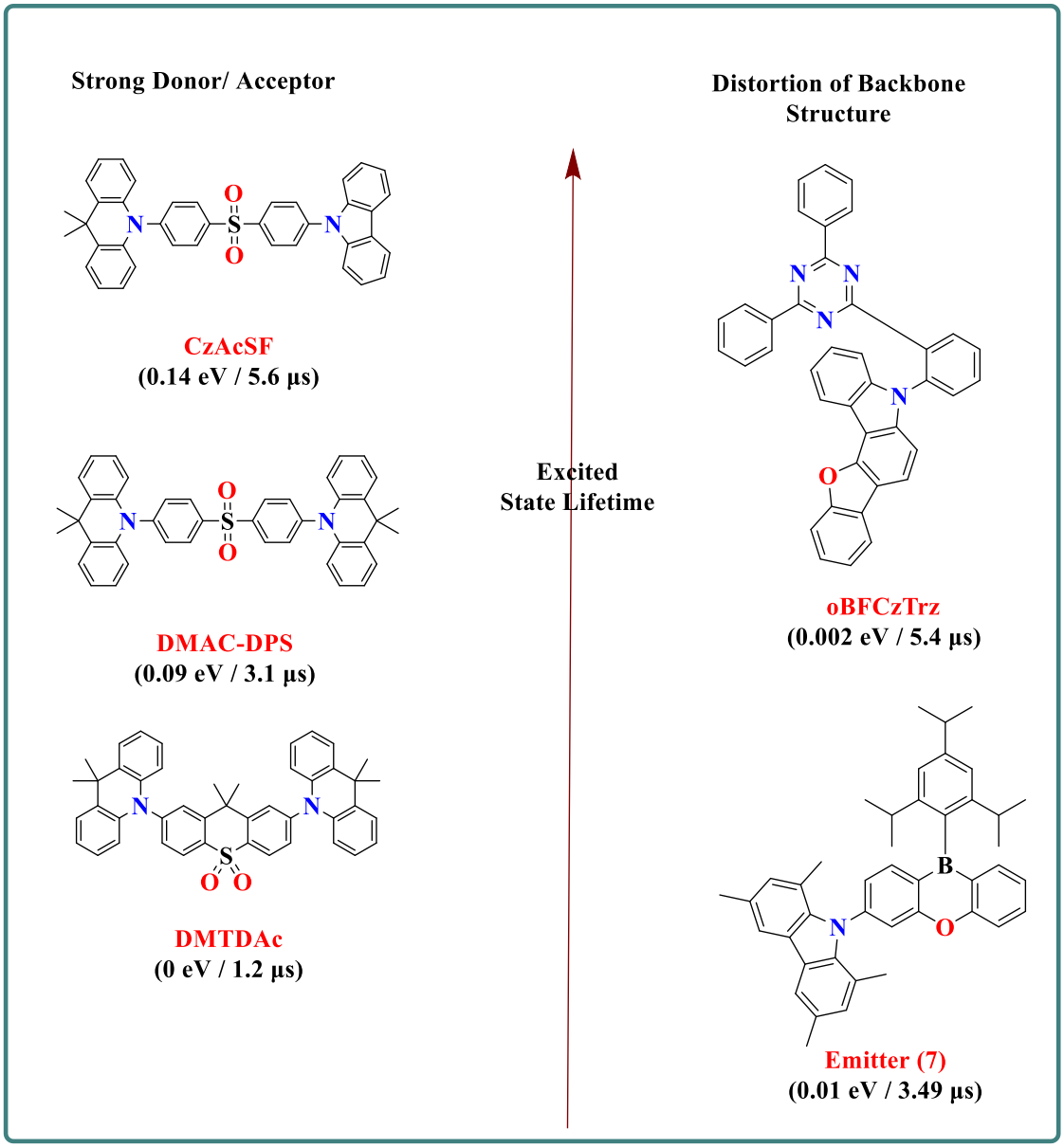

Figure 1.9 Emitters' chemical structures associated with short lifetimes for delayed fluorescence. On the left side of the figure, increasing the strength of the donor molecules from CzAcSF to DMTDAc results in a decrease in the band gap between singlet and triplet, which in turn reduces RISC's delayed fluorescence time. On the right side of the figure, the distortion of backbone structure (how donor and acceptor link together); the ortho-phenyl linker to the acceptor (diphenyl triazine) in oBFCzTrz increases the steric hindrance and results in increasing the CT, which in turn minimises the band gap and reduces the delayed fluorescence time of RISC compared to the m and p phenyl linkers that provide less steric hinderance.

1.3.3.3 High PLQY Molecular Design

1.3.3.3.1 Design of Phenyl Linker

Various molecular designs have been suggested to enhance the PLQY of TADF emitters such as (phenyl linker, HOMO dispersion and dual emitting core). Research has revealed some

chemicals that exhibit high PLQY. These compounds, however possessing different chemical structures, can be categorised into three categories based on their design strategy for achieving high PLQY: firstly, the design including a phenyl linker; secondly, the design involving HOMO dispersing; and finally, the design with a dual emitting core.[58] Prior studies on TADF materials primarily emphasised the phenyl linker-free design, without necessitating the mention of the phenyl linker principle. However, the Adachi group's innovative research also suggested using a phenyl linker to alter the molecular design in order to achieve a high PLQY by overlapping the HOMO and LUMO levels. In earlier TADF emitters, such as 9-(4,6-diphenyl- 1,3,5-triazin-2-yl)-9′-phenyl- 9H, 9′H-3,3′-bicarbazole (**CzT**), 9,9″ -(6-phenyl-1,3,5-triazine-2,4-diyl) bis- ((9H-3,9′-bicarbazole)) (**CC2TA**), 12,12′-(6-([1,1′-biphenyl]-4-yl)-1,3,5-triazine-2,4-diyl)bis(11-phenyl-11,12-dihydroindolo[2,3-a]carbazole) (**PIC-TRZ**), and 12-(4,6- diphenyl-1,3,5-triazin -2-yl)-5-phenyl -5,12- dihydroindolo [3,2-a] carbazole (**PIC-TRZ2**). It was observed that the PLQY of these emitters was less than 70%. This was attributed to the high energy gap between the HOMO and LUMO, which prevented the absorption and emission of light.[66-70] Therefore, studies indicate that high PLQY can be achieved by employing the design of a phenyl linker and effectively managing the gap between the HOMO and LUMO levels. The phenyl linker design reduces the gap between the HOMO and LUMO levels by extending them to the aromatic phenyl linker. Significantly, the achievement of high oscillator strength is reliant upon the HOMO - LUMO extension to the phenyl linker in the TADF emitter. This advancement ultimately results in a greater PLQY by increasing the light-absorbing ability of the emitter.

The implementation of the initially developed phenyl linker-based TADF emitter, specifically 2,4,5,6-tetra(9H-carbazol-9-yl) isophthalonitrile (**4CzIPN**), demonstrated notable advantages in enhancing the PLQY to more than 90% in both solution and solid states. Regarding **4CzIPN**, the phenyl linker was used to connect two CN moieties, which are electron acceptors, and four carbazole moieties, which are electron donors. The linkage in the **4CzIPN** structure has a crucial function in elevating the PLQY to a level above 90% and encouraging the EQE to rise above 20%. These specific results in the enhancement of PLQY and EQE were produced by the overlap between HOMO - LUMO at the phenyl linker based on molecular orbital calculation.[71-74] Since the phenyl linker strategy was proven to improve PLQY, various TADF materials were created by connecting donor and acceptor units to it. The utilisation of the phenyl linker strategy in TADF emitters has effectively exhibited the great performance of this design in terms of increasing the PLQY.

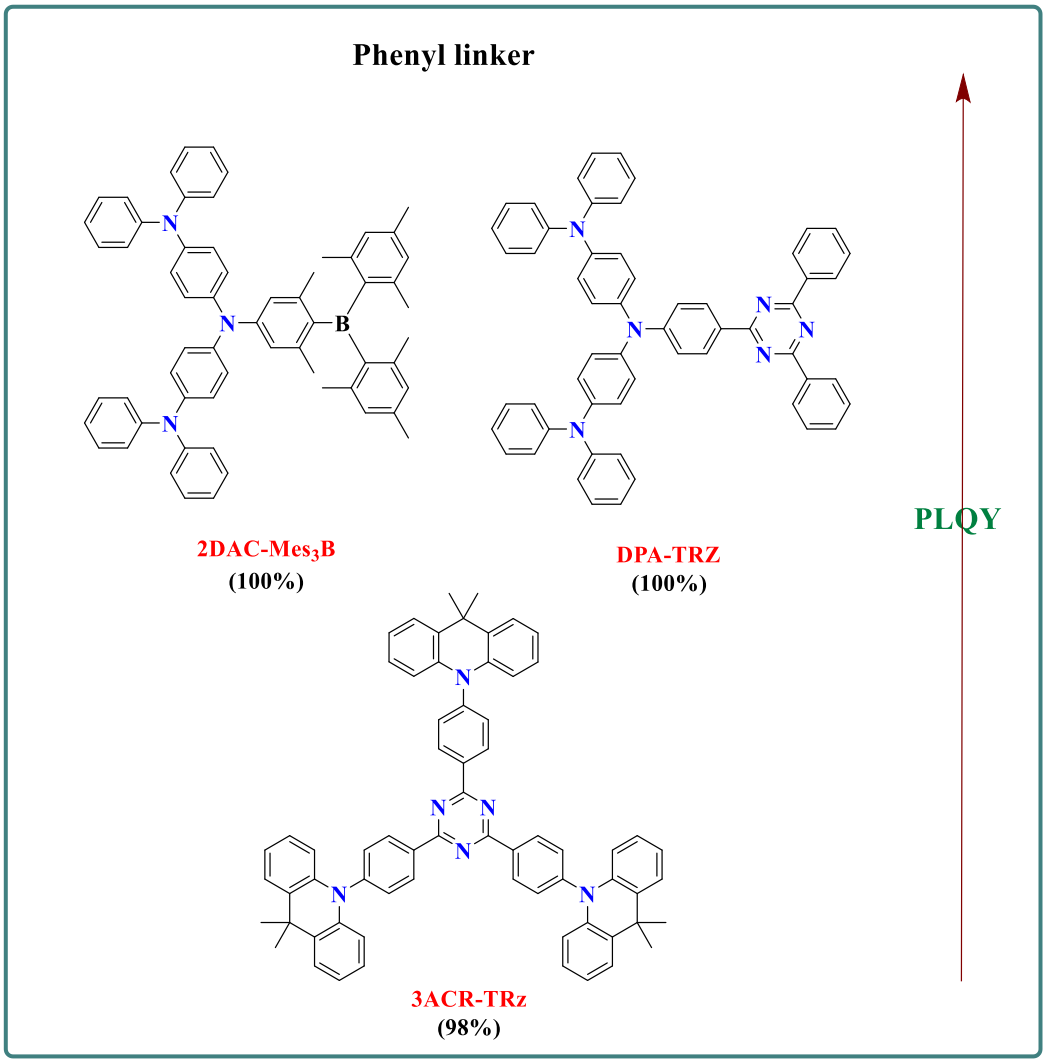

Figure 1.10 TADF emitter chemical structures with high PLQY with regard to phenyl linker design. Emitters abbreviated with 2DAC-Mes3B and DPA-TRZ can achieve 100% PLQY; this is attributed to using multi-strong donors (triphenylamine) connected to the acceptors through the phenyl linker. The emitter 3ACR-TRz can reach 98% PLQY due to using multiple donors of acaridan (less strength), which is connected to the acceptor (triazine) through the phenyl linker.

Studies illustrated that 4, 4′, 4″-(1, 3, 3a-1, 4, 6,7, 9-heptaazaphenalene-2, 5, 8-triyl) tris(N, N-bis(4-(tert-butyl)-phenyl) aniline) (**HAP-3TPA**), is considered a highly effective red TADF emitter due to its effective designation of heptazine as an acceptor and t-butyl-modified aromatic amine as a strong donor with the phenyl linker. The outcome of this advancement is that the PLQY achieves a notable level of 95%, while the EQE reaches a significant value of 18 %.[75] Furthermore, the observation that the PLQY surpasses 90% and the EQE value is as high as 27% indicates that DMAC-Trz is among the most efficient green TADF materials in terms of performance.[76] The formation of the **DMAC-Trz** as a TADF emitter was accomplished by linking 9,9-dimethyl-9,10-dihydroacridine (DMAC) as a robust donor with 2,4,6-triphenyl-1,3,5-triazine (TRZ) (acted as an acceptor) to the phenyl linker at the para

position. Similarly, the design approach used for blue TADF emitters, employing compounds such as spiroacridan-triazine hybrid, spiroAc-Trz,[77] and 9,9′,9″-(5-(4,6-diphenyl-1,3,5-triazin-2-yl)-benzene-1,2,3-triyl)tris(9H-carbazole) (**TCzTrz**), involved the implementation of the phenyl linker concept. This involves attaching donors and acceptors to the phenyl linker to achieve the desired design.[58, 78-81] The strategies of molecular design based on high PLQY and representative emitters with phenyl linker design are summarised in Figure 1.10 above.

1.3.3.3.2 HOMO Dispersing Design

The successful implementation of the HOMO-dispersing molecular design (The distribution of the HOMO over the molecular structure) has led to high-performance levels in TADF emitters (critical factor in determining the behaviour of TAD) , particularly in terms of PLQY. This design has been effectively combined with the phenyl linker principle in the molecular structure. The HOMO-dispersing molecular design concept aims to create a substantial overlap of the HOMO and LUMO in the backbone structure between donors and acceptors respectively . This is achieved by uniformly distributing the HOMO across the structure. Therefore, by increasing the degree of overlap between the HOMO and LUMO, the oscillator strength and PLQY of TADF emitters are enhanced. The HOMO dispersion strategy was effectively implemented into the design of **4CzIPN** by employing four carbazole donor units that handle the HOMO.[82] When comparing 4,6-di(9H-carbazol-9-yl)isophthalonitrile (**DCzIPN**), which contains two carbazole units, it was found that **4CzIPN** achieved a significantly better PLQY of 94%. This can be attributed to the superior ability of the four carbazole donor units in **4CzIPN** to disperse the HOMO.[83] The initial increase in PLQY led to the EQE of the TADF device beyond 20%, and the subsequent operation of an additional TADF device further improved the EQE to over 30%. By employing the identical principle, high PLQY emitters were identified in compounds containing three carbazole donor moieties, 9, 9′, 9″- (5- (4, 6- diphenyl-1, 3, 5- triazin-2-yl) - benzene -1, 2, 3-triyl) tris (3, 6-dimethyl-9Hcarbazole) (**TmCzTrz**) and (**TCzTrz**). These emitters exhibiting elevated PLQY were developed from the compound with two carbazole donor molecules 9,9′-(5-(4,6-diphenyl-1,3,5-triazin-2-yl)-1,3-phenylene)bis(9H-carbazole) (**DCzTrz**). When comparing both emitters with **DCzTrz**, it was found that both emitters obtained a 100% PLQY, but **DCzTrz** only produced a 43% PLQY due to the presence of extra carbazole units. This circumstance suggests that the presence of the extra carbazole molecule enhances the PLQY through the delocalisation of the HOMO.

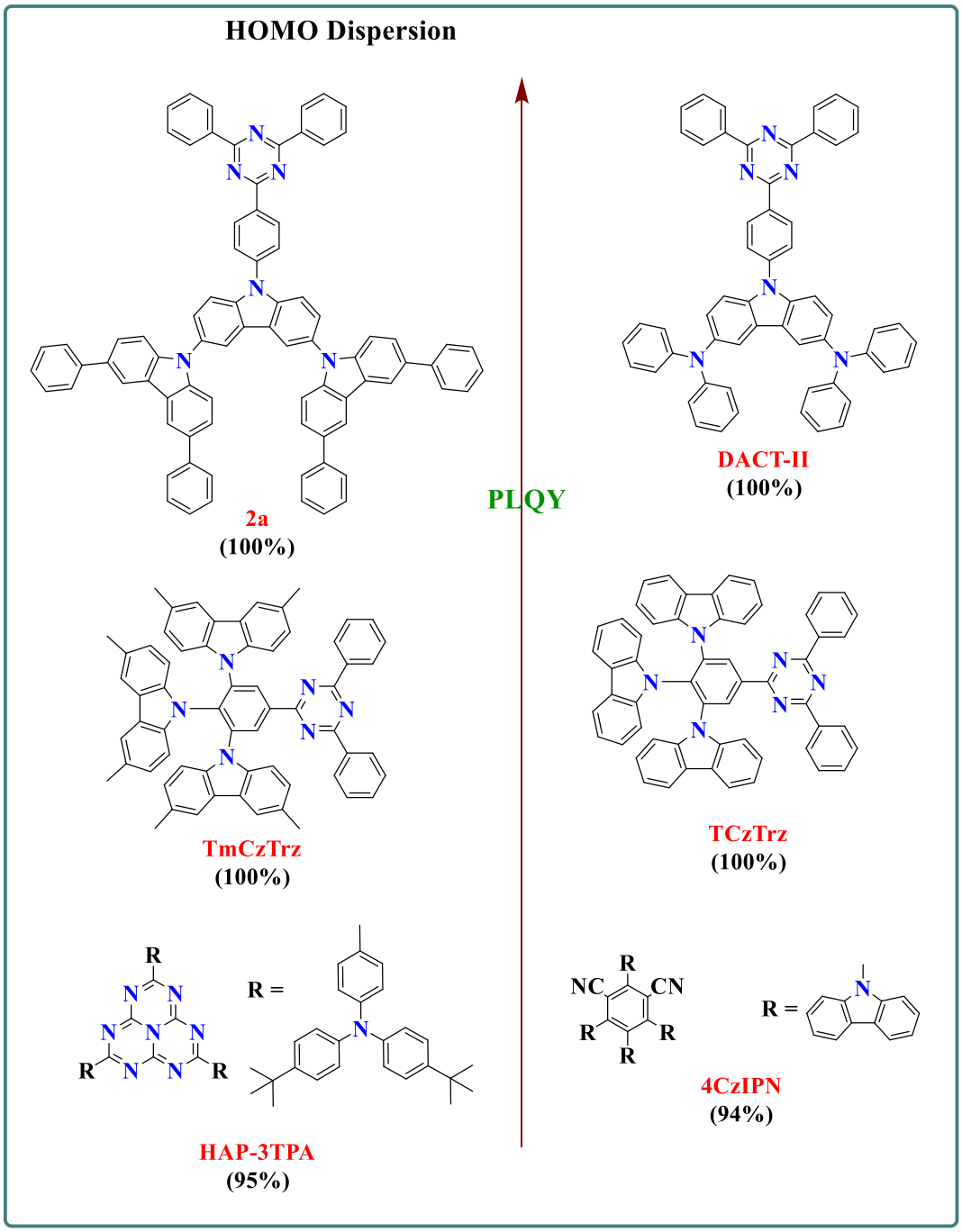

Figure 1.11 TADF emitter chemical structures with high PLQY with regard toHOMO dispersion design. In compounds such as 2a, TmCzTrz, DACT-II and TCzTrz, the HOMO (donors) are dispersed fully and connected to the acceptor through the phenyl linker. This achieved 100% PLQY compared to compounds such as HAP-3TPA and 4CzIPN which achieved 95% and 94% respectively, the reduced percentages in both two last compounds are attributed to weak dispersed of HOMO over the structures, as they attached directly to the acceptors, Therefore, the HOMOs are not dispersed efficiently compared the first fourth compounds.

Remarkably, **TCzTrz** achieved a high EQE (external quantum efficiency) of 25% in devices-based blue TADF emitters, thanks to its increased PLQY. Furthermore, five donor groups,

derived from carbazoles such as 3-(3-(tert- butyl)-9H- carbazole -9-yl)-2, 4, 5, 6- tetra (9H-carbazol -9- yl) benzonitrile (**5CzBN**(**5CzCN**)), demonstrated that the enhanced PLQY is attributed to the uniform distribution of HOMO caused by the five donor units.[84] The EQE value of 17% provided by the (**5CzBN**(**5CzCN**)) emitter was brilliant. Aside from delocalising the HOMO through the use of multiple donors, wide HOMO dispersion was an additional technique for attaining a high PLQY. The reason for this phenomenon is the presence of a bulky structure of the donor in the TADF emitters.[85] In the TADF emitter known as 9′-(4-(4,6-diphenyl-1,3,5- triazin-2-yl)- phenyl)-3, 3″,6 ,6″- tetraphenyl- 9′H-9, 3′:6′,9″- terbenzo [b] indole (**2a**), two carbazoles substituted with 3,6-diphenylcarbazole were employed as donor moieties. Research has determined that the (**2a**) emitter's PLQY yielded a value of 100%. The increase in both the PLQY and the HOMO-dispersing capability resulted in the 2a emitter's EQE reaching 21%. In addition, 9-(4-(4, 6- diphenyl-1,3, 5-triazin-2-yl)- phenyl)-N^3,N^3,N^6,N^6-tetraphenyl-9H-carbazole-3,6-diamine (**DACT-II**), which is designed from diphenyltriazine acceptor exhibited a 100% PLQY and a 29% EQE; as a result of the distribution of the HOMO of two carbazoles substituted with diphenylamine at positions 3 and 6.[58, 86-89] Figure 1.11 above, presents a summary of the molecular design approaches that focus on achieving high PLQY and highlights the typical emitters with regard to the design of HOMO dispersion.

1.3.3.3.3 Design of Dual Emitting Core

A recent advancement involves the use of a dual emitting core design, which enhances the creation of high PLQY. This design consists of two linked TADF emitter components within a single molecular architecture. The underlying concept of the dual-emitting core design proposes that the combination of two emitter moieties will greatly enhance the light-absorbing ability together with the emission of the TADF emitters in comparison to the single-emitting core design. Furthermore, 3,3′,5,5′-tetra(9H-carbazol-9-yl)-[1,1′-biphenyl]-2,2′,6,6′-tetracarbonitrile (**DDCzIPN**), which was effectively synthesised through the reaction of direct coupling of two **DCzIPN** emitters, was the initial TADF emitter to be designed in this manner utilising the dual emitting core method.[90] A comparison between **DCzIPN** and **DDCzIPN** revealed that **DDCzIPN** showed a higher absorption coefficient from 1.1×10^5 to $3.7 \times 10^5 M^{-1}$ cm^{-1} as a result of the two TADF units' absorption.[90] As a consequence, the PLQY and EQE of **DDCzIPN** experienced noticeable increases up to 91% from 67%, and 19% from 16% respectively. Additionally, it was observed that dual-emitting core TADF emitters, including **DDCzIPN**, exhibited a shift in emission spectrum towards longer wavelengths. The observed transition can be attributed to the elevated degree of conjugation, which was initiated

by the direct coupling of two phenyls. To handle the colour shift issue associated with the dual-emitting core design, one potential strategy is to couple two TADF emitter units *via* a donor molecule in the molecular structure. This enabled efficient management of the emission spectrum emitted by the dual-emitting core TADF emitters. This concept has been demonstrated to effectively manage the emission spectrum of dual emitting core emitters, according to the results of investigations involving two types of molecules with acceptor units consisting of diphenyltriazine and dicyanobenzene. When considering dicyanobenzene compounds such as 6,6′-(9H,9′H-[3,3′-bicarbazole]-9,9′-diyl)-bis(4-(9H-carbazol-9-yl)isophthalonitrile) (**33TCzPN**), 6,6′-(9H, 9′H- [3, 4′- bicarbazole]-9, 9′-diyl)- bis(4-(9H -carbazol- 9-yl) isophthalonitrile) (**34TCzPN**), and 6, 6′ -(9H, 9′H-[4, 4′- bicarbazole]-9, 9′-diyl)- bis(4-(9H-carbazol-9-yl) isophthalonitrile) (**44TCzPN**) that contained carbazole moieties interlinked in various positions, distinct emission spectra were observed depending on the interlinked position.[91] In particular, the emission spectrum of the 33TCzPN, which is composed of two carbazole units joined at the 3- position of each carbazole, was red-shifted. Hence, this evolution may be ascribed to the minimal dihedral angle of 33TCzPN, which exists between the two carbazole units. A noteworthy advancement occurred when the PLQY of dual emitting core TADF emitters increased substantially due to enhanced light absorption, which in turn led to the increased EQE in the devices-based TADF. A summary of the molecular design approaches that focus on achieving high PLQY and illustrate the typical emitters in relation to the design of a dual-emitting core is presented in Figure 1.12 below.[58]

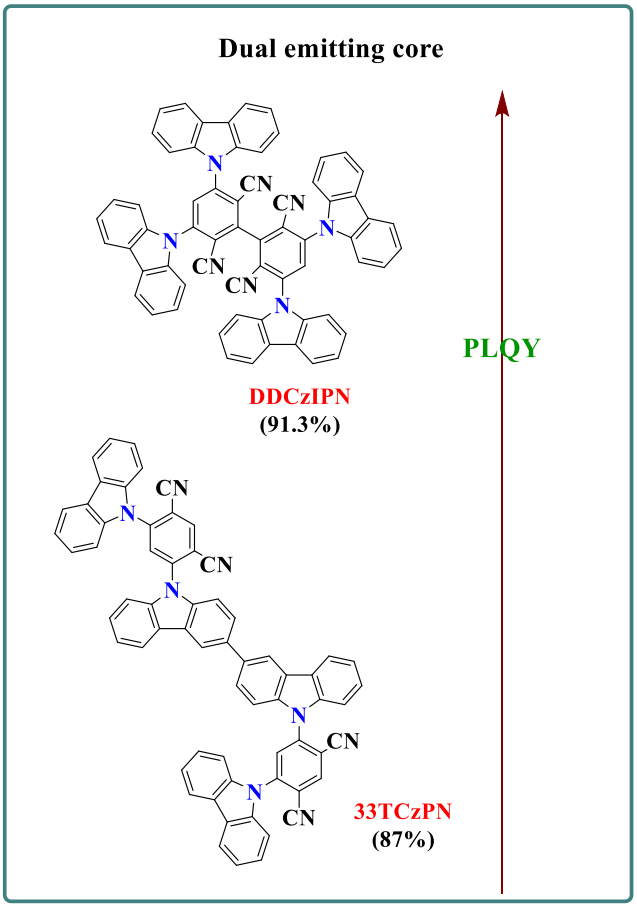

Figure 1.12 TADF emitter chemical structures with high PLQY with regard to dual emitting core design. Compounds such as DDCzIPN exhibited higher PLQY than 33TCzPN, this is due to the direct coupling of two TADF emitter's cores compared to 33TCzPN which has two TADF emitters connected via donors.

1.3.3.4 Molecular Design for Improving Stability

OLED devices with a limited lifespan are not suitable for practical application. Specifically, the lifespan of blue OLEDs is roughly 10-40 times less than that of red and green OLEDs, which is currently unsuitable for use in commercial applications. The limited lifespan of blue devices is mostly related to emitters' vulnerability.[92-96] Hence, the lifespan of OLED devices is crucial for their performance. Therefore, it is imperative for the TADF materials design to guarantee their ability to resist and permit degradation when used in OLED displays. While numerous studies have examined the lifespan of TADF devices, only a limited number of studies have specifically addressed the molecular design criteria for TADF emitters with extended lifespans.[58] From a chemical structural standpoint, the TADF emitters' design only allows for the inclusion of stable units to ensure stable operation. The OLED device operation involves the collection of both positive and negative polarons, together with excitons

by the TADF emitters. This also highlights the importance of maintaining molecular stability under charged circumstances (electron and hole transporting materials' selectivity). Bond dissociation energy (BDE) is a measure of the stability of molecules in the presence of either negative or positive polarons. Donor units which contain acridan derivatives or aromatic amine compounds possess lower BDE values for negative polarons. On the other hand, donor units with carbazole derivatives have higher values of BDE. Acceptor molecules with compounds such as diphenylphosphine oxide or diphenylsulfone exhibit relatively lower values of BDE in comparison with other acceptor molecules including benzonitrile or diphenyltriazine which exhibit elevated values of BDE. In order to address the aforementioned factors, the design of the TADF emitter focused on creating emitters with high stability that consist of donor and acceptor units with high BDE. These units include carbazole derivatives, diphenyltriazine, benzonitrile, and triazine derivatives. Figure 1.13 illustrates some stable materials with respect to their long-term stability.[58, 97-100]

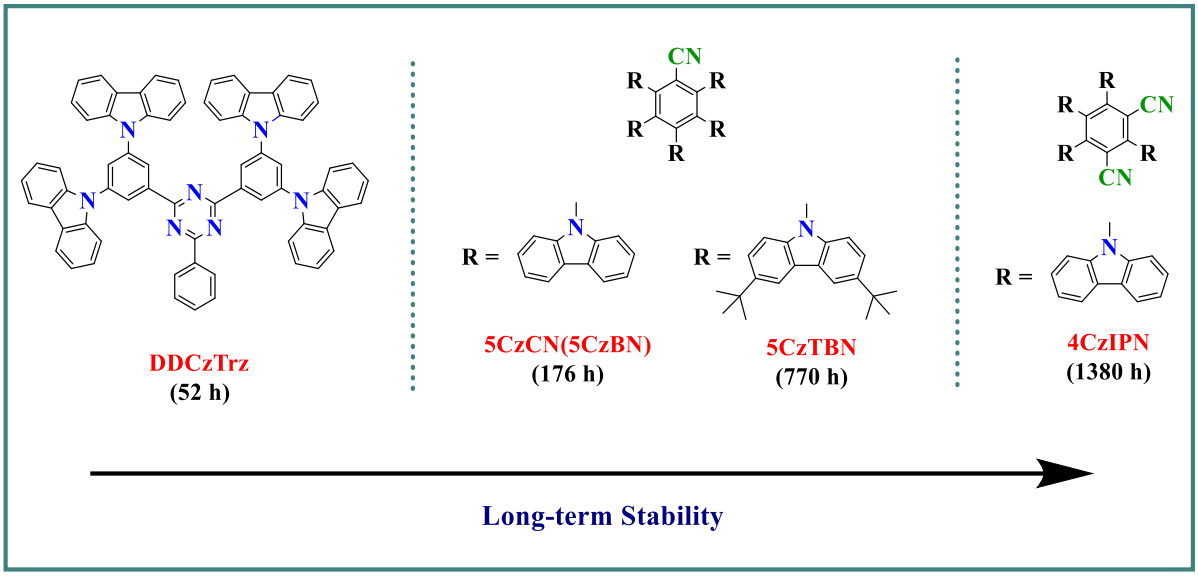

Figure 1.13 The influence of TADF emitters' stability by their chemical structures. DDCzTrz exhibited the shortest long-term stability compared to other compounds, this is due to the use of a weak acceptor attached to the donors (carbazole). With increasing the strength of the acceptor (cyanobanzene) with the same donor, the 5CzCN(5CzTBN) exhibited longer-term stability (176 h). In comparison to 5CzCN(5CzTBN), 5CzTBN showed a higher value in terms of stability (770 h) as the donor strength increased. The last compound 4CzIPN exhibited the highest long-term stability of (1380 h), with increasing the acceptor's strength.

1.3.4 Solution-Processable TADF Material Design Strategy

1.3.4.1 TADF small molecules

Among the several materials for vacuum-processed OLEDs, small TADF molecules (have a molecular weight of 1000 daltons or less) have received the greatest amount of attention and production. Soluble TADF small molecules can be used as emitters in EL devices based on solution processing, which is a totally reasonable and apparent attempt considering the reasons given above. The development of small molecules of TADF based on solution processing also requires considering numerous other factors besides the TADF property, which is essential for triplet harvesting to attain IQE of 100%. To enable solution process manufacturing, the material must initially possess sufficient solution processing ability in the commonly organic solvent. An additional important factor applies to guaranteeing that the devices are capable of utilising a solution-processed film, that exhibits adequate morphological consistency and stability across varying temperatures and when subjected to a current of electricity. Furthermore, for the device to operate at peak efficiency, high PLQYs should be achieved in the thin film, which is made of small molecules. Additionally, to simplify device configuration, it is highly advised that the TADF materials can transport and inject charges in a balanced manner. So far, only a limited number of classes of TADF small molecules that accomplish effective solution processing have met these requirements.[101] Small molecules such as 4CzIPN (see figure 1.13) is a commonly utilised as a green TADF emitter due to its high PLQYs and unique TADF properties. It is extensively employed in vacuum-deposited OLEDs.[7] Adachi and his colleagues achieved a significant improvement in the stability and efficiency of solution-processed OLEDs by utilising a high molecular weight carbazole-based host material with a high Tg. The OLEDs, based on 4CzIPN, demonstrated an impressive EQE of 12% and exhibited enhanced stability even at high brightness levels.[102]

1.3.4.2 Dendrimers as TADF materials.

Generally speaking, dendrimers have a configuration that consists of a core, determining the essential properties together with a shell that has manifold branches comprising the functional tuning units.[103-106] The given configuration empowers the dendrimers, both the polymers and the small molecules. More precisely, dendrimers characteristically demonstrate polymer behavior; they are very stable, and they can be processed in solution, being morphologically

steady. Moreover, condensed dendrimers have high PLQYs due to the fact that they are not cumulative; they have unreserved dendritic structures. In the meantime, the most favorable reproducibility can be realised with dendrimers that display the steady chemical configuration property which can be modified through chemical decoration.

Extensive research has been carried out on several dendrimers that are potential emitters of OLEDs. Creating TADF dendrimers typically entails integrating exterior branches with a core that represents a standard TADF chromophore which dictates the emission properties: (TADF character, colour PLQYs). The former comprises HOMO distributions spatially dispersed on the electron donor unit whereas the LUMO distributions are divided on the electron acceptor unit. The exterior branches behave as charge transporters; besides, they make the structure soluble and easily processed: they can also improve the nature of the TADF core. There are two main types of TADF dendrimers that differ with respect to the manner of the dendron-core connection: TADF dendrimers that contain both conjugated and non-conjugated linkages, as illustrated in figure 1.14

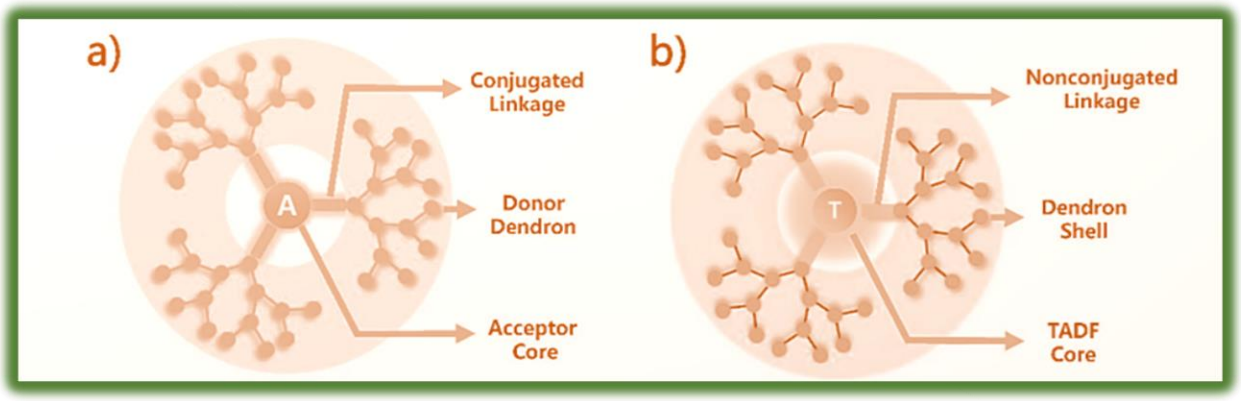

Figure 1.14 Configurational structure of TADF dendrimers with (a) conjugated linkages; In this type of TADF dendrimer, the acceptor (acting as a core) is connected to the donors (acting as dendrons) through the conjugated linkers. (b) nonconjugated linkages; In this type of TADF dendrimer, the core is connected to the donors through non-conjugated linkers such as aliphatic chains.

1.3.4.2.1 TADF Dendrimers Featuring Conjugated Linkages

TADF dendrimers featuring conjugated linkages are distinguished by their electron-acceptor units being positioned at the core, while the dendrons that acted as electron-donor units are connected to the core *via* conjugated linkages. As a result of the widespread availability and low cost of the carbazole (Cbz), which also enhances chemical functionality, this particular dendrimer category is frequently synthesised using Cbz dendrons.[107] Dendrons based on Cbz

derivatives, comparable to capsular structures, possess the ability to hinder molecular interactions and decrease concentration quenching due to their extensive branching and twisted structure.[108-110] Furthermore, due to their high triplet energy levels (ranging between 2.8 eV – 3 eV), Cbz dendrons with 3- and 6-substitutions can function as host substances for the emissive core.[111, 112] Thus, the ability to create EL devices in the absence of hosts is enabled. The formation of dendrons can be regulated by adjusting the HOMO distribution (distributing the donor's units through the structure effectively), which enables the attainment of the best TADF character through an efficient overlapping of HOMO and LUMO between the core (electrons acceptor) and the Cbz dendrons. Expressed differently, Cbz dendrons exhibit a possibly gradient HOMO level with the peripheral regions forming a significant number of electrons.[79, 113] Figure 1.15 depicts an example of a TADF dendrimer including Cbz dendrons and acceptor core with respect to its configuration.

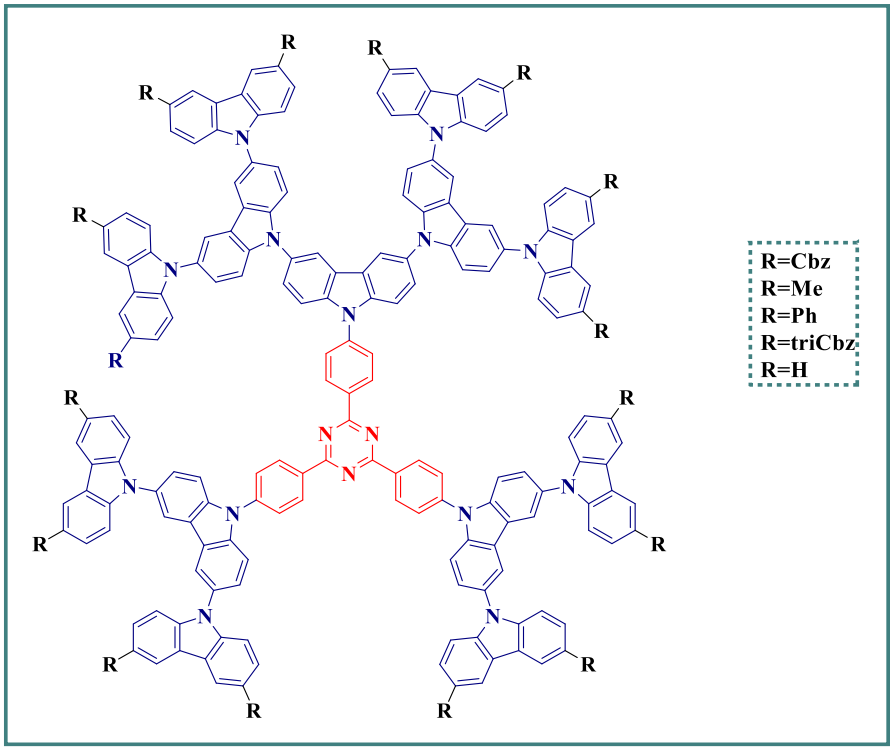

Figure 1.15 The molecular configurations of TADF dendrimer with conjugated linkages. The acceptor (Triphenyltriazine) acted as a core is connected to the carbazole dendrons (donors) via the conjugated linkages, the selectivity of R groups in both positions 3 and 6 of the carbazoles play crucial roles in terms of donor strength.

1.3.4.2.2 TADF Dendrimers Featuring Non-Conjugated Linkages

While TADF dendrimers with conjugated linkages and those with non-conjugated linkages share the same core-shell configuration, they are distinguished by the presence of aliphatic

chains that support the core-dendron connection *via* non-conjugated linkages. TADF dendrimers featuring non-conjugated linkages possess more solubility in common organic solvents, own more stability in terms of morphology and their dendritic configuration effectively impedes intermolecular interactions among molecules. Additionally, because of the core-shell non-conjugated linkages, peripheral units do not exert any influence on the TADF architecture.[114-117] To clarify, TADF dendrimers featuring unconjugated linkages have a TADF structure determined by the core, whereas the function of aliphatic chains (connected to the core-shell) is to isolate the linkages. Thus, additional functionalities (such as charge transport and host ability) can be performed by the external dendrons, while the TADF nature of the core is effectively preserved. Figure 1.16 illustrates an example of a TADF dendrimer with non-conjugated Linkages including core and shells.

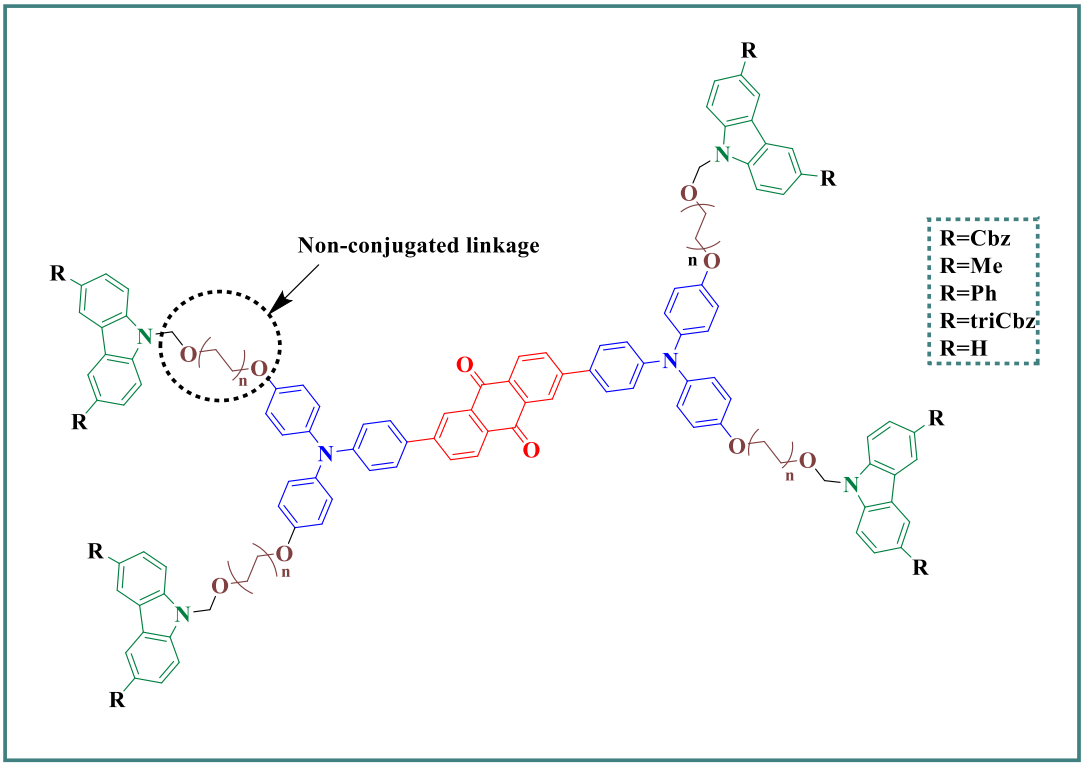

Figure 1.16 The molecular configurations of TADF dendrimer with non-conjugated linkages. Introducing the non-conjugated linker in the TADF dendrimer is beneficial as it increases the dendrimer solubility and prevents the internal interactions between the molecules. In addition, it isolates the properties of terminal dendrons (e.g. charge transport property and host mobility) and keeps the core's properties maintained such as controlling the zone's position where the combination takes place and create charge transfer units.

1.3.4.3 TADF Polymers

Dendrimer and polymer-based TADF devices have garnered significant attention due to their straightforward solution-processed fabrication and optimised performance.[118] A demonstration

of the concept of OLED with improved solubility is described by Cho and his colleagues in their work on the generation of solution-processed high-efficiency OLEDs based on adapted TADF small molecules.[98] In the framework of TADF emitter development, small or dendritic molecules have been the subject of extensive research due to their simple synthesis and reproducibility, as well as the widely recognised technology for device fabrication. However, the utilisation of polymers in sectors such as manufacturing can yield substantial advantages due to their exceptional morphological stability and ability to be processed in solution, thereby enabling the generation of affordable and readily adaptable devices that utilise solution processing.[82, 119, 120] There are numerous molecular design strategies that can be utilised to generate TADF polymers, capitalising on the fact that polymers enable the simple introduction of a vast array of functional units (see figure 1.17). Amongst these strategies, main-chain TADF polymers and side-chain TADF polymers are considered as the fundamental categories of TADF polymers. Main-chain TADF polymers have a structure where donors and acceptors are arranged alternately along the polymer backbone or where acceptors are attached to donors through conjugated linkages. on the other hand, the synthesis of side-chain TADF polymers involves the grafting of TADF molecules into the backbone of the polymer *via* non-conjugated linkages.

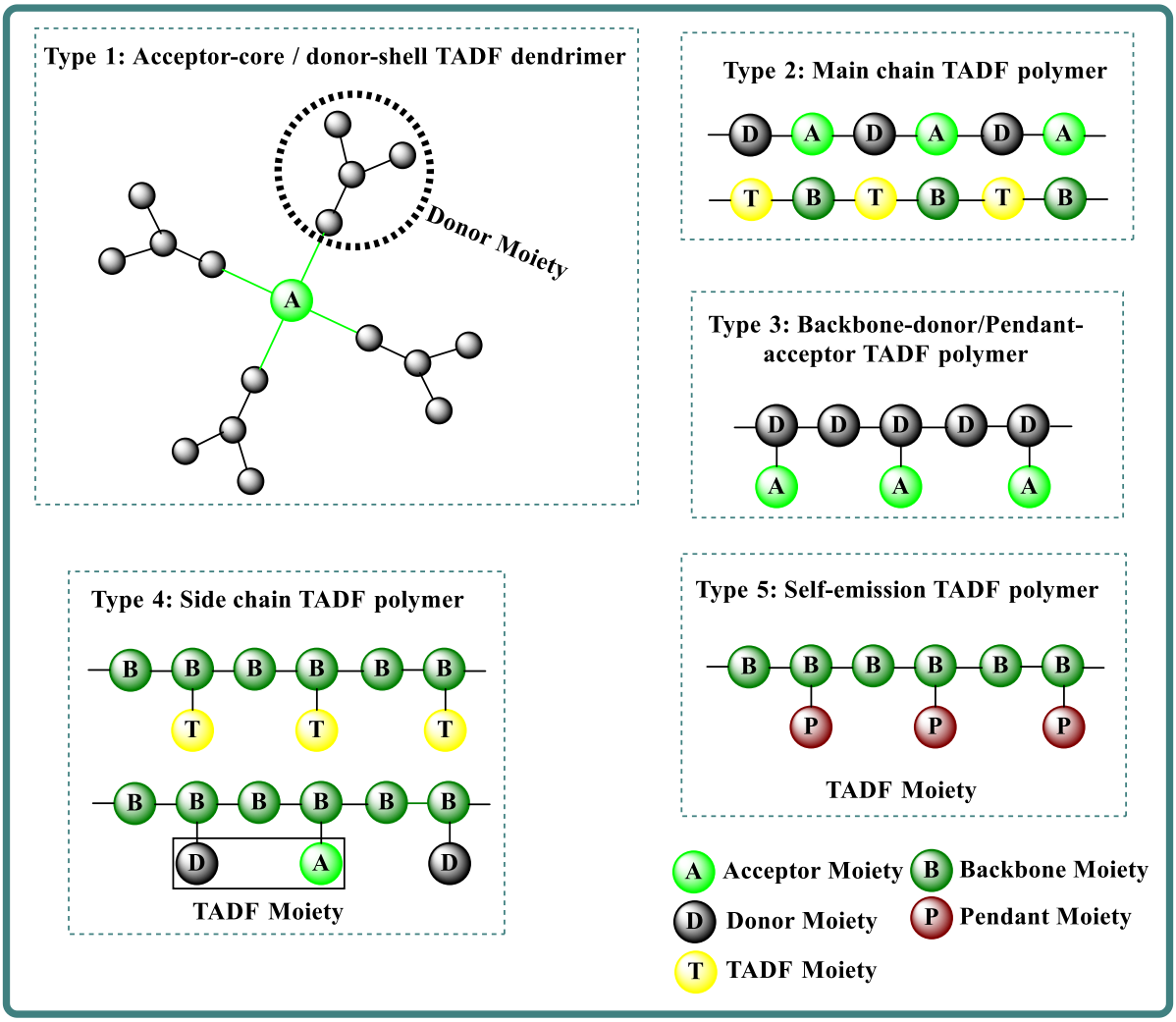

Figure 1.17 Design strategies for TADF polymer.[52] Category 1: A TADF dendrimer where the central core serves as the acceptor and the dendrons on the periphery act as the donor. Category 2: TADF polymer with a fully alternating arrangement of donor and acceptor connections (the top); TADF units separated by backbone spacer units (bottom). Category 3: Donors are selected to be the main backbone, while acceptors are attached as a side chain. The letters B, D, P, and A represent the terms backbone, donor, pendant, and acceptor, respectively. Category 4 involves the incorporation of TADF components into the backbone structure as pendant groups (the top), where the donor and acceptor moieties are molecularly separated yet spatially adjacent to each other (bottom). Category 5: The TADF effect is observed in the entire polymer instead of the monomer.

1.3.4.3.1 Main-chain TADF Polymers

TADF polymers with main chains are commonly synthesised and designed with donor and acceptor units in consideration. The TADF potential of these polymers has been demonstrated through their narrow ΔE_{STS} and large recombination zone. These properties can be further enhanced through the regulation of acceptor and donor unit counts. The donor unit within the chain is typically the TADF active part, which is linked to the backbone of the polymer. Active

units and other components of the TADF main chain exhibit significant influence on one another. Inter-monomer TADF is a novel approach introduced by Nikolaenko et al. for producing TADF active units through indirect means from non-conjugated main-chain TADF polymers through the polymerisation of acceptor and donor monomers.[121] Researchers produced the main chain light-emitting polymers through the incorporation of triphenylamine (5%) as an electron donor unit, triphenyltriazine (50%) as an electron acceptor monomer, and a non-conjugated host with a high triplet energy (45%) as a spacer connected to the main chain, as depicted in figure 1.18. The role of triazine is to control the zone's position where the combination takes place and create charge transfer units. Meanwhile, the spacer is responsible for distributing all of the emitters within the light-emitting polymer.[121] By means of solution processing, non-doped OLEDs were manufactured with TADF polymers serving as the emissive layer. These OLEDs displayed a narrow value of ΔE_{ST} (less than 0.23 eV) and an adequate PLQY value. Polymers with acceptor units that linked alternately within their backbone are known as conjugated main-chain TADF polymers. This design strategy can lead to substantial overlap between acceptors and donors, which in turn leads these conjugated polymers to lose their TADF features, making it very challenging and difficult to produce alternating D-A with TADF capabilities.

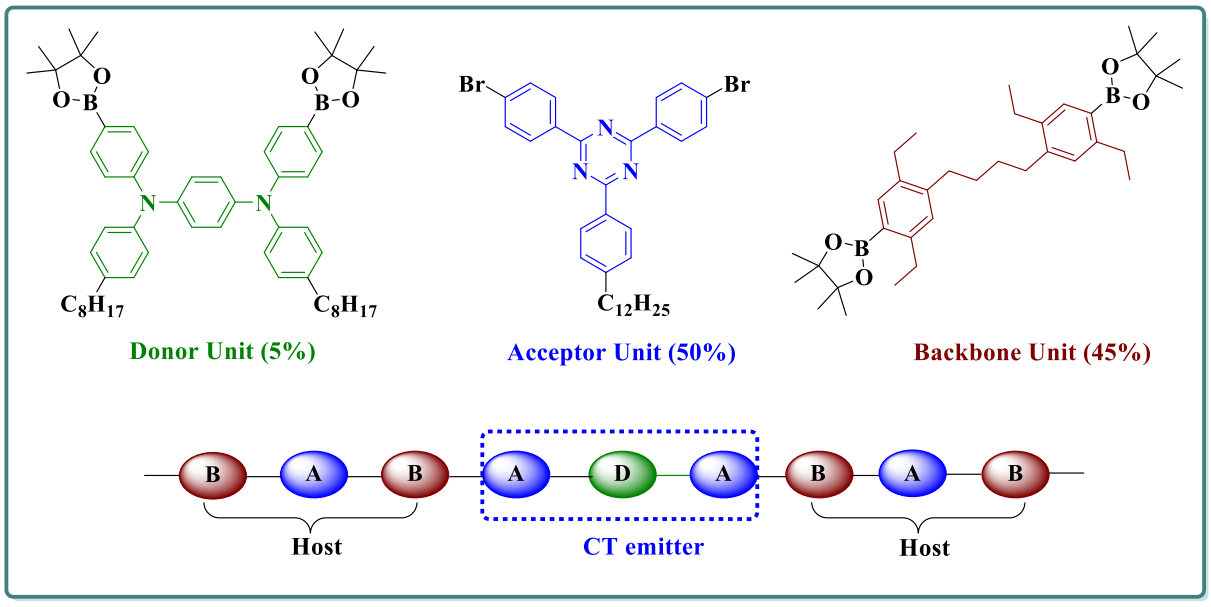

Figure 1.18 ' Inter-monomer' structure of TADF polymers' main chain.[121] In this strategy, the TADF polymer structure is composed of different ratios of donor (5%), acceptor (50%), and backbone unit (45%). All components are attached alternately within the main polymer backbone. The host comprised of acceptor and backbone units while the CT emitter consisted of acceptor and donor units (alternately arranged).

1.3.4.3.2 Side-Chain TADF polymers

The strategy of side-chain engineering is the most effective approach employed for TADF polymers.[122] The composition of these polymers mostly comprises side chains that are functionalised with TADF molecules, which are attached to the backbone of the polymer. The TADF characteristics, injection of charge features, and transport of charge properties are all determined by the constituents of these polymers, whether they are part of the backbone or side chains. In side-chain polymers, the key difference lies in the fact that the chains connecting the side chain and backbone are non-conjugated, contrasted with main-chain polymers. Hence, the side chain does not influence the electronic characteristics of the backbone. In contrast to the main chain type TADF, the synthesis of sizable conjugated structures of this sort is relatively unchallenged, and they provide significant processing advantages for the devices. The insertion of the TADF-linked molecule into the backbone of the polymer is accomplished *via* chemical bonding in TADF polymers that rely upon side chain structures. Effective blue OLEDs have successfully utilised side-chain TADF polymers on account of their polymer backbone stability.[123] It is possible to create TADF polymer emitters by grafting the monomer onto the polymer's side chain. Implementing the TADF approach has been demonstrated to enhance the potential for effectively utilising excitation in polymeric compounds.[101, 124, 125] An innovative engineering approach to creating solution-processed TADF polymers with exceptional efficiency was presented in 2019 by Zhou et al. This approach is based on the idea of creating and synthesising TADF copolymers, which integrate the TADF active unit's character onto a side chain. Furthermore, the structure can reach the balance as the polymer's backbone consists of both conjugated and non-conjugated units of CBz and tetraphenylsilane respectively.[126]

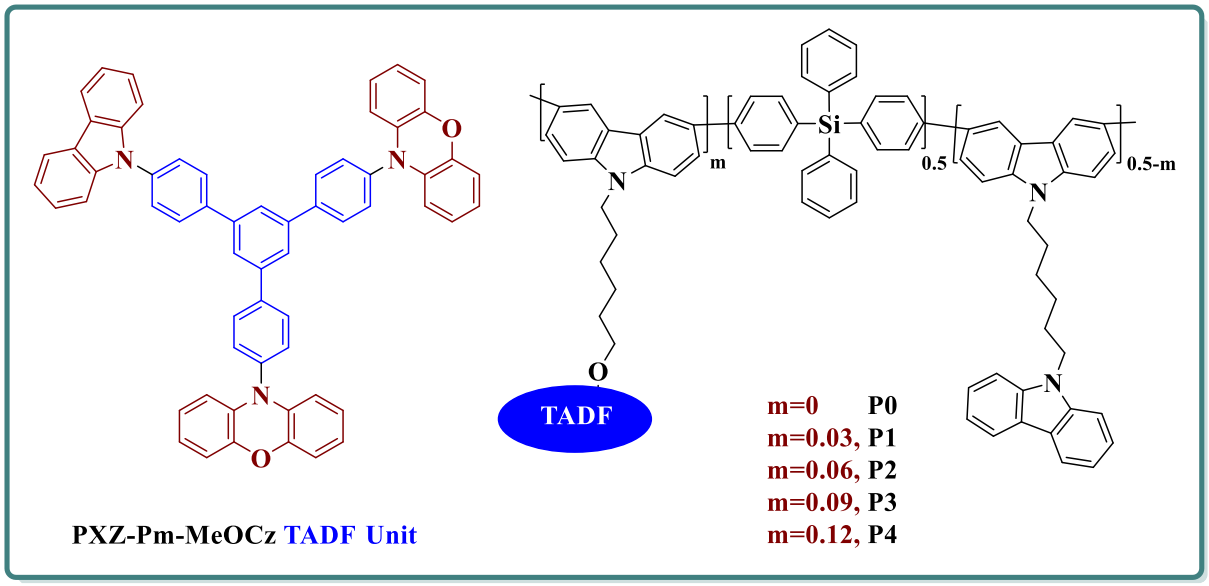

Figure 1.19 Synthesis of TADF copolymer via side chain conjugated backbone.[126] In this strategy, the polymer main chain is composed of both donor and acceptor, while the TADF units are attached to the polymer main chain as a side chin via a non-conjugated linker (aliphatic chain). This strategy is more effective for maintaining the properties of the polymer backbone, and thus cannot be influenced by the TADF functionalities.

1.4 The Required Criteria for Host Materials

A number of issues, including concentration quenching and aggregation, are known to cause TADF emitters to function poorly in the emitter's thin films. Consequently, both the photophysical properties and the efficiency of the devices are enhanced by mixing the TADF emitters with host materials at concentrations up to 30% of the emitter.[127] High triplet-state energy is one of the crucial requirements for the host materials to own. The T_1 state of the host material should ideally possess higher energy than the T_1 state of the TADF emitter to effectively inhibit the occurrence of Dexter energy transfer from the TADF emitter to the host material. This transfer of triplet excited states represents a significant loss channel in OLEDs based on TADF emitters. Additionally, it is important to ensure that the energy level gaps between HOMO and the LUMO of the host and emitter materials are appropriately regulated. If the host and emitter have significantly distinct energy levels, the emitter could experience direct charge trapping or an undesirable exciplex could form. Therefore, to enhance the performance of the emissive layer, it is critical to ensure that the energy levels of the materials (HOMO and LUMO) are precisely aligned so that the required energy and charge carrier transfer can efficiently occur between the TADF emitters and host materials.

In addition to the two critical aspects delineated earlier, TADF requires more characteristics to be possessed by the host materials,[42, 128, 129] such as thermal and morphological stability; these can prevent crystallisation and stabilise the film morphology. Furthermore, host materials should be highly stable materials; this is mainly evaluated by measuring the bond dissociation energies (BDEs) of individual bonds in a molecule under three different conditions: cationic, anionic, and neutral. To further reduce the impact of the emitter's and host's local dipole interactions which cause the emission peak to move towards the bathochromic shift, it is advised to select hosts with low polarity such as *N,N′*-dicarbazolyl-3,5-benzene (*m*CP).[130]

More factors can affect significantly the level of triplet energy T_1,[42, 131-134] such as extending the π-conjugation, which reduces the triplet energy. As the π-conjugation is increased from benzene < biphenyl < *p*-terphenyl respectively, the triplet energy level is decreased. Furthermore, the triplet energy decreases in fused ring systems such as naphthalene compared to biphenyl, which has a higher triplet energy due to its larger conjugated system.

It has been found that strongly twisted molecular structures decrease conjugation, which increases the triplet level; meta-linkage, as compared to para-linkage, results in less conjugation and is better for achieving high triplet levels. Moreover, bulky substituents on π-conjugated host molecules negatively affect intermolecular interactions, causing the energy of the T_1 state to rise and the red-shift of phosphorescence spectra to decrease. Hence, it is possible for the measurement of T_1 in solution to be higher than that in neat films, based on the degree of the interactions.[135]

The availability of stable host materials for blue TADF emitters remains limited, as they necessitate triplet energies over 3.0 eV to provide effective confinement of excitons. Carbazole, thiophene, and benzofuran are frequently employed as versatile building blocks in the development of host and emitter materials specifically designed for deep blue applications. This preference is attributed to their high triplet energies, which range from 2.8 to 3.0 eV.

DPEPO has a strong preference as a host material for blue TADF emitters owing to its notably high triplet energy level of 3.0 eV.[136] DPEPO's instability results in OLED devices being subject to significant efficiency roll-off,[137] which is regrettably prevalent. The figure 1.20 below, illustrates additional examples of conventional hosts categorised according to their prospective charge transport properties.[42, 138, 139]

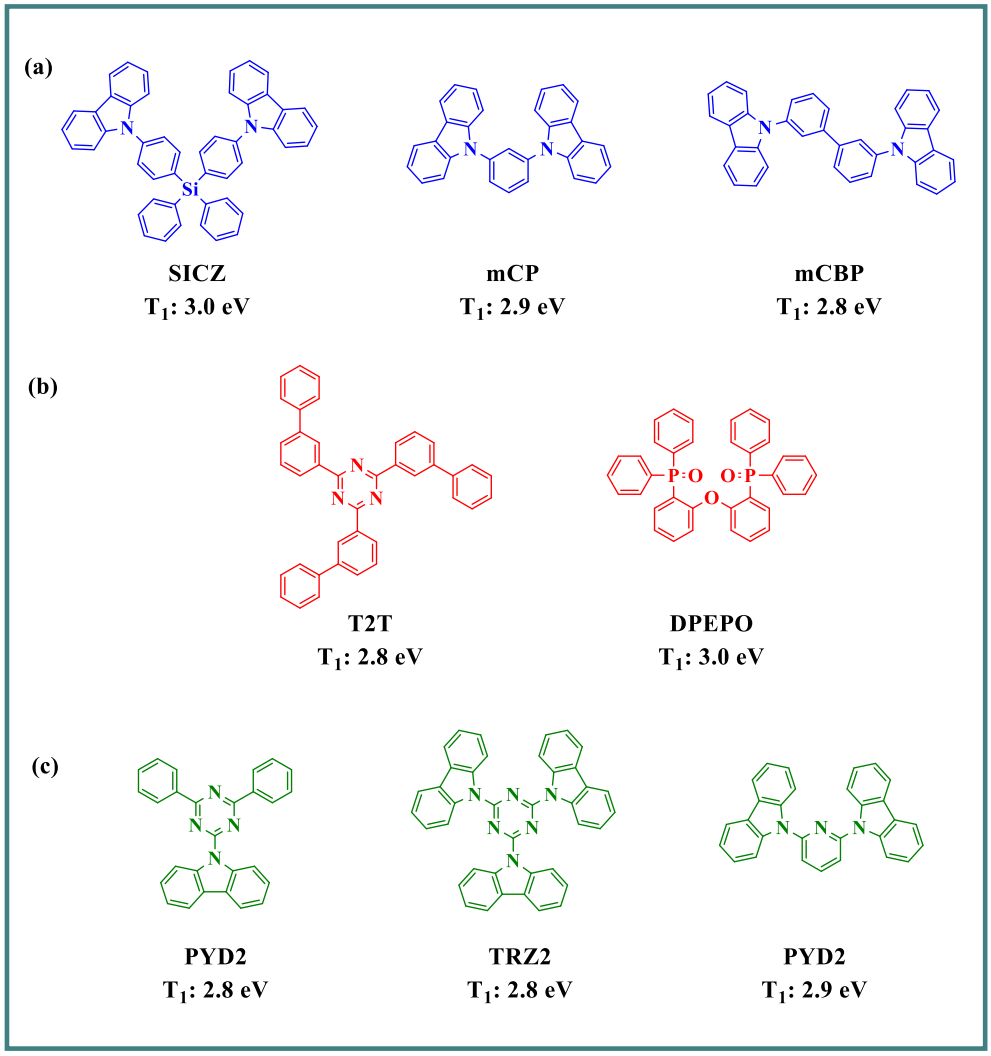

Figure 1.20 Different TADF host materials; (a) Host with hole transport characteristics (p-type), (b) Host with electron transport characteristics (n-type) and (c) Ambipolar host with hole and electron properties (e.g. charge transporting ability, high triplet energy).

.

1.5 The Selection of Carbazole and DPEPO as OLED Host Materials

1.5.1 Carbazole (Cbz)

Cbz is characterised by a rigid fused ring. The ring is heterocyclic featuring the nitrogen component of Cbz. The structure is shown in figure 1.21. Oligomers, dendrimers, and polymers as some form of emitters that use Cbz as host materials in the wide application in optoelectronic devices.[140, 141] Cbz has been identified as a near-perfect hole-transporter in these applications.[142] As an organic material, Cbz has fundamental advantages. These include the fact that the nitrogen atom is easier to functionalise and that the raw material is quite cheap. It

is, therefore, possible to make alterations without modifying the backbone in the Cbz linkage positions. This is important to retain the aromatic properties because they are responsible for the observedstability despite a variety of conditions.[143] Cbz dendrimers[144] have been studied and found to have high hole-transporting performance [145, 146] as host[147-149] and emission materials.[150, 151] The high hole-transporting performance, triplet energy, and thermal stability make up for a robust crosslinking in the backbone of Cbz.[116, 152]

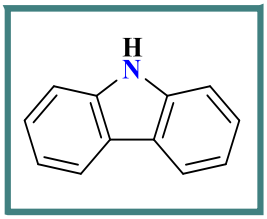

Figure 1.21 Chemical structure of carbazole. Featuring a hole-transporting material with high triplet energy (2.8–3 eV), thermal stability, and commercial affordability.

1.5.2 DPEPO

DPEPO has been extensively utilised as a host material for blue TADF-based OLEDs,[136, 153] owing to its high triplet energy of approximately (3 eV) and its utilisation as an electron transporting layer. The structure of DPEPO possesses two distinct insulating bonds, namely the P=O bond and the -O- bond. These bonds exhibit contrasting electron-absorbing and electron-donating properties, respectively. The introduction of six distinct phenyl groups results in the division of DPEPO, leading to a distortion in its spatial arrangement. Consequently, this distortion contributes to a rise in its T_1 state.[136, 154] The electron-donating effect of the O atom is noteworthy, while the electron- withdrawing effect is exhibited by the P=O moiety. As a result, the electron cloud density of the four phenyl rings exclusively connected to P=O exhibits a significantly lower value in comparison to the two phenyl groups that are attached to the O atom. As a consequence, DPEPO's electron injection capability is enhanced due to the bipolar structure, which further increases the energy difference between the frontier molecular oritals. DPEPO, therefore, addresses the criteria for an effective host material. While DPEPO has demonstrated its efficacy as a preferable host material, it has been observed that the utilisation of ET-type host materials often leads to decreased stability of the device and a drop in efficiency over time.[155-158]

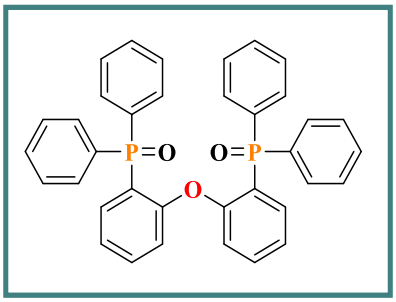

Figure 1.22 Chemical structure of DPEPO. It is commonly used as a host material for blue OLEDs due to its high triplet energy (3 eV), thermal stability, and affordability commercially. Additionally, it functions as an electron-transporting material.

1.6 Hyperbranched Polymers

1.6.1 Brief History

Undesired side reactions and the complications that come about due to multistage synthetic procedures in the preparation of dendrimers are some of the reasons why several studies have been done to produce branched polymers without these complications. The architecture that has come out of these investigations is fragmental and irregular leading to incomplete branch points. In 1952 highly branched polymers were hypothesised by Flory as he suggested a new synthetic class that would make a synthesis of these polymers possible. This new synthesis involved polycondensation of single-A (core molecule) and multiple B functional groups (branching units) in a single monomer. The reaction is between the A function group with at least one B functional group from another monomer (AB_n monomer, $n \geq 2$).[57] It is from Flory's suggested synthetic theory that Kim and Webster synthesised the first functional hyperbranched polymer.[159]

The architecture of repeating units A,B functionalities and the final end groups can identify the final properties and applications of hyperbranched polymers (HBPs).[160] There are several advantages in the preparation of HBPs as they could be made in a one-pot process, they require as short time to synthesise (such as 6 hours for polymerising 3,5-diacetoxybenzoic acid, AB_2 monomer). In addition, they are made with a lower production cost, and have many inherent synthetic advantages. In contrast, the synthetic steps for dendrimers could be done through multi-steps synthesis, involving protection, deprotection and purification procedures. Another advantage is that the HBPs possess some physical and chemical properties of an exceptional level compared to dendrimers. HBPs have large internal spaces within their molecular structure; these increase their ability to encapsulate guest molecules within their cavities, making them

valuable carriers. Furthermore, HBPs have a low viscosity, which is advantageous in terms of processing simplicity and flow characteristics. Moreover, the branching structure of these materials results in rich surfaces with functional groups, allowing for the modification of these groups' functionality.[161] HBPs can also be obtained at a low cost with a high scale of production. Due to the previous unique features of HBPs, these materials have therefore been suggested as competent and realistic alternatives to dendrimers.[162] Three methodologies can be applied to the synthesis of HBPs with the first being the self-condensation of vinyl polymerisation in the AB* monomer. The second methodology entailed polycondensing the AB_x and the A_2+B_3 monomers *via* a step-growth. The third synthetic methodology for HBPs is by polymerising latent AB_x monomers by multi-branch ring-opening.[163, 164]

1.6.2 Hyperbranched Polymers (HBPs) as OLED Materials

HBPs are generally known to have special qualities such as unique molecular shape and branching coupled with a lower intrinsic viscosity. These polymers also have shown higher solubility that comes with their added processability and better stability in the spectrum of luminescence. The HBPs also allow tuneable emission colours in view of their 3D structures.[165, 166] Some of the previous challenges such as aggregation in linear polymer chains are mitigated by the high branching of the globular 3D structures also eliminating other undesirable and significant intermolecular interactions. In some special cases, the thermal stability is also improved besides the emission efficiency.[167, 168] HBPs can prevent crystallisation and improve the efficiency and stability of PLEDs when the HBPs are used to improve the morphologies of the thin films.[169, 170] The convenience in the synthetic accessibility of HBPs typically by one-spot synthesis has attracted considerable interest for industrial-scale production.

1.7 Proposed strategies for preparing the target hyperbranched polymers

1.7.1 The proposed methods for synthesising HBPs using single or multi-functional monomers

Numerous methods have been employed for the synthesis of HBPs, which can be broadly classified into two categories based on the number of monomers utilised: single-monomer and double-monomer approaches. The utilisation of the AB_2 step-growth polycondensation method and the A_2 B_3 methodology in the preparation and design of hyperbranched polymers has been widely employed.[171] These will be explained in the following sections with respect to their structures and properties.

1.7.1.1 Strategy of using a single monomer.

This method employs only one variety of monomer, AB_n ($n \geq 2$), with AB_2 being the most commonly used monomer. The reaction between two A groups from two molecules and two B groups from a single molecule generates one branch within the structure as shown in scheme 1.1 below. Although there is no possibility of gelation (the point at which a polymer becomes solid and unsoluble, signifying the occurrence of cross-linking)[172]with this technique, monomers must typically be prepared in advance.[173-175]

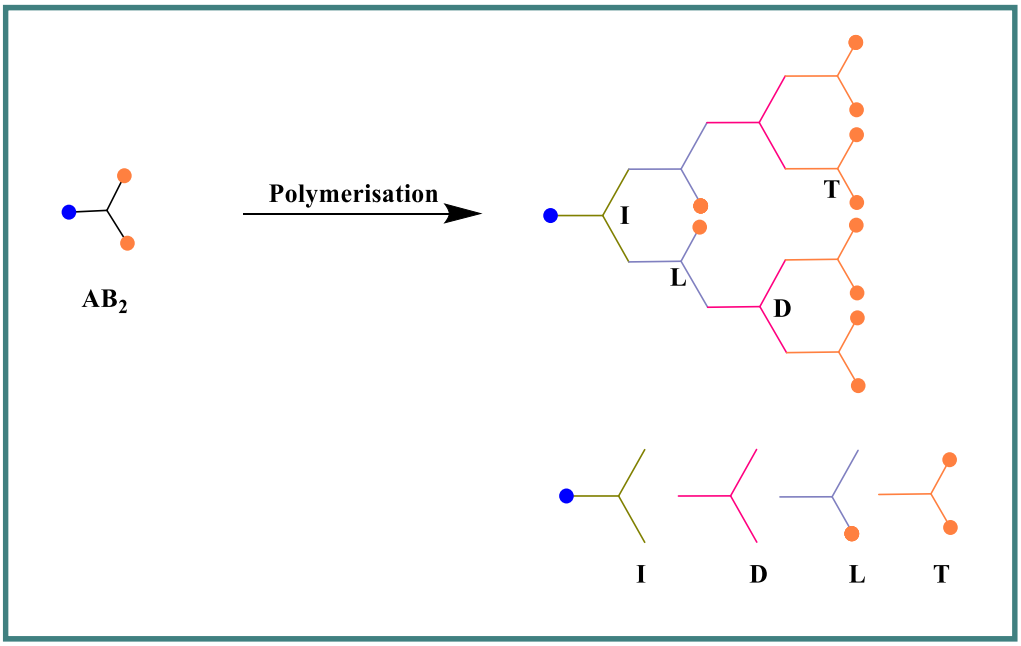

Scheme 1.1 Proposed scheme of AB_2 polycondensation approach. The hyperbranched polymer type AB2 consists of three types of units: dendritic units (D), linear units (L), and terminal units (T). The number of unreacted B groups on the structural units determines these units. The initial units (I) are considered insignificant.[176]

1.7.1.2 Strategy of using two monomers.

The most commonly employed monomers in this approach are "A_2" and "B_3". Two distinct functional groups, designated as A and B, are present in two different molecules, hence facilitating the production and storage of monomers. Furthermore, by adjusting the initial ratio of monomers, the final group ratio can be regulated. Polymerisation should be halted, or capping molecules should be introduced prior to reaching the gelation point, as this is the typical route by which gelation occurs.[172, 177, 178] Solvents such as DMF and selective base are required in this polymerisation.

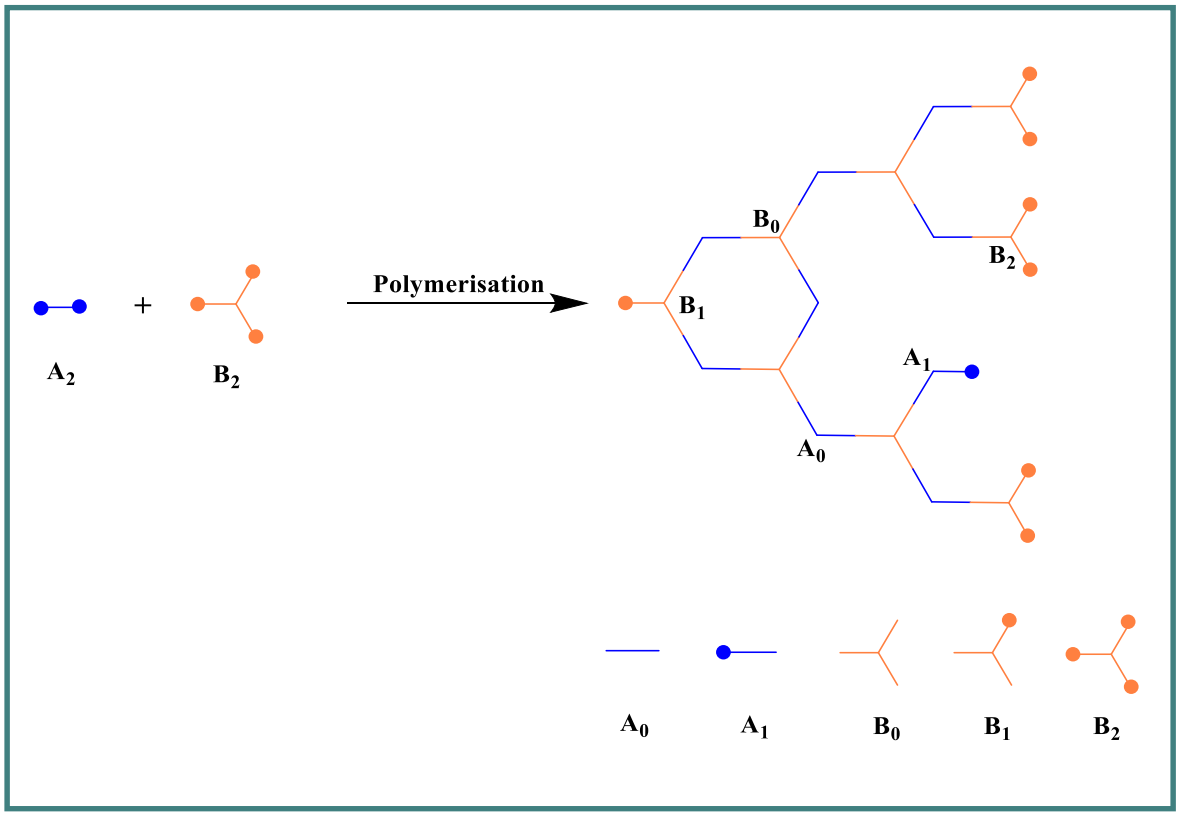

Scheme 1.2 Proposed scheme of A_2 + B_3 polycondensation approach. The structural units of general hyperbranched polymers are classified based on the number of unreacted groups. These units are A_0, A_1, B_0, B_1, and B_2. The A units, A_0 and A_1, and the B units, B_0, B_1, and B_2, are formed from the A_2 and B_3 monomers, respectively.[176]

1.7.2 Suzuki Cross-Coupling in the preparation of HBPs

This particular polymerisation method has attracted significant attention in the context of C-C bond formation. Scheme 1.3 depicts the procedure involving the palladium-catalysed cross-coupling of aryl halides with organoboronic acids or esters. This process is conducted in the presence of a selective base, such as potassium carbonate (K_2CO_3) or sodium hydroxide (NaOH).

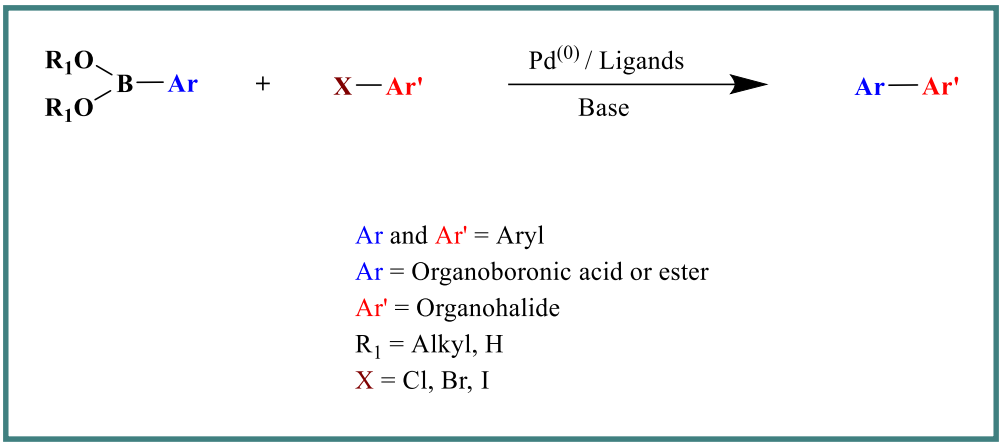

Scheme 1.3 Synthetic conditions of Suzuki cross-coupling reaction. Reagents and conditions; THF, Sat.$NaHCO_3$, $Pd(OAc)_2$, $P(o\text{-}tol)_3$, K_2CO_3, 24 h, Reflux.

To accelerate transmetallation and enhance the polarisation of organic ligands, this method requires the activation of the boron atom. The reaction can be carried out under mild reaction conditions, and the necessary reagents are easily obtainable in the commercial industry. Furthermore, organoboron compounds possess properties such as thermal stability, resistance to water and oxygen reactivity, and the ability to incorporate a wide range of functional groups.[179-181] This method comprises four synthetic stages, as depicted in scheme 1.4. To start the process, an aryl halide [i] is oxidatively added to the palladium (0) catalyst to generate a palladium (II) complex [ii]. The hydroxyl group from the base is then introduced to replace the halide group in the complex, resulting in the formation of an aryl palladium (II) complex [iii]. In the subsequent step, intermediate palladium (II) [iv] is produced by reacting the aryl palladium (II) complex with organoboronic acid or ester. The aryl group of the organoboronic acid or ester becomes more nucleophilic as a result of the activation of the boron atom during the transmetallation process via a base reaction. Therefore, the transmetallation reaction is more facilitated. In the last stage, the intermediate palladium (II) [iv] is reductively eliminated to generate the desired coupling product [v]. The palladium (0) catalyst undergoes the same catalytic cycle with different aryl halides to produce more compounds of interest.[182]

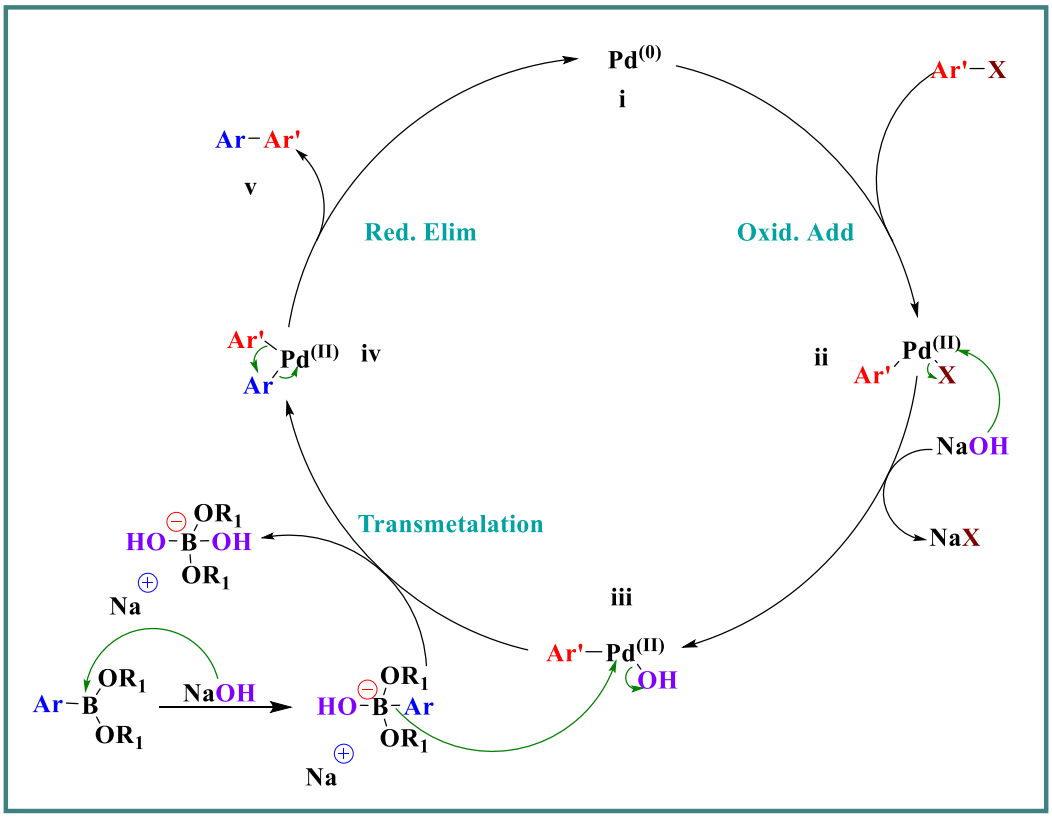

Scheme 1.4 The proposed mechanism of Suzuki cross-coupling reaction. This mechanism allows for the production of the target product through a series of synthetic steps, as follows: (i) Generating the palladium (II) complex through the oxidative addition of aryl halide to the palladium (0) catalyst. (ii) the formation of an aryl palladium (II) complex by replacing the complex's halide group with the base's hydroxyl group. (iii) In the transmetallation step, the aryl palladium (II) complex reacts with organoboronic acid or ester to generate the intermediate palladium (II). (iv) In the last step, the intermediate palladium (II) is reductively eliminated to obtain the desired coupling product (v).

1.8 Project Objectives

The development of lighting technology has led to significant changes in our contemporary lifestyles, and there is a global shift towards the use of environmentally friendly products (e.g. decreased hazardous substances such as mercury and limited greenhouse gas emissions). Manufacturing OLED devices requires the use of less environmentally damaging compounds compared to fluorescent tubes, resulting in the production of highly effective lighting panels. Several providers, including Samsung, Sony, Toshiba, and Philips, have included this technology in their lighting display products. OLED is utilised in a variety of devices, including laptop screens, television displays, and mobile phones. In addition to their sustainability (e.g. long lifetime and easily to be recycled), OLEDs provide more brightness, adaptability, flexibility, high quality performance and less energy consumption as benefits.

OLEDs have the potential to revolutionise the manufacturing of flat-panel screens and portable electronic devices taking into account all of these characteristics. In order to attain displays of superior quality, it is important to thoroughly investigate all available approaches to device manufacture. In addition, it is critical to investigate the potential mechanisms by which the triplet excitons can be harvested and converted into singlet excitons in order to achieve high IQE. Amongst the three generations of OLEDs, the latest generation, which is based on the properties of TADF, makes it possible for the use of triplet states that are produced in OLED devices by means of thermal energy. This is accomplished by converting them into singlet levels through the process of RISC. Therefore, the highest values of IQE can be efficiently achieved.

The aim of this project is to prepare and design solution processable (More suitable for solution processing rather than vacuum deposition) hyperbranched polymers using host materials with high triplet energy such as carbazole and DPEPO to be used in OLED devices. Incorporating efficient hyperbranched polymers into OLED emissive layers is the focus of this work. Hyperbranched polymers which can be used using solution processing technology are required for several reasons, including the ability to develop materials with varying host-guest ratios and increase the affordability of materials and devices in order to support commercial growth. The presence of branches results in spatial occupation and efficient separation of the core chromophores within the TADF, hence limiting concentration bursts. Due to their affordability, hyperbranched polymers have been intensively researched as solution-processable OLED materials.

In chapter 2, AB_2 approach of polycondensation is to be utilised in terms of synthesising the target hyperbranched polymers. This approach requires a single monomer, and the polymerisation can be carried out through one pot preparation with short conversion time. Carbazole as a host material is chosen as a monomer for incorporation in the HBPs, as it possesses high triplet energy, classified as an efficient hole carrier and is affordable commercially. In chapter 3, A_2B_3 polycondensation approach is selected to be applied to prepare the target hyperbranched polymers using double monomers strategy. This approach has been widely applied to synthesis a significant number of hyperbranched polymers, and this is due to the presence of a good number of bi and tri functionalised monomers. The non conjugated aliphatic chains of monomer (B_3) is to be used in the polymerisation to enhance the solubility of the target hyperbranched polymers as well as to restrict electronic conjugation. Suzuki coupling polycondensation is to be applied to synthesise a series of TADF hyperbranched polymers in chapter 4 and chapter 5. Side chain strategy consists of partially conjugated and non-conjugated molecules of polymer's backbone together with TADF moieties as a side chain and is to be utilised to design the required TADF hyperbranched polymers in chapter 4 and chapter 5.

In chapter 4, to enhance the charge transporting mobility of the HBPs, carbazole is to be incorporated as a host material in the polymer's backbone. Grafting the TADF moieties (PXZ-TRZ) into the side chain of the polymer's backbone in the designed polymers provides other functionalities such as improving polymers' emission, without affecting the electronic properties of the polymer's backbone, which works as host and charge transporting carrier. In chapter 5, DPEPO units are to be incorporated in the polymer's backbone to facilitate the electrons transport characteristics and reach the balance along the polymeric backbone in the presence of a non-conjugated branched structure of 1,3,5-tris((6-phenoxyhexyl)oxy)benzene. Moreover, the incorporation of branched structures in the polymer's backbone is beneficial to reduce the conjugation along the polymeric backbone and improve the solubility of the designed polymers.

Chapter 2: Synthesis and Properties of AB_2 Hyperbranched Polymers Based on Carbazole Derivatives for OLED Applications

Abstract

Progress in OLEDs research is still required to improve both the costs of their manufacture and their efficiency. Various synthetic approaches based on the preparation of purely organic molecules are underway. Amongst the applied approaches, HB polymers have gained more attention due to their unique features. The multi-dimensional architecture of HB polymers improves their film morphology, increases their thermal stabilities, and provides them with good solution processability and low viscosity, which should enhance device efficiency. In this chapter, two HB polymers were designed *via* the AB_2 approach based on CBZ derivatives. P1 and P2 were synthesised in the absence and presence of a core, respectively. Both polymers were obtained in low yields and exhibited low molecular weights with polydispersity index (PDI) of 2.6 and 2.1 for P1 and P2 respectively. Additionally, the crude of both polymers exhibited low solubility in common solvents such as THF, DMSO, and 1,2-dichlorobenzene. The thermal degradations were also determined for both polymers, resulting in low thermal stabilities. The optical properties showed that P2 absorbed light at a longer wavelength in a solid state (thin film) compared to P1; this could be due to the effect of the presence of the electro withdrawing nitro group on the core of the HB polymer. Conversely, P1 showed long emission in the thin film around 425.5 nm, attributed to the inter-molecular aggregation in the polymeric chains of P1. The band gaps for P1 were calculated to be 3.48 eV and 3.38 eV for P2. The lower band gap of P2 was associated with the increase of carbazole rings in the polymeric backbone, enhancing the conjugated system and the electronic delocalisation. The electrochemical investigation revealed that P1 showed a shallower HOMO level at -5.05 eV, attributed to the increase of the conjugation system compared to P2 which showed a deeper HOMO level of -5.08 eV.

2.1 Introduction

Organic light-emitting diodes (OLEDs) have garnered significant attention due to their considerable potential for use in full-colour flat-panel displays and solid-state lighting[183]. In contrast to the majority of small molecule organic materials that rely on high-vacuum thermal deposition for device construction, polymers provide the advantage of using a comparatively simple solution technique (using a solution (polymers and solvents) directly on the surface is more controlled than vacuum deposition. In addition, the full amount of solution can be exploited on the surface compared to vacuum deposition, which could lose some of it), for providing electroluminescent films.[82, 184] Solution-processed polymer light-emitting diodes (PLEDs) have gained significant interest within scientific and industrial fields due to their notable attributes, including favourable thermal stability, cost-effective processing, flexibility, and the potential for large-scale mass manufacturing.[185-190]

The most often researched conjugated polymers are those with one-dimensional (1D) linear architectures[191]. When compared to linear polymers, the three-dimensional (3D) architectures of the electroluminescent hyperbranched polymers (HBPs) possess distinct molecular shapes, branching patterns, lower intrinsic viscosity, higher solubility, improved processability, a more stable luminescent spectrum, and the ability to tune emission colours.[166, 167] Furthermore, HBP materials are attractive because their highly branched and globular 3D shape decreases or eliminates significant interactions between molecules and clusters of the polymer chains (once the branching increases, the surface volumes among the branches will also increase; therefore, the possibility of internal cyclisation between molecules rarely occurs), and in certain cases, improves emission efficiency and thermal stability (Increasing the branching leads to a proportional increase in the terminal groups, which are responsible for light tuning, thereby enhancing the light efficiency. In addition, increasing the branching leads to a high molecular weight, which contributes to high thermal stability).[168, 169] The utilisation of HBPs has been shown to enhance the morphological characteristics of thin films and inhibit crystallisation (crystalline structures may exhibit imperfect alignment with the substrate structure. Furthermore, crystalline OLEDs have a high degree of sensitivity to changes in temperature. Moreover, the cost of producing crystalline OLEDs is higher compared to amorphous OLEDs), hence leading to improved stability and efficiency of PLEDs.[140, 170] In addition, the HB polymers have garnered significant attention due to their advantageous synthetic accessibility,

often achieved by a one-pot synthesis method, enabling their large-scale manufacturing industrially.

In 2019, a series of hyperbranched polymers were synthesised by Li et al.[192], using the $A_4 + B_2$ polymerisation approach through a Suzuki-Miyaura coupling reaction as illustrated in scheme 2.1. In this synthesis, di(hexyl)-tetraphenylcyclopentadiene was applied as the A_4 monomer, while 9-phenylcarbazole, tetraphenylethene and fluorene were used as B_2 monomers, providing HB polymers **1**, **2** and **3** respectively. All designed three HB polymers showed a significant enhancement in photoluminescence quantum yield (PLQY) in various states, including solution and thin film solid state. Additionally, they displayed favourable thermal stability properties. Amongst three the designed HB polymers, the HB polymer (**2**) demonstrated the highest electroluminescent (EL) performance when incorporated into OLEDs using 1,3-Bis(N-carbazolyl)benzene (mCP) as the host material, achieving an external quantum efficiency (EQE) of up to 6.36%.

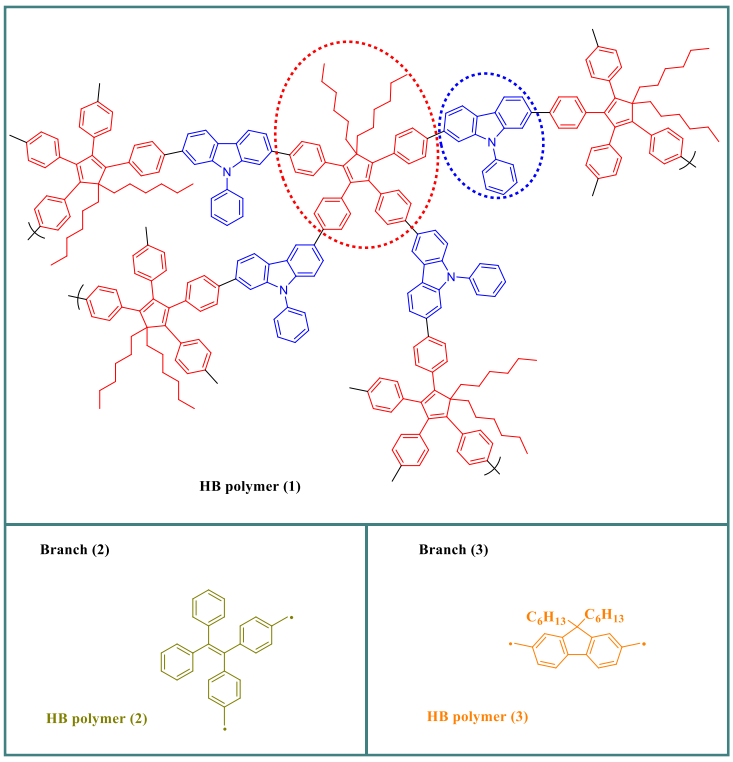

Scheme 2.1 Design of Three HBPs via $A_4 + B_2$ Approach. The host material in HB polymers 1 was 2,7-dimethyl-9-phenyl-9H-carbazole, which connected to the core 4,4'-(2,2-dihexyl-4,5-diphenylcyclopenta-3,5-diene-1,3-diyl)bis(methylbenzene) via a conjugated linker. While HB polymers 2 and 3 used 9,9-dihexyl-2,7-dimethyl-9H-fluorene and 4,4'-(2,2-diphenylethene-1,1-diyl)bis(methylbenzene) as host materials, respectively. Introducing the aliphatic chains in the HB polymers generally assists and increases the solubility.

2.2 Results and Discussions

In this chapter, a sequence of reactions has been applied using carbazole as a raw material to prepare the required polymers P1 and P2. Positions 3- and 6- of carbazole rings have been brominated, obtaining product (1), which was then methoxylated in the same positions to produce product (2). The nitrogen atom from the carbazole has been functionalised with 4-methoxycarbonyl phenyl, allowing product (3) to be formed (see scheme 2.2). Subsequently, product (4) was afforded by hydrolysing the ester group from the methyl benzoate substituent on the carbazole nitrogen atom. The 3,6-dimethoxy substituents of carbazole rings are then hydrolysed to afford product (5), which was acetoxylated in the same positions to afford the product (6) as monomer 1 (M1) as shown in the scheme 2.2 below.

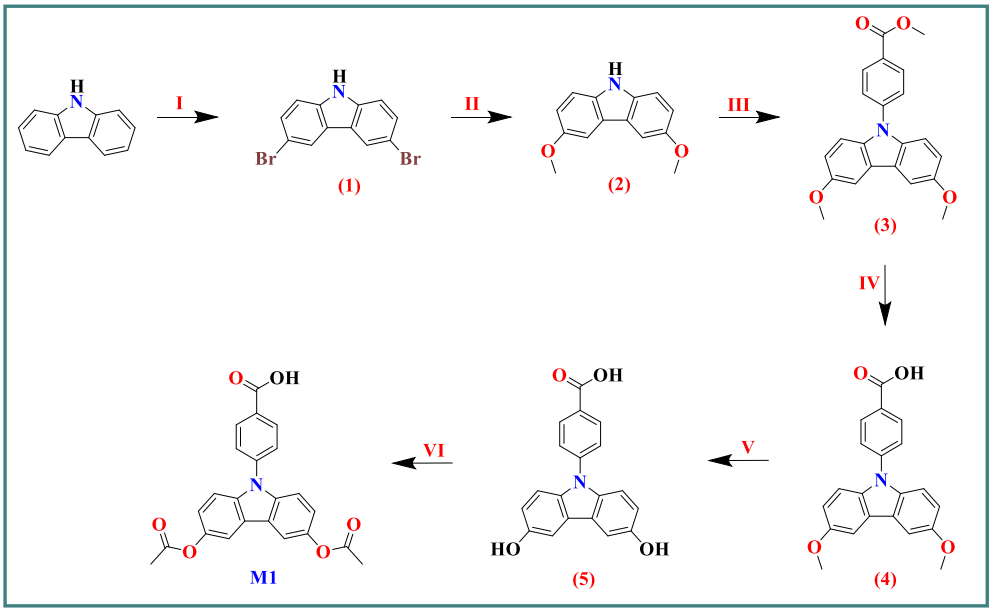

Scheme 2.2 Monomeric steps of synthesis M1. Reagents and conditions; (I) NBS, Toluene, DMF, RT. (II) $NaOCH_3$, CuI, DMF, 120 ^{0}C. (III) Methyl 4-fluorobenzoate, NaH, DMF, 70 ^{0}C, 72 h. (IV) MeOH, NaOH, 70 ^{0}C, 6 h. (V) Pyridinium chloride, 160 ^{0}C, 1 h. (VI) Et_3N, CH_3COCl, THF, RT.

M1 was polymerised *via* AB_2 polycondensation in one single reaction in the absence and the presence of a core to obtain the target P1 and P2 (see scheme 2.3). The final structure of required polymers has been identified initially using ^{1}H NMR to calculate the polymers' protons (by comparing the integration and the intensity of the acetoxy spectrum in both polymers 1 and 2 to the acetoxy spectrum in the monomer 1, it can be seen a dramatic decrease in the intensity and integration of both polymers as the acetoxy consumed through the polymerisation, also in P2 the spectrum of the incaporated core (4-nitrophenyl acetate) was observed and explained in the discussion of polymers section), followed by the GPC analysis

to investigate the molecular weights of both polymers. The thermal, optical and electrochemical properties have been investigated *via* analyses using TGA, UV, PL and cyclic voltammetry respectively.

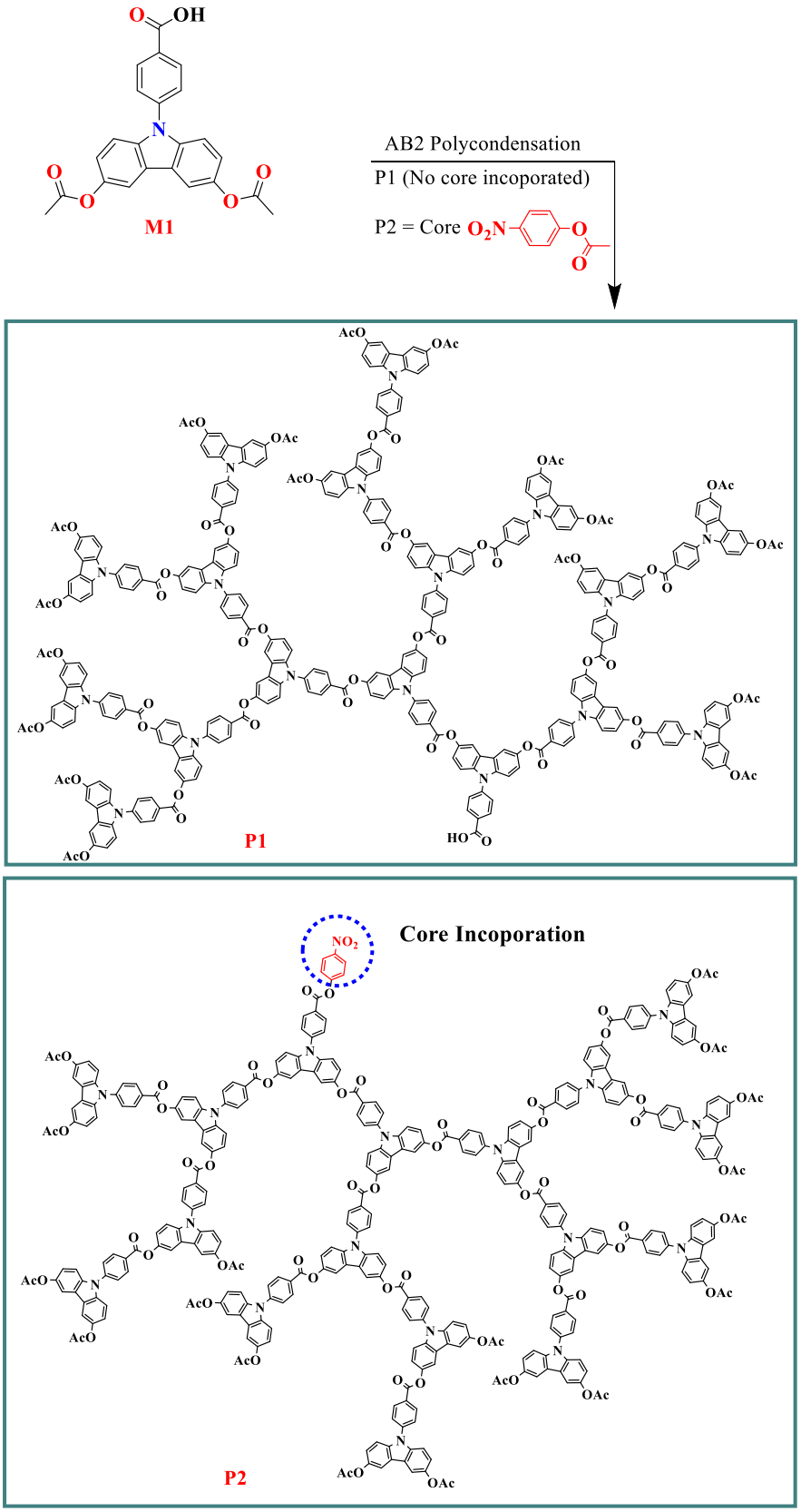

Scheme 2.3 The proposed AB_2 approach to prepare P1 and P2, In polymer 1, M1 was copolymerised in the absence of a core. While polymer 2 was compolymerised in the prescence of 4-nitrophenyl acetate as a core. Diphenyl ether was used as a solvent for both polymerisations.

2.2.1 Synthesis of Monomer M1

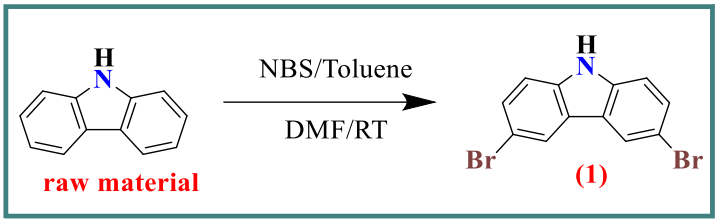

Scheme 2.4 Synthetic conditions of compound (1). Reagents and conditions; (I) NBS, Toluene, DMF, room temperature.

The preparation of monomer M1 involved a number of steps (outlined in scheme 2.2.). It starts with compound (1) which was prepared according to a synthetic route suggested by Ludwiczak et al.[193] NBS was used in this reaction as a brominating agent, DMF was used as a co-solvent with toluene. Light affects the reaction dynamics and causes a free radical reaction from the decomposition of active NBS which causes a loss of selectivity in the brominating substitution position on the carbazole ring. So, the reaction was carried out in the dark environment. An electrophilic aromatic substitution reaction takes place, and the bromide ions on NBS attack the carbazole rings at the 3,6 position and with progress a succinimide anion removes protons from the carbazole ring to produce 3,6-dibromo-carbazole (1) as shown in scheme 2.5.

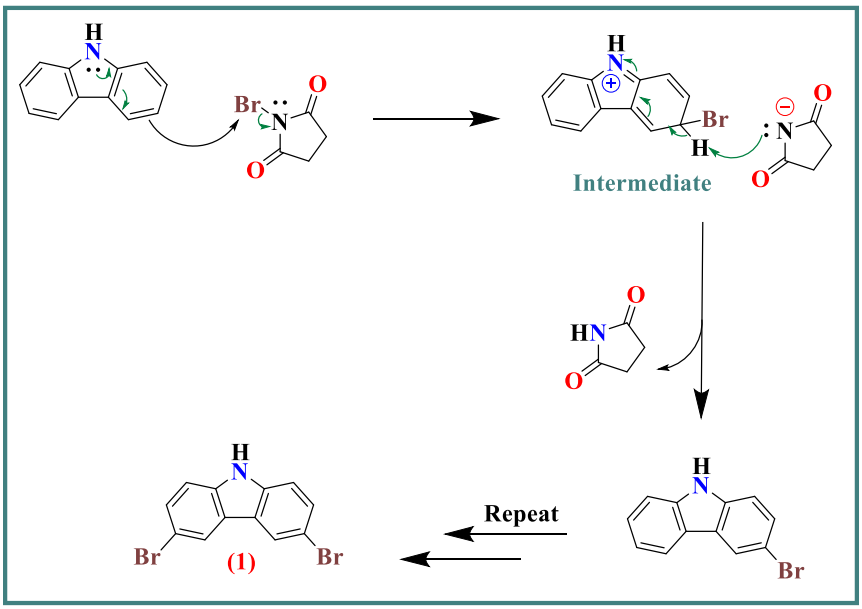

Scheme 2.5 The proposed mechanism for compound (1). Carbazole was used as a starting material which was brominated in both positions 3 and 6 using N-Bromosuccinimide (NBS) as a brominating agent with respect to other reaction conditions to afford the required 3,6-dibromocarbazole.

There were no impurities from the product as can be noted from the analysis and characterisation *via* ^{1}H NMR, ^{13}C NMR, Mass Spectrometry and Elemental Analysis. The characterisation by ^{1}H NMR displayed a broad singlet peak at 11.60 ppm, corresponding to the nitrogen proton of the carbazole ring, at 8.44 ppm, a deshielded singlet was noticed corresponding to the two protons located in positions 4- and 5- of the carbazole rings. Shielded protons in a multiplet was also observed between 7.58 – 7.45 ppm, corresponding to the four carbon protons of the carbazole rings in the positions (1- and 8-) and (2- and 7-), see figure 8.1 in the appendix . The elemental analysis of product (1) was found to be C 44.54, H 2.69, N 4.13, matching the calculated values of C 44.35, H 2.17, N 4.31, Br 49.17, which confirms that product (1) has been successfully prepared.

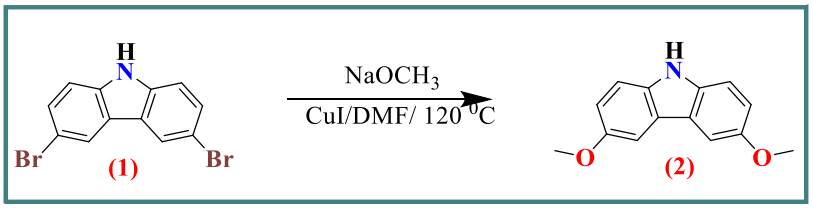

Scheme 2.6 Synthetic conditions of compound (2). Reagents and conditions $NaOCH_3$, CuI, DMF, 120 ^{0}C, overnight.

Synthesis of compound (2) was done following the proposed synthetic procedure reported in the literature[194]. The reaction used copper(I) iodide as a catalyst along with sodium methoxide and goes throughnucleophilic aromatic substitution reaction . In the reaction mechanism, the substitution reaction from the methoxy anion can be enhanced, forming the ether if an electron-withdrawing group can be found on the aromatic ring as illustrated in scheme 2.7. Unactivated aromatic hydrocarbons however require a catalyst. These aromatic hydrocarbons have rings with high electron density. Cuprous halides have been identified as significant catalysts during the methoxylation of non-activated aromatic hydrocarbons. This catalyst is used in the reaction between 3,6-dibromo-carbazole and sodium methoxide with DMF as the solvent. Sodium methoxide is prepared from the MeOH reacting with sodium metal in an inert gas and ice bath conditions. The particular catalyst in this reaction is the monovalent copper ion present in the copper iodide. There is a valence change in the copper salt and oxidization of the monovalent copper ions to a divalent state.

The purity of the product (2) was confirmed by both ^{1}H NMR spectra and mass spectrometry. It was observed a broad singlet at 11.59 ppm, corresponding to the N-H, at 7.53, 7.33 and 7.08 ppm was noticed a singlet, doublet and doublet of doublet referring to the aromatic protons on the carbazole rings. The new substituent methoxy group has been assigned by observing a

highly intense singlet at 3.96 ppm (see figure 8.2 in the appendix). The mass spectrometry also confirmed the success of the product (2) by giving 228.1.

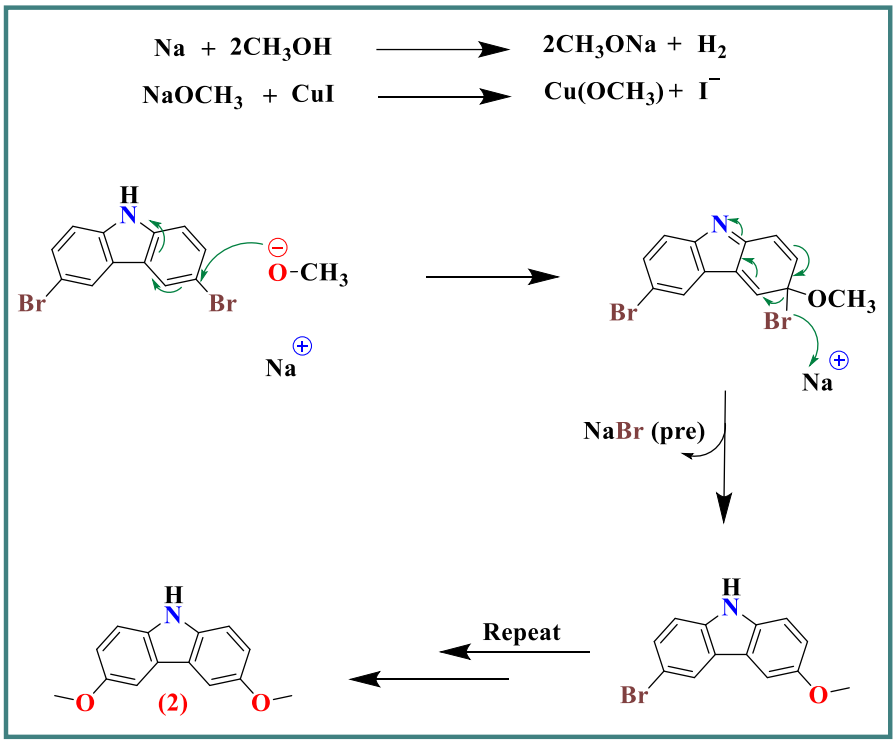

Scheme 2.7 The proposed mechanism for compound (2). The methoxylation of 3,6-dibromocarbazole was carried out via the nucleophilic aromatic substitution reaction to obtain 3,6-dimethoxycarbazole and sodium bromide as a byproduct (precipitate).

Compound (3) was synthesised following the modified preparation suggested by Zhang et al.[195] through the nucleophilic substitution reaction using NaH as a base. The NaH has strong basicity that in multiple structures can drive the reaction by deprotonation. DMF was used as the solvent, methyl 4-fluorobenzoate undergoes an aromatic nucleophilic substitution reaction through replacement of the fluoride substituent with the 3,6-dimethoxy-*9H*-carbazole anion to provide the desired product. The substitution reaction is favoured given the electron withdrawing effect from the methyl ester functional group at the *para*-position of the fluorine substituent.

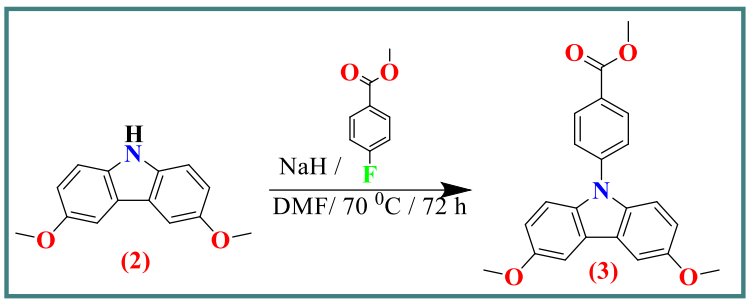

Scheme 2.8 Synthetic conditions of compound (3). Reagents and conditions; Methyl 4-fluorobenzoate, NaH, DMF, 70 ^{0}C, 72 h.

Characterisation *via* ^{1}H NMR confirmed the structure of product (3) by showing two aromatic doublets with different chemical shifts to those observed in compound (2), a more deshielded doublet observed at 8.28 ppm referring to the aromatic protons on the phenyl group of the methyl benzoate substituent. The deshielding occurred due to the ester group. The other shielded protons on the same phenyl ring resulted in a doublet observed at 7.67 ppm. The methyl protons of the ester group give a singlet at 4.01 ppm (see figure 8.3 in the appendix). ^{13}C NMR spectroscopy revealed peaks at 52.31 and 56.10 ppm representing respectively the 3-methoxy groups on the carbazole ring (in positions 3 and 6) and the methyl carbon of the ester group. Peaks corresponding to the different carbons on the carbazole ring are also observed, confirming the structure of the product (3).

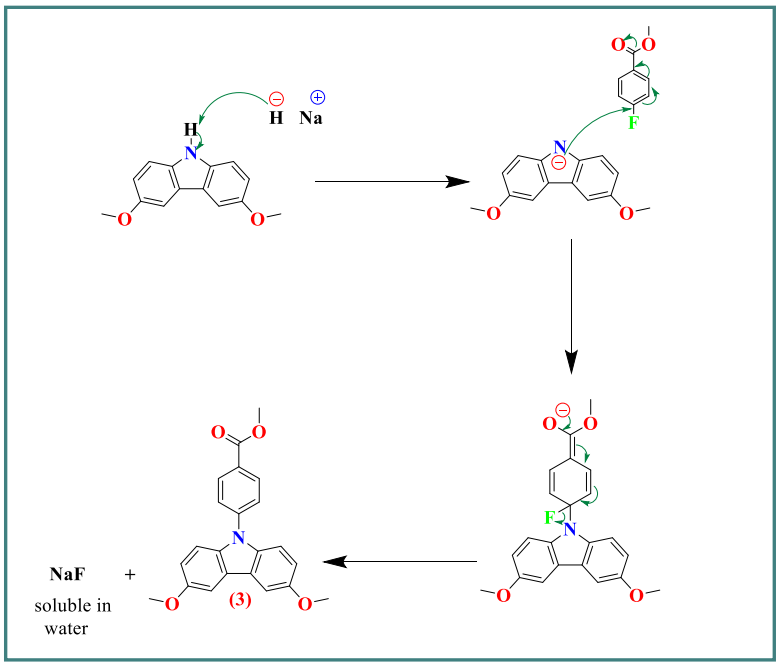

Scheme 2.9 The proposed mechanism for compound (3). The synthesis of methyl 4-(3,6-dimethoxy-9H-carbazole-9-yl)benzoate was achieved via nucleophilic substitution reaction using sodium hydride

as a strong base and DMF as a reaction solvent within 72 hours with respect to other reaction conditions mentioned above.

Compound (4) was synthesized on hydrolysis of the ester group according to literature procedures[196]. The reaction was performed under basic conditions using 1M aqueous sodium hydroxide solution solution in methanol at reflux temperature for 6 hours. The reaction mechanism is through a nucleophilic attack on the acyl substitution in two steps.

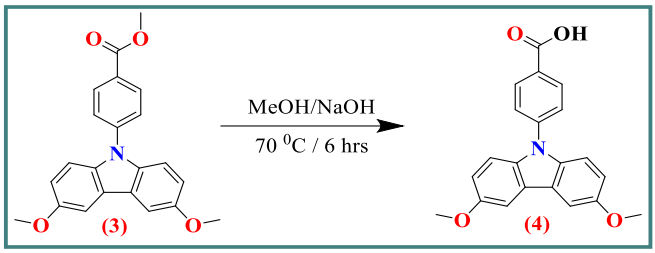

Scheme 2.10 Synthetic conditions of compound (4). Reagents and conditions; MeOH, NaOH, 70 ^{0}C, 6 h.

The first step consists of the nucleophilic addition of the hydroxide anion to the carbonyl group, which resulted in a tetrahedral intermediate as shown in scheme 2.11. This is followed by the elimination of methoxide group to obtain the target carboxylic acid. The ^{1}H NMR spectrum confirmed the synthesis of a product (4) by observing the disappearance of the signal from the ester group (see figure 8.4 in the appendix). The chemical shift of the carbon of the C=O group of the carboxylic acid appeared at 171.2 ppm compared to the C=O in the ester group, which was observed at a chemical shift of 166.31 ppm.

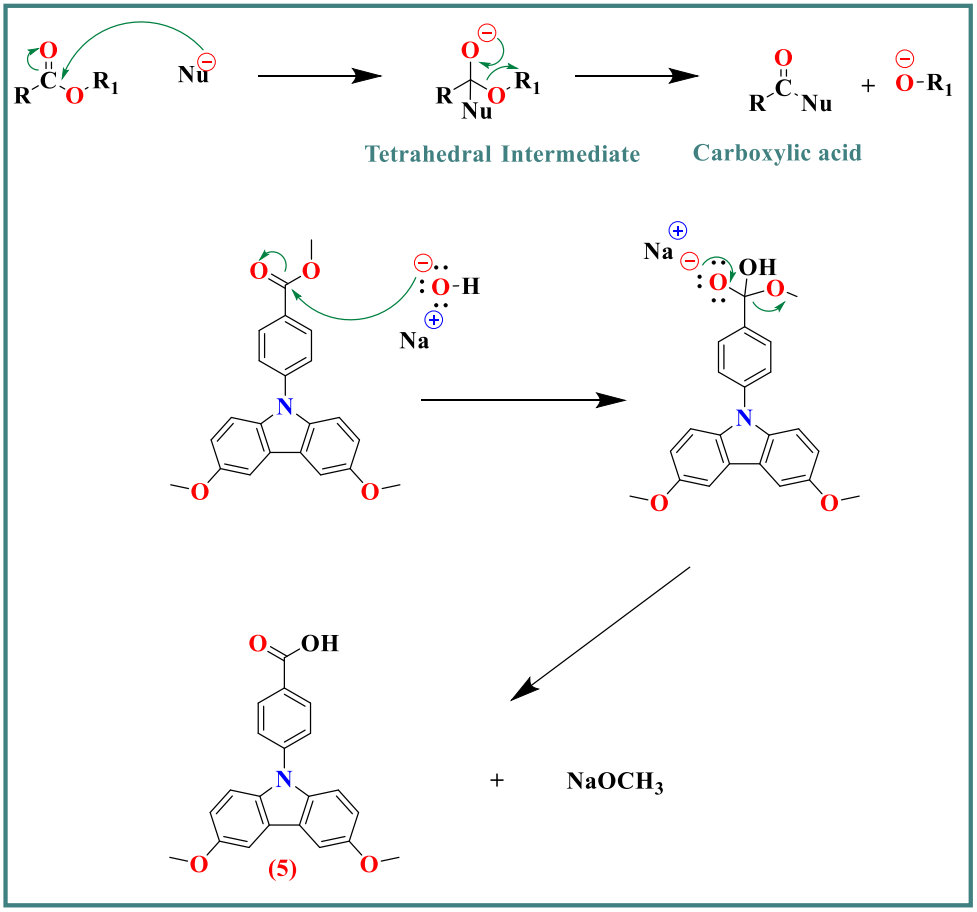

Scheme 2.11 The proposed mechanism for compound (4). The hydrolysis of the ester group in compound (3) was carried out under basic conditions using sodium hydroxide as a base and methanol as a solvent with respect to other reaction conditions mentioned above, affording the 4-(3,6-Dimethoxy-9H-carbazol-9'-yl)benzoic acid (compound 4).

Compound (5) was synthesised following a literature procedure.[197] There are many difficulties with the cleavage of methyl groups of aryl ethers. First it is a challenge to overcome the mild reaction conditions when demethylation is desired. Second, with harsher conditions, as required, there are structural and stereochemical alterations which could lead to the formation of undesired products. This calls for alternative reagents to confer deprotection on the methyl aryl ethers, such as BBr_3, $AlCl_3$, trimethylsilyl iodide, and pyridine hydrochloride, which are examples of Lewis acids. Lewis acids, however, are classic reagents and they are not only expensive but also require the use of chlorinated solvents.

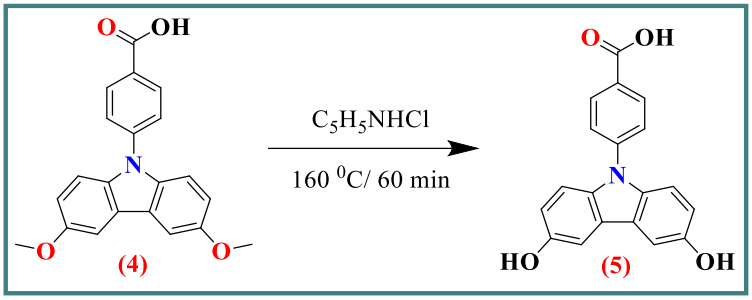

Scheme 2.12 Synthetic conditions of compound (5). Reagents and conditions; Pyridinium chloride, 160 ^{0}C, 1 h.

Pyridine hydrochloride is cheap and does not require the use of a solvent. It is also readily available and hence preferred among the other reagents. To achieve demethylation a timeof one hour and a temperature of 160 ^{0}C for the pyridinium chloride to complete the reaction before being quenched using ice-water, then extracted the mixture using ethyl acetate. Drying of the ethyl acetate solution using sodium sulfate and evaporation of the solvent to afford the product as a white solid without any further purification. Proton transfer takes place from the pyridinium ion when the reaction starts and gets transferred to the oxygen of the aryl methyl ether. The next step features an attack by the chloride ion on the aryl methyloxonium ion, which takes place on the methyl group. The result of the step is the phenolic ring. Finally, the N-methylpyridinium chloride to give, then pyridine takes up the methyl from methyl chloride (see scheme 2.13).

After the analysis and characterization of the data *via* ^{1}H NMR, it was observed that the methoxy peak at 3.96 ppm disappeared. The appearance of a broad peak at 4.6 ppm was noticed, confirming the new substituents of two hydroxy groups on positions 3- and 6- of carbazole rings (see figure 8.5 in the appendix). The elemental analysis by giving the values of C 71.50, H 4.12, N 4.41 and the mass spectrometry by giving the value of 320.1, both analysisconfirmed the structure and purity of product (5).

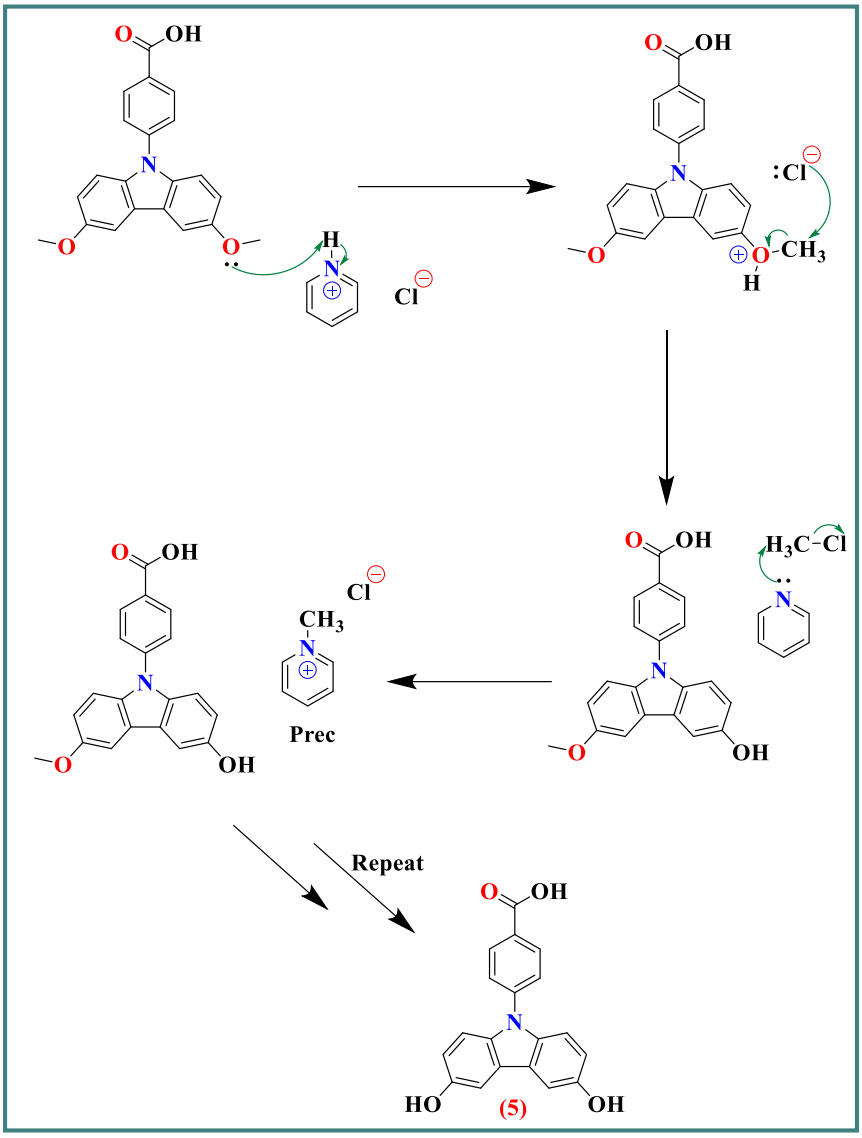

Scheme 2.13 The proposed mechanism for compound (5). The demethylation of the two methoxy groups on the positions 3 and 6 of the carbazole rings was achieved under harsh conditions (160 °C) using pyridinium chloride to obtain the required 4-(3',6'-dihydroxy-9H-carbazol-9'-yl) benzoic acid.

Compound (6) (monomer M1) was prepared according to the reported procedures suggested by Milzarek et al.[198] The acetylation reaction was carried out in the presence of acetyl chloride, THF as a solvent and triethylamine as a base under an inert atmosphere. The first step of the process involves a nucleophilic attack of the hydroxy groups of the carbazole on acetyl chloride to form a tetrahedral intermediate structure followed by deprotonation of the oxygen atom by triethylamine and leaving of the chloride group resulting in the formation of the acetylated product as shown in scheme 2.15.

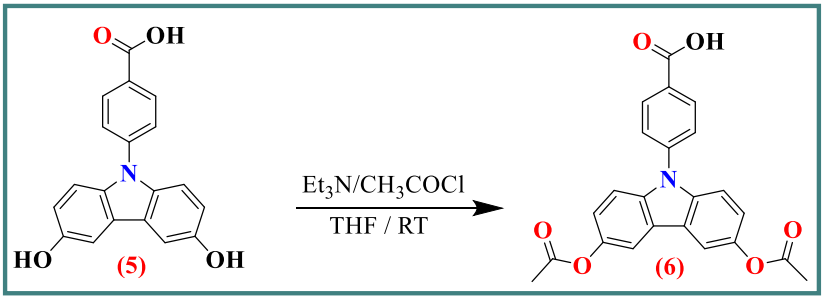

Scheme 2.14 Synthetic conditions of compound (6) M1. Reagents and conditions; Et_3N, CH_3COCl, THF, RT.

Compound (6) M1 was obtained as a yellow oil, which was precipitated from cold petroleum ether to afford brown solids. M1 was obtained as a white solid in a yield of 74 % after purification of the crude product with column chromatography using a petroleum ether: ethyl acetate mixture (3:1).

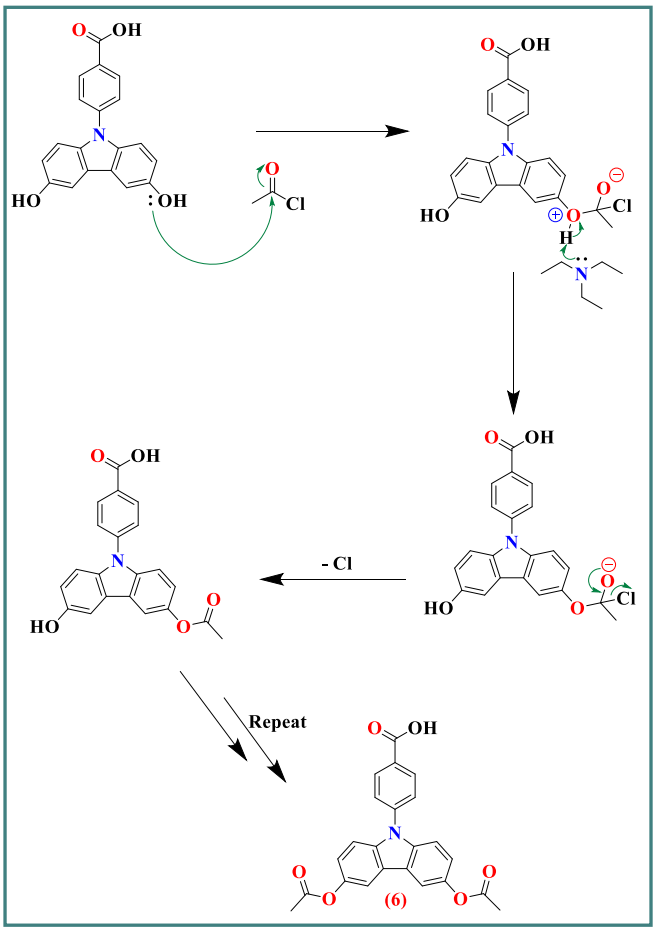

Scheme 2.15 The proposed mechanism for compound (6) M1. The acetylation of compound (5) was carried out via acetyl chloride as an acetylating agent, in the presence of triethylamine as a base to assist the deprotonation and DMF as a solvent at room temperature, affording the first monomer (4-(3,6-Diacetoxy-9H-carbazol-9-yl) benzoic acid).

The structure of product (6) M1 was confirmed using ^{1}H NMR (Figure 2.1). The spectrum displayed an additional singlet peak at 2.33 ppm corresponding to the 6 protons of the acetoxy functional groups. The purity of 4-(3,6-diacetoxy-*9H*-carbazol-9-yl) benzoic acid was also confirmed by mass spectrometry with the latter showing a mass of 404.1 corresponding to the molecular ion.

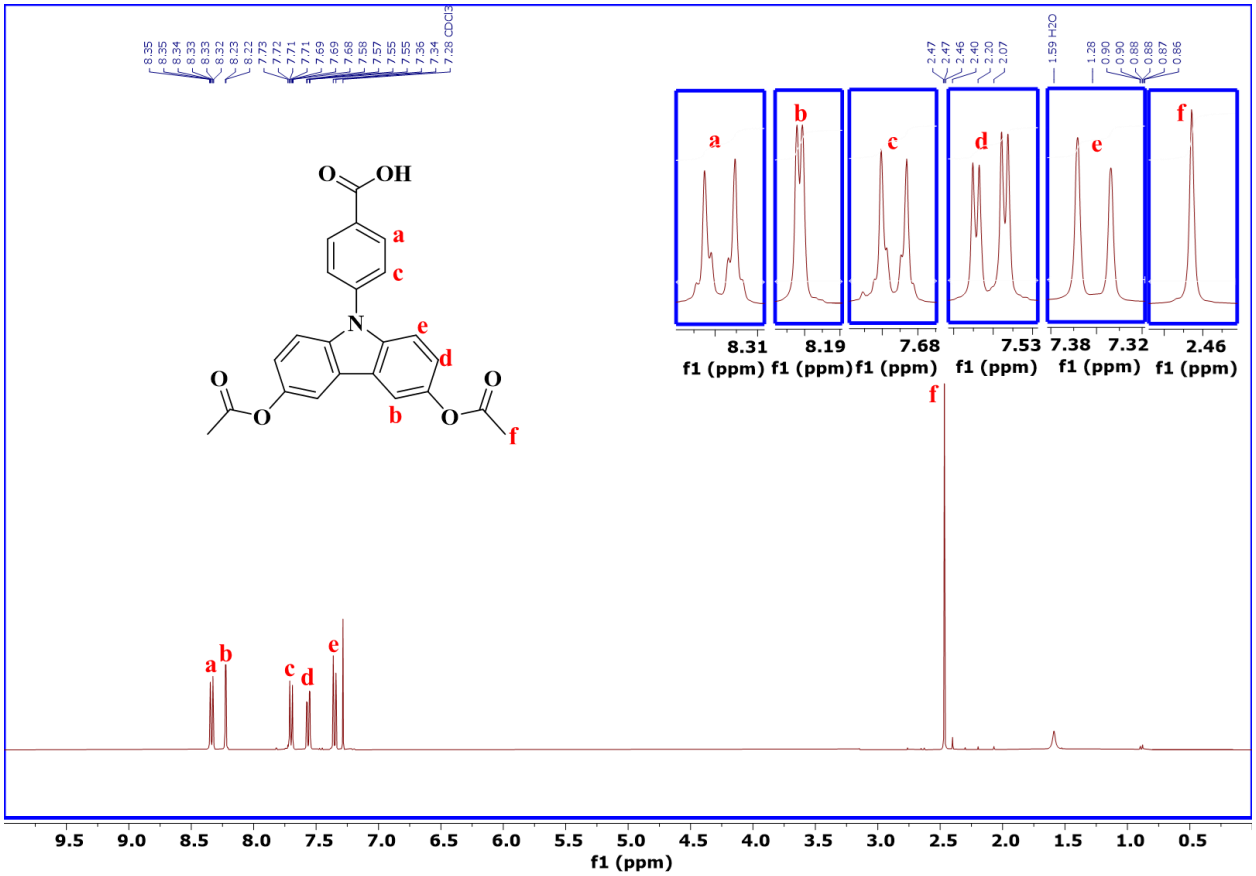

Figure 2.1 ^{1}H NMR Spectrum of monomer (1) M1 in $CDCl_3$. 13.11 (br,s, 1H) 8.34 (d, J = 8.5 Hz, 2H), 8.22 (d, J = 1.9 Hz, 2H), 7.69 (d, J = 8.5 Hz, 2H), 7.55 (dd, J = 8.7, 2.0 Hz, 2H), 7.35 (d, J = 8.7 Hz, 2H), 2.46 (s, 6H).

2.2.2 Synthesis of Polymers P1 and P2

P1 and P2 were synthesised *via* AB_2 approach following the reported procedure in the literature[199]. M1 was polymerised using diphenyl ether as a rection solvent, in the absence and the presence of core (4-nitrophenyl acetate) with the ratio of 1:20 of M1 respectively. The polymerisation was done at high temperature conditions by initially heating up the mixture of monomer M1 in diphenyl ether up to 225 ^{0}C for the first three hours with stirring. Next, the temperature was reduced to 180 ^{0}C and a low vacuum was applied for a further hour to remove any acetic acid by-product produced during the polymerisation. Upon completion, solids were

formed, and the temperature allowed to cool down to 25 ^{0}C. The crude polymer was dissolved partially in hot THF followed by precipitation from cold MeOH to afford the required polymers as white-yellow solids in low yields 25% and 28% respectively. Different solvents were used with different polarities in an attempt to dissolve the crude polymers such as THF, DMSO and 1,2-dichlorobenzene. Unfortunately, none of the solvents selected was able to dissolve the crude polymers completely, even at reflux conditions. This is possibly due to the occurrence of internal cyclisation reactions, which prevents the completion of polymerisations and limits the molar mass of the required polymers to be increased. Besides this phenomenon, undesired side reactions could happen, resulting in cross-linking during the polymerisation. P1 was obtained after polymerising M1 in the absence of a core; in this case, some factors should be considered, such as less control of polymerisation, polymer topology and reaching the focal point early before the completion of polymerisation, which limits the molar mass of the polymer. In comparison, P2 was synthesised in the presence of 4-nitrophenyl acetate as a core, assuming to produce ideal polymer with well-controlled molar mass and better morphology.

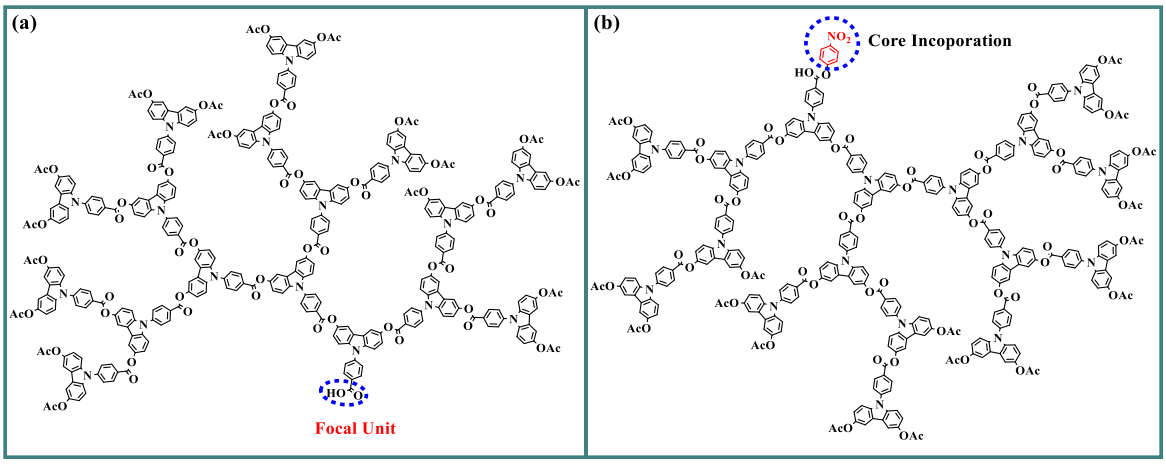

Scheme 2.16 Polymeric scheme for: (a) P1 and (b) P2 (core incorporation). Polymer 1 was obtained via polymerising M1 in the absence of core, while polymer 2 was obtained using the same monomer in the presence of core 4-nitrophenyl acetate. Diphenyl ether was used as a solvent for the polymerisation.

Despite the low yields, the success of polymerisations for both P1 & P2 was confirmed *via* ^{1}H NMR spectroscopy (figure 2.2). The absence of carboxylic proton peaks at 13.11 ppm was noticed. Furthermore, the acetoxy peak was reduced in terms of intensity dramatically in both P1 & P2 compared to the acetoxy peak, which was observed at 2.40 ppm for the methyl group in monomer M1 before the polymerisation took place. As the acetoxy is consumed with every single propagation internally, the size of the polymer increases and the terminal acetoxy groups decrease in intensity. The incorporation of the core units (4-nitrophenyl acetate) in polymer P2

is demonstrated by the appearance of a multiplet observed at 8.39 ppm which is absent from the NMR spectrum of polymer P1, at the same region, confirming the incorporation of core units in polymer P2, (see figure 2.2).

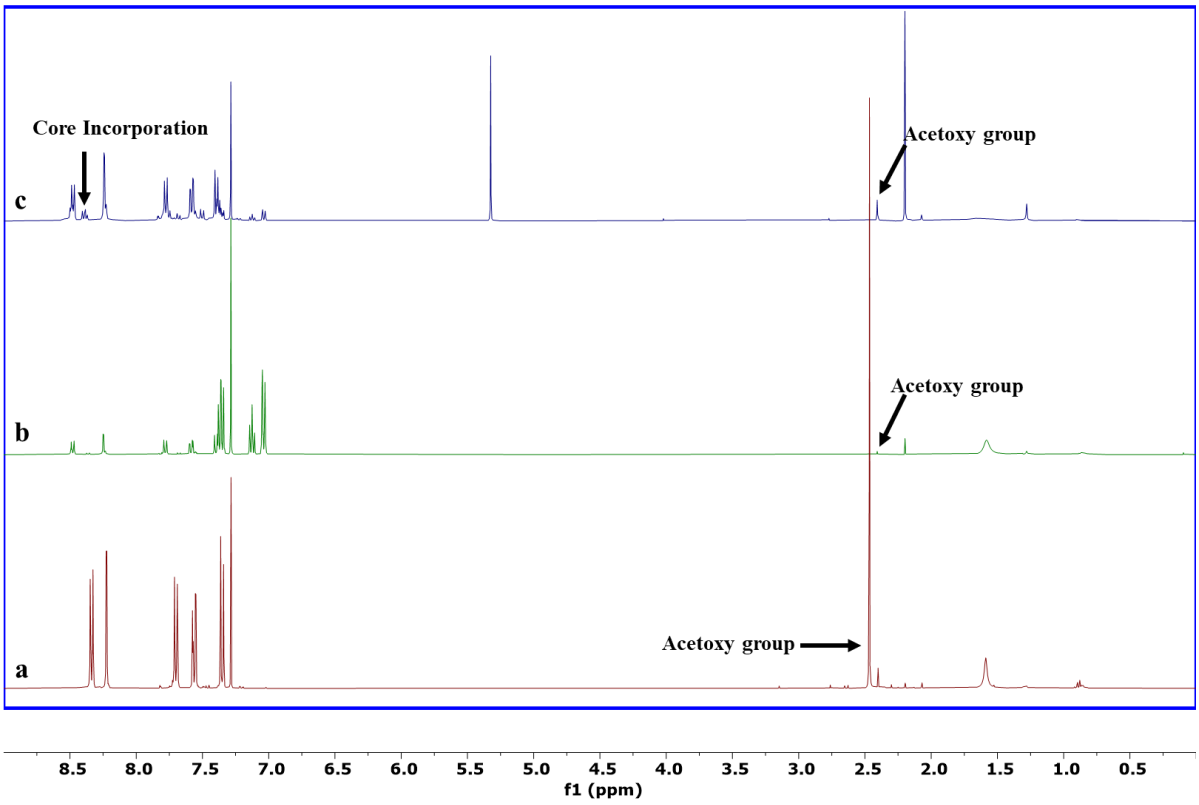

Figure 2.2 ^{1}H NMR Spectra of (a) M113.11 (br,s, 1H) 8.34 (d, J = 8.5 Hz, 2H), 8.22 (d, J = 1.9 Hz, 2H), 7.69 (d, J = 8.5 Hz, 2H), 7.55 (dd, J = 8.7, 2.0 Hz, 2H), 7.35 (d, J = 8.7 Hz, 2H), 2.46 (s, 6H). , (b) **P1**, 8.51 – 8.45 (m, 2H), 8.28 – 8.20 (m, 3H), 7.82 – 7.74 (m, 2H), 7.62 – 7.54 (m, 3H), 7.41 (s, 1H), 7.40 – 7.32 (m, 13H), 7.16 – 7.08 (m, 6H), 7.07 – 7.00 (m, 11H), 2.41 (s, 0.67H). and (c) **P2**, 8.55 – 8.44 (m, 6H), 8.42 – 8.35 (m, 2H), 8.28 – 8.20 (m, 7H), 7.85 – 7.66 (m, 9H), 7.65 – 7.47 (m, 10H), 7.46 – 7.31 (m, 9H), 7.26 – 7.20 (m, 1H), 7.16 – 7.09 (m, 1H), 7.07 – 7.01 (m, 1H), 2.41 (s, 2H). in $CDCl_3$.

2.2.3 Molecular Weight of P1 and P2

Gel permeation chromatography (GPC) is known to provide underestimated values of the molecular weights of hyperbranched polymers especially when using linear polymers as standards in these measurements (MALDI could be used to measure the molecular weight if they are estimated to be below 10000 Da). This is due to the hyperbranched structure and globular nature of HBPs. In the GPC, the prepared solution can pass through a column that contains controlled porosity, usually a polymeric porous gel (also called a "stationary phase"). The molecular weights of polymers P1 and P2 were nevertheless investigated *via* Gel

Permeation Chromatography (GPC) using THF as an eluent and a drop of toluene as a marker. The measurements were done at 40 °C using polystyrene standards to calculate the weight average molecular weight (Mw) and the number average molecular weight (Mn). The polydispersity index (PDI) for the designed polymers were measured using the following equation **PDI = Mw/Mn.**

Table 2.1 GPC data of P1 and P2

Polymers	Mn(Da)	Mw(Da)	PDI	Yield	Fraction
P1	2800	7200	2.6	25%	Chloroform
P2	3600	7900	2.2	28%	Chloroform

Both polymers showed relatively low molecular weights, Mn and Mw for both P1 and P2 as shown in the table 2.1, with Mn at 2800 and 3600 Da and Mw at 7200 and 7900 Da respectively. The PDI was measured for the designed polymers to be 2.5 and 2.1 respectively. Chen et al.[200] reported that the designed polymers based on 3,6-CBZ and its derivatives showed low molecular weight, this is a reason for the occurrence of steric hindrance which prevents the conjugation from being done by forcing the chain to twist. The PDI for P1 was higher than P2 by 0.4 which could be attributed to the absence of a core, leading P1 to have less controlled structure of the polymeric backbone and resulting in a high distribution of branching.

2.2.4 Thermal Properties of P1 and P2

The thermal properties of the designed polymers P1 and P2 were investigated *via* thermogravimetric analysis (TGA) under the protection of N_2 at heating rate of (10°C min^{-1}). As can be seen from figure 2.3, P1 and P2 revealed low thermal stabilities with increasing temperature.

Table 2.2 Thermal data of P1 and P2

Polymers	Td (˚C)
P1	142/327
P2	133/276

Both P1 and P2 started losing weight dramatically with 10 % weight loss initially (20 mg as an actual weight) and degradation temperatures of 142 ^{0}C and 133 ^{0}C respectively. At 327 ^{0}C, P1 showed a dramatic decrease in terms of weight loss (15 %) and with the same decrease for P2

at 276 ^{0}C, which means that both polymers possess low thermal stability at low temperatures. Carbazole-based dendrimers in the literature[201] have shown higher thermal stabilities (Td over 300 °C). However, the carbazole monomers in those materials are more electronically conjugated than those in polymers P1 and P2 as the linkages between them are through C-C bonds between carbazole units rather than through ester bonds in P1 and P2. The low thermal stabilities of P1 and P2 are therefore easily explained for these materials.

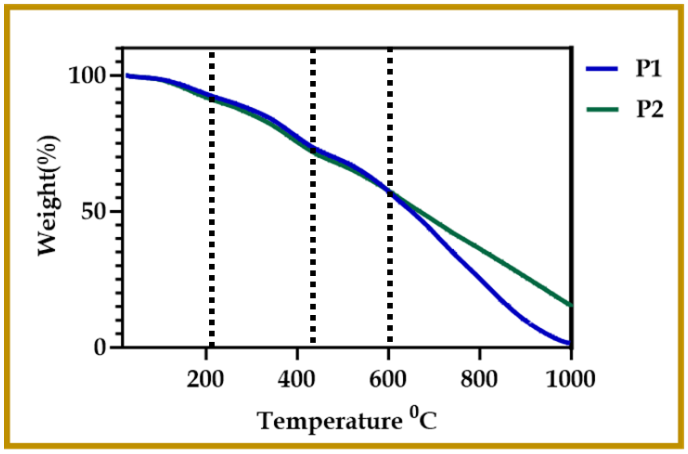

Figure 2.3 TGA analysis of P1 and P2. Three degradation stages of both polymers 1 and 2, the first degradation between 0 and 205 °C, the second degradation between 205 and 410 °C and the last degradation between 600 – 1000 °C.

2.2.5 Optical Properties of P1 and P2

Investigation of the optical properties of polymers P1 and P2 were conducted *via* UV-Vis spectroscopy and photoluminescence spectroscopy. The optical band gaps of the polymers were obtained from the onset of their absorption spectra in thin films using the equation:

$$\mathbf{Eg_{opt} = 1240/\lambda_{Onset}\ eV}\ \text{(in thin films)} \qquad \text{(Eq 2.1)}$$

P1 and P2 were measured in solution using chloroform as a solvent in quartz cuvette and in solid state by drop-cast the polymers as a thin film on a glass substrate.

Table 2.3 Optical data of P1 and P2 in (a) solution and in (b) thin film. PL data of P1 and P2 in (c) solution and in (d) thin film. (e) Error in the range at the maximum of the absorbance curve for different extinction coefficients. The optical band gap of P1 and P2.

Polymers	$\lambda_{abs\ (a)}$ Solution (nm)	$\lambda_{abs\ (b)}$ Film (nm)	λ_{Onset} thin film (nm)	$\lambda_{em\ (c)}$ Solution (nm)	$\lambda_{em\ (d)}$ Film (nm)	$E_{g\ opt}$ (eV)
P1	321	326	356	400	452	3.48 ± 0.007[(e)]
P2	324	330	366	368	426	3.38 ± 0.003[(e)]

In solution, P1 and P2 showed two maximum absorptions at 321 and 324 nm respectively. While in solid state (thin film), the maximum absorptions were observed at 326 and 330 nm respectively. Absorptions at low wavelengths of P1 and P2 at ~ 269 and 272 nm respectively correspond to the π-π* transition of the polymeric backbone, which are caused by the non-conjugated polymeric system. The red-shifted absorptions with low intensity of both P1 and P2, attributing to the n- π* transition of the nitrogen atom from the incorporated CBZ moieties in the carbazole repeat units. In the thin film, both polymers exhibited more shifted absorptions to the red region, this is due to a degree of aggregation of carbazole repeat units in polymeric films compared to solutions. There is an increase in aggregation of molecules going from solution to films and enhances the inter-molecular interaction. The band gaps for P1 was calculated to be 3.48 eV and 3.38 eV for P2. Hypothetically, the lower band gap of P2, associating with the increase of carbazole rings in the polymeric backbone, enhancing the conjugated system and the electronic delocalisation. The band gap between the conduction band (where electrons are restricted in terms of movement) and the valence band (where electrons move freely) refers to the optical band gap. This is required to be minimised, as photons with energy below the band gap are excluded from absorption. In addition, the optical band gap has a significant impact on the colour and emission characteristics of a material. The photoluminescence (PL) properties for both P1 and P2 were measured in solution using chloroform and in solid state (thin film). As illustrated in figure 2.4 (b), the PL spectra for P1 and P2 in solution were measured to be 400 and 368 nm, and in thin film to be 452 and 426 nm respectively. In comparison, P2 showed more blue-shifted emission than P1 in both solution and film, this is due to some factors that require to be considered, one of these factors is attributed to the presence of withdrawing group (NO_2) attached to the core in P2. It has been reported that the incorporation of withdrawing groups contribute to the increase of inter-system crossing from S_1 to T_1, hence the emitted photons from S_1-S_0 will be decreased, leading to the fluorescence to be degreased.[202] P1 observed a high redshifted emission at 452nm compared to P2 which observed a low redshifted emission at 426.5 nm, this is due to the inter-molecular aggregation in the polymeric chains of P1.

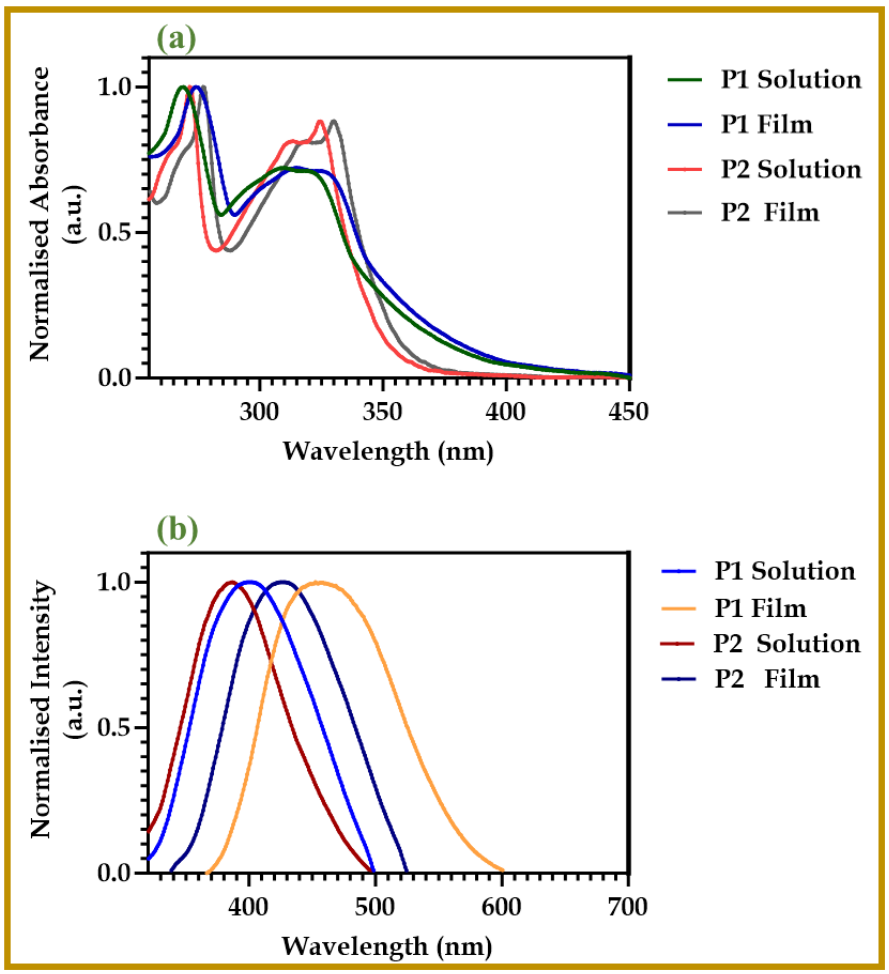

Figure 2.4 (a) Normalised UV vis absorption spectra of P1 and P2 in solution and film.(b) Normalised PL emission spectra of P1 and P2 in solution and film. In terms of the UV-vis spectra, P1 exhibited a hypsochromic shift in both solution and film, while P2 exhibited a bathochromic shift in both solution and film in comparison with P1. In the PL spectra, P1 exhibited a bathochromic shift in both solution and film, while P2 exhibited a hypsochromic shift in both solution and film compared to P1.

2.2.6 Electrochemical Properties of P1 and P2

Investigation of the electrochemical properties of the polymers was conducted *via* cyclic voltammetry analyses. The electrochemical band gaps were calculated from the difference between the HOMO and LUMO energy levels values obtained from the oxidation and reduction curve's onsets respectively, using the following equation.

$$\textbf{\textit{HOMO/LUMO}} = -\left[(E_{OX/Red\ Onset} - E_{fec}) + E_{ref}\right]\ (eV) \qquad \text{(Eq 2.2)}$$

$\mathbf{E_{fec}}$ refers to the potential of the ferrocene/ferrocenium ion (measured to be 0.084 *vs.* Ag/Ag^{+} reference electrode), and $\mathbf{E_{ref}}$ refers to the ionisation potential I_P of ferrocene (4.8 eV) which was used as a calibrant. The measurements were achieved on drop-cast polymer thin films on

platinum disc electrodes, which were used as a working electrodes in the electrolyte 0.1 M (tetrabutylammonium perchlorate in acetonitrile) with a reference electrode made from a silver wire in 0.01 M silver nitrate solution in the electrolyte solution (Ag/Ag^{+}). The scan rate used was 100 mV s^{-1}.

Table 2.4 CV data of P1 and P2, (a) HOMO and (b) LUMO level values, (c) The electrochemical band gaps.

Polymers	**HOMO (eV)[(a)]**	**LUMO (eV)[(b)]**	**$E_{g\ elect}$ (eV)[©]**
P1	-5.05	-1.57	3.48 ± 0.07
P2	-5.08	-1.7	3.38 ± 0.03

HOMO values were obtained from the anodic (oxidation) curve onset, whereas the LUMO values were calculated from the difference between the HOMO and the optical band gap values.

As mentioned in the table 4 above, the HOMO levels of P1 and P2 were calculated from the onset of first oxidation peak of both polymers to be -5.05 and -5.08 eV. Where the LUMO levels of P1 and P2 were obtained by subtracting the optical bandgap (Eg) of both polymers from the HOMO values to be -1.57 and -1.7 eV respectively, as the reduction potential peaks are not clearly defined. The HOMO levels of the polymers indicate fairly shallow oxidation levels given the lack of electronic conjugation in these materials, however, their low onset of oxidations and as a result their shallow HOMO levels could be due to aggregation of the carbazole units which could explain the observed values obtained. The results from the absorption data seem to support this given the high absorption onsets observed in films compared to those in solution. It must be mentioned that the reduction potential peaks are not clearly defined. However, it is noticed that P2 showed slightly shallower value, this is due to the effect of electron withdrawing group, favouring lower reduction potentials[203]. The deeper HOMO level of P2 at -5.08 eV, and the lower electrochemical band gap of 3.38 eV, attributing to the decrease of conjugation system compared to P1.

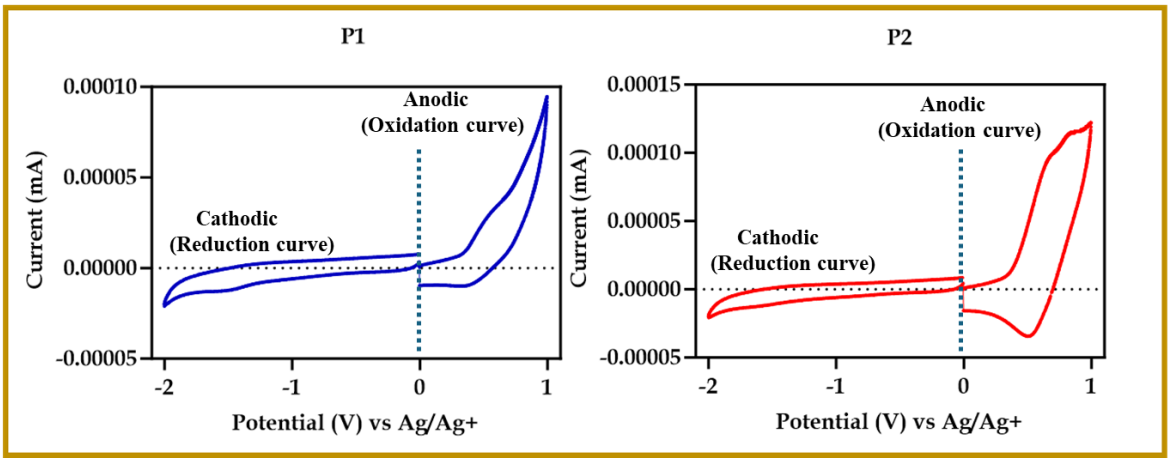

Figure 2.5 The CV analysis of P1 and P2. Both polymers 1 and 2 showed oxidation and reduction peaks, the HOMO values of both polymers were measured from the oxidation peak onset. However, the reduction curve onsets of both polymers could not be measured, so the LUMO values were calculated from the HOMO values and the optical band gap values.

2.3 Conclusion

Improvements in OLEDs technology for use in a wide range of applications requires the development of new materials with improved solution processability, thermal stability, high photoluminescence efficiency and low production costs. Two hyperbranched polymers P1 and P2 were prepared and fully characterised in this work. Polymer P1 was obtained in low yields, poor solubility and with low molecular weights. The poor yield and low molecular weights of polymer P1 is due to its low solubility, probably due to aggregation of the carbazole units in the final polymer as well as gelation of the growing polymer chains during the polymerisation reaction. The polymerisation therefore required an enhancement and control in some of its properties. The preparation of polymer P2 was then undertaken upon adding *p*-nitrophenyl acetate during the polymerisation which provides a core to the hyperbranched polymer P2 and which should also reduce the cyclisation side reactions and limit the gelation of the growing polymer. HBP P2 was obtained with a slightly higher molecular weight than that of P1, however, despite the incorporation of p-nitrophenyl core unit in polymer P2 as demonstrated from the 1H NMR studies, the molecular weight of polymer P2 was still low resumably as a result of aggregation of carbazole units in P2 limiting the growth of polymer chains. Both polymers P1 and P2 exhibited low thermal stabilities with degradation temperature just above 100 °C. These low thermal stabilities were explained by the nature of the hyperbranched polymer chains and the ester linkages between repeat units in these materials as opposed to other hyperbranched carbazole-based molecules where the linkage is through C-C bonds from carbazole repeat units.

The optical band gaps of both P1 and P2 were obtained to be 3.48 eV and 3.38 eV respectively, the high optical band gaps of P1 is attributing to the high distribution of the polymer chain. At last, the designed Hb P1 and P2 undesired to be used with current conditions in the device fabrications as they suffered from low molecular weight, poor solubility and exhibited low thermal resistance.

Chapter 3: Synthesis and Properties of A_2B_3 Hyperbranched Polymers Based on Carbazole Derivatives for OLED Applications

Abstract

Hyperbranched polymers (HBPs) are becoming increasingly popular because of their unique features and broad range of properties made possible by their highly branched topological architectures. Efficiencies of OLEDs based on hyperbranched polymers have been greatly enhanced in terms of the material's solubilities, allowing to obtain high molecular weight polymers with excellent thermal stability and improved film morphology. In this chapter, carbazole derivatives have been used to design and synthesise HBPs *via* $A_2 + B_3$ approach of polycondensation; offering great control of branching and molecular weight by avoiding the internal cyclisation interaction and preventing gelation from being reached. In addition, polymer stability and hole-transporting material abilities are improved. P3 and P4 have been designed and prepared using the $A_2 + B_3$ approach to polycondensation. A good control of polymerisation and molecular weight was observed by exhibiting Mn values of 8500 Da and 11700 Da for P3 and P4 respectively. Both P3 and P4 were obtained in good yields of 70% and 72 %, with excellent solubilities in common organic solvents. Both polymers exhibited good thermal stability, and in comparison, P3 showed better thermal stabilities by observing one thermal degradation at 365 ^{0}C compared to P4 which observed two thermal degradations at 214 ^{0}C and 409 ^{0}C. The optical band gaps for both P3 and P4 were determined to be 3.08 eV and 2.95 eV respectively. The difference in the optical band gaps is attributed to the decrease of HOMO - LUMO levels due to the effect of Phenyl substituents electron withdrawing group in P4.

3.1 Introduction

Extensive research has been conducted on polymeric light-emitting diodes (PLEDs) for their incorporation into several domains and applications[186]. Factors such as preventing molecules' aggregation and enhancing the polymer's stability (thermally stable when it is applied as thin film) need to be considered. In the solid state, it is common for linear polymeric light-emitting materials to undergo aggregation and produce excimers, which subsequently leads to both a red shift of emission and quenching of fluorescence.[191] The phenomenon known as Aggregation Caused Quenching (ACQ) has the potential to hinder the effective utilisation of a substance. However, the incorporation of polymer branches has been shown to mitigate aggregation and enhance stability to a certain level.[204, 205] While seeking unique specifications for performance, extensive research is being conducted to explore the design and synthesis of hyperbranched polymers for application in light-emitting diodes (LEDs), with a particular focus on identifying unique performance criteria such as (high conducticity and solubility, high thermal and lumincescence spectrum stability), .

Hyperbranched polymers with three-dimensional (3D) topological architectures can enhance steric hindrance, hence efficiently impede quenching of fluorescence and the formation of crystalline domains that could occur due to the π-π stacking phenomena between molecules. In addition, the prevention of polymer chain aggregation can lead to the formation of multi-dimensional topological structures of hyperbranched polymers.[191] This, in turn, can result in enhanced polymers' light-emitting performance and an enhancement in the electroluminescence of the respective devices. As a result, a variety of methodologies are used in the design of monomers that exhibit advantageous steric hindrance characteristics, facilitating the production of hyperbranched polymers. Fluorene derivatives possessing alkyl chains have been found to efficiently mitigate the buildup amongst conjugate skeletons, primarily due to steric hindrance. Consequently, these compounds have been extensively included into hyperbranched polymers utilised in OLEDs, resulting in the generation of optimal emission intensities[206].

Among these methods, the AB_2 step-growth polycondensation strategy has been extensively employed for the synthesis of HB Polymers.[171] It is worth noting that Flory was the pioneer in utilising this approach, as documented in the literature.[207] The lack of control over the polycondensation reaction involving AB_2 monomers has been observed, leading to challenges

in regulating the reduced molecular weight and polydispersity.[208] Furthermore, the utilisation of polycondensation AB_2 monomers in the synthesis process has been found to result in the formation of HB polymers exhibiting elevated viscosity, as documented in previous studies[209]. This phenomenon should be avoided as the desired HB polymers should be with low viscosity.

In order to mitigate the potential drawbacks associated with the utilisation of AB_2 polycondensation, the second approach of $A_2 + B_3$ has been widely employed in the synthesis of hyperbranched polymers (HPs) through the polycondensation reaction involving bi-functionalised monomer A (identical functionalities) and tri-functionalised monomer B (same functionalities)[171] , as depicted in scheme 3.1. The fundamental principles of the $A_2 + B_3$ approach are as follows: the monomeric and polymeric A_2 and B_3 groups share a similar reactivity, and the A_2 functional groups interact selectively with the B_3 sites of activity[172, 178].

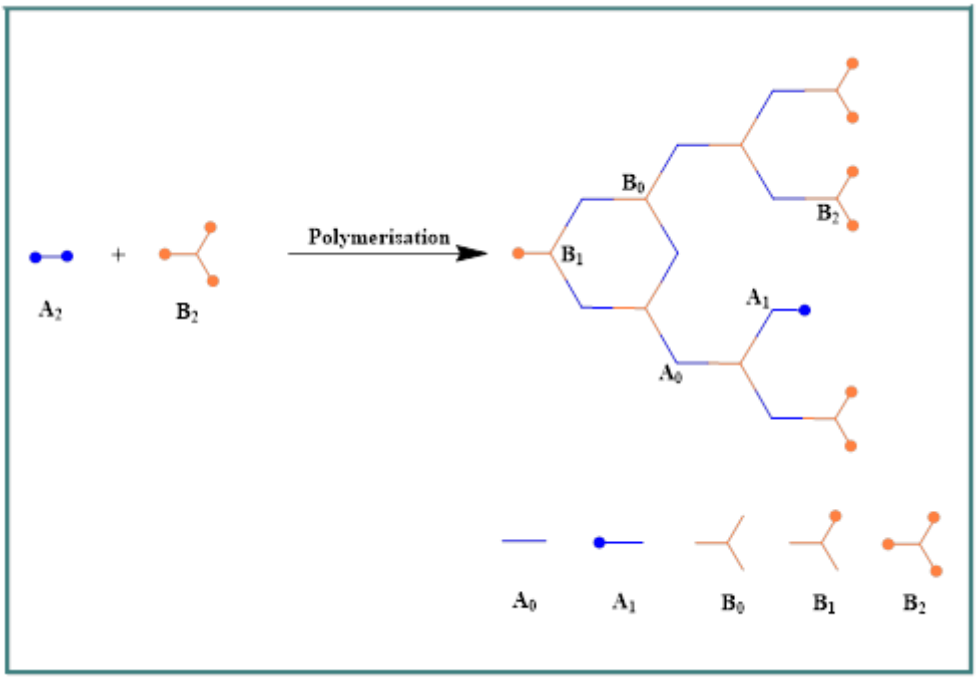

Scheme 3.1 The proposed traditional approach of $A_2 + B_3$ polycondensation. The structural units of general hyperbranched polymers are classified based on the number of unreacted groups. These units are A_0, A_1, B_0, B_1, and B_2. The A units, A_0 and A_1, and the B units, B_0, B_1, and B_2, are formed from the A_2 and B_3 monomers, respectively.[176]

This technique exhibits distinctive characteristics, such as the restriction of intramolecular cyclisation, which is recognised as a crucial element in achieving well-defined extremely hyperbranched architectures with abundant terminal functionalities.[176] Furthermore, the production of soluble polymers can be achieved by preventing gelation and adjusting the level

of branching through the incorporation of solubilising groups into the polymeric structures. Moreover, an advantageous aspect of this technology lies in the wide range of monomers that are readily accessible, hence enabling the versatile synthesis of hyperbranched polymers.[210-215]

Lu et al.[216] have synthesised two partly conjugated hyperbranched polymers, referred to as HBP1 and HBP2, using the $A_2 + B_3$ and $A_2 + B_4$ polycondensation techniques, respectively. The compound 1,4-distyrylol-2,5-butoxybenzene was synthesised and designated as A_2. The compounds 1,1,1-tris-(p-tosyloxymethyl)-propane and pentaerythritol tetra(methyl benzene sulfonate) were also synthesised and denoted as B_3 and B_4, respectively, as depicted in scheme 3.2. The characterization revealed that HBP1 demonstrated great solubility in widely used organic solvents and showed remarkable capabilities for forming films. Regarding thermal properties, it is seen that both polymers exhibit favourable thermal stabilities, as evidenced by their decomposition temperatures falling within the range of 396 - 405 ^{0}C. Additionally, these polymers demonstrate elevated glass-transition temperatures (refers to the temperature at which polymer undergoes a transition from a rigid, fragile condition to a softer state, similar to a cooled liquid), which confer advantages in the production of light-emitting devices with superior performance characteristics. The relative photoluminescence quantum efficiencies of HBP1 and HBP2 in dilute chloroform solution were investigated to be 56.8 and 49.3 % respectively, indicating that HBP1 possesses greater features than HBP2.

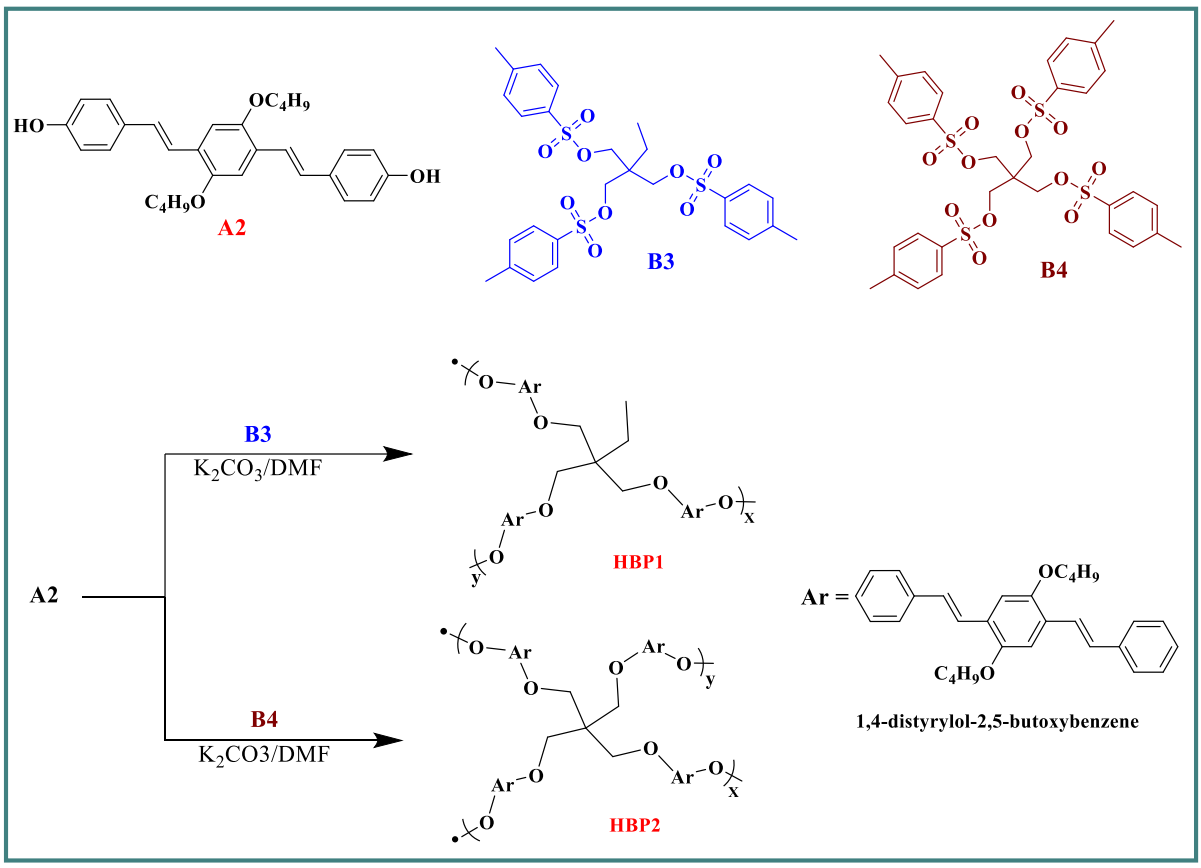

Scheme 3.2 Synthesis of HBP1 and HBP2 via A_2+B_3 and A_2+B_4 approaches from Lu et al.[216] HBP1 was prepared using 2-ethyl-2-((tosyloxy)methyl)propane-1,3-diyl bis(4-methylbenzenesulfonate) as a core (B_3) with 4,4'-(2,5-dibutoxy-1,4-phenylene)bis(ethene-2,1-diyl))diphenol as partially conjugated donor (A_2). While HBP2 was prepared using the same partially conjugated donor (A_2) with 2-(((phenylsulfonyl)oxy)methyl)-2-((tosyloxy)methyl)propane-1,3-diyl bis(4-methylbenzenesulfonate) as a core (B_4). Introducing the central aliphatic chains in the core are benfecial to increase the solubility of both HBP1 and HBP2.

3.2 Results and Discussions

In the previous chapter, P1 and P2 were synthesised in low yields and characterised thermally, optically and electrochemically. It has been noticed that both P1 and P2 suffered from poor solubility in many organic solvents, low molecular weights and less control of the polymerisation due to the occurrence of internal cyclisation reactions, gelation and less control of the topology. To overcome these issues, step growth polymerisation using the A_2 + B_3 approach offers many benefits, such as limiting the internal cyclisation reaction, preventing gelation and good control of the topological structures, compared to polycondensation using the AB_2 approach.

In this chapter, different functionalised monomers were synthesised to be polymerised using the A_2 + B_3 approach of polycondensation. Bi-functionalised monomers A_2 (M2, M3 and M4)

were prepared using both 3,6-dibromo- and 3,6-dimethoxy-carbazole as raw materials, respectively, as shown in scheme 3.3 with respect to other reaction conditions. Tri-functionalised monomer B_3 (M5) was synthesised in one step using trimethylolpropane (TMP) as a starting material, see scheme 3.3.

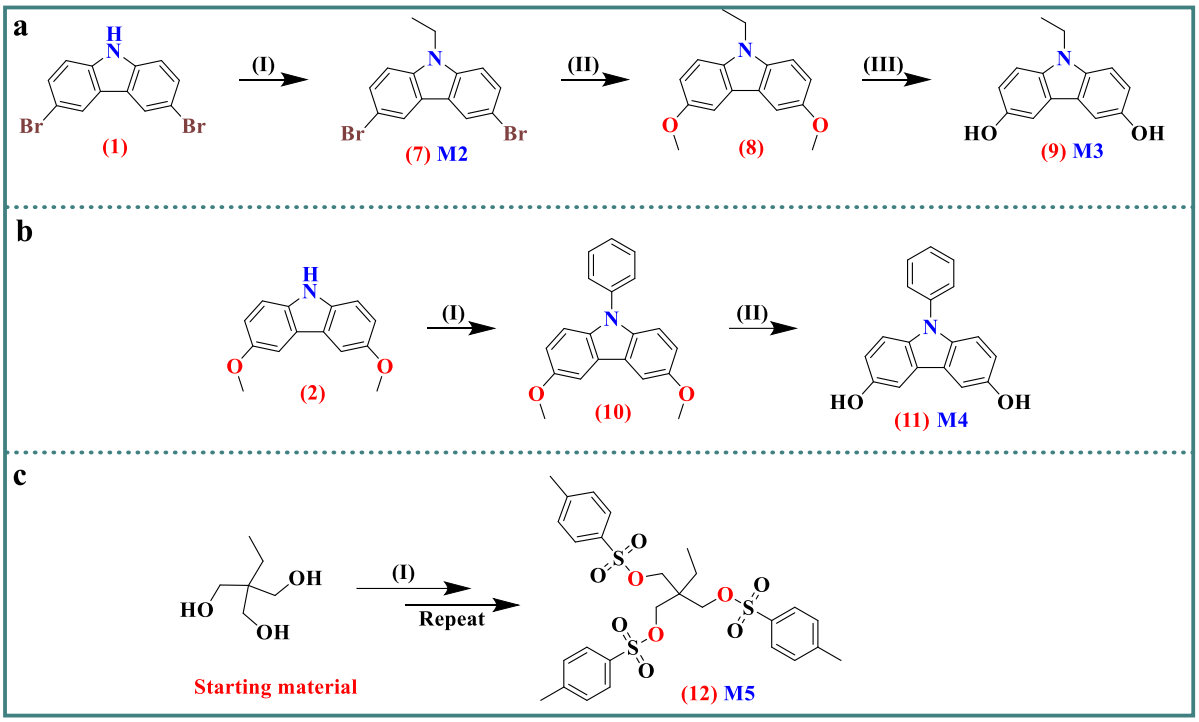

Scheme 3.3 Monomeric Synthetic steps of M2, M3, M4 and M5. Reagent and conditions; a (I) Ethyl bromide, KOH, DMF, 24 ^{0}C, overnight. (II) $NaOCH_3$, CuI, DMF, 120 ^{0}C, 24 h. (III) BBr_3, ice bath-room temperature, 24 h. b (I) Cu, 1-Iodobrnzene, CH_3CN, Cs_2CO_3, 90 ^{0}C, 48 h. (II) BBr_3, ice bath-room temperature, 24 h. C (I) . 4-methylbenzene-1-sulfonyl chloride, Et_3N, DCM, room temperature, 72 h.

P3 and P4 were prepared using M3 and M4 as an A_2 with M5 as a B_3, respectively. The designed polymers P3 and P4 were characterised to be investigated in terms of solubility, polymers' molecular weight and controlling the topology. In addition, the investigation of thermal, optical and electrochemical properties.

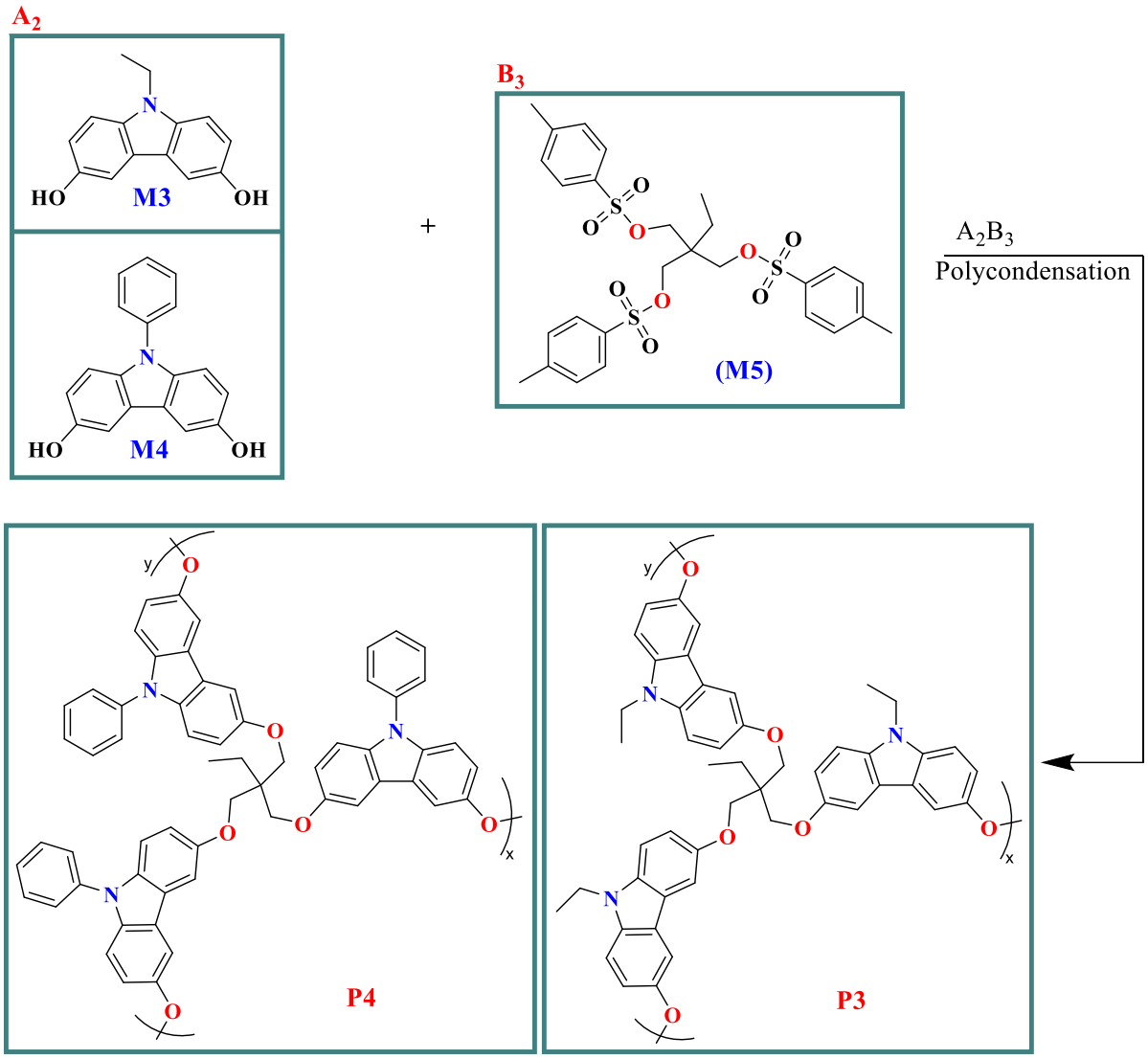

Scheme 3.4 Synthesis of P3 and P4 *via* $A_2 + B_3$ approach. P3 was prepared using M3 (A_2) as a donor with M5 (B_3) as a central core. While P4 was prepared using M_4 (A_2) as a donor with the same central core (B_3). The central aliphatic alkyl chains play a crucial role in terms of increasing both polymers's solubility.

3.2.1 Synthesis of Monomers

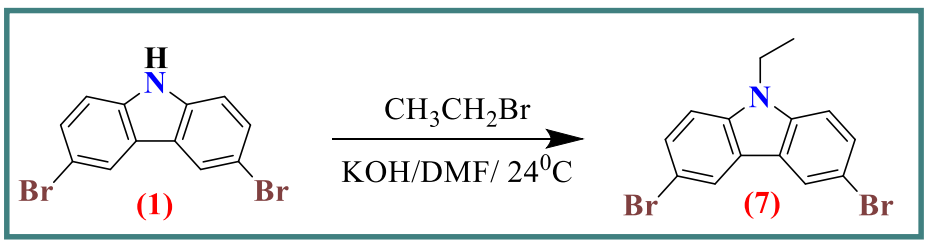

Scheme 3.5 Synthetic conditions of compound (7). Reagent and conditions; Ethyl bromide, KOH, DMF, 24 ^{0}C, overnight.

Compound (7) was synthesised following the modified procedures reported by Guo et al.[217] The reaction was conducted at room temperature using dry DMF as a reaction media and potassium hydroxide as a base to help in deprotonation. The alkylation by ethyl bromide was achieved through the nucleophilic substitution reaction in two steps: firstly, by generating the anion which resulted from the deprotonation of the carbazole nitrogen atom. This is followed by the attack of the anion on the ethyl bromide, affording the target compound. The purification was done using column chromatography once the TLC observed two intense spots with different (R_f).

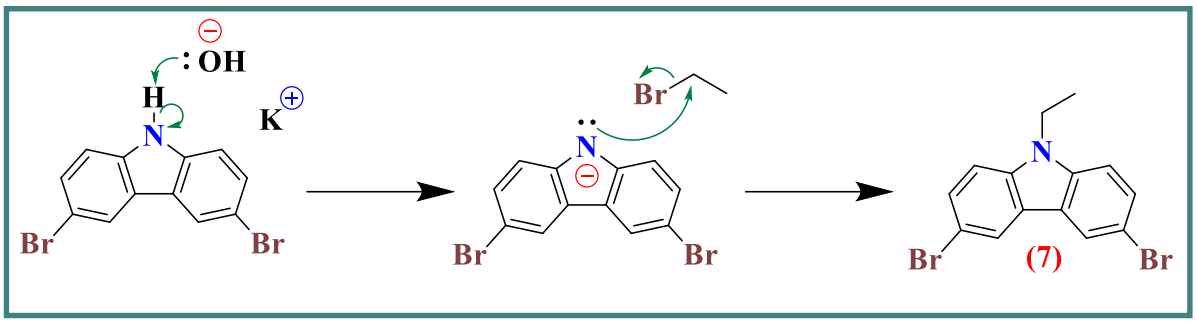

Scheme 3.6 The proposed mechanism for compound (7). The alkylation of the nitrogen from the carbazole was carried out through the nucleophilic substitution in the presence of KOH as a base to assist the deprotonation and using DMF as solvent to afford 3,6-dibromo-9-(2-ethyl)-carbazole (M2).

The ^{1}H NMR spectra confirmed the structure of the desired product by observing the disappearance of the N-H peak, which appeared at 11.60 ppm. A deshielded quartet appeared at 4.47 ppm, assigned to (N-CH_2). In the aliphatic area, a shielded triplet was noticed at 1.30 ppm, corresponding to the terminal methyl group, (see figure 3.1). Furthermore, mass spectrometry confirmed the preparation of the required compound by giving the value of 351.93. In addition the elemental analysis confirmed the preparation of the required product (7) by giving the values of C 47.62; H, 3.12; Br, 45.30; N, 3.99, maching the theoretical values of C, 47.63; H, 3.14; Br, 45.28; N, 3.

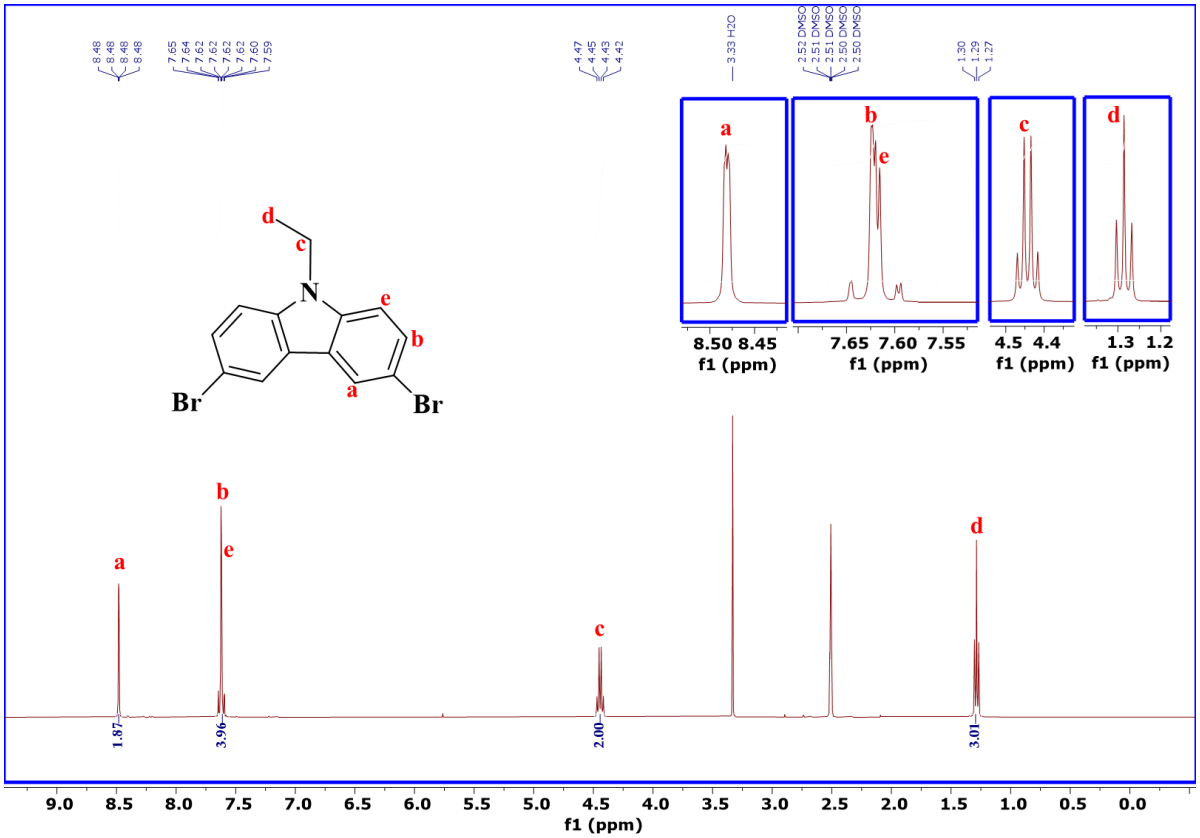

Figure 3.1 ^{1}H NMR Spectrum for M2 in DMSO-d6. 8.48 (s, 2H), 7.67 – 7.55 (m, 4H), 4.44 (q, J = 7.1 Hz, 2H), 1.29 (t, J = 7.1 Hz, 3H).

The preparation of compound (8) was carried out according to a reported synthetic methoxylation procedure in the literature[194]. The required product was obtained as a pale yellow solid with a yield of 79 % after purifying the crude, using column chromatography with ethyl acetate and petroleum ether (1:6). The reaction mechanism was explained in chapter (2) for the preparation of compound (2).

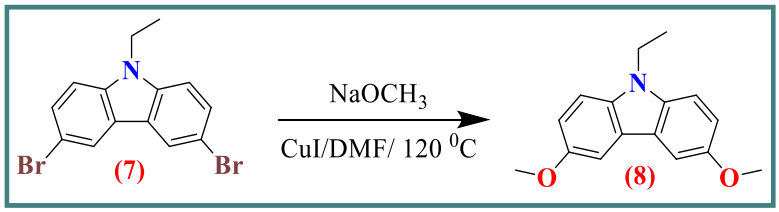

Scheme 3.7 Synthetic conditions of compound (8). Reagent and conditions; $NaOCH_3$, CuI, DMF, 120 ^{0}C, 24 h.

The characterisation of compound (8) using ^{1}H NMR showed more a deshielded intense singlet at 3.96 ppm ascribing to the new substituents of two methoxy groups in the 3- and 6- positions of carbazole rings (see figure 8.6 in the appendix). Moreover, the elemental analyses confirmed

the success of the prepared compound through the obtained values of C 47.64; H, 3.16; N, 3.99 which indeed matched the calculated values C, 47.63; H, 3.14; N, 3.97

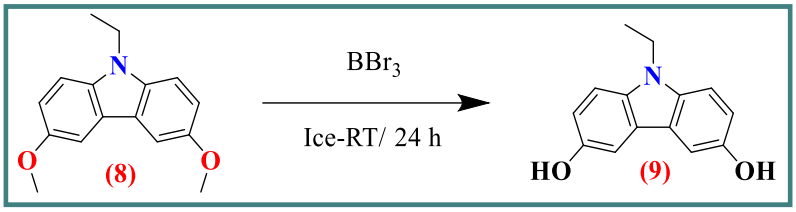

Scheme 3.8 Synthetic conditions of compound (9). Reagent and conditions; BBr_3, ice bath-room temperature, 24 h.

Compound (9) was prepared following the synthetic procedure reported by Hillyer et al. [218]. The reaction was carried out using boron tribromide (Lewis acid) as the ether cleaving reagent, and dichloromethane as a solvent. The carbazole phenolic rings were obtained through the demethylation of aryl methyl ether (compound 8) as shown in scheme 3.9. The addition of boron tribromide was completed at 0 ^{0}C to reduce the reactivity of the reagent, and then ice was removed allowing the reaction temperature to reach 24 ^{0}C after the complete addition. A saturated solution of sodium hydrogen carbonate was added to neutralise the pH of the reaction mixture and remove the resulting boric acid $B(OH)_3$ (water miscible) which is known as a weak acid.

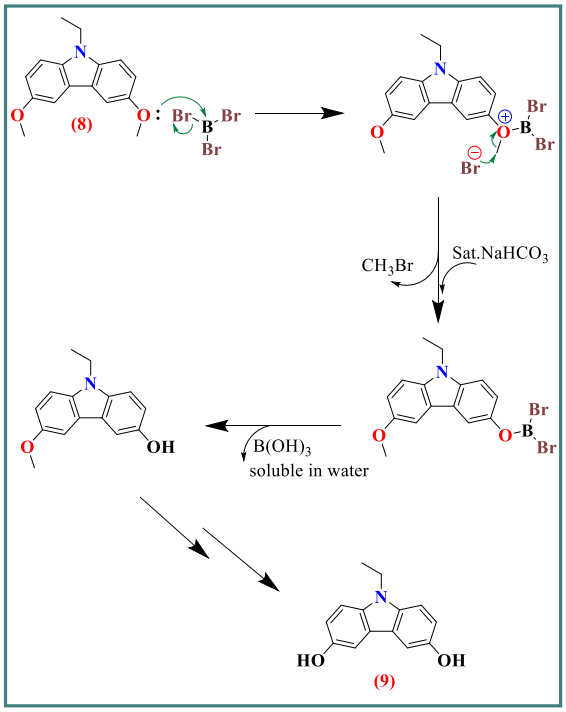

Scheme 3.9 The proposed mechanism for compound (9) M3. The preparation of phenolic rings of compound (9) was carried out in dry conditions (under N_2), using boron tribromide (Lewis acid) as the

ether-cleaving reagent, and dichloromethane as a solvent with respect to other reaction conditions mentioned in the scheme above.

The analysis of compound (9) using ^{1}H NMR confirmed the final structure successfully by the disappearance of the intense peaks for the 6 protons from the two methoxy groups. The new phenolic rings of carbazole showed a broad singlet peak at 8.87 ppm attributed to the presence of the two new OH substituents in the 3- and 6-positions of the carbazole rings, (see figure 3.2). Moreover, ^{13}C NMR confirmed the obtained structure by disappearance of the methoxy peak at 56.20 ppm. Further analysis was conducted using elemental analyses to confirm the elements' values to be C, 73.99; H, 5.77; N, 6.16 which relatively matched the calculated values C, 74.05; H, 5.80; N, 6.20.

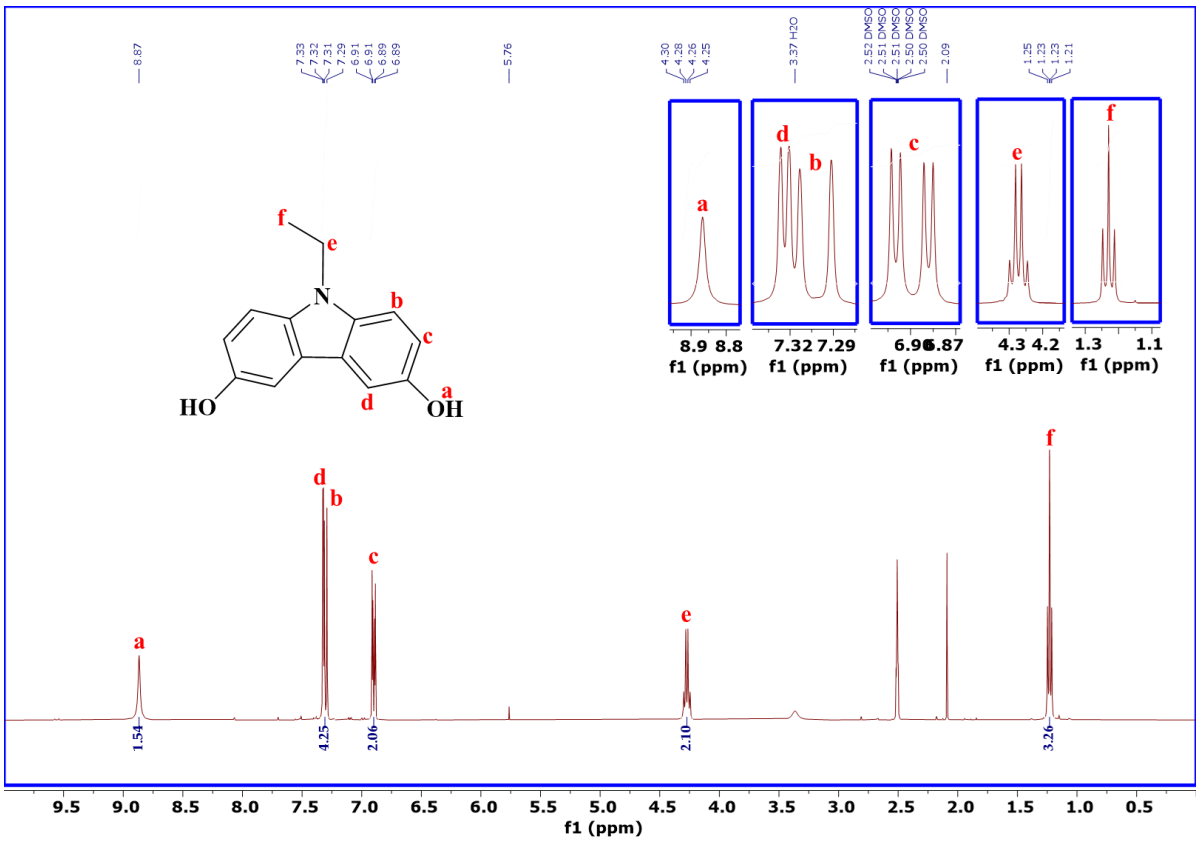

Figure 3.2 ^{1}H NMR Spectra for M3 in DMSO-d6 8.87 (s, br, 2H), 7.35 – 7.27 (m, 4H), 6.90 (dd, J = 8.7, 2.4 Hz, 2H), 4.27 (q, J = 7.1 Hz, 2H), 1.23 (t, J = 7.1 Hz, 3H).

Compound (10) was successfully prepared according to the proposed synthetic procedure reported by Teng et al.[219] This reaction was conducted under the protection of N_2 atmosphere using dry acetonitrile as a solvent, copper metal as a catalyst, and caesium carbonate as a base. The reaction was left under stirring for 48 hours at 90 ^{0}C until completion. As caesium carbonate is considered a strong base, the reaction is not required to be carried out at a high

temperature. Furthermore, using caesium carbonate as a base in the reaction is favourable, due to the high solubility in aprotic solvents compared to other carbonates such as potassium and sodium carbonate, also leading to producing a high-yield products as stated by Rabie et al.[220] Caesium carbonate has distinctive characteristics, including an extremely large ionic radius, low density of charges, and strong polarising ability. As a result of these characteristics, caesium carbonate is a more desirable compound for sensitive reactions that necessitate a precisely balanced base strength.[221]

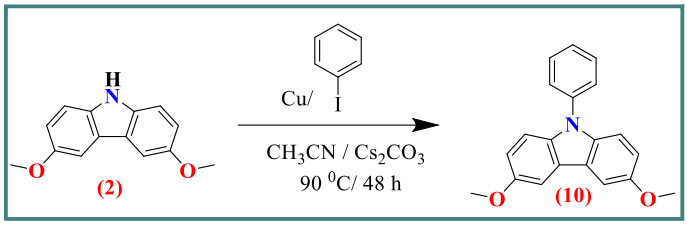

Scheme 3.10 Synthetic conditions of compound (10). Reagent and conditions; Cu, 1-Iodobrnzene, CH_3CN, Cs_2CO_3, 90 ^{0}C, 48 h.

In terms of reaction mechanism, Ullman coupling reaction was applied to prepare product (10) in three mechanistic steps; firstly by the oxidative addition process Cu metal to 1-iodobenzene, resulting in the complex (A) as shown in scheme 3.11 followed by the second steps which includes the transmetalation between the deprotonated compound (2) and complex (A) to obtain the complex (B). The last step was achieved through the reductive elimination of complex (B) affording the required product (10).

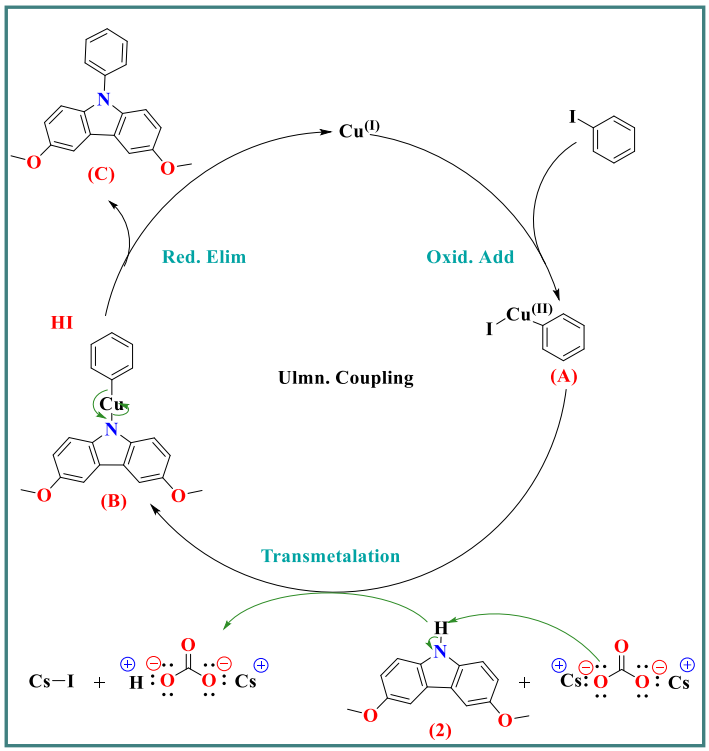

Scheme 3.11 The proposed mechanism for compound (10). Ullman coupling reaction includes three mechanistic steps; (I) The oxidative addition (to form complex A), (II) The transmetalation (to form complex B), (III) The reductive elimination of complex (B) to produce the required 3,6-dimethoxy-9-phenyl-9H-carbazole (10).

The characterisation by ^{1}H NMR, mass spectrometry and elemental analysis confirmed the success of the preparation of the product (10). ^{1}H NMR revealed the disappearance of a broad peak at 11.59 ppm which was assigned to the N-H group. New deshielded aromatic doublet of triplet peaks were observed at 7.55 ppm, attributed to the two protons (chemically equivalent) located on the *ortho* positions of the new attached phenyl group. Another less shielded multiplet was observed from 7.47 to 7.37 ppm assigned to the two protons in the meta position and one in the *para* position from the same new phenyl substituent (see figure 8.7 in the appendix). Further analysis by mass spectrometry confirmed the molecular weight of the required product as m/z of 304.34 matching peak to the calculated value was observed. The elemental analysis indeed confirmed the purity of the product by obtaining the values of C, 79.25; H, 5.70; N, 4.60, which are similar to the calculated values of C, 79.19; H, 5.65; N, 4.62

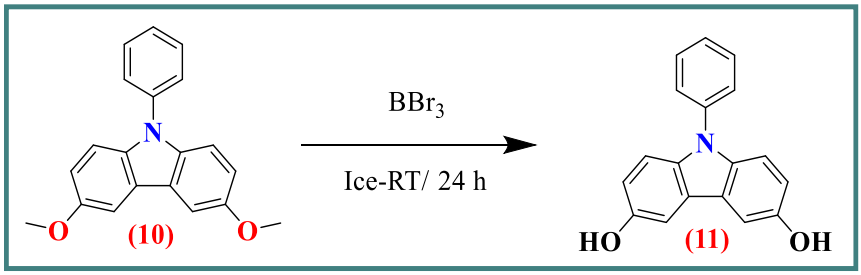

Scheme 3.12 Synthetic conditions of compound (11) M4. Reagent and conditions; BBr_3, ice bath-room temperature, 24 h.

Compound (11) was prepared following the modified procedure mentioned in the literature[218]. The condition and mechanism to prepare compound (11) were used and explained in the preparation of compound (9). M4 was obtained as a faintly grey solid in a yield of 74 %. The phenolic carbazole rings were confirmed through the ^{1}H NMR characterisation, by observing a singlet peak at 9.08 ppm, ascribed to the new substituents of two hydroxy groups as shown in figure 3.3. Furthermore, the disappearance of the intense methoxy peak which was located at 3.96 ppm was also observed. Further analysis was done *via* mass spectrometry confirming the molecular mass of the required product (11) of 276.28. In addition to confirm, the characterisation of elemental analysis provided the values of C, 78.56; H, 4.75; N, 5.11, maching the calculated values of C, 78.53; H, 4.76; N, 5.09.

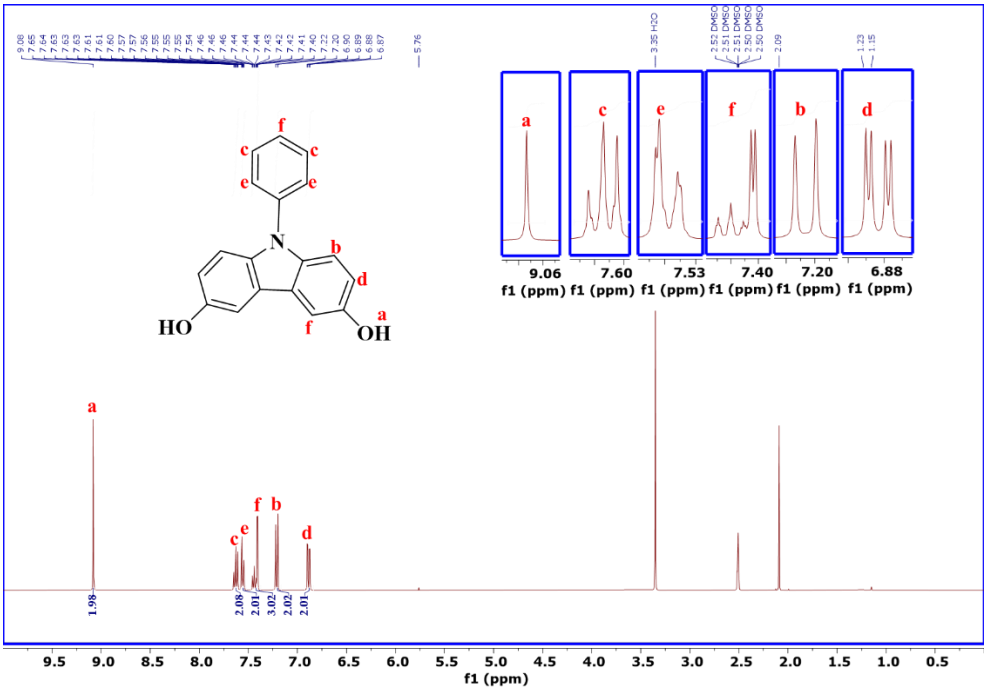

Figure 3.3 ^{1}H NMR Spectrum for M4 in DMSO-d6. 9.08 (s, 2H), 7.63 (dd, J = 8.2, 2.2 Hz, 2H), 7.55 (dd, J = 7.2, 1.4 Hz, 2H), 7.47 – 7.37 (m, 3H), 7.21 (d, J = 8.7 Hz, 2H), 6.89 (dd, J = 8.8, 2.4 Hz, 2H).

The preparation of compound (12) was achieved according to the synthetic procedure reported by Matsukizono et al.[222] TMP was treated using triethylamine as a base in the presence of 4-toluenesulfonyl chloride under the protection of N_2 at room temperature using anhydrous DCM as a solvent. The reaction was given 72 hours until completion, resulting in a dark brown oil as residue. The required product (12) was afforded as a white solid (84 %) once precipitating the residue in a mixed solvent of methanol and 0.25 M of HCl solution.

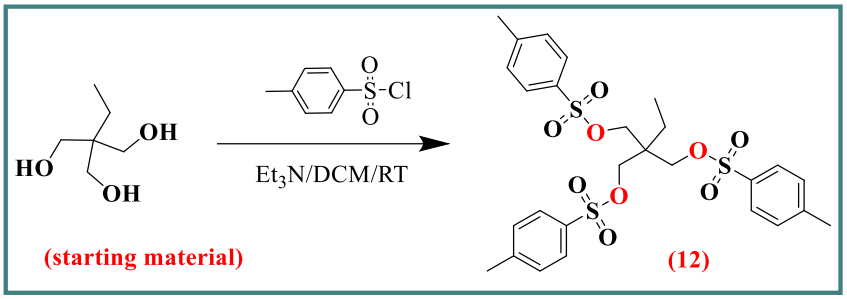

Scheme 3.13 Synthetic conditions of compound (12). Reagent and conditions; 4-methylbenzene-1-sulfonyl chloride, Et_3N, DCM, room temperature, 72 h.

In terms of reaction mechanism, the lone nitrogen pair form triethyl amine deprotonated the hydroxy group forming the oxygen anion (O^-), which in turns attacked the sulfur atom in 4-toluenesulfonyl chloride through the nucleophilic addition, generating the tetrahedral intermediate as can be seen in scheme 3.14. Next, the S-Cl bond was broken through the elimination of the chloride anion to afford the product (12).

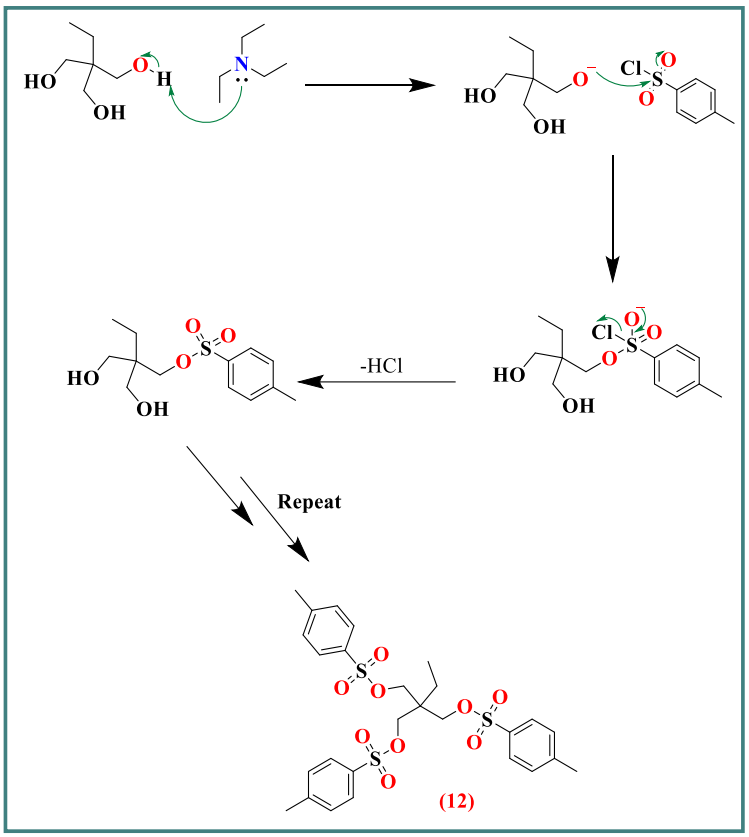

Scheme 3.14 The proposed mechanism for compound (12). The nueclphilic substitution was applied to prepare the required 2-ethyl-2-((tosyloxy)methyl)propane-1,3-diyl bis(4-methylbenzenesulfonate) (12) M5 in the presence of triethylamine as a base and dry DCM as a solvent with respect to other reaction reagents and conditions mentioned above.

The ^{1}H NMR spectrum confirmed the structure of the product and revealed two aromatic doublets with chemical shifts at 7.75 and 7.40 ppm. The deshielded peaks assigned to six protons located in position (a) from the phenyl rings as noticed in the figure 4.3 below, and the shielded peaks corresponding to the six protons in position (b) from the same phenyl rings. A singlet was observed at 3.79 ppm confirming the presence of six protons from three methylene groups next to the oxygen atoms. At 2.49 ppm an intense singlet was noticed attributed to the nine protons of the three terminal methyl groups in position (d), the more deshielding of these protons is due to the delocalisation caused by phenyl rings. Two protons of the ethyl group located in (e) position were observed as a quartet at 1.41 ppm. The shielded terminal methyl group located in (f) position was viewed as a triplet at 0.69 ppm. further characterisation *via* mass spectrometry, confirmed the successfull preparation of product (12) by providing an m/z peak at 597.73.corresponding to molecular weight of the product.

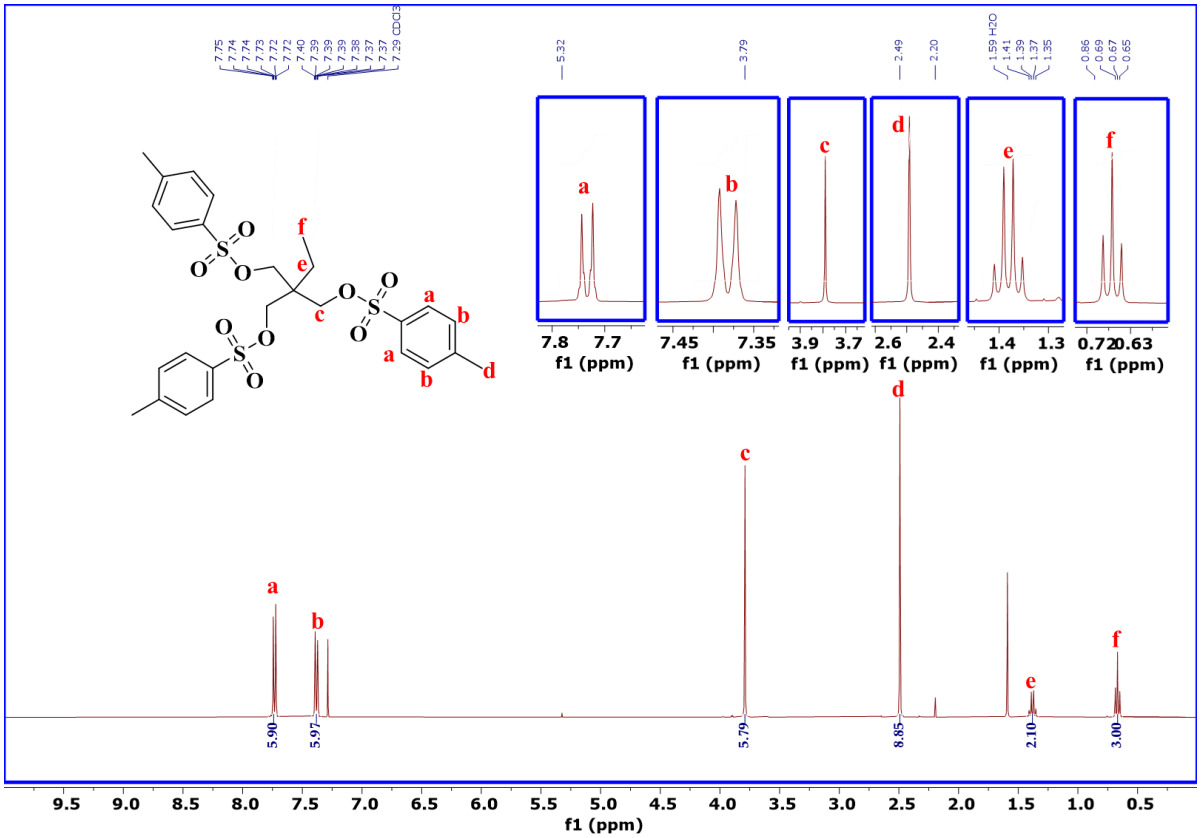

Figure 3.4 ^{1}H NMR Spectrum for M5 in $CDCl_3$. 7.74 (d, J = 8.6 Hz, 6H), 7.38 (d, J = 7.8 Hz, 6H), 3.79 (s, 6H), 2.49 (s, 9H), 1.38 (q, J = 7.6 Hz, 2H), 0.67 (t, J = 7.6 Hz, 3H).

3.2.2 Synthesis of P3 and P4

P3 and P4 were synthesised *via* A_2 + B_3 polycondensation reaction following the proposed synthetic procedures reported by Lu et al.[216] M3 and M4 (difunctionalised monomers, A_2) were polymerised with M5 (tri-functionalised monomer, B_3) in the monomeric ratios of (1.5:1), obtaining hyperbranched polymers P3 and P4 respectively as shown in scheme 3.15. The polymerisation was conducted under N_2 protection, using dry DMF as a solvent and K_2CO_3 as a base (30 eq.). The reaction was conducted over 72 hours at 120 °C and monitored throughout the polymerisation time. At the end of the polymerisation, the residue was precipitated using deionised water, then filtered and dried overnight. The dried solids were dissolved in chloroform and precipitated in methanol, affording polymers P3 and P4 as yellow solids in good yields of 70% and 72% respectively. Both synthesised P3 and P4 using the A_2B_3 approach exhibited good properties. In terms of solubility, both P3 and P4 showed very good solubilities in common organic solvents such as (chloroform, DCM, THF and toluene) as opposed to the poor solubilities of P1 and P2, which means that the gelation point was overcome. Moreover, the prevention of internal cyclisation reaction, and gaining excellent control of topological

structure were achieved compared to the synthesised P1 and P2 which were prepared via the AB_2 approach of polycondensation in chapter 2. The good solubility of P3 and P4 should be beneficial in the fabrication of devices as their solution processability should enable the deposition of uniform films.

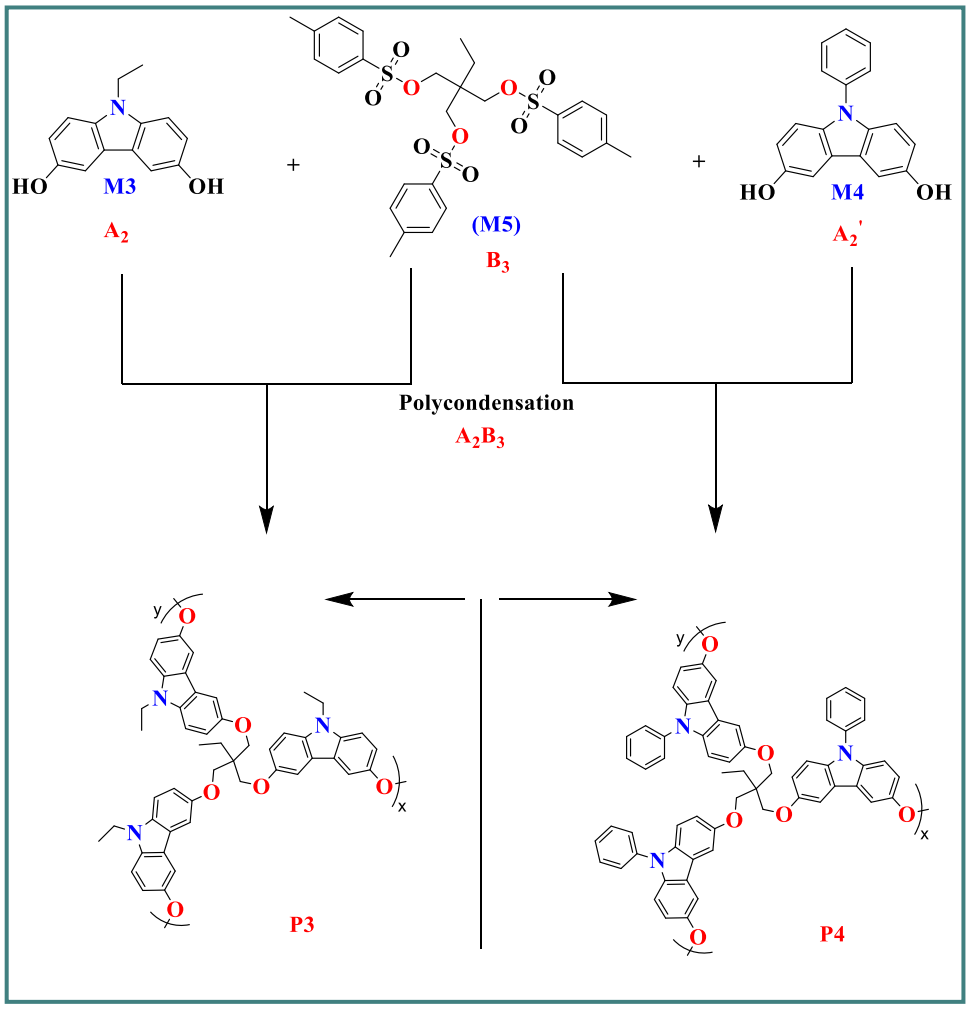

Scheme 3.15 Synthesis of P3 and P4 via $A_2 + B_3$ approach. P3 was prepared using M3 (A_2) as a donor with M5 (B_3) as a central core. While P4 was prepared using M_4 (A_2') as a donor with the same central core (B_3). The central aliphatic alkyl chains play a crucial role in terms of increasing both polymers's solubility. The selection of 4-toluenesulfonyl chloride in the core as a terminal groups is favoured as they considered as a good leaving groups.

The characterisation of P3 and P4 using ^{1}H NMR confirmed the success of the preparation of both polymers. Broad aromatic peak between 7.97 - 6.67 ppm assigned to (Ar-CH) protons were observed for P3. Peaks for the (O-CH_2) and (N-CH_2) protons were observed as two broad peaks at 4.71 ppm and 4.06 ppm respectively. Furthermore, a broad peak was observed at 1.89 - 1.49 ppm corresponding to (-CH_2-) protons, as well as a broad peak at 1.18 - 0.78 ppm for the (-CH_3) protons (see appendix, figure 8.21). The structure of P4 was also confirmed through

^{1}H NMR analyses. The spectrum of P4 revealed broad peaks at 8.39 - 6.59 ppm (Ar-CH), 4.71 - 4.04 ppm (N-CH_2), 4.0 - 3.59 ppm (O-CH_2), 1.98 - 1.57 ppm (-CH_2-) and 1.18 - 0.77 ppm assigned to (-CH_3) (see appendix, figure 8.22).

3.2.3 Molecular Weights of P3 and P4

The Mn, Mw and PDI for P3 and P4 were determined *via* the GPC, using polystyrene standards, THF as a solvent and toluene as a marker. The obtained Mn values for P3 and P4 were found to be 8500 Da and 11700 Da respectively as shown in table 3.1. The Mw values were measured as 13500 Da and 16200 Da respectively. From the obtained results, it can be seen that P4 possesses a slightly higher Mn value compared to that of P3. The PDI values were calculated at 1.6 for P3 and 1.4 for P4, the slight difference in PDI was attributed to a slightly high distribution of P3. In comparison, P3 and P4 exhibited lower PDI values compared to P1 and P2. The difference between these PDI values and the high PDI values obtained for P1 and P2, prepared using AB_2 approach could probably be linked to the side reactions in the preparation of P1 and P2 land their lower solubities.[223]

As the two polymers were synthesised *via* the $A_2 + B_3$ approach, high molecular weights can be expected compared to the preparation of P1 and P2 which were synthesised using AB_2, and which provided lower molecular weights. The degree of branching can be controlled by controlling the internal reactions between monomers, which limits the inter-molecular cyclisation and prevents the gelation point from occurring[176], which can be avoided by end-capping the polymerisation.

Table 3.1 GPC data of P3 and P4

Polymers	Mn(Da)	Mw(Da)	PDI	Yield	Fraction
P3	8500	13500	1.6	70%	Chloroform
P4	11700	16200	1.4	72%	Chloroform

3.2.4 Thermal Properties of P3 and P4

Investigation of the thermal stabilities of P3 and P4 were undertaken using thermal gravimetric analyses under nitrogen atmosphere at heating rate of (10°C min^{-1}). The thermal degradation of P3 and P4 were estimated based on the thermal degradation curves. As shown in figure 3.5, P3 exhibited a good thermal stability up to 364 ^{0}C, as the sample weight remained constant

with the increase of temperature. At 365 ^{0}C, the polymer started degrading thermally with a drop in the polymer sample weight.

Table 3.2 Thermal data of P3 and P4.

Polymers	Td (˚C)
P3	365
P4	217- 409

In comparison, P4 was revealed to be less thermal stability than P3 by showing multiple thermal degradations. With increasing the temperature the polymer started degrading dramatically with losing sample's weight of 7% by reaching 95 ^{0}C. Further gradual degradation was observed between 217 ^{0}C- 409 ^{0}C by losing about 10 % of the sample weight. The low thermal stability of P4 could be attributed to the increase of branching in the polymeric backbone[224], which affect the thermal stability of polymer.

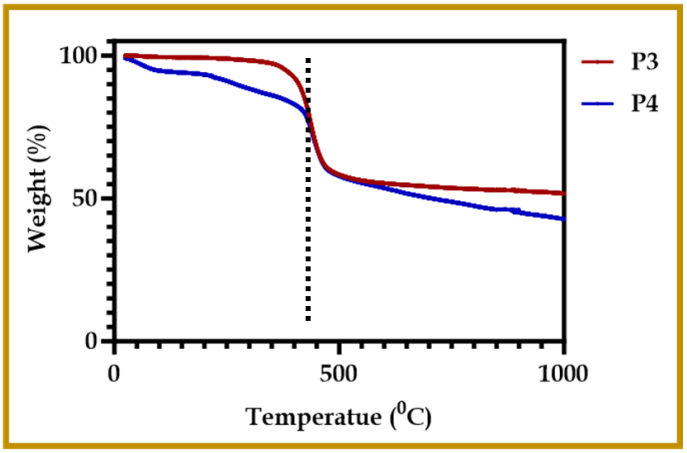

Figure 3.5 TGA analysis of P3 and P4. Both P3 and P4 showed relatively good thermal stability proportionally with increasing the temperature. However, P3 showed better thermal stability as the polymer's weight was not affected from 0 ºC to ~ 365 ºC compared to P4.

3.2.5 Optical Properties of P3 and P4

The optical properties of P3 and P4 were investigated *via* UV-Vis spectroscopy in solution of dilute samples in toluene and in thin films. Both P3 and P4 exhibited two absorptions at short and long wavelengths in solution and in net film as well. In the solution, P3 and P4 showed maximum absorption at 369 and 372 nm respectively, whilst in the film thin at 375 and 378 nm respectively. The short and long wavelengths observed in figure 3.6 (a), correspond to π-π* transitions and n- π* transitions of the carbazole moieties on the polymers' framework. P4

showed more red-shifted absorption compared to the P3. This is due to electron delocalisation from the carbazole to the phenyl group in P4 which leads to a red-shifted absorption.[225]The optical band gaps for both P3 and P4 were calculated from the maximum absorption onset in the film to be 3.08 eV and 2.95 eV respectively. The optical band gap of P4 is lower than the optical band gap of P3. The smaller band gap attributed to the decrease of HOMO - LUMO separation due to the effect of electron delocalisation on carbazole repeat units in P4, and probably to increased aggregation between n-phenyl-carbazole units on the polymer.

Table 3.3 Optical data of P3 and P4 in (a) solution and in (b) thin film. PL data of P3 and P4 in (c) solution and in (d) thin film. (e) Error in the range at the maximum of the absorbance curve for different extinction coefficients. The optical band gap P3 and P4.

Polymers	$\lambda_{abs\ (a)}$ Solution (nm)	$\lambda_{abs\ (b)}$ Film (nm)	λ_{Onset} thin film (nm)	$\lambda_{em\ ©}$ Solution (nm)	$\lambda_{em\ (d)}$ Film (nm)	$E_{g\ opt}$ (eV)
P3	369	375	402	411.6	426.5	3.08 ± 0.003 [(e)]
P4	372	378	420	382.5	415.5	2.95 ± 0.005[(e)]

The PL spectra of P3 and P4 were measured in both solution (dilute in toluene) and in solid state (thin film). The emissions of P3 and P4 were obtained in solution to be 411.6 nm and 382.5 nm, while in film were obtained to be 426.5 nm and 415.5 nm respectively, see figure 3.6 (b). It can be noticed from the figure 3.6 (b) below, P4 showed more blue shifted emission in solution compared to the P3 which revealed more red shifted emission by 29 nm, this is due to the effect of weak electron withdrawing (phenyl substituents) which decrease the number of emitted photons from S_1-S_0 by increasing the inter-system crossing from S_1-T_1, leading to decrease of fluorescence. P3 presented the longest emission in film at 426.5 nm compared to the P3 that observed less red shifted emission by 11 nm, this is attributed to the presence of electron donating group (ethyl substituents). It is widely believed that electron-donating groups have a role in stabilising positive charges on the nitrogen atom and promoting conjugation. As a consequence, there is a reduction in the energy gap between π-π* or n- π*orbitals, leading to a shift in absorption towards longer wavelengths.[226] The broadness of the emission peak of P4 in film could be attributed to the presence of multi states of vibration and rotation in both ground and the excited states in the polymer.[226]

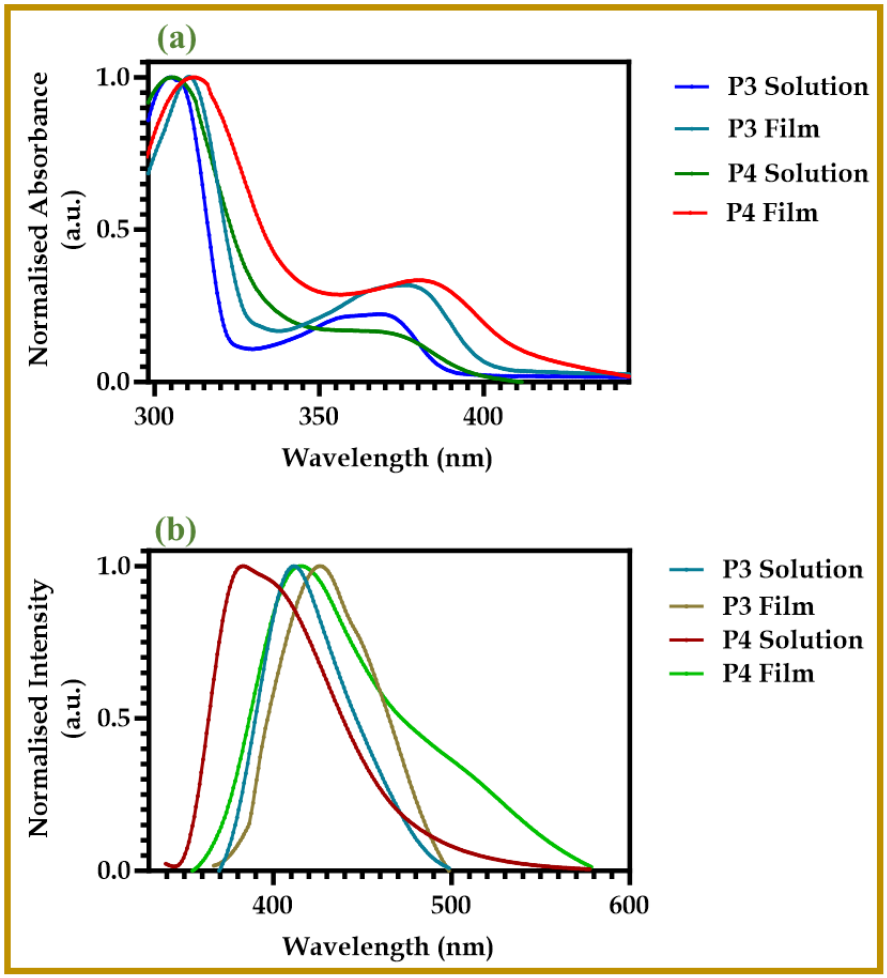

Figure 3.6 (a) Normalised UV vis absorption spectra of P3 and P4 in solution and film.(b) Normalised PL emission spectra of P3 and P4 in solution and film. In terms of the UV-vis spectra, P3 exhibited a shorter wavelength (blue shift) in both solution and film, while P4 exhibited a longer wavelength (red shift) in both solution and film. In the PL spectra, P3 exhibited a bathochromic shift in both solution and film, while P4 exhibited a hypsochromic shift in both solution and film.

3.2.6 Electrochemical Properties of P3 and P4

The electrochemical properties of P3 and P4 were investigated using cyclic voltammetry, the HOMO level for each P3 and P4 were calculated from the onset of the first oxidation curve, while the LUMO levels were calculated from the onset of the first reduction curve.

Table 3.4 CV data of P3 and P4, (a) HOMO and (b) LUMO level values.

Polymers	HOMO (eV)[a]	LUMO (eV)[b]
P3	-5.14	-2.06
P4	-5.18	-2.23

HOMO values were obtained from the anodic (oxidation) curve onset, whereas the LUMO values were calculated from the difference between the HOMO and the optical band gap values.

The HOMO values for P3 and P4 were calculated to be -5.14 and -5.18 eV, whilst the LUMO values were calculated by deducting the optical bandgap (Eg) values of both polymers from the HOMO values to be -2.06 and -2.23 eV respectively, (the substantial LUMO value exhibited by P4 is adequate to block the flow of electrons from the host to the hole-transporting layer in the OLED).[227] It must be noted that the onset of reduction is not clearly defined and as a result there is limited confidence in the values presented. P4 showed a similar HOMO energy level to that of P3

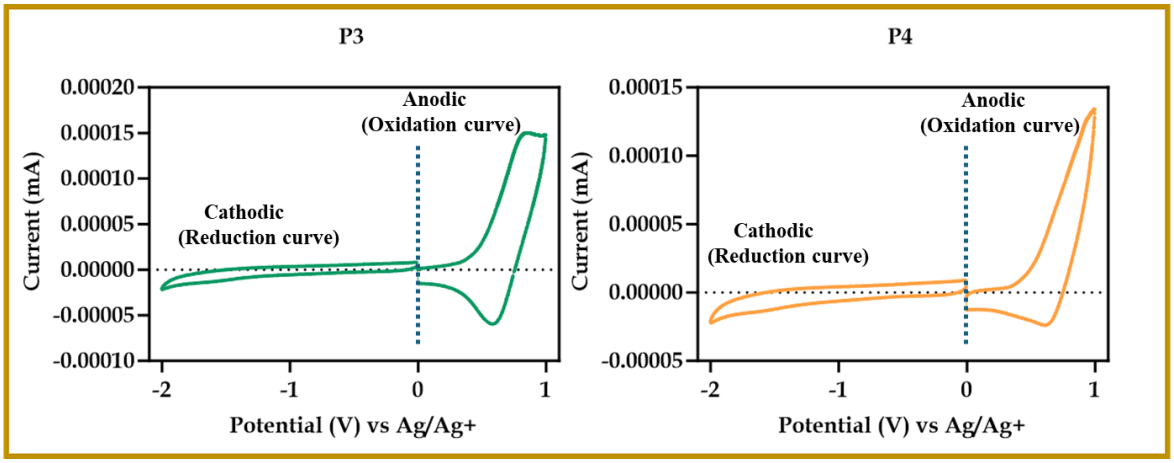

Figure 3.7 The CV analysis of P3 and P4. Each P3 and P4 showed oxidation and reduction peaks, the HOMO values of both polymers were calculated from the oxidation peak onset. However, the reduction curve onsets of both polymers could not be measured, so the LUMO values were calculated from the HOMO values and the optical band gap values.

3.3 Conclusion

Design and control HBPs via $A_2 + B_3$ for OLEDs has notably exhibited great properties, making this approach more desired and favourable to synthesis numerous HBPs. The limitation of internal cyclisation interaction, preventing the gelation point and achieve good control of polymerisation are required to obtain HBPs with ideal properties such as high molecular weights, less viscosity, good thermal properties, exhibiting desired solubility in common solvents, less molecular aggregations. P3 and P4 were designed and controlled using $A_2 + B_3$ approach of polycondensation. The characterisation showed that both P3 and P4 exhibited ideal properties compared to the design P1 and P2 which were synthesised in chapter (1) via AB_2 approach, where the low yields, low molecular weight and low thermal stability were observed. These due to the effect of internal cyclisation interactions which took place during the polymerisation. In contrast. P3 and P4 showed excellent solubility in common organic solvents such as chloroform, DCM, toluene and THF. P3 and P4 were obtained in high yields of 70% and 72% with desired Mn values of 8500 Da and 11700 Da respectively. In terms of thermal properties, both P3 and P4 exhibited good thermal resistance with increase of the temperature, especially P3 which showed just one degradation stage at 365 ^{0}C compared to P4. Therefore, these polymers can be used in the device fabrication as they showed more solution processability and good thermal stability. In terms of optical characterisation, both P3 and P4 displayed more red-shifted absorptions in thin film at 375 nm and 378 nm than in solution with calculated optical band gaps 3.08 eV and 2.95 eV respectively. The CV measurements revealed that both P3 and P4 showed similar HOMO levels.

Chapter 4: Synthesis and Design of TADF Hyperbranched Polymers Based on Carbazole Derivatives for OLED Applications

Abstract

The use of TADF polymers in electroluminescent devices has garnered considerable attention owing to their distinctive characteristics (completely modifiable, thermally stable, 100% internally quantum efficient TADF polymers, narrow bandgap and free heavy metals). By employing the side-chain engineering approach, a number of highly efficient copolymers were synthesised and enhanced, incorporating TADF units in varying portions. The successful incorporation of the green (TADF) emitter, PXZ-TRZ, into polymers, was achieved through the utilisation of Suzuki polycondensation. The backbone of the copolymer consisted of non-conjugated 1,3,5-tris((6-phenoxyhexyl)oxy)benzene and partially conjugated derivative units of carbazole. P5, one of the synthesised polymers, was specifically synthesised using TADF-free moieties in order to facilitate a comparative analysis. The photophysical, thermal resistance and electrochemical behaviour of the synthesised polymers have been investigated. All of the designed polymers were highly soluble in common organic solvents, making them excellent options for the emitting layer of solution-processed polymers used in OLEDs. Moreover, P5-P8 exhibited close optical band gap values (ranging from 3.28 eV to 3.21 eV); this characteristic can be ascribed to the materials' non-conjugated states. Excellent thermal stability is exhibited by all polymers from 5-8 at degradation temperatures exceeding 251 °C. The incorporation of TADF units in the polymers' sidechains with different ratios of 5%, 10% and 20%, increased the thermal stabilities of these polymers from P5 > P6 > P7 > P8. The gedradting temperatures of these polymers were observed to 251 °C, 332 °C, 359 °C and 375 °C respectively.

4.1 Introduction

OLEDs have experienced rapid growth as a result of the increasing commercial interest in their potential as next generation displays and lighting sources. The principal organic emissive materials used in OLEDs have rapidly progressed over the past few years, from fluorescent materials to phosphorescent and, most recently, to TADF materials.[228-231] The new generation of materials with TADF characteristics can turn triplet excitons into singlet excitons, resulting in about 100% exciton utilisation efficiency (EUE), (25% of singlet excitons plus 75% of triplet excitons via the RISC) without using any heavy-metal components as used in the phosphorescent (second generation of OLEDs).[59, 232, 233]

There have been recent impressive developments in cutting-edge OLED technologies utilising TADF materials. In OLED devices, for specific examples, 12.5%, 19%, and 28.6% of the external quantum efficiencies (EQEs) of the red emitter (D-Ph-A-Ph-D-type molecule), blue emitter (DMAC-DPS), green emitter (4CzIPN) have been achieved.[7, 73, 234] These devices were made using evaporation deposition techniques such as chemical vapour deposition (CVD), but such approaches require complex designs, higher costs, and precise control. A solution-processing approach is a more effortless, cost-effective, and easily regulated option when compared to alternative manufacturing processes, as well as providing the capability to produce devices on a large scale. Solution processing is inappropriate with the vast majority of published TADF dopants, which are fundamentally small molecules. This is due to the difficulties in making films with small molecules using solution processing. As a result, it is crucial to develop organic emissive materials that can be processed in a solution and possess TADF properties.[90, 121, 124, 235, 236]

Fabrication of efficient devices through solution-processing requires materials with enhanced properties. This can be achieved through the utilisation of soluble polymeric materials, with excellent emissive properties.[186, 237] Nevertheless, since the non-radiative decay mechanism induces the deactivation of 50–75% of triplet excitons, the decreased EUE in the EL process limits the performance of conventional polymer-based devices to some degree.. As a consequence; devices constructed using these polymers exhibit singlet and triplet ratios ranging from 1:1 to 1:3.[238-241] Consequently, increasing the EUE of a polymeric material may be possible through the use of a TADF mechanism comprised of metal-free organic emissive materials.

Amongst π-conjugated polymers that exhibited high quantum yield, polycarbazoles have shown remarkable characteristics.[242] Carbazole-based polymeric hosts exhibit distinctive characteristics compared to other π-conjugated polymers due to their notable attributes, including a reduced redox potential and an intense absorption capacity within the near-UV range of the spectrum. Consequently, extensive research has been dedicated to investigating the electrochemical and spectroscopic characteristics of carbazole and its derivatives. They can be used as functional units for incorporation into organic molecules due to their advantageous chemical, electrical, and optical properties. Moreover, they sustain hole transport layers and emit light in OLEDs.[243-245] Additionally, they function as host materials in phosphorescent OLED applications and as active components in solar cells.[246] The inclusion of carbazole units within the structure of organic molecules additionally enhances their resistance in terms of thermal stability.

Yeng et al.[124] effectively synthesised blue and blue-green TADF polymers PCz0, PCz3, PCz6, PCz9, and PCz12 by grafting 10-(4-(5-phenyl-1,3,4-oxadiazol-2-yl)phenyl)-10H-phenoxazine, a TADF emitter, into the backbone of polycarbazole as illustrated in scheme 4.1 below. The carbazole monomer units in the polymers above are linked through their 3,6-positions along the polymer backbones owing to its high triplet energy (2.6 eV) and its excellent hole-carrying ability; in this role, it only serves as the host and charge-transporting material. The grafted units perform additional functions that are not influenced by the electronic properties of the polymer backbone. The above polymers PCz0-PCz12 were designed using three monomers, as shown in the scheme below, with different ratios incorporated. The success of synthesis was verified once the ^{1}H NMR analysis integrated the total number of protons. The molecular weights of the designed polymers PCz0, PCz3, PCz6, PCz9, and PCz12 were calculated to be 5329 Da, 7358 Da, 5530 Da, 6273 Da and 5806 Da respectively. Furthermore, the photoluminescence quantum yield of fluorescence (PLQY) in the solid state for the designed polymers PCz3, PCz6, PCz9, and PCz12 were obtained to be 27.5%, 27.2%, 33.6% and 33.7% respectively. Moreover, polymers from PCz3- PCz12 exhibited 1.2%, 1.1%, 4% and 4.3% respectively in terms of the maximum EQE of non-doped OLEDs,

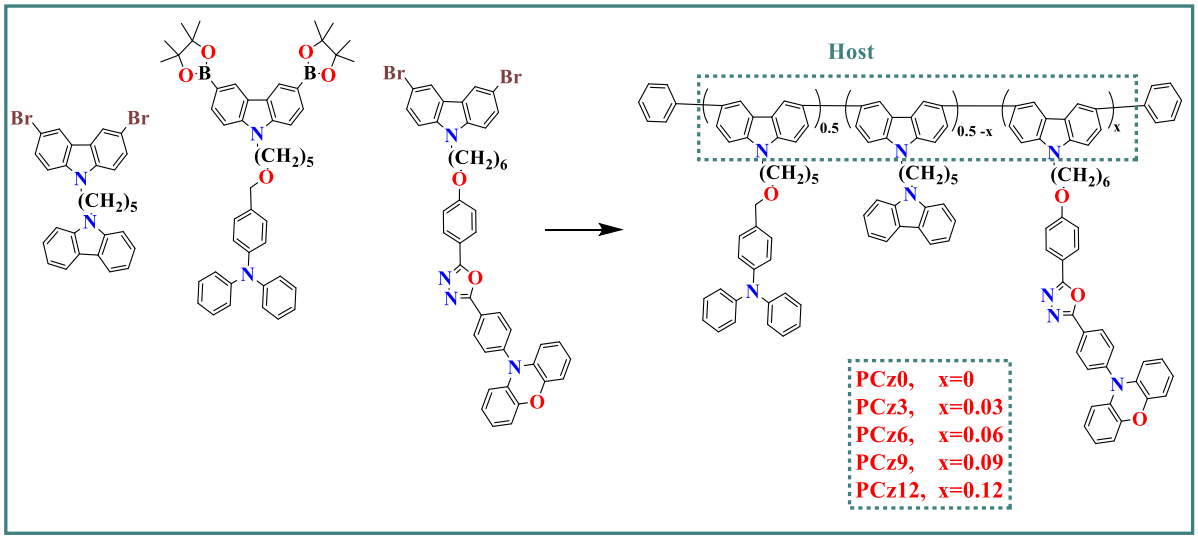

Scheme 4.1 Design of green TADF copolymers by Yeng et al. Five polymers have been prepared using a polymer sidechain strategy. The polymer sidechains have been grafted with different ratios of the TADF emitter (0%, 0.03%, 0.06%, 0.09% and 0.12%). Grafting the TADF emitter as a sidechain with different ratios was applied to investigate the polymers' properties, such as the thermal, optical and electrochemical properties.

4.2 Results and Discussion

A series of green emitting hyperbranched polymers with TADF properties were designed and investigated in this chapter. Side-chain engineering strategy was applied using conjugated and non-conjugated molecules as a polymer main chain. Moreover, the polymer was grafted withsidechains with a green emitting TADF dye (TRZ-PXZ) containing phenoxazine moiety as donor and with a triazine moiety as an electron acceptor. Utilising only non-conjugated molecules in this approach is aimed at a reduced electronic conjugation in these systems so as to obtain a carbazole framework with a high triplet state energy. The carbazole repeat units are substituted with ethyl substituent to improve solubility.

The choice of the carbazole moieties in M2 as a host can be explained by its exceptional ability to transport holes and its possession of a high triplet energy state, measuring 3.05 eV. This energy state is significantly greater than the E_T of the TADF emitter PXZ-TRZ. The purpose of this is to prevent the phenomenon of triplet energy back-transfer from the TADF emitter to the host material, while also maximising its ability to efficiently transport holes. Because of the high steric hindrance caused by the CBz host in M2, the triplet energy of the polymer should be similar to that of the carbazole repeat units in view of a lack of electronic delocalisation in the final hyperbranched polymers. In order to disturb the conjugation system of the polymer

backbone, 1,3,5-tris((6-phenoxyhexyl)oxy)benzene from M6 was introduced into the polymeric backbone of M2 which includes saturated hexamethylene segments.

PXZ-TRZ in M7 was used as a guest (TADF emitter) in this work. Commonly used as an OLED TADF dye. It's utilised in OLEDs to create active layers using *vacuum* thermal evaporation. The *vacuum* thermal evaporation technique is a specific method of dry deposition utilised in the production of OLEDs. The process referred to as the physical vacuum deposition method is widely employed for commercial purposes. The substrate is coated with organic molecules in the gaseous phase. The organic compounds are placed into a crucible, while the substrate is maintained at a specific distance from the crucible. A consistent temperature differential remains preserved between the substrate and crucible within the vacuum chamber, which has a considerably reduced pressure ranging from 10^{-5} to 10^{-7} torr. By increasing the temperature of the crucible, solid organic substances convert to gaseous form. This technique is classified into three distinct categories based on the evaporation source, substrate, and distance between them: point evaporation source, linear evaporation source, and planar evaporation source.[247] The deposition technique offers the following benefits: this deposition technique deposits complex or multilayer constituents of various materials. Furthermore, the layer thickness can be precisely controlled through the utilisation of masks. Furthermore, it is an inexpensive and straightforward deposit method. Additionally, it offers higher efficiency and a lengthy lifetime. This deposition method has a significantly reduced possibility of contamination and impurity compared to others because of its high vacuum chamber system. Nonetheless, the following drawbacks can be identified when employing this method: Organic substances degrade rapidly when exposed to high temperatures due to their high thermal sensitivity. Additionally, eliminating deposited organic materials by scaling is a difficult process. An additional drawback of employing this technique is the relatively low yield of materials, with the residual organic substances being discarded during the deposition process.[248, 249] In contrast to *vacuum* thermal evaporation, solution processing techniques, including spin coating and spray coating, offer several benefits. To facilitate the implementation of this strategy, the TADF unit was grafted into the side chains of polymer backbones.

All Monomers M2, M6 and M7 illustrated in scheme 4.2 below, were polymerised with different ratios via Suzuki polycondensation, yielding the desired polymers P5 in the ratio of (50:50:0), P6 (45:50:5), P7 (40:50:10) and P8 (30:50:20) respectively. P5 was designed with no feeding of M7 (TADF) in comparison with other designed polymers P6 – P8, which grafted

with different ratios of M7 (TADF moiety). The structural verification of the yellow-green hyperbranched polymers P5 - P8 was conducted using ^{1}H NMR analysis. All designed polymers P5 – P8 have been investigated in terms of the polymer's molecular weight and solubility in common solvents such as DCM, Chloroform and THF. Moreover, characteristics such as thermal resistance, photophysical properties and electrochemical behaviours were also examined and investigated.

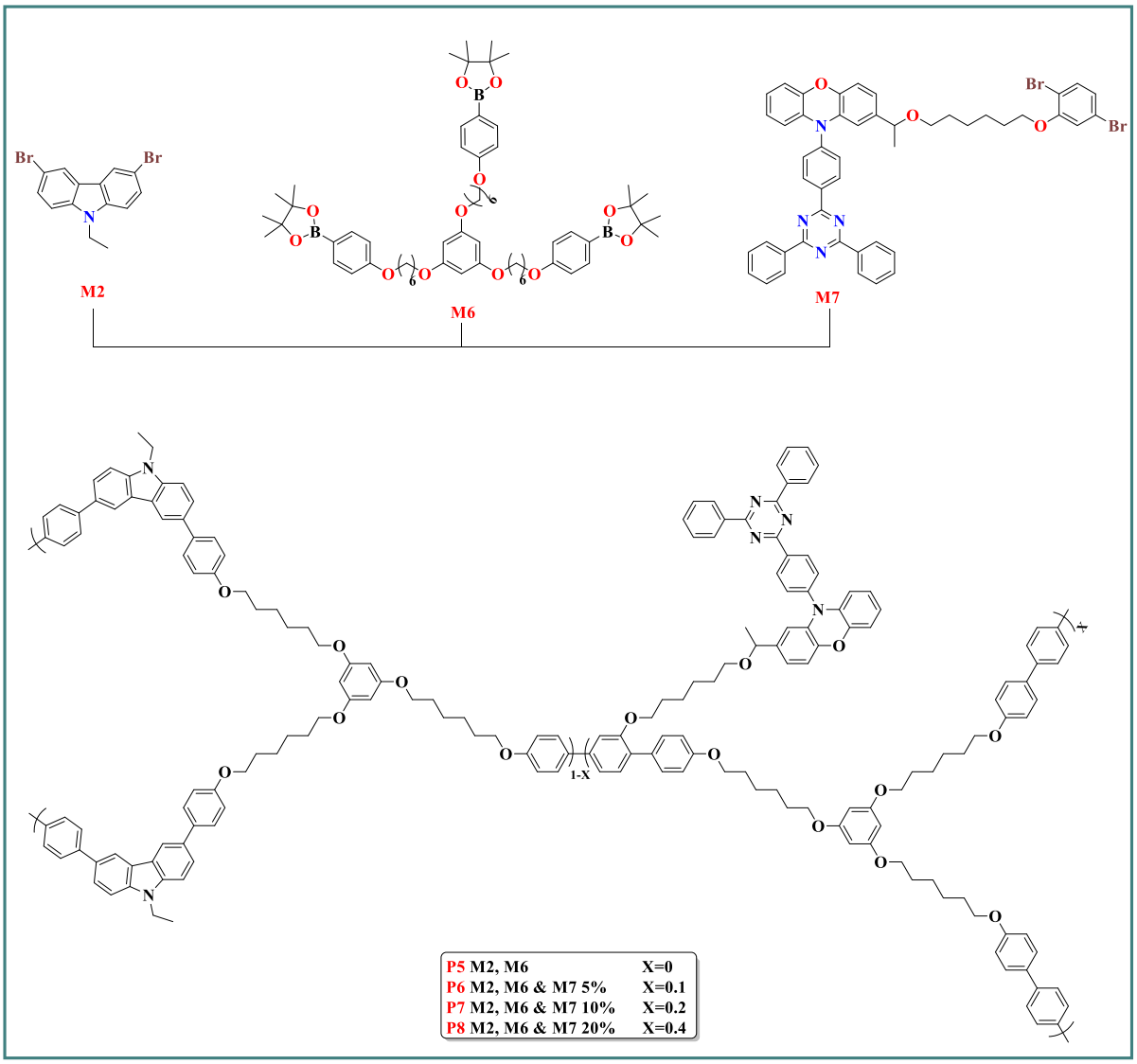

Scheme 4.2 Design of yellow-green TADF hyperbranched polymers P5 – P8. Four hyperbranched polymers were prepared using different molar ratios of M2, M6 and M7. P5 was prepared using the ratio of (50:50, M2:M6), while the polymer from P6 – P8 were prepared using the ratio of (45, 50, 5), (40, 50, 10) and (30, 50, 20) of the selected M2, M6 and M7 respectively. Reagents and conditions; THF, Sat.$NaHCO_3$, $Pd(OAc)_2$, $P(o\text{-}tol)_3$, K_2CO_3, 24h, Reflux.

4.2.1 Synthesis of monomers

4.2.1.1 Synthesis of M6

Three synthetic steps were carried out to obtain M6 using phloroglucinol as the starting material (see scheme 4.3). The different steps are outlined in the scheme together with reaction conditions.

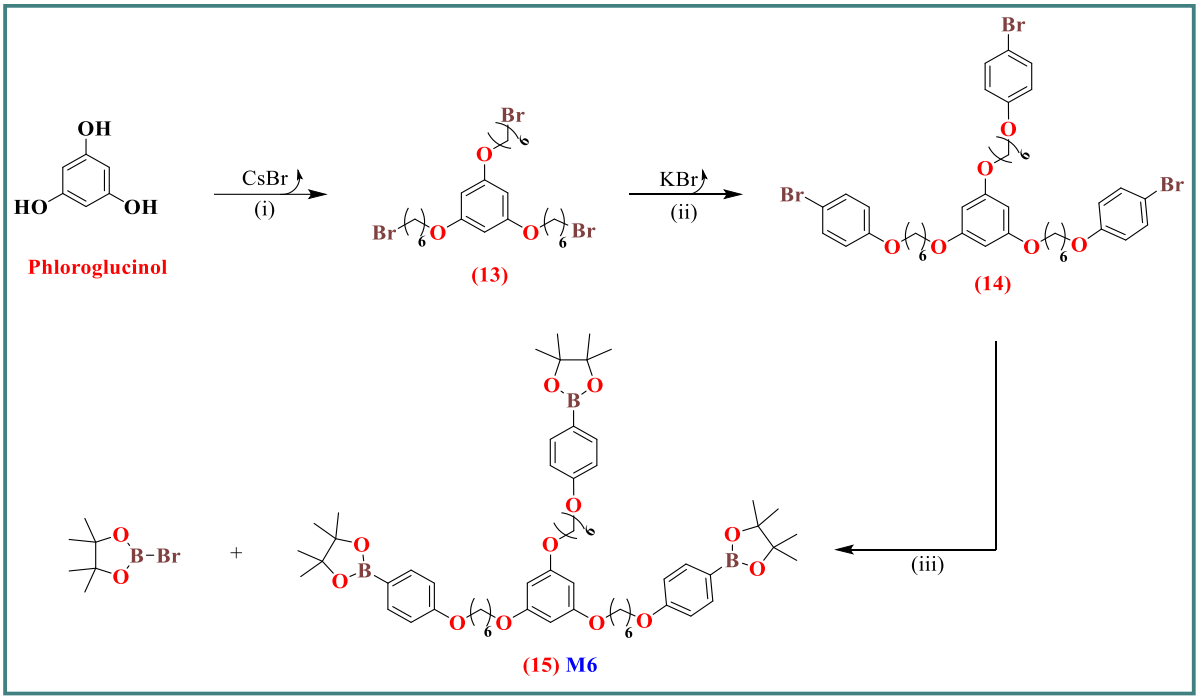

Scheme 4.3 Monomeric steps to prepare M6. The preparation of 1,3,5-tris((6-(4-(4,4,5,5-tetramethyl-1,3,2-dioxaborolan-2-yl)phenoxy)hexyl)oxy) benzene was carried out within three synthetic steps as illustrated in the scheme above. Reagents and conditions; (i) 1,6-dibromohexane, DMF and $CsCO_3$. (ii) 4-bromophenol, butanone, 18-Crown-6, K_2CO_3, reflux. (iii) DMF, $Pd(dppf)Cl_2$, CH_3CO_2K, bis (pinacolato) diboron, 100 ^{0}C.

Product (13) was obtained after purifying the crude using column chromatography as a dense pale yellow oil with a yield of 66.3% following the synthetic procedures reported by Shi et al.[250] The reaction was conducted under the protection of N_2, at ambient temperature using DMF as a solvent and caesium carbonate as a base, as it can be dissolved in the common polar aprotic solvents such as DMF, DMSO and acetone. Additionally, obtaining products with high yield compared to the ones obtained using potassium and sodium carbonates.

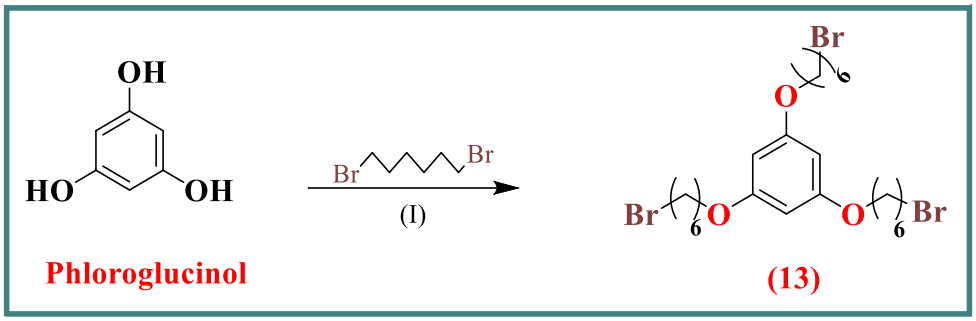

Scheme 4.4 Synthetic conditions of compound 13.Reagents and cnditions ; 1,6-dibromohexane and (I) DMF, $CsCO_3$, room temperature..

The reaction was done through Williamson's ether reaction between aryloxide and the primary alkyl halide. The S_N2 nucleophilic substitution reaction occurred once the nucleophile deprotonated the hydroxy group of the phenolic phenyl ring forming the anion (O^-), which in turn attacked the primary brominated carbon of 1.6-dibromohexane resulting in the elimination of the bromide (good leaving group) to achieve the first step of product (13). the same mechanism was applied twice to obtain the target product (13) as illustrated in scheme 4.5.

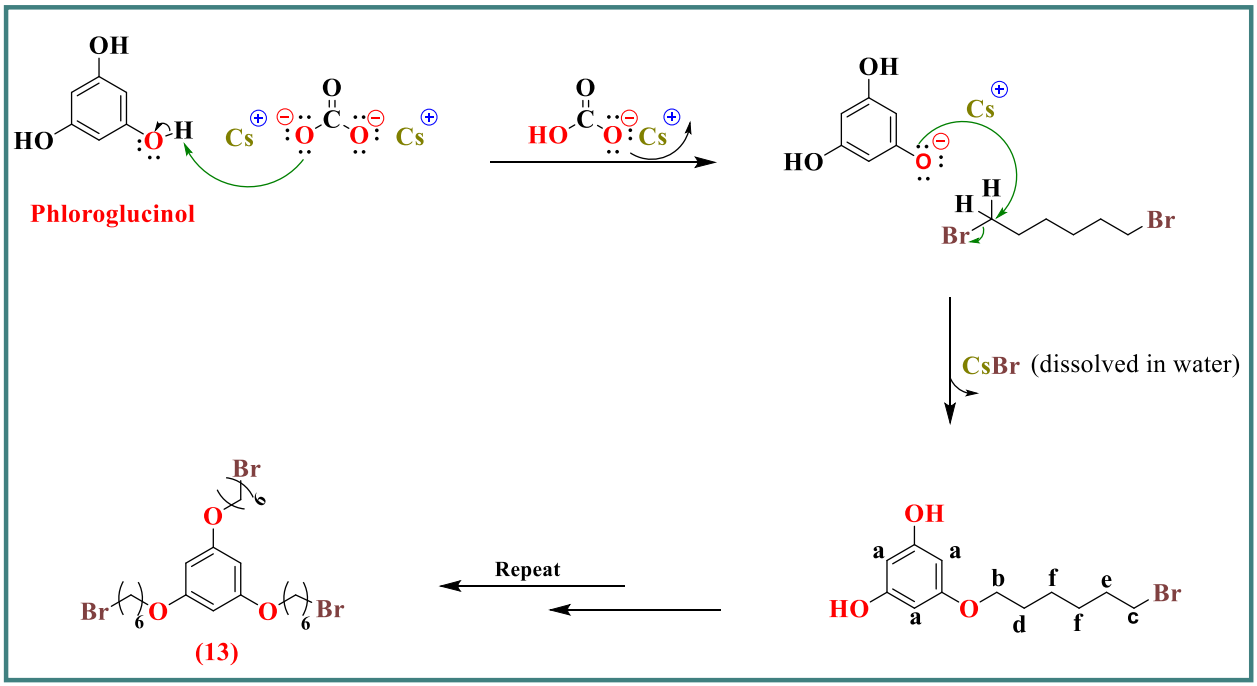

Scheme 4.5 The proposed mechanism of compound 13. The synthesis of 1,3,5-tris(6-bromohexyloxy)benzene was carried out via Williamson's ether reaction, in the prescence of DMF as a solvent and caesium carbonate as a base under the protection of N_2 with respect to other reaction conditions mentioned above.

To confirm the success of the product (12), ^{1}H and ^{13}C NMR were utilised along with mass spectrometry and elemental analysis. The analysis by ^{1}H NMR showed a singlet at 6.08 ppm, assigned to the three protons (a) of the phenyl ring see scheme 4.5. More deshielded triplet was observed at 3.94 ppm, attributing to the six protons (b) attached to the oxygen and a less deshielded triplet was also noticed at 3.45 ppm, corresponding to the six protons (c) attached to the carbon with the bromine substituents. The difference in electronegativity between oxygen and bromine caused the first triplet to be more deshielded due to the high electronegativity of an oxygen atom. A further aliphatic multiplet was observed at 1.97 ppm, attributing to six protons in position (d) of the alkyl chain. Another less deshielded multiplet was observed at 1.85 ppm, corresponding to six protons in position (e) of the methylene chain. As there was not any effect of the electronegativity on the position (f) of the methylene chain, a shielded multiplet was observed at 1.56 ppm, assigned to the 12 protons of the methylene chain (see figure 8.8 in the appendix). Elemental analysis of the product (12) revealed the values of C, 46.55; H, 6.25; Br, 38.69, similar to the calculated values of C, 46.85; H, 6.39; Br, 38.96. In addition, mass spectrometry confirmed the mass of the final product by indicating a value of m/z value of 613.05.

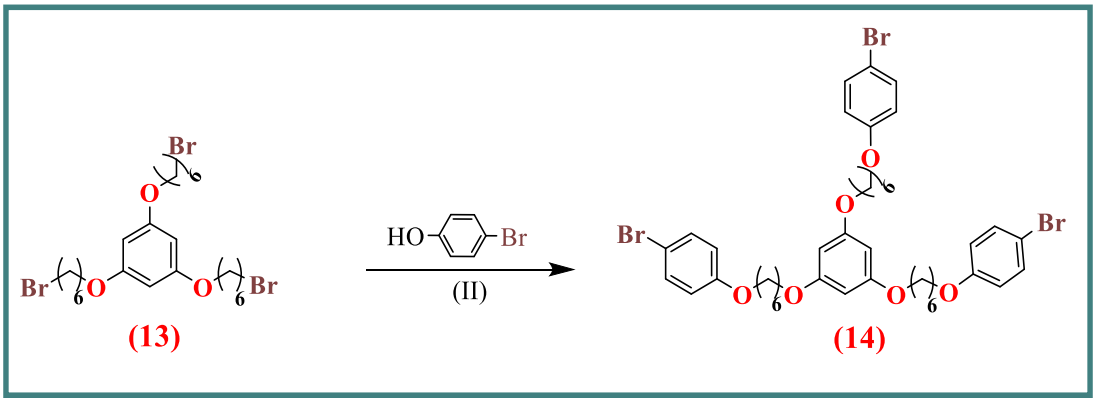

Scheme 4.6 Synthetic conditions of compound 14. Reagents and conditions; 4-bromophenol, (II) butanone, 18-Crown-6, K_2CO_3, reflux.

Compound (14) was synthesised according to a modified synthetic procedure reported by Nithyanandhan et al.[251] The reaction was done under mild conditions at 90 ^{0}C, using the selective solvent 2-butanone, potassium carbonate as a base and 18-Crown-6 as a catalyst. The TLC showed three spots until the completion of the reaction. The final product was successfully afforded as white crystals in a high yield of 94% once the crude was purified *via* column chromatography with the eluent of (Hex/EA) in a ratio of 15 to 1 respectively and recrystallised

finally from ethanol. The reaction mechanism is similar to the mechanism in the synthesis of product (13) which followed Williamson's ether reaction (ether formation) as shown in scheme 4.7. The analysis of compound (14) *via* ^{1}H NMR revealed two new doublets with different shifts in the aromatic region. A more deshielded doublet was observed at 7.38 ppm, corresponding to six protons in the position (e) illustrated in the scheme 4.7 below. The other doublet has been noticed at 6.79 ppm, attributed to the presence of six protons in the position (f). The less electronegativity effect results in more shielded peaks. Additionally, the triplet which was observed at 3.45 ppm in position (c) of the product (13) disappeared, this is due to the elimination of the bromine atoms which possess less electronegativity than the new substituents of oxygen atoms. Hence, the electronegativity increased, allowing both sides of the methylene chain to be chemically equivalent and have the same chemical shift observed at 3.94 ppm which is assigned to 12 protons. Furthermore, the disappearance of the shielded triplet at 1.85 ppm was noticed as the 12 protons in both positions (d) and (e) became chemically equivalent and their presence was assigned by giving a multiplet at 1.88 ppm (see figure 8.9 in the appendix).

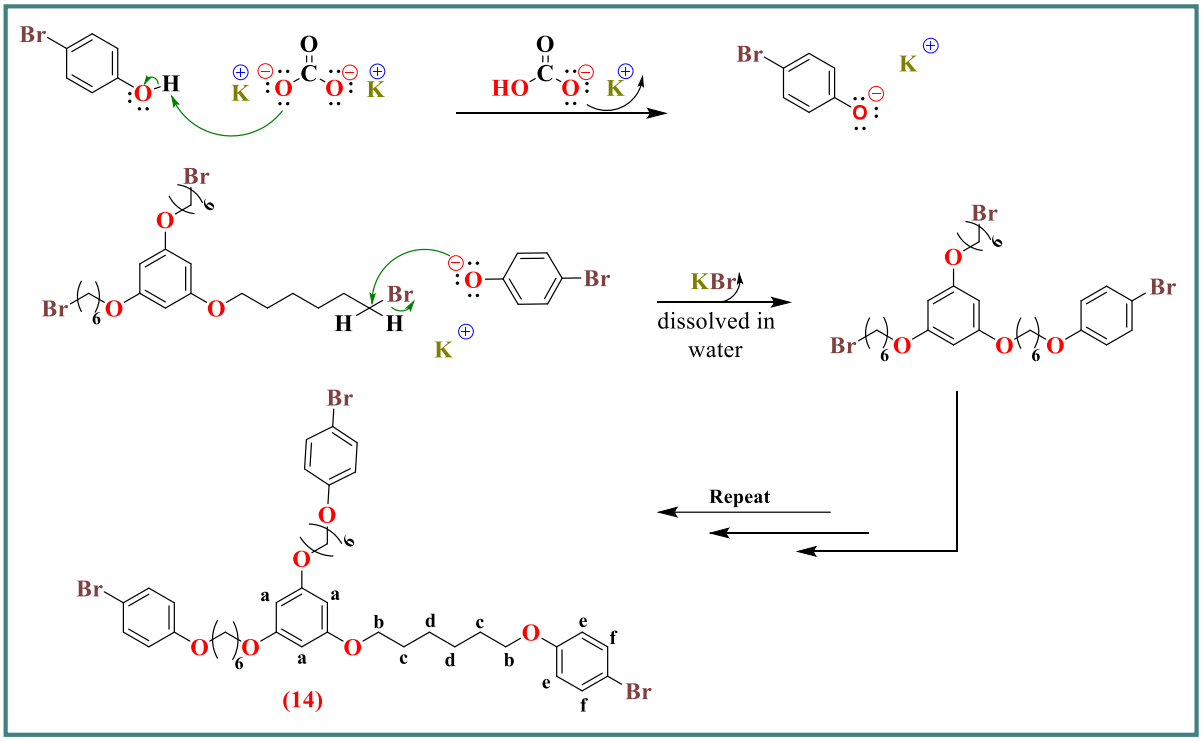

Scheme 4.7 The proposed mechanism of compound 14. The synthesis of 1,3,5-Tris[[6'-(4"-bromophenoxy)hexyl]oxy]benzene was achieved via Williamson's ether reaction (ether formation), using the selective solvent 2-butanone, potassium carbonate as a base and 18-Crown-6 as a catalyst. The reaction was performed under mild condition of temperature (90 ^{0}C) with respect to other reaction conditions mentioned in the scheme above.

Further characterisation was conducted *via* ^{13}C NMR, confirming the structure of product (14) by showing five new peaks at 158.20 (C-O from new phenyl ring), 132.22 (C=C-Br) , 116.31 (C=C-O), 112.64 (C-Br) and 67.81 ppm (C-O) from the alkoxy group. The confirmation of product (14) by the mass spectrometry analysis showed a peak with an m/z value of 889.12, indicating that product (14) has been successfully obtained.

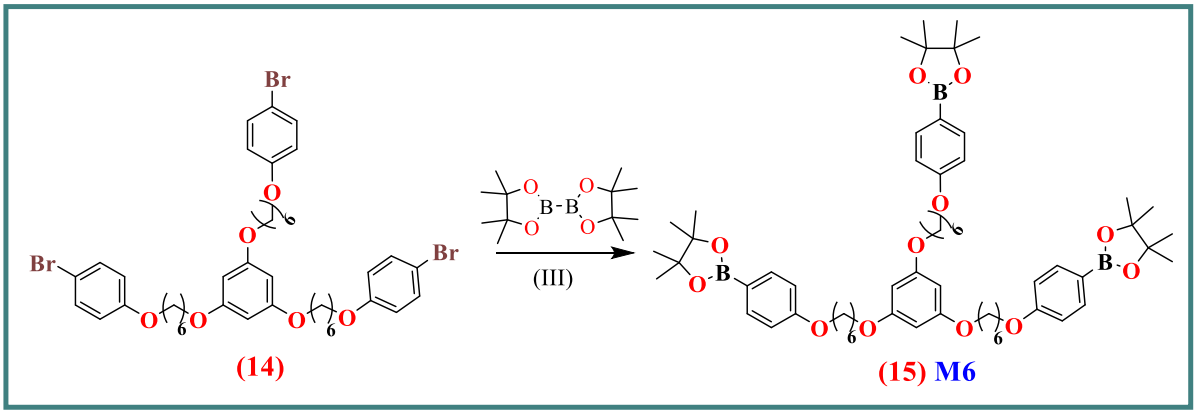

Scheme 4.8 Synthetic conditions of compound 15 M6. Reagents and conditions; Bis(pinacolato)diboron, (III) DMF, $Pd(dppf)Cl_2$, CH_3CO_2K, 100 ^0C.

Product (15) M6 was synthesised following the modified synthetic procedure of cross-coupling reaction suggested by Ishiyama et al.[252] This reaction is catalysed by $Pd(dppf)Cl_2$ and involves the reaction of an aromatic halide with bis(pinacolato)diboron to form an aryl boronic ester. The mechanism for the formation of M6 goes through three steps including oxidative addition of aryl halides, trans-metallation and reductive elimination see scheme 4.9. The boronic ester compound (15) was obtained as white crystals in a yield of 81% after purification of the crude product using column chromatography and recrystallised from methanol. The selection of dimethylformamide (DMF) as the reaction solvent was based on the observation that polar solvents such as (DMSO and THF) can significantly enhance the yield of the coupling reaction, as the nionic transition states can be stabilised for oxidative addition by using polar solvents.[253] The most appropriate base for this reaction was determined to be potassium acetate as the utilisation of other bases with more basicity such as K_3PO_4 or K_2CO_3 could result in more self-coupling reactions of the crude aryl halides. $PdCl_2(dppf)$ was used in this reaction as a catalyst as it is the most widely utilised catalyst class at present owing to its favourable catalytic performance.

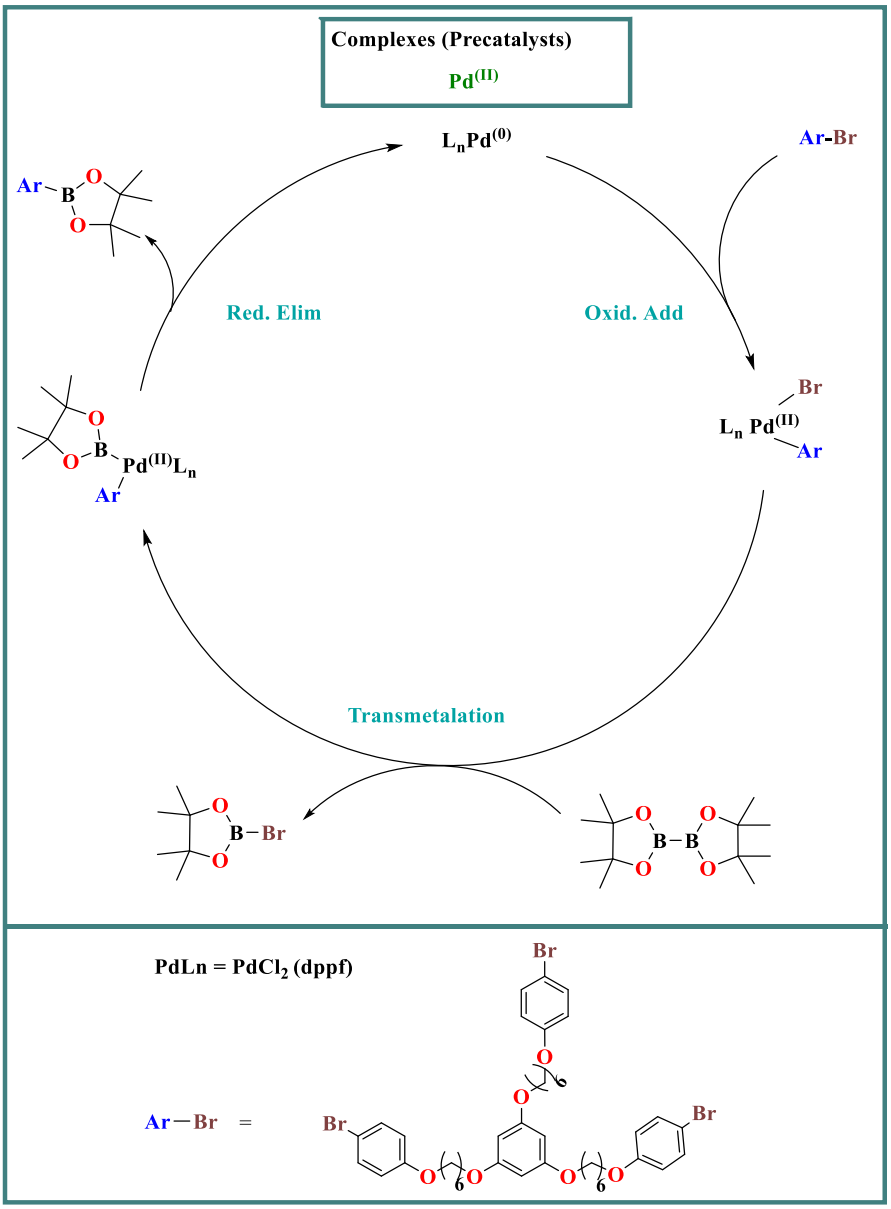

Scheme 4.9 The proposed mechanism for the cross-coupling reaction of compound 14. The formation of 1,3,5-tris((6-(4-(4,4,5,5-tetramethyl-1,3,2-dioxaborolan-2-yl)phenoxy)hexyl)oxy) benzene was carried out under the protection of N2 using DMF as a reaction medium at 100 ^{0}C. The reaction was catalysed by Pd(dppf)Cl_2 and involves the reaction of an aromatic halide with bis(pinacolato)diboron to form an aryl boronic ester in three steps; the oxidative addition of aryl halides, trans-metallation and reductive elimination.

The confirmation of the structure of M6 was achieved *via* ^{1}H NMR, ^{13}C NMR, elemental analysis and mass spectrometry. ^{1}H NMR characterisation showed a new intense aliphatic peak at 1.35 ppm, attributed to the new 36 protons of the terminal twelve methyl groups of the new substituents boronic esters in position (g) as illustrated in figure 4.1 below. The ^{13}C NMR spectrum showed a new peak at 83.52 ppm, corresponding to the ring carbons from the boronic

ester. Further characterisation was carried out *via* the elemental analysis, illustrating the values of C, 69.70; H, 8.55, which closely match the calculated values of C, 69.78; H, 8.49 for M6.

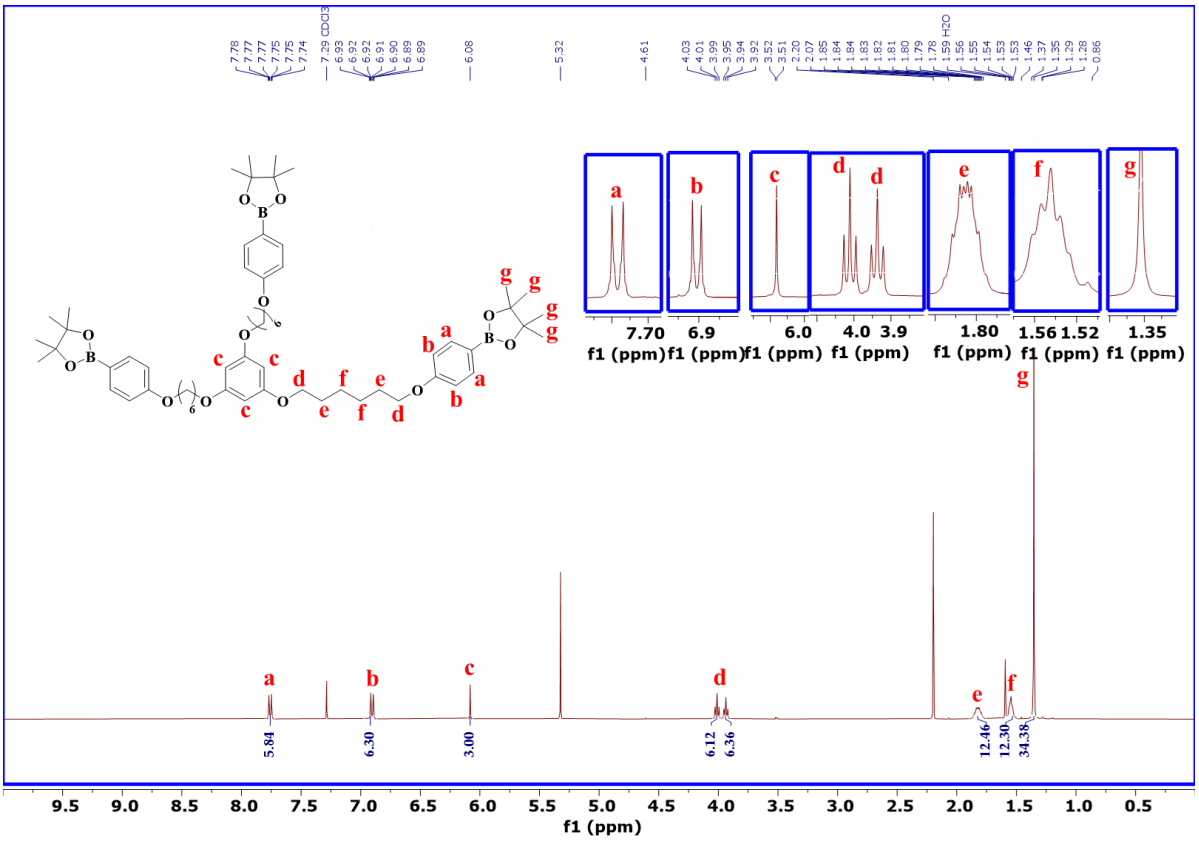

Figure 4.1 ^{1}H NMR spectrum of M6 in $CDCl_3$.; 7.76 (d, J = 9.0 Hz, 6H), 6.91 (d, J = 8.2 Hz, 6H), 6.08 (s, 3H), 4.01 (t, J = 6.5 Hz, 6H), 3.94 (t, J = 6.4 Hz, 6H), 1.89 – 1.76 (m, 12H), 1.58 – 1.49 (m, 12H), 1.35 (s, 36H).

4.2.1.2 Synthesis of TADF Emitter M7

The TADF (M7) monomer was prepared through nine synthetic steps as shown in scheme 4.10. Three starting materials namely 10*H*-phenoxazine, cyanuric chloride and 2.5-dibromophenol respectively were used in the synthesis of the target monomer as illustrated in the scheme below. The various conditions and different reaction mechanisms for the synthesis of the TADF monomer are discussed below.

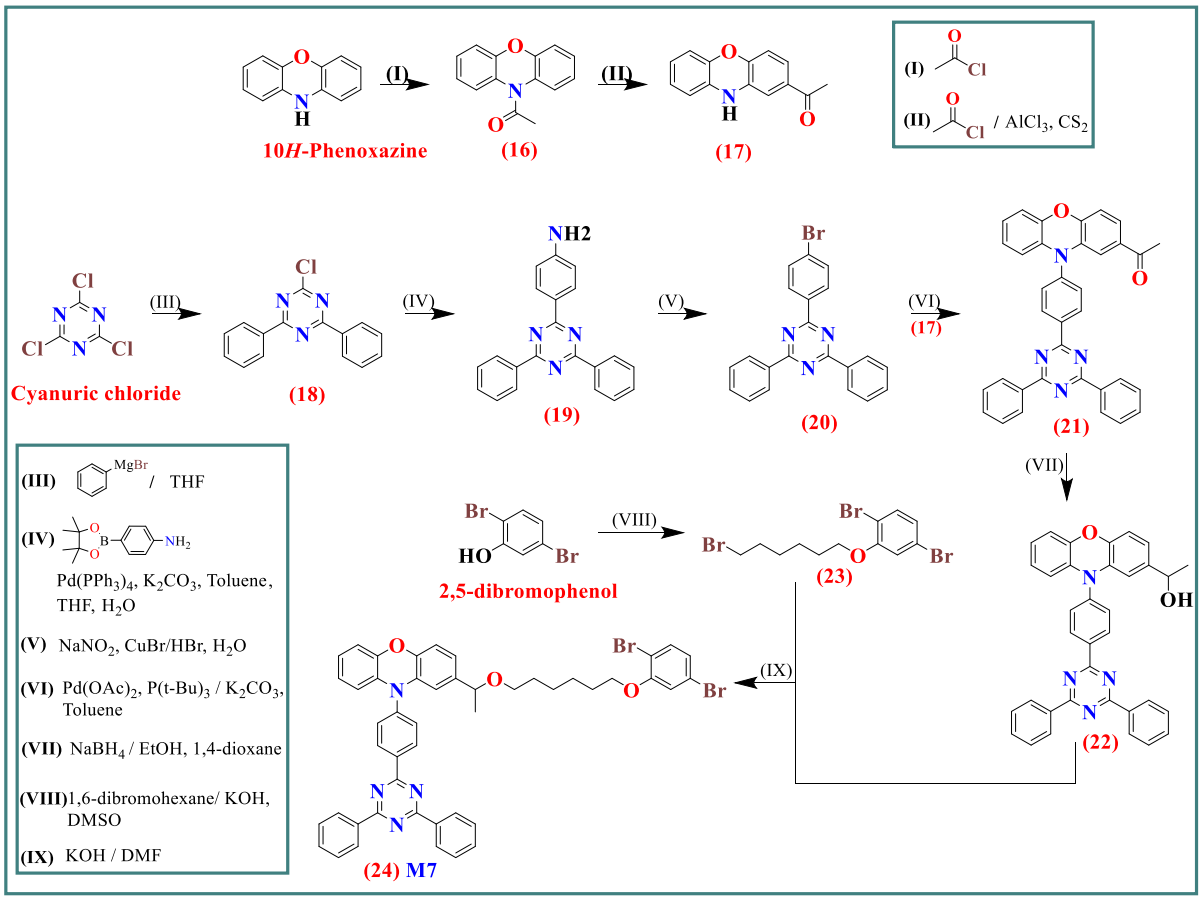

Scheme 4.10 Synthetic steps for TADF monomer M7. The yellow TADF emitter was prepared using three starting materials namely; 10*H*-phenoxazine, cyanuric chloride and 2,5-dibromo phenol, as illustrated in the scheme above. Nine synthetic steps were carried out to afford the required emitter (24) M7. Reagents and conditions; (I) Acetyl chloride, triethylamine, DCM, 0 °C, 24 h. (II) Aluminum chloride, acetyl chloride, CS_2, reflux, 3 h. (III) Bromobrnzene, Phenylmagnesium bromide, THF, 60 °C, overnight. (IV) 4-(4,4,5,5 tetrame-thyl1,3,2-dioxaborolan-2-yl) aniline, $Pd(PPh_3)_4$, K_2CO_3, THF, reflux. 72 h. (V) NaNO2, CuBr, HBr, reflux, 24 h. (VI) $Pd(OAc)_2$, $P(t\text{-}Bu)_3$, K_2CO_3, Toluene, reflux, 24 h. (VII) $NaBH_4$, EtOH, 1,4-dioxane, room temperature (3 h), 60 °C (1 h). (VIII) 1,6-dibromohexane, KOH, DMSO, room temperature, overnight. (IX) KOH, DMF, 55 °C, 24 h.

The acylated product (16) was synthesised according to the synthetic procedure illustrated by Vanderhaeghe.[254] The reaction was carried out under a nitrogen atmosphere using DCM as a solvent and 10*H*-phenoxazine as a raw material in the presence of triethylamine as a base. The crude was purified using column chromatography with the eluent of (PE/EA, 5:1), affording the 10-acetylphenoxazine as a pale green solid in a high yield of 90%. The reaction mechanism proceeds through the acetylation reaction between 10*H*-phenoxazine and the acid chloride which is considered as a type of the nucleophilic addition-elimination reaction. The mechanism

involves three steps, starting by the nucleophilic attack on the carbonyl group of acetyl chloride by the nitrogen of 10*H*-phenoxazine which acted as a nucleophile, forming the

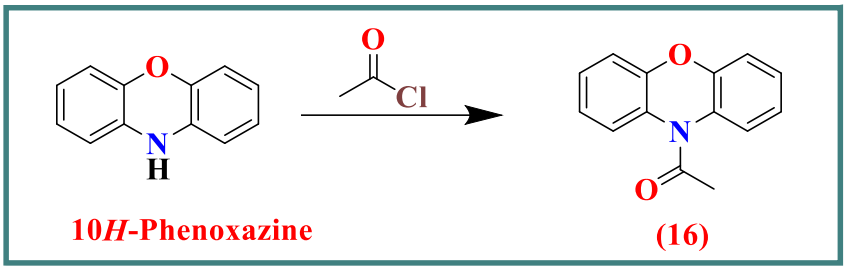

Scheme 4.11 Synthetic conditions of compound (16). Reagents and conditions; (I) Acetyl chloride, triethylamine, DCM, 0 ºC, 24 h.

tetrahedral intermediate (see scheme 4.12) which is followed by elimination of chloride ion, resulting in the formation of carbonyl group. The last step was achieved once the nitrogen atom of the nitrogen group is deprotonated by the nucleophilic attack of the nitrogen lone pair from the triethylamine, resulting in the elimination of the proton as illustrated in the scheme 4.12 below.

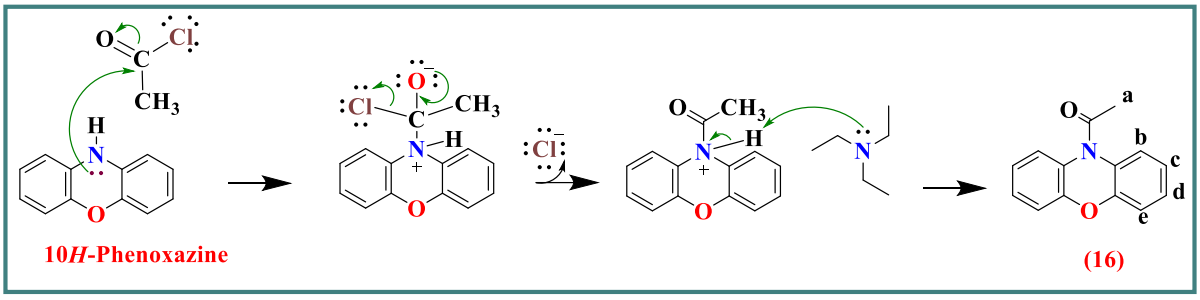

Scheme 4.12 The proposed mechanism for the preparation of compound 16. The reaction mechanism proceeds through the acetylation reaction between 10*H*-phenoxazine and the acid chloride which is considered as a type of the nucleophilic addition-elimination reaction to afford the required 10-acetylphenoxazine.

The purity and structure of compound (16) was confirmed *via* ^{1}H NMR, where the disappearance of broad singlet at 8.20 ppm was observed and a new singlet appeared at 2.36 ppm, attributed to the presence of methyl protons from the acetyl group (see figure 8.10 in the appendix) . Further characterisation was carried out *via* mass spectrometry, revealing the value of 226.12 which matched the theoretical molecular weight of the product (16).

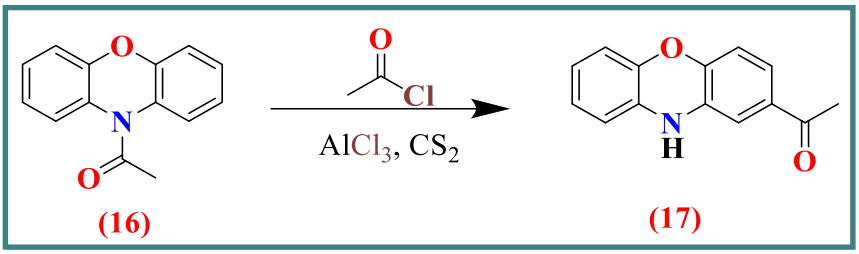

Scheme 4.13 Synthetic conditions of compound (17). Aluminum chloride, acetyl chloride, CS_2, reflux, 3 h.

The synthesis of product (17) namely 2-acetylphenoxazine was carried out following a modified procedure reported by Müller et al.[255] The required compound was obtained as yellowish green crystals in high yield of 93%, once the crude was purified by extraction with ethyl acetate, followed by a water wash and evaporation of the solvent to obtain the pure target product which did not require any further purifications. The chemical mechanism involved in this reaction was a Friedel-Crafts acylation, which ultimately resulted in the formation of the required product by a subsequent hydrolysis process.

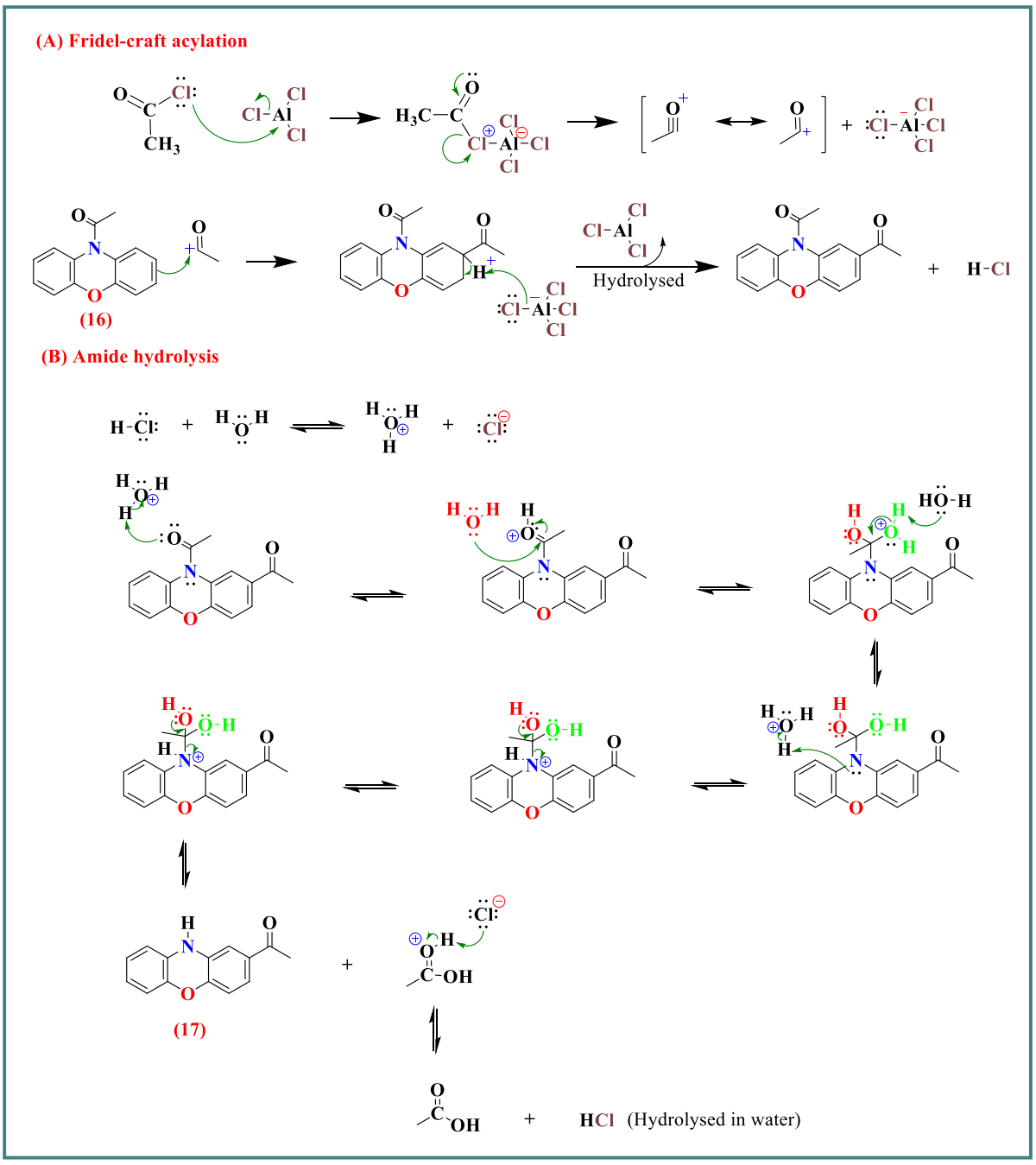

Scheme 4.14 The proposed mechanism Friedel-Crafts acylation of compound (17). The chemical mechanism involved in this reaction was a Friedel-Crafts acylation, which ultimately resulted in the formation of the required 2-acetylphenoxazine (17) by a subsequent hydrolysis process. The reaction was carried out in two mechanistic steps including; Friedel-Crafts acylation and amid hydrolyses. In the first step; 1,1'-(10H-phenoxazine-2,10-diyl)diethanone was formed together with HCl as byproduct. In the second step; the required procudt was obtained with both acetic acid and hydrochloric acid as byproducts.

In the initial step of the Friedel-Crafts acylation, aluminium trichloride ($AlCl_3$) was employed as a Lewis acid catalyst to facilitate the reaction with acetyl chloride. This resulted in the

generation of a carbon with more electrophilicity, known as the acylium ion. Following this, the nucleophile generated at the para position of the aromatic C=C bond attacks the electrophilic carbon (C^+). Therefore, at this point, the formation of an intermediate cation known as cyclohexadienyl resulted from breaking the aromatic system. Ultimately, the C=C bond of the targeted phenyl is regenerated, while simultaneously regenerating the active catalyst through the elimination of a hydrogen ion (H^+) from the carbon atom owned the new substituent of acyl group, resulting in the formation of HCl as drawn in the scheme 4.14. The last step of the mechanism involved the utilisation of acid-catalyzed amide hydrolysis, resulting in the synthesis of the desired 2-acetylphenoxazine. The purity and the success of the target product was confirmed by the ^{1}H NMR analysis, where a broad singlet was appeared at 8.42 ppm, assigned to one proton of the amine group. Additionally, an intense singlet was observed at 2.44 ppm, corresponding to the three protons of the acetyl group (see figure 8.11 in the appendix). Further analysis was conducted via the elemental analysis, exhibiting the values of C, 74.70; H, 4.90; N, 6.15, which agreed with the calculated values (C, 74.65; H, 4.92; N, 6.22) of the target product.

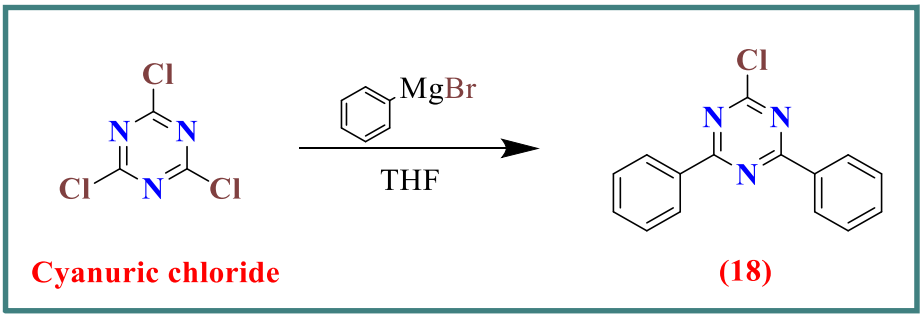

Scheme 4.15 Synthetic conditions of compound 18. Reagents and conditions; Bromobrnzene, Phenylmagnesium bromide, THF, 60 °C, overnight.

The proposed procedure for synthesis of product (18) was reported by Zhong et al.[256] The reaction was carried out under the protection of N_2, using the THF as a reaction medium. The reaction was treated via HCl (14%, 60 ml) to form the residue, which in turnwas purified using column chromatography with the selective eluent of PE/DCM, 3:1, obtaining the 2-chloro-4,6-diphenyl-1,3,5-triazine as a white solid in a yield of 80%. In terms of reaction mechanism, two steps were involved in the synthesis of the required product. The first step was carried out *via* a free radical reaction that generates a Grignard reagent, which consists of two primary stages as illustrated in scheme 4.16. In the first stage, the Grignard reagent namely (phenylmagnesium bromide) is created by reacting magnesium turnings with bromobenzene, generating a polar

intermediate. The second step was achieved once the intermediate (Grignard reagent) attacked the cyanuric chloride yielding the target compound (18) namely 2-chloro-4,6-diphenyl-1,3,5-triazine.

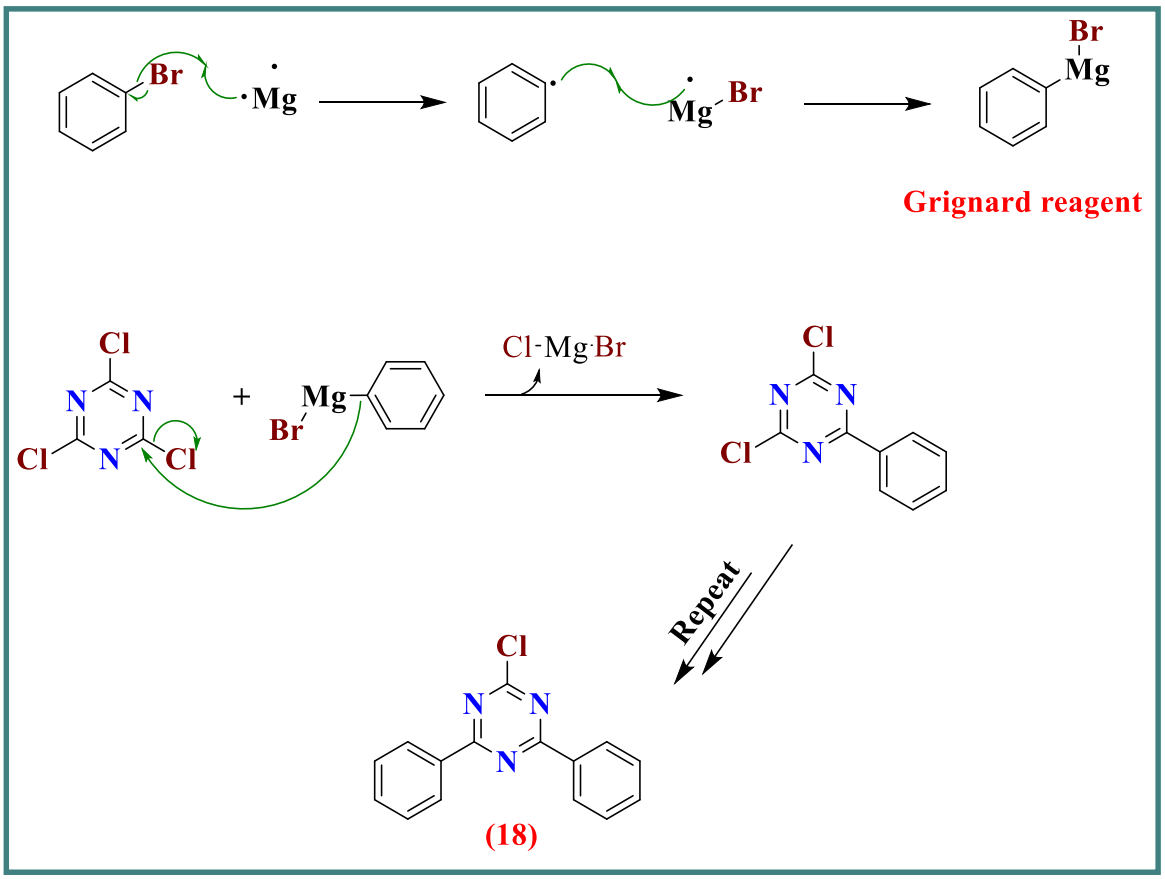

Scheme 4.16 The proposed mechanism of product (18). The synthesis of the required 2-chloro-4,6-diphenyl-1,3,5-triazine was achieved within two mechanistic steps; In the first step, the Grignard reagent namely (phenylmagnesium bromide) was formed by reacting magnesium turnings with bromobenzene, generating a polar intermediate. The second step was achieved once the intermediate (Grignard reagent) attacked the cyanuric chloride yielding the target compound.

The chemical structure of compound (18) was confirmed *via* various characterization techniques including ^{1}H NMR, ^{13}C NMR, elemental analysis and mass spectrometry. The analysis of product (18) using ^{1}H NMR showed three aromatic signals with different splitting; doublet of doublet was observed at 8.69 ppm, assigned to the four protons located in ortho position from the new substituents of two phenyl groups. The effect of strong electronegativity resulted from the triazine ring causing the ortho protons to be shifted more downfield. In addition, two triplets were noticed at 7.68 ppm and 7.60 ppm, corresponding to the two para and four meta protons respectively (see figure 8.12 in the appendix). The analysis *via* ^{13}C NMR also confirmed the structure of compound (18) by indicating intense peaks at 173.4 ppm and

172.6 ppm, corresponding to the two *ipso* carbon atoms attached to the two phenyl rings and one *ipso* carbon atom bonded to the chlorine respectively. The mass spectrometry showed the value of 268.09, verifying the molecular weight of 2-chloro-4,6-diphenyl-1,3,5-triazine.

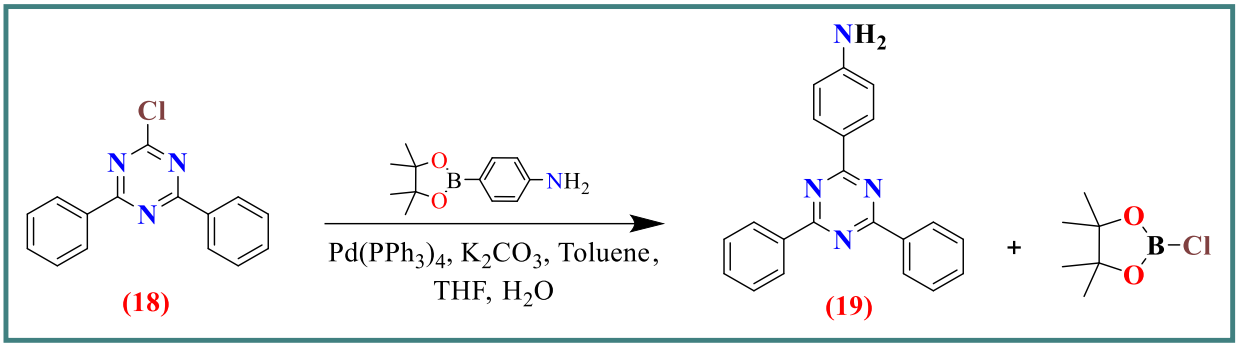

Scheme 4.17 Synthetic conditions of compound (19). Reagents and conditions; 4-(4,4,5,5 tetramethyl1,3,2-dioxaborolan-2-yl) aniline, $Pd(PPh_3)_4$, K_2CO_3, THF, reflux. 72 h.

Compound (19) namely 2-(4-aminophenyl)-4,6-diphenyl-1,3,5-triazine was prepared following the synthetic procedures reported by Tanaka et al.[257] The reaction was conducted under N_2 protection, using dry THF as a solvent and potassium carbonate as a base. The crude product was obtained once the reaction left stirring for 72 hours at refluxed. The required compound (19) was purified *via* extraction with ethyl acetate, followed by evaporation of the solvent reduction and a chloroform wash, to obtain 2-(4-aminophenyl)-4,6-diphenyl-1,3,5-triazine as a white powder in a yield of 79% without any further purification required. The mechanism of the Suzuki coupling reaction was discussed in the first chapter. The ^1H NMR analysis confirmed the chemical structure of compound (19). Two doublets appeared at 8.46 ppm and 6.74 ppm, attributed to the total of four protons; two located on the *ortho*-position and the other two on the *meta*-position of the new substituent phenyl ring. In addition, a broad singlet was observed at 4.18 ppm which was assigned to two new protons of amine group (see figure 8.13 in the appendix).

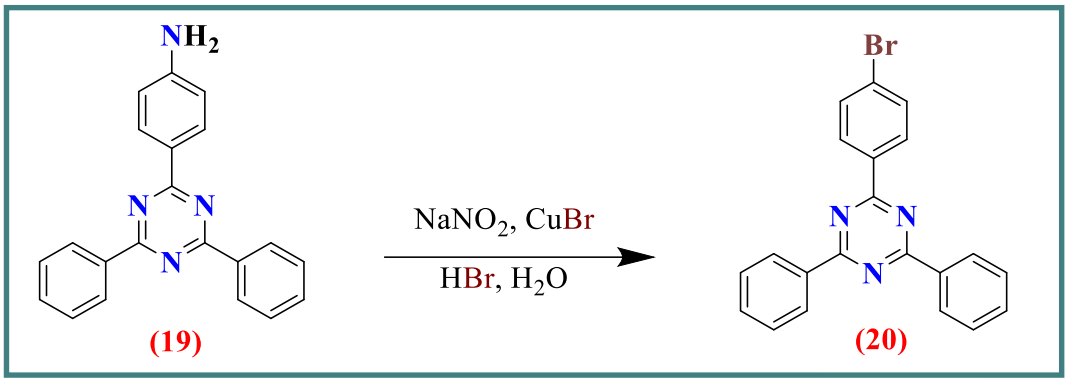

Scheme 4.18 Synthetic conditions of compound (20). Reagents and conditions; $NaNO_2$, CuBr, HBr, H_2O, reflux, 24 h.

The synthesis of compound (20) namely 2-(4-bromophenyl)-4,6-diphenyl-1,3,5-triazine was carried out following a modified procedure reported by Tanaka et al.[257] The required product was obtained as a white powder in a yield of 68% once the crude purified *via* column chromatography with the eluent of (hexane/$CHCl_3$, 4:1). The proposed mechanism for producing compound (20) is based on the Sandmeyer reaction, a type of substitution reaction that generates aryl halides from aryl diazonium compounds as shown in the scheme 4.19 below.

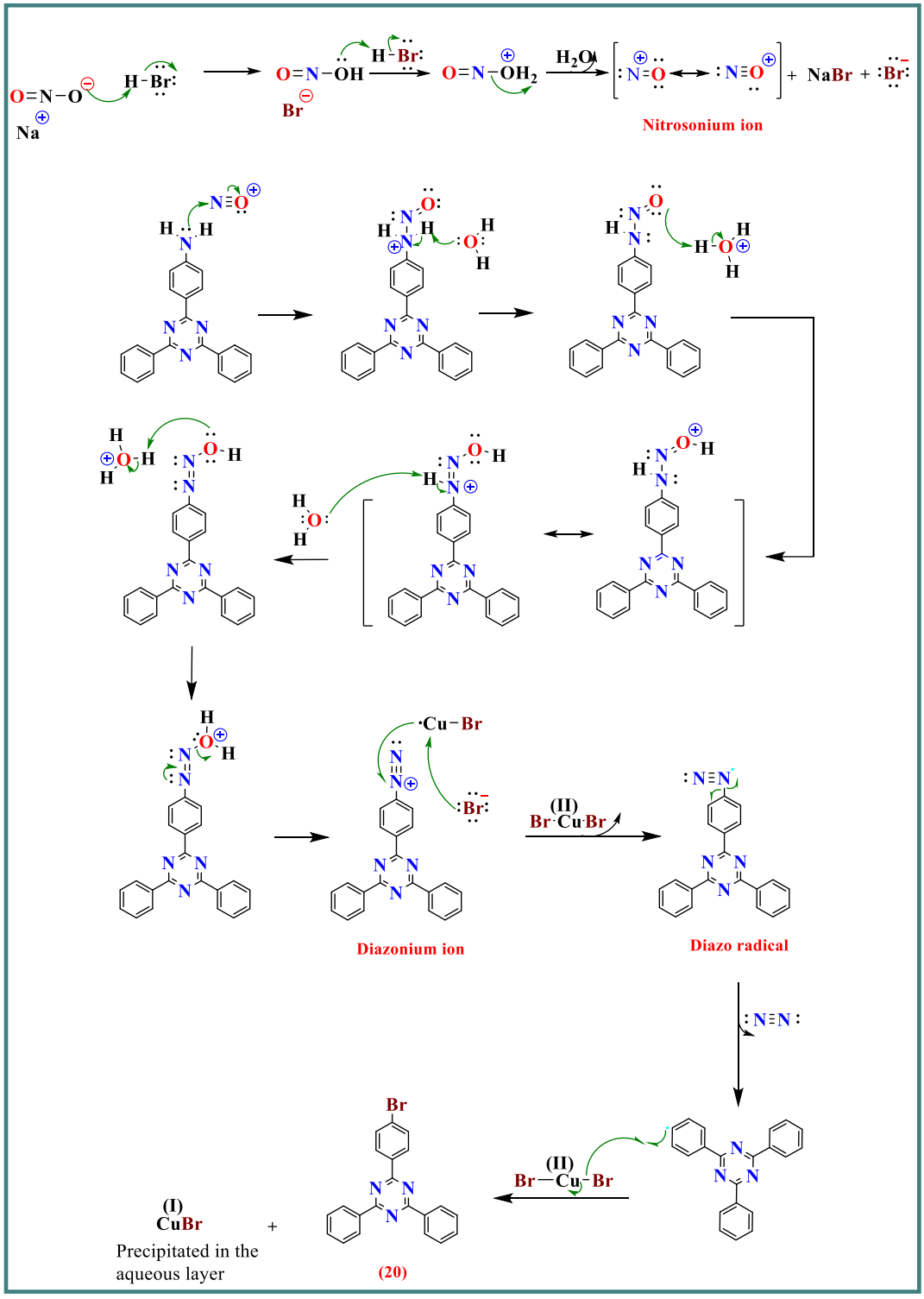

Scheme 4.19 The proposed mechanism for the preparation of compound (20). The reaction mechanism for producing the required product is based on the Sandmeyer reaction which is a type of substitution reaction that generates aryl halides from aryl diazonium compounds. The mechanism involved four synthetic steps including the generation of generating both bromine ion and nitrosonium in the first step. Secondly, diazonium salt was produced via the electrophilic nitrosonium . The third step was included the formation of a diazo radical and Cu(II)Br_2 with respect to other mechanistic conditions mentioned below. In the last step, the required 2-(4'-Aminophenyl)-4,6-diphenyl-1,3,5-triazine (20).

The mechanism involves four stages; firstly by generating both bromine ion and nitrosonium once the two protonations occurred through the reaction between sodium nitrite and hydrobromic acid. Followed by converting the amine to diazonium salt by the electrophilic nitrosonium as illustrated in scheme 4.19. Subsequently, the oxidation state of copper (Cu) undergoes a rise to +2, facilitated by the migration of a lone electron from Cu towards the diazonium salt. This electron transfer results in the formation of a diazo radical. Additionally, the bromide ion coordinates to Cu(II)Br, leading to the formation of Cu(II)Br_2. Ultimately, nitrogen gas is released from the diazo radical, generating a radical which in turn reacts with Cu(II)Br_2 to regenerate the Cu(I) and obtain the required product (20). The analysis by ^{1}H NMR, elemental analysis and mass spectrometry successfully approved the confirmation of the target product. ^{1}H NMR revealed the disappearance of a broad singlet at 4.18 ppm for the amine group (NH_2). In addition, the two doublets which are assigned to the two *ortho* and two *meta* protons from the bromophenyl group were deshielded and appeared at 8.66 ppm and 7.72 ppm; this is due to the inductive effect caused by the new substituent of bromine. Further characterisation by elemental analysis showed the values of C, 64.84; H, 3.71; Br, 20.48; N, 10.73 %, which match the calculated values of C, 64.85; H, 3.72; Br, 20.50; N, 10.75 % for the required product. Furthermore, the mass spectrometry showed apeak with an m/z value of 388.04, verifying the successful synthesis of product (20).

The next step in the preparation of the TADF monomer involved the reaction of compound (17) with compound (20) *via* a palladium-catalysed coupling reaction to obtain product (21). The synthetic procedure reported by Moon et al.[258] was followed as shown in the scheme below.

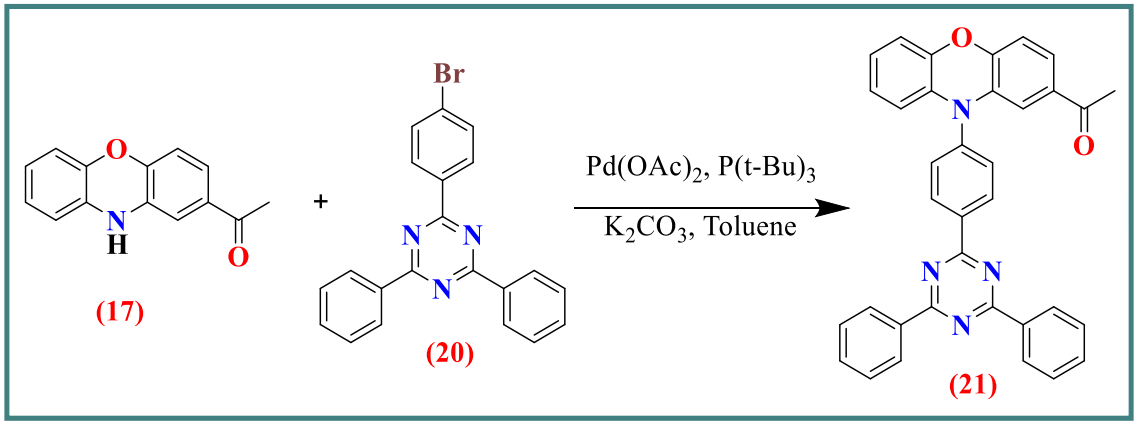

Scheme 4.20 Synthetic conditions of compound (21). Reagents and conditions; $Pd(OAc)_2$, $P(t\text{-}Bu)_3$, K_2CO_3, Toluene, reflux, 24 h.

The reaction was conducted under the protection of N_2 at reflux (110 ^{0}C) for 24 h, using dry toluene as a reaction solvent, potassium carbonate as a base and palladium acetate as a catalyst. The crude product showed three spots on the TLC plate, indicating the presence of some impurities. The crude was purified *via* column chromatography, using DCM/PE eluent with a starting ratio of 1:2 and changing the polarity progressively to 1:1 to obtain the target product as a yellow solid in a yield of 80%. In terms of reaction mechanism, Buchwald-Hartwig cross-coupling reaction (catalysed by palladium) was applied to prepare the required product through a number of steps as illustrated in the scheme 4.21 below.

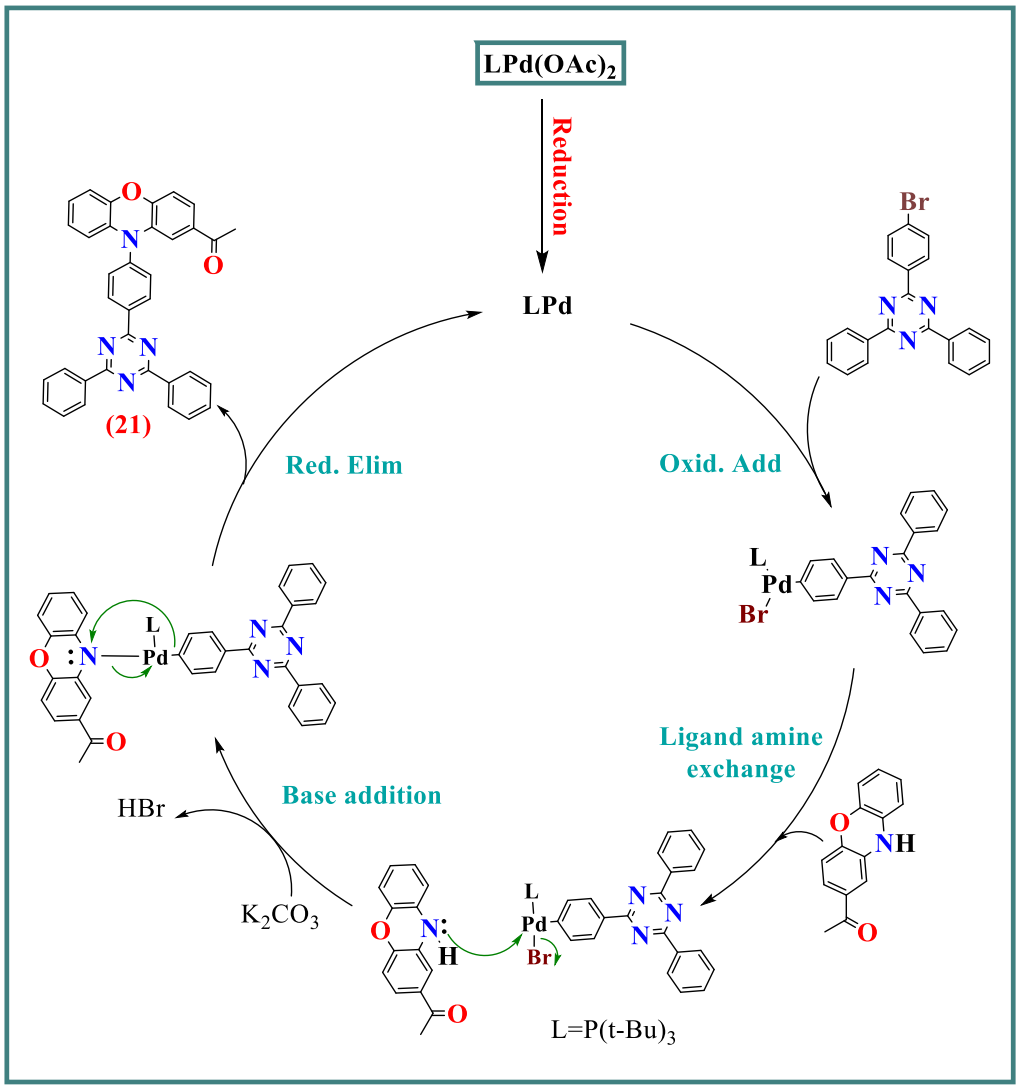

Scheme 4.21 The proposed mechanism Buchwald-Hartwig cross-coupling of compound (21). Buchwald-Hartwig cross-coupling reaction (catalysed by palladium) was applied to prepare the required product through several steps; compound (21) is oxidatively added to the palladium. Next, the resulting complex reacted with phenoxazine (17). Deprotonation ultimately occurred, followed by a reductive elimination, to obtain the required 10-(4'-(4",6"-diphenyl-1,3,5-triazin-2"-yl)phenyl)-10*H*-phenoxazin-2-yl)ethan-1-one.

After the modification of the palladium oxidation state, compound (21) is oxidatively added to the palladium. Next, the resulting complex reacted with phenoxazine (17). Deprotonation ultimately occurred, followed by a reductive elimination, to obtain the required compound. The successful synthesis of compound (21) was verified *via* ^{1}H NMR, elemental analysis and mass spectrometry. The NMR analysis showed the disappearance of the broad singlet at 8.24 ppm assigned to the amine proton from compound (17). Additionally, deshielded aromatic peaks were observed from 7.33 ppm to 6.06 ppm, verifying the presence of phenoxazine aromatic protons. Furthermore, a singlet appeared at 2.38 ppm , corresponding to the three protons from the acetyl group in the phenoxazine (see figure 8.15 in the appendix). Mass spectrometry analysis also confirmed that product (21) was prepared successfully with observation of an accurate mass value of 533.20.

The next stage of preparing the TADF monomer was achieved by reduction of the carbonyl group in compound (21) to obtain alcohol (22). This was prepared following reported synthetic procedure by Kamogawa et al.[259]

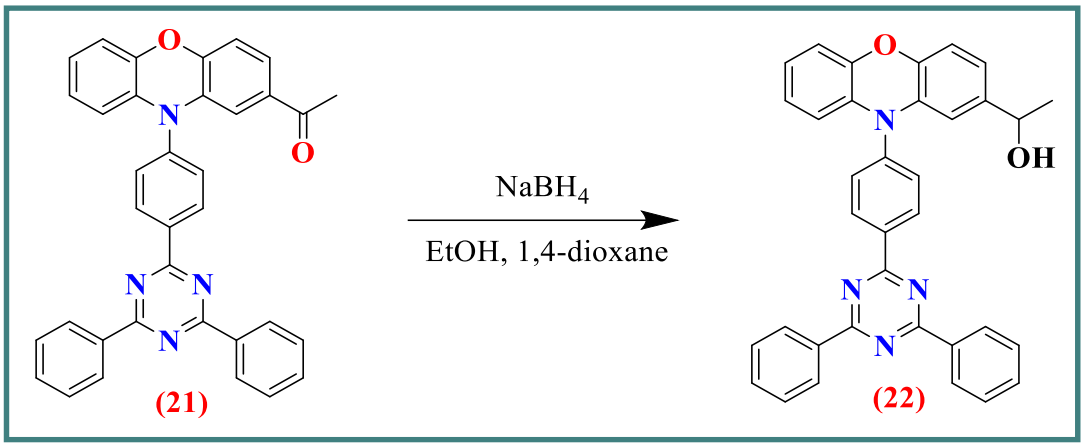

Scheme 4.22 Synthetic conditions of compound (22). Reagents and conditions; $NaBH_4$, EtOH, 1,4-dioxane, room temperature (3 h), 60 °C (1 h).

The reaction was carried out at mild conditions (60 ^{0}C) using two solvents, ethanol and 1,4-dioxane, as a reaction medium and sodium borohydride as a reducing agent. The reduced pure compound was obtained as golden orange crystals in a yield of 75.3%, once the crude was recrystallised from toluene/petroleum ether mixture. The reduction mechanism of the carbonyl group occurs in two steps. Firstly, the alkoxide ion was formed once the carbonyl (C=O) attacked by the hydride anion (H^-) which acted as nucleophile from (BH_4^-). This was followed by the protonation of the alkoxide ion to generate the alcohol as illustrated in the scheme 4.22

below. The confirmation of the final structure for compound (22) was confirmed by ^{1}H NMR analysis, where a quartet observed at 4.59 ppm, assigned to one proton bonded to the secondary carbon atom. Additionally, a broad singlet appeared at 4.19 ppm, verifying the presence of new (OH) group (see figure 8.16 in the appendix). This is indeed confirmed the successful synthesis of compound (22).

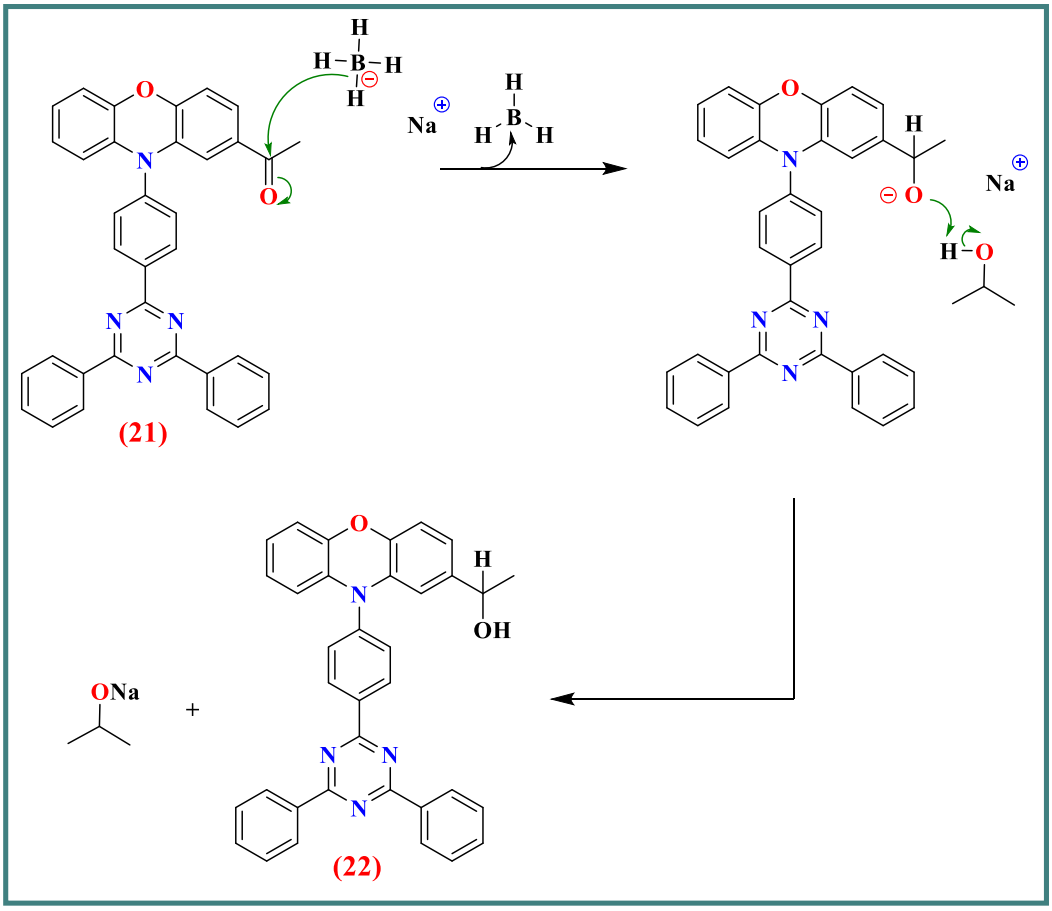

Scheme 4.23 The proposed mechanism for compound (22). The reduction mechanism of the carbonyl group occurs in two steps. Firstly, the alkoxide ion was formed once the carbonyl (C=O) attacked by the hydride anion (H^-) which acted as a nucleophile from (BH_4^-). This was followed by the protonation of the alkoxide ion to generate the alcohol (22).

As a part of preparing the TADF monomer, compound (23) was prepared according to the synthetic procedures reported by Hsieh et al.[260] Regarding the reaction conditions, 1,6-dibromohexane was reacted with 2,5-dibromophenol under the protection of N_2 in the presence of anhydrous DMSO as a solvent and potassium hydroxide as a base to assist the deprotonation. The reaction was given 24 hours for completion and consists of an etherification reaction. The crude was purified using column chromatography with an eluent of (DCM/PE, 1:10) to obtain the required product (23) as white crystals in a high yield of 96%.

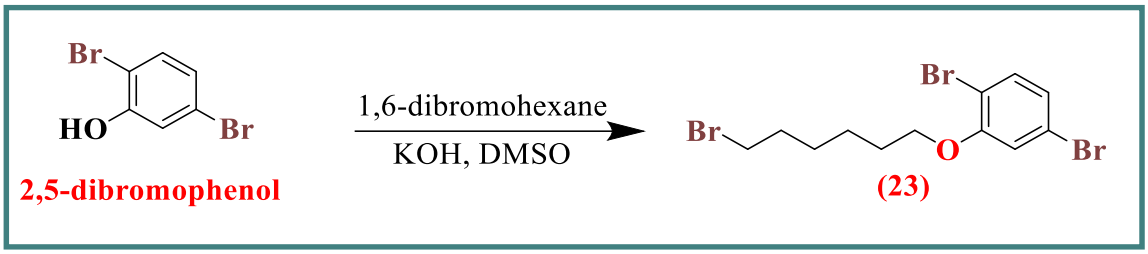

Scheme 4.24 Synthetic conditions of compound (23). Reagents and conditions; 1,6-dibromohexane, KOH, DMSO, room temperature, overnight.

In terms of the structural confirmation, the analysis by ^{1}H NMR showed the disappearance of the broad singlet at 5.60 ppm, which was assigned to the hydroxyl proton from 2,5-dibromophenol. In addition, three aromatic peaks were observed with different splitting; two doublets and one doublet of doublet at 7.40 ppm, 7.02 ppm and 6.98 respectively, which correspond to the three protons of the phenyl ring. Moreover, two triplets appeared at 4.03 ppm and 3.46 ppm, assigned to two protons from (OCH_2) and two protons from ($BrCH_2$) respectively. The more electronegativity effect results in more downfield shift (O>Br). Furthermore, two triplets were observed at 2 ppm and 1.64 ppm, corresponding to four protons from two methylene groups neighbouring to (OCH_2) and four protons also from the two methylene groups neighbouring to ($BrCH_2$). The total number of protons indeed confirmed the successful synthesis of compound (23), (see figure 8.17 in the appendix). Further analysis *via* the elemental analysis confirmed the presence of compound (23), which indicated concordance between the measured elemental percentages with the values of C, 34.65; H, 3.80; Br, 57.85 and those calculated (C, 34.73; H, 3.64; Br, 57.77).

The final step in the preparation of the required TADF monomer (M7), involved the reaction of the product (22) with the product (23) using the reaction conditions in scheme 4.25. A modified synthetic procedure reported by Luo et al.[261] was followed. TLC showed two spots under the UV light. The purification of the crude product was achieved using column chromatography with the eluent (DCM/PE, 1:1) followed by recrystallisation from methanol, affording the target monomer as a yellow powder in a yield of 74%.

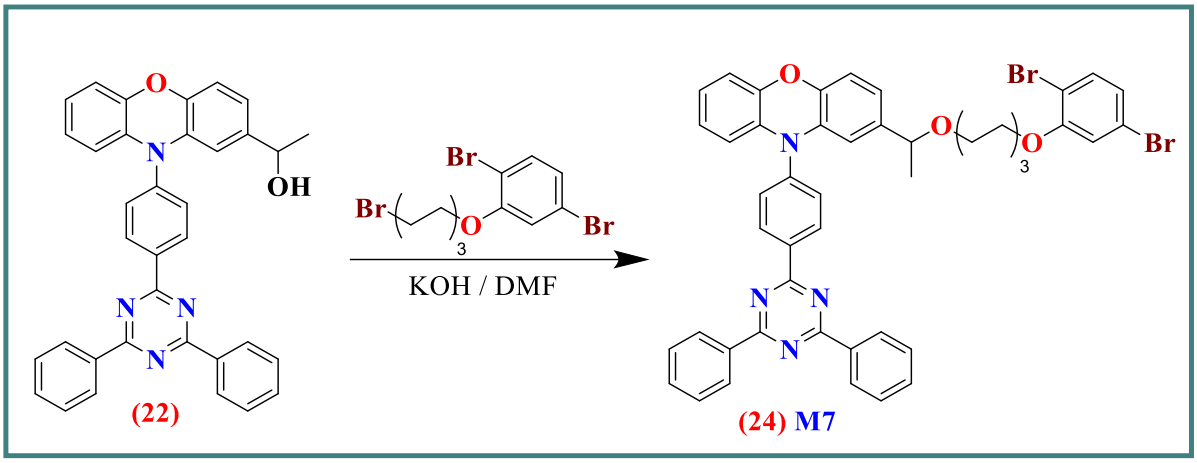

Scheme 4.25 Synthetic conditions of TADF monomer M7. Reagents and conditions; KOH, DMF, 55 °C, 24 h.

The mechanism of this reaction follows the same mechanism used to prepare product (23). The structural confirmation of the TADF monomer (M7) was successfully achieved *via* ^{1}H NMR, mass spectrometry and elemental analysis. Characterisation using ^{1}H NMR showed the disappearance of the broad singlet at 4.19 ppm, which correspond to the hydroxyl proton from the TADF moiety (product 22) confirming the success of the etherification reaction and synthesis the TADF monomer M7. Moreover, a quartet was observed at 4.08 ppm, assigned to the one of the TADF moiety protons in the position (i) as illustrated in figure 4.2 below. In addition, two triplets were observed at 3.84 ppm and 3.23 ppm, corresponding to the four protons of the two alkoxy groups in positions (j) and (k) respectively. The more downfield shift of the alkoxy protons in position (j), attributed to the increase of the electronegativity of phenol ether group compared to the aliphatic ether groups. Elemental analysis, values of C, 65.15; H, 4.55; Br, 18.50; N, 6.40 were found. These matched the calculated values of C, 64.99; H, 4.64; Br, 18.40; N, 6.45 for the TADF monomer, which indeed approved the final structure of the required product. Ultimately, the mass spectrometry revealed the value of 866.90, verifying the success in the preparation of target monomer M7.

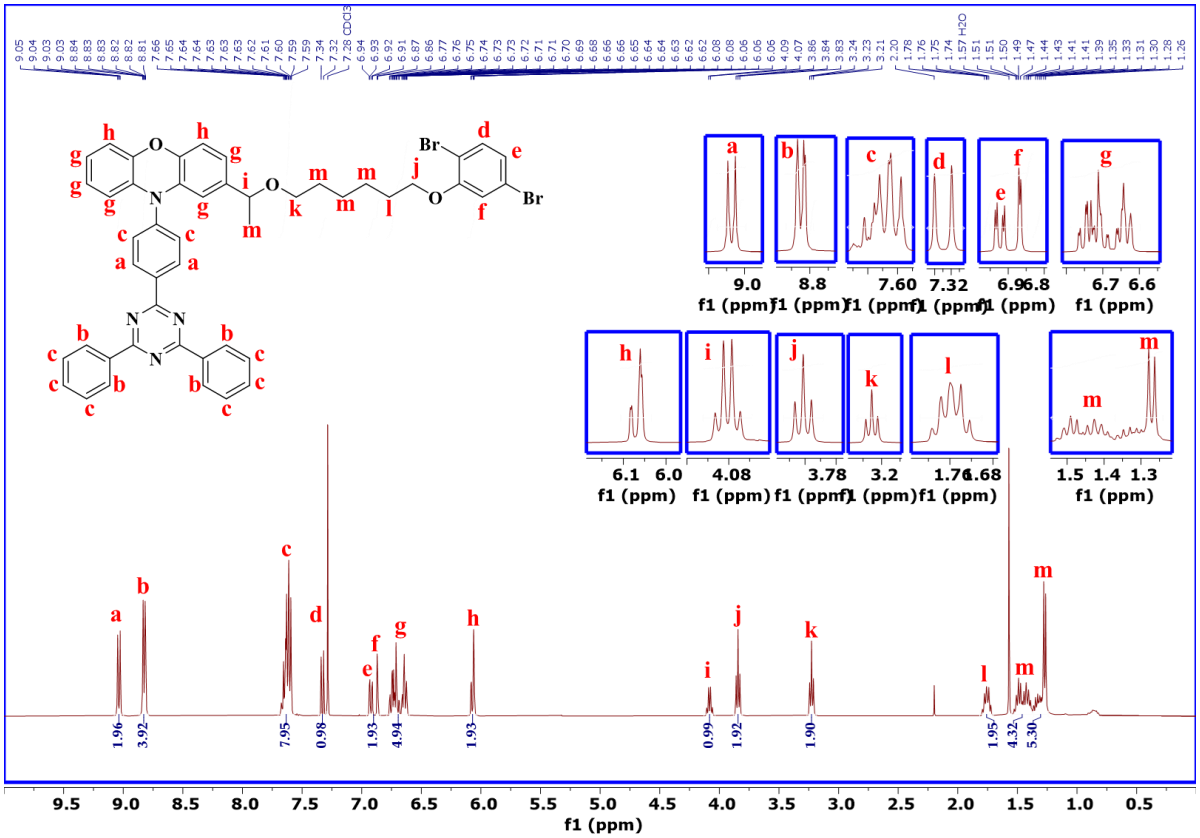

Figure 4.2 ^{1}H NMR spectra of TADF M6 in $CDCl_3$; 9.04 (d, J = 8.5 Hz, 2H), 8.83 (dd, J = 6.5, 1.4 Hz, 4H), 7.69 – 7.54 (m, 7H), 7.33 (d, J = 8.3 Hz, 1H), 6.92 (dd, J = 8.4, 2.1 Hz, 1H), 6.87 (d, J = 2.2 Hz, 1H), 6.78 – 6.67 (m, 3H), 6.64 (ddd, J = 7.6, 5.8, 1.7 Hz, 2H), 6.13 – 5.97 (m, 2H), 4.08 (q, J = 6.4 Hz, 1H), 3.84 (t, J = 6.4 Hz, 2H), 3.23 (t, J = 6.4 Hz, 2H), 1.76 (m, J = 14.0, 6.7 Hz, 2H), 1.53 – 1.29 (m, 6H), 1.27 (d, J = 6.5 Hz, 3H).

4.2.2 Design and synthesis of polymers P5, P6, P7 and P8

All polymers P5 – P8 were synthesised and designed following modified synthetic procedures of Suzuki polycondensation. P5 was prepared in molar ratio of 50:50 of M2 and M6, compared to the P6, P7 and P8 which were prepared on incorporation of different molar ratio feeds of M7 (TADF) in their sidechains. The molar ratios selected for M2, M6 and M7 to design P6, P7 and P8 were 45:50:5, 40:50:10 and 30:50:20 respectively. P5 which included no molar ratio of the TADF monomer M7 has been prepared to be compared with the other polymers P6 - P8 which have different molar ratios of the TADF monomer.

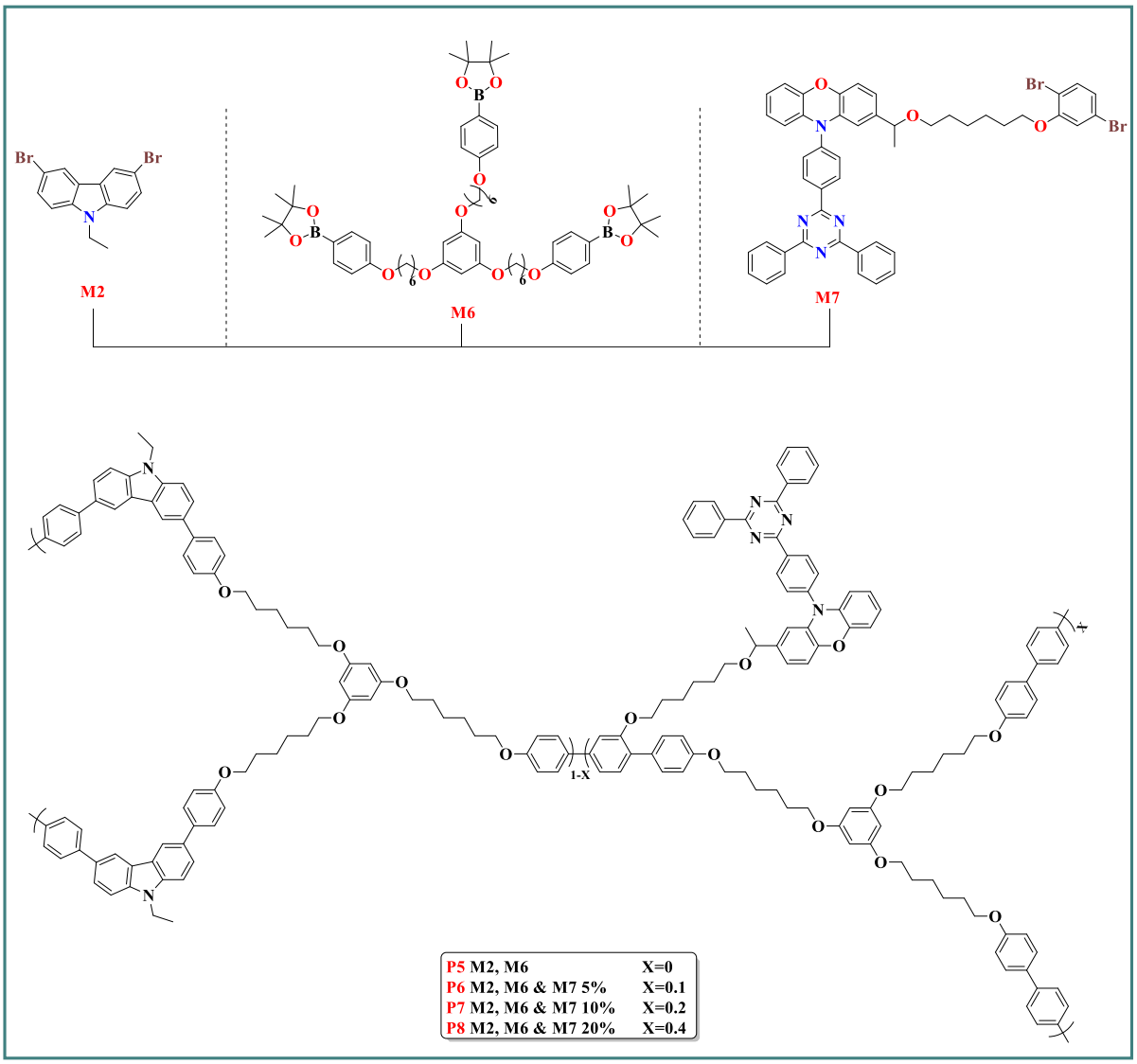

Scheme 4.26 Design of P5 – P8 with different ratios of TADF. Four hyperbranched polymers were prepared using different molar ratios of M2, M6 and M7. P5 was prepared using the ratio of (50:50, M2:M6), while the polymer from P6 – P8 were prepared using the ratio of (45, 50, 5), (40, 50, 10) and (30, 50, 20) of the selected M2, M6 and M7 respectively. Reagents and conditions; THF, Sat.$NaHCO_3$, $Pd(OAc)_2$, $P(o\text{-}tol)_3$, K_2CO_3, 24h, Reflux.

In terms of the polymerisation conditions, all reactions were undertaken under the protection of N_2, using small volumes of THF as a solvent with pre-degassed solutions of sodium hydrogen carbonate used as a base, with both palladium (II) acetate ($Pd(OAc)_2$) and tri(o-tolyl) phosphine ($P(o\text{-}tol)_3$) as catalysts. The polymerisations were conducted over 24 hours at reflux. The polymerisation reactions were confirmed once precipitation of polymers were observed by the end of the reactions.[182] Bromobenzene and phenylboronic acid were added successively to end cap the polymers, followed by a reflux of a further 12 hours. The polymer's end-capping is designed to improve the polymers' stability while used in OLED devices.[262, 263]

Polymerisation can be effectively stopped by adding a specific reagent to the end of a polymer chain. This prevents the polymer's overgrowth and aggregation. In addition, stabilises unstable polymer's end groups and therefore improves the product's reaction abilities.[264]

Chloroform was used to dissolve all polymers, followed by the addition of ammonium hydroxide solution to remove catalyst residues. All polymers solutions were extracted and washed with water several times to eliminate the ammonium hydroxide. The required polymers P5, P6, P7 and P8 were obtained in yields of 58%, 55%, 52% and 60% respectively, once the polymers precipitated from methanol without any further purification. All polymers exhibited great solubility in most common solvents such as (chloroform, DCM, toluene and THF). The confirmation of the structures of all polymers was successfully verified *via* analysis using ^{1}H NMR spectroscopy as shown in figure 4.3 below.

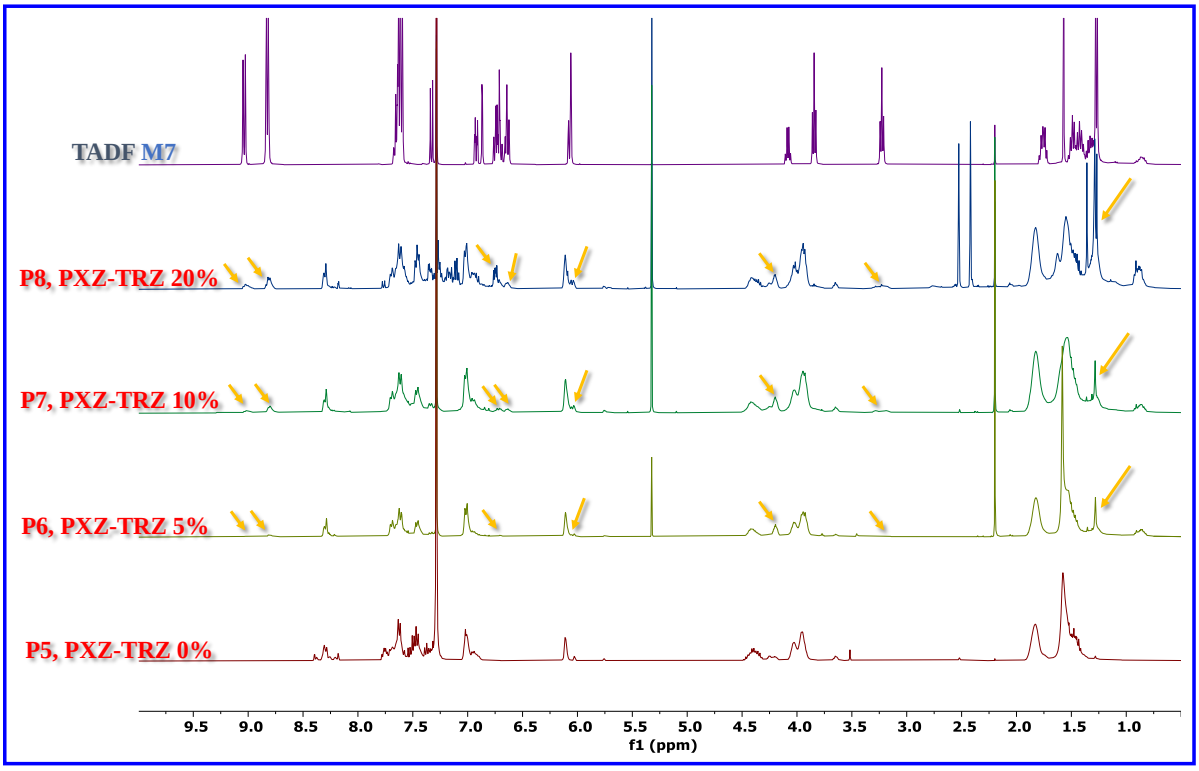

Figure 4.3 ^{1}H NMR spectra of the designed polymers P5 – P8 and TADF M7 in $CDCl_3$. The five NMR spectra for TADF M7, P8, P7, P6, and P5 were stacked, respectively (from top to bottom). These spectra showed the comparison among all TADF hyperbranched polymers grafted with TADF (M7) in different mole ratios. In P5, the TADF units were not grafted into the polymer's sidechain; therefore, no TADF spectra were observed in the polymer. However, in the polymers 6, 7, and 8, the corresponding TADF spectra increased proportionally with increasing feeding molar ratios from 5% to 20%. The data of all stacked spectra in $CDCl_3$ are as follows; **TADF M7**; 9.04 (d, J = 8.5 Hz, 2H), 8.83 (dd, J = 6.5, 1.4 Hz, 4H), 7.69 – 7.54 (m, 7H), 7.33 (d, J = 8.3 Hz, 1H), 6.92 (dd, J = 8.4, 2.1 Hz, 1H), 6.87 (d, J = 2.2 Hz, 1H), 6.78 – 6.67 (m, 3H), 6.64 (ddd, J = 7.6, 5.8, 1.7 Hz, 2H), 6.13 – 5.97 (m, 2H), 4.08 (q, J = 6.4 Hz, 1H), 3.84 (t, J = 6.4 Hz, 2H), 3.23 (t, J = 6.4 Hz, 2H), 1.76 (m, J = 14.0, 6.7 Hz, 2H), 1.53 – 1.29 (m,

6H), 1.27 (d, J = 6.5 Hz, 3H). **P5;** 8.33 – 8.23 (m, 4H), 8.23 – 8.15 (m, 1H), 7.81 – 7.71 (m, 4H), 7.66 – 7.55 (m, 10H), 7.55 – 7.43 (m, 9H), 7.41 – 7.29 (m, 8H), 7.01 (s, 11H), 6.11 (s, 3H), 4.52 – 4.29 (m, 7H), 4.28 – 4.15 (m, 3H), 4.10 – 3.86 (m, 15H), 3.64 (s, 2H), 1.83 (s, 17H), 1.66 – 1.34 (m, 41H). **P6**; 9.02 (bs, 0.09H), 8.81 (bs, 0.1H), 8.30 (m, 1H), 7.85 – 7.31 (m, 2H), 7.14 – 6.52 (m, 1H), 6.11 (bs, 1H), 4.58 – 3.56 (m, 3H), 1.82 (bs, 2H), 1.52 (bs, 4H), 1.28 (s, 1H), 0.97 – 0.64 (m, 0.31H). **P7**; 9.01 (bs, 0.20H), 8.82 (bs, 0.38H), 8.34 – 8.04 (m, 1.08H), 7.75 – 7.39 (m, 5H), 7.12 – 6.83 (m, 3H), 6.77 – 6.55 (m, 0.59H), 6.17 – 5.97 (m, 1.38H), 4.52 – 4.12 (m, 2H), 4.11 – 3.79 (m, 4H), 1.82 (s, 5H), 1.68 – 1.38 (m, 9.41H), 1.28 (s, 2H), 0.87 (s, 1H). **P8**; 9.02 (bs, 0.40H), 8.80 (s, 0.63H), 8.36 – 8.14 (m, 1H), 7.73 – 7.52 (m, 4H), 7.51 – 7.38 (m, 2H), 7.37 – 7.30 (m, 1H), 7.28 – 7.06 (m, 3H), 7.05 – 6.83 (m, 3H), 6.78 – 6.59 (m, 1H), 6.17 – 5.96 (m, 2H), 4.20 (s, 2H), 4.11 – 3.74 (m, 5H), 3.34 – 3.11 (m, 1H), 1.83 (s, 5H), 1.70 – 1.39 (m, 10H), 1.38 – 1.01 (m, 8H), 0.89 (s, 2H).

Polymer P5 showed broad peaks in both aromatic and aliphatic regions. A broad multiplet was observed at 8.39 ppm, assigned to the aromatic carbazole rings protons from M2. In addition, a broad multiplet was observed at 7.79 ppm which is attributed to the presence of terminal phenyl ring protons from M6. Furthermore, a broad singlet was observed corresponding to the methylene protons attached to the nitrogen atom from M2. Moreover, a broad singlet appeared at 1.83 ppm which is assigned to methylene groups protons attached to the alkoxy groups in M6. Hence, this is totally in agreement with the structure of polymer P5. As can be seen from the figure 4.3 above, all polymers P6, P7 and P8 showed the incorporation of TADF monomer (M7) in their side chains by observing new ^{1}H NMR peaks at 9 ppm, 8.80 ppm, 6.75 ppm, 6.64 ppm, 4.19 ppm, 3.22ppm and 1.27 ppm which indeed corresponding to the TADF (M7) protons. As noticed in figure 4.3 above, the intensity of TADF peaks increased proportionally with increasing the TADF (M7) percentage used in the polymerisations from 5% to 20%, verifying that TADF (M7) has been incorporated successfully in the polymeric sidechains of P6, P7 and P8. The actual feeding values of the TADF (M7) were calculated from the ratios of the integrated protons in M2 and M7 to be 5%, 7.2% and 12.6% for the designed polymer P6, P7 and P8 respectively, as illustrated in table 4.1 below.

Table 4.1 The actual feeding molar ratio of M7 in the polymeric side chains of P5-P8

Polymers	Feed Molar Ratio %	Actual Molar Ratio %
P5 0% TRZ-PXZ	0	0
P6 5% TRZ-PXZ	5	5
P7 10% TRZ-PXZ	10	7.6
P8 20% TRZ-PXZ	20	12.6

P5 was prepared with 0% molar ratio of M7 in comparison with P6, P7 and P8, which were prepared using molar ratios of 5%, 10% and 20% respectively. The calculated molar ratio of M7 in P6 – P8 using the integrated NMR spectra showed values of 5 %, 7.6 % and 12.6 % respectively.

4.2.3 Molecular Weight of P5, P6, P7 and P8

The values of the number average molecular weight (Mn), weight average molecular weight (Mw) and the polydispersity index (PDI) for the designed polymer were measured using gel permeation chromatography (GPC), in THF as an eluent, against polystyrene standards and toluene as a marker. It is well known that the use of linear polymer standards such as polystyrene in this case, provides under-estimated values of Mn and Mw molecular weights in view of the globular structure of hyperbranched polymers.

Table 4.2 GPC data of the designed polymer P5 – P8

Polymers	Mn(Da)	Mw(Da)	PDI	Yield	Fraction
P5 0% TRZ-PXZ	19000	23200	1.2	58%	Chloroform
P6 5% TRZ-PXZ	14600	39400	2.7	55%	Chloroform
P7 10% TRZ-PXZ	13000	42000	3.2	52%	Chloroform
P8 20% TRZ-PXZ	14000	47400	3.3	60%	Chloroform

As illustrated in the table 4.2 above, the Mn values of P5 was calculated to be 19000 Da, whereas the polymers with incorporated TADF monomer M7 i.e., P6 – P8 the Mn values observed are calculated to be ranged between 13000 Da and 14600 Da. Polymer P5 which contains 0% of the TADF monomer showed a higher Mn value as compared to the other polymers P6 – P8. This is attributed to the increase of branching in the polymeric backbone of P5. The low molecular weight values of P6 – P8, this is due to the effect of the high steric hindrance of the carbazole molecule from M2.[265] The PDI results of the TADF polymers increased gradually from P6 to P8 by illustrating the values between 2.7 – 3.3, this is the result of an increase in steric hinderance in the polymeric backbone, which causes a greater repulsion between the chains of polymers P6, P7, and P8. Different values of yield were obtained for the designed polymers P5-P8, ranging from 52% to 60%. The purification of polymers was carried out using different purification methods, such as precipitation from alcohol and Soxhlet extraction using different solvents to eliminate dimers, oligomers, and unreacted monomers. So, due to multiple purification steps, polymers could lose some of their weight, which leads to low yield values for the designed polymers.

4.2.4 Thermal Properties of P5, P6, P7 and P8

The thermal properties of the newly designed polymers P5 – P8 were investigated using thermogravimetry analysis (TGA) under inert atmosphere conditions with a heating rate of 10 °C min^{-1}. As illustrated in table 4.3, the thermal degradations of all designed polymers from P5 – P8 were determined to be 251 °C, 323 °C, 359 °C and 375 °C respectively.

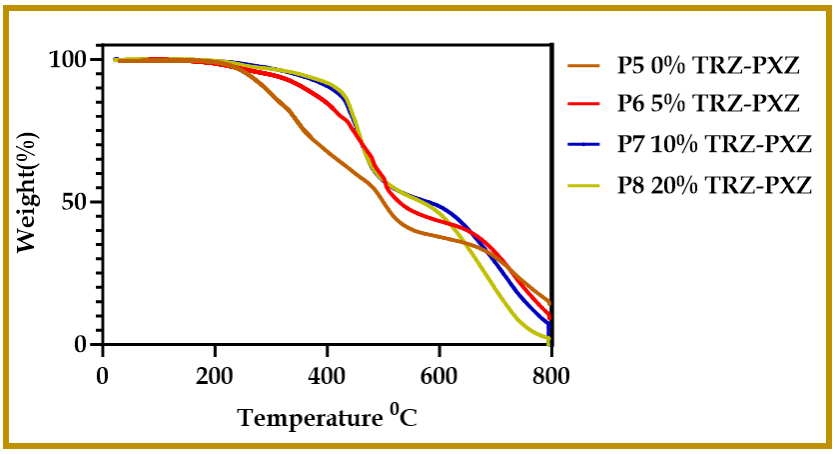

Figure 4.4 TGA analysis of P5 – P8. The thermal stability of all designed polymers 5 – 8 showed a proportional increase with increasing the TADF feeding ratios (0% > 5% > 10% > 20%). The degradation temperatures of all designed polymers were measured from the decomposition curves to be 251 °C, 323 °C, 359 °C and 375 °C respectively.

As shown in the figure 4.4 above, all the designed polymers showed evidently higher thermal stabilities than polymers P1-P4 described in chapters 2 and 3. These increased thermal stabilities could be due to the nature of linkage between monomer units in this new class of polymers compared to the previous class of polymers. The bonding of repeat units in P5 – P8 uses ether functional groups as linkages that are different to the ether linkages in polymers P3-P4, while polymers P1-P2 rely on ester linkage between monomer repeat units which could explain the higher thermal stabilities of P5-P8 series of polymers. Polymers P6 – P8 which incorporate TADF monomer units exhibit better thermal stability compared to polymer P5 which has no TADF monomers. The TADF units containing phenoxazine and triazine possess a high conjugated system, therefore Indeed, the thermal stability of specific materials can be improved by the presence of a highly conjugated system. For instance, optimising the intrinsic thermal conductivity (TC) is essential for the effective dissipation of heat in polymeric materials that are employed for thermal management.[266] Moreover, the increase of thermal stability, specifically in P6, P7 and P8, could be attributed to the increase of steric hindrance of the incorporated TADF emitters which leads to an increase in the rigidity and stability in the polymeric side chains in P6, P7 and P8. Higher temperatures are required to induce cleavage

in TADF polymers as a result of their rigidity during the degradation process. The desirable thermal properties of TADF polymers P6 – P8 present a good advantage for the use of these solution-processable materials in OLEDs' emitting layers.

Table 4.3 Thermal data of P5 – P8

Polymers	Td (˚C)
P5 0% TRZ-PXZ	251
P6 5% TRZ-PXZ	332
P7 10% TRZ-PXZ	359
P8 20% TRZ-PXZ	375

4.2.5 Optical Properties of P5, P6, P7 and P8

Ultraviolet-visible absorption spectroscopy (UV-Vis) and photoluminescence (PL) spectroscopy were employed to investigate the photophysical properties of polymers P5 - P8. The absorption and emission spectra of polymers P5-P8 which include a gradual increase of TADF monomers incorporated in their structures are presented in figure 4.5 and figure 4.6 respectively. Spectra of the free TADF dye (PXZ-TRZ) are also included in the figures to enable a comparison with the TADF functionalised polymers P6-P8. The investigations were conducted on diluted toluene solutions and on thin films (solid state). The optical band gaps for all designed polymers were calculated from polymers' onsets of absorption in thin films. The UV-vis an PL data of all polymers P5 – P8 as well as for the free TADF dye are summarised in table 4.4 below.

Table 4.4 Optica data of P5 - P8 in (a) solution and in (b) thin film. PL data of P5 - P8 in (c) solution and in (d) thin film. (e) Error in the range at the maximum of the absorbance curve for different extinction coefficients. The optical band gap of P5 - P8.

Polymers/ Compounds	**λ_{abs} (a) (nm)**	**λ_{abs} (b) (nm)**	**λ_{Onset} Film (nm)**	**λ_{em} (c) (nm)**	**λ_{em} (d) (nm)**	**$E_{g\ opt}$ (eV)**
P5 0% TRZ-PXZ	355	361	378	394.5	397.5	3.28 ± 0.03 [e]
P6 5% TRZ-PXZ	363	366	383	413.5	528.5	3.23 ± 0.06 [e]
P7 10% TRZ-PXZ	362	365	382	417.5	534.5	3.24 ± 0.02 [e]
P8 20% TRZ-PXZ	368	370	386	421.5	545.5	3.21 ± 0.06 [e]
TRZ-PXZ	435	445	----	543.5	550.5	---

As can be observed in figure 4.5 below, all polymers P5-P8 showed the maximum absorption peaks in solution between 355 – 368 nm, respectively. In addition, all polymers absorb light in the short and long wavelengths. The short wavelengths of P5-P8 observed between 290 nm and 296 nm are attributable to the π-π* transition originating from the polymer backbone. While the long wavelengths correspond to the n-π* transition from the carbazole molecule in the polymeric backbone as well as absorptions from the (PXZ – TRZ) substituents. In comparison, the TADF (PXZ – TRZ) showed a weak broad absorption from 375 – 493 nm, this is attributed to the ICT process occurring between the donor molecule, phenoxazine, and the acceptor molecule, triphenyltriazine.[267] This has been observed in the polymers P6 – P8 which were susbstituted with varying molar ratios of the TADF moieties, confirming the successful incorporation of TADF molecules in the polymeric repeat units. All designed polymers P5 – P6 displayed similar absorptions in films, with more red-shifted absorption bands compared to their absorption in solutions. This is due to the effect of increasing the intermolecular π-π interaction of carbazole repeat units in thin films. The optical band gaps for the designed polymers P5 – P8 were calculated to be 3.28 eV, 3.23 eV, 3.24 eV and 3.21 eV respectively. The lower and high optical band gap values obtained for the designed polymers P5-P8 correspond to an increase and decrease in the electronic conjugation of polymers, respectively.[268] Minimising the optical band gaps is necessary because photons with energy lower than the band gap cannot be absorbed. Furthermore, the optical band gap exhibits a substantial influence on both the colour and emission properties of a substance.

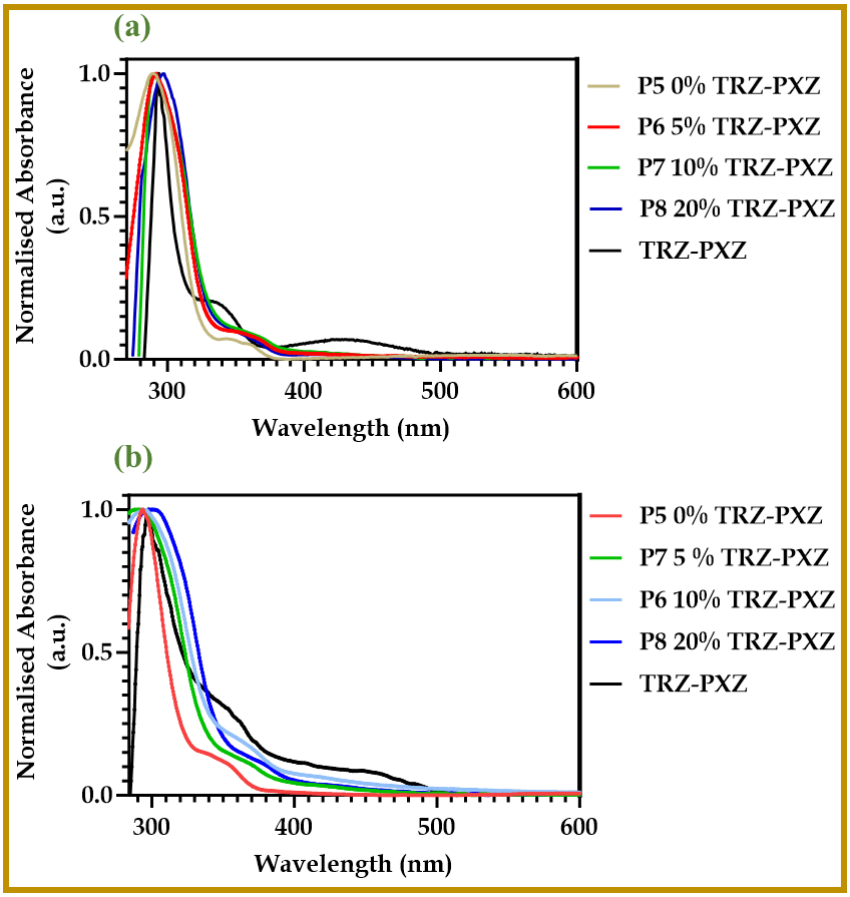

Figure 4.5 (a) Normalised UV vis absorption spectra of P5 – P6 in solution and (b) in thin film. In terms of the UV-vis spectra, all polymers from P5-P8 exhibited hypsochromic shifts in solution with notable broad absorptions from 375 – 493 nm in P6, P7 and P8. These weak absorptions are attributed to the ICT process occurring between the donor molecule, phenoxazine, and the acceptor molecule, triphenyltriazine. In the thin film of P5, P6, P7 and P8, bathochromic shifts were observed compared to the absorptions of the same polymers in solution. This is attributed to the effect of increasing the intermolecular π-π interaction of carbazole repeat units in thin films.

Figure 4.6 (b) shows the photoluminescence spectra of the designed polymers P5 – P8 and the free TADF (PXZ – TRZ) molecule in both toluene solution and film. In solution, P5 which possess 0% of the TADF moieties presented only one emission peak at 394.5 nm compared to the other modified polymers with TADF which presented dual emission peaks at 413.5 nm and 543.5 nm respectively. These are assigned to the emissions of the polymeric backbone and the TADF moieties respectively. Notably, the intensity of the longer emission peaks at 543.5 nm increased proportionally with increasing the ratio of TADF, signifying that energy is transferred from the polymeric backbone to the TADF units more efficiently when the ratio of TADF substituents is higher.[267] In contrast, the polymers P6 - P8 with different ratios of the TADF units exhibited distinct features in thin film. The PL spectrum of P6, which possessed 5% of

the TADF units, displayed a small peak around 383–450 nm. This peak is likely attributed to the emission originating from the polymeric backbone, due to incomplete energy transfer from the polymeric backbone to the TADF (PXZ – TRZ) units. Whereas the PL spectra of P7 and P8, which were grafted with 10% and 20% of the TADF units, exhibited only one TADF peak at 543.5 and 545.5 nm accompanied by tail residual peaks at 396.5 and 403.5 nm, emitted from the backbone of the main chain, respectively. This is clear evidence that interchain and intrachain energy transfer is more efficient in the solid state given the short space separation between the carbazole repeat units and the TADF moities.[269]

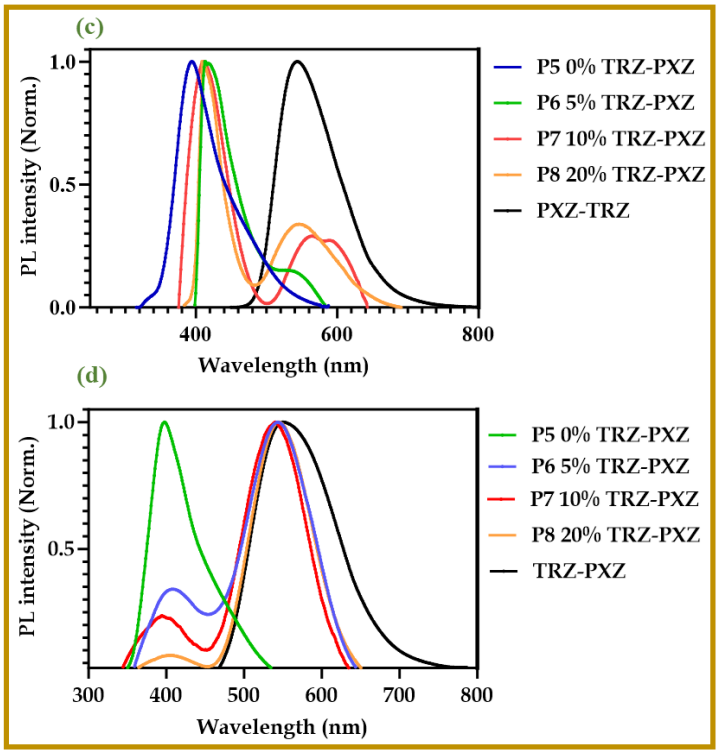

Figure 4.6 (c) Normalised PL emission spectra of P5 – P8 in (c) solution and (d) in the thin film. In solution, P5 showed only one polymeric emission in comparison with the grafted P6, P7 and P8 with different molar ratios of TADF, which exhibited dual emissions corresponding to the polymer (at short wavelength) and the TADF sidechain (at long wavelength). The intensity of TADF sidechain emissions increases proportionally with increasing the molar ratios of the TADF, indicating that energy is transferred more effectively from the polymeric backbone to the TADF units. In the thin film, P5 exhibited the same behaviour in solution by showing one polymeric peak with more red shifting. P6 (grafted with 5% of TADF) in comparison with P7 and P8, showed one small polymeric peak ~ 400 nm. This means incomplete energy transfer from the polymeric backbone to the TADF (PXZ – TRZ) units. However, both P7 and P8 exhibited only one TADF emission at ~ 454 nm, confirming the complete and efficient energy transfer from the polymers' main chain to the TADF sidechains.

It can be noticed from Figure 4.6 (d), that in the solid state once the incorporation of TADF increased, the PL spectra of the polymers P6 – P8 possess the TADF units presented more

hypsochromic shift from 528.5 – 545.5 nm, indicating the increase of aggregation caused by increasing the TADF moiety. Therefore, demonstrating the obvious influence of the TADF moiety on the emission characteristics of the copolymers.

4.2.6 Electrochemical Properties of P5, P6, P7 and P8

The electrochemical behaviour of all designed polymers P5 – P8 (grafted with 0% to 20% of TADF units) was investigated using cyclic voltammetry (CV) on films prepared from solutions with a concentration of 1 mg/ml in chloroform using similar measurement conditions to those mentioned in Chapter 2. The HOMO level values were calculated from the onset of oxidation of the polymers, while the LUMO level values were determined from the difference between the optical band gap and the HOMO level as summarised in table 4.5 below. It is more common to determine the LUMO levels from the onset of reduction in cyclic voltammetry. Unfortunately, in this case, the reduction peaks were not easily observed in our measurements. All designed polymers were measured in acetonitrile solutions of Tetrabutylammonium perchlorate. Therefore, during the reduction process, the larger sidechains of polymers may have impeded the diffusion of the bulky BuN+ cation into the polymer film, resulting in the unobserved reductions of all polymers P5–P8. Because of this, charge balance would be impossible, leading to a huge overpotential and a change in the reduction to occur outside of the solvent window.[270]

Table 4.5 CV data of P5 – P8, (a) HOMO and (b) LUMO level values. (c) the electro band gap

Polymers	HOMO (eV)[(a)]	LUMO (eV)[(b)]	$E_{g\ elect}$ (eV)[©]
P5 0% TRZ-PXZ	-5.20	-1.92	3.28
P6 5% TRZ-PXZ	-5.09	-1.86	3.23
P7 10% TRZ-PXZ	-5.05	-1.81	3.24
P8 20% TRZ-PXZ	-4.98	-1.77	3.21

HOMO values were obtained from the anodic (oxidation) curve onset, whereas the LUMO values were calculated from the difference between the HOMO and the optical band gap values.

As illustrated in figure 4.7 below, P5 which has no TADF monomer units showed a single oxidation peak, compared to the P6 – P8 (grafted with TADF 5% - 20% respectively), which presented two oxidation peaks. The first semi-oxidation peak corresponds to the phenoxazine (electron donor) from the TADF unit, whilst the second oxidation peak is assigned to the polymeric backbone and the carbazole-based host units. Polymers from P6 – P8 which possess

TADF units, presented shallower values of the HOMO level from -5.09 to -4.98. This is due to the effect of increasing the feeding ratio of the TADF from 5% - 20 %. In contrast, P5 which has no TADF repeat units exhibited the deepest value of the HOMO level -5.20 eV. This is due to oxidation only affecting the carbazole units from the polymeric structure. It can be observed that P6 – P8 showed deeper values of the LUMO level from -1.86 eV to -1.77 eV compared to P5, this can be attributed to the presence of triazine units (electron acceptor) in the TADF units. Therefore, the electrochemical behaviour of the designed polymers P5 – P8 is comparable to the electrochemical behaviour of the designed yellow-green TADF polymers by Zong et al.[267] It was advantageous for the designed polymers to gain the electrochemical properties of both the host units and emissive units since the polymer backbone and TADF units or host units are linked via the non-conjugated linkage. This could significantly reduce the mutual interference of the TADF units, host units, and polymer backbone.[116, 271]

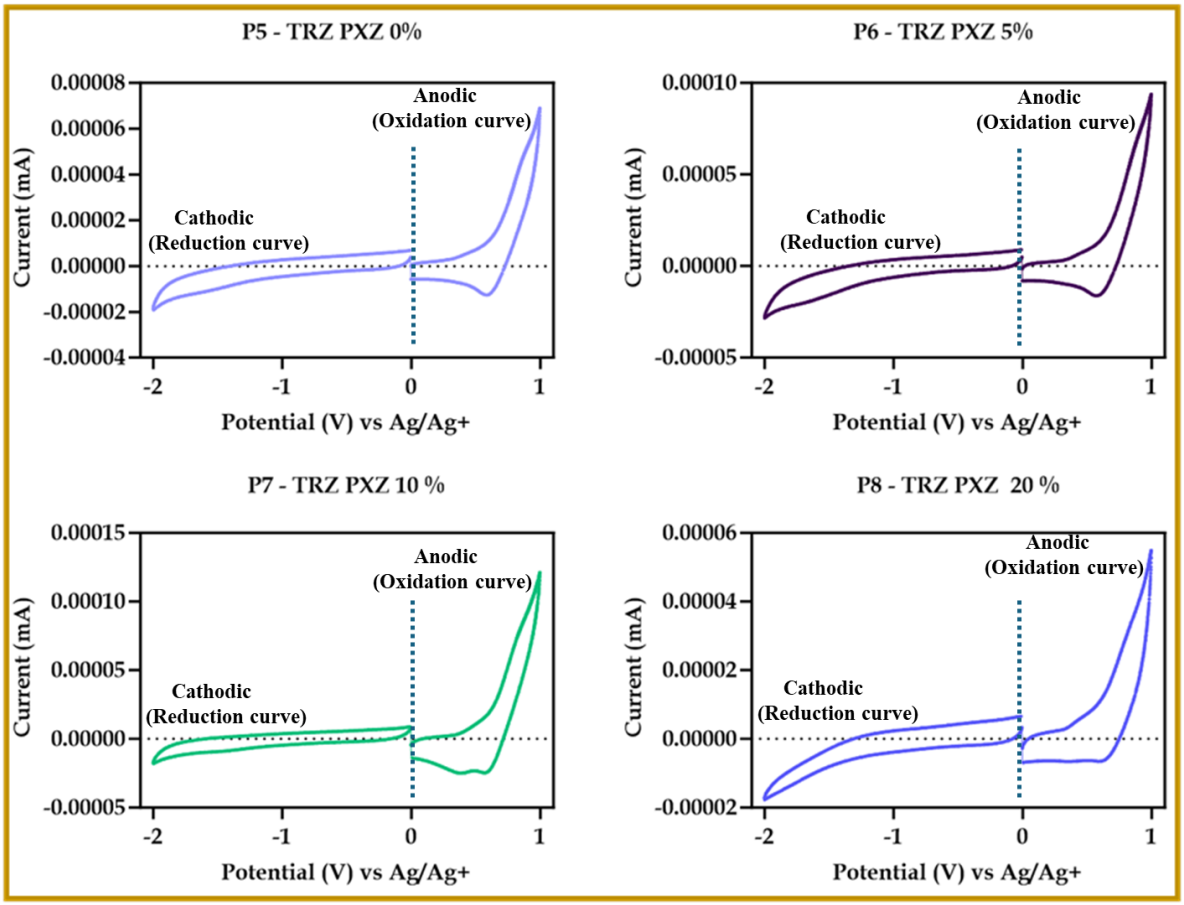

Figure 4.7 The CV analysis of P5 – P8. P5 (containing 0% of the TADF) exhibited only one oxidation and reduction peak. Polymers from P6-P8, which grafted with different molar ratios of the TADF (5%, 10% and 20% respectively) exhibited two peaks of oxidations; the first oxidation peak which corresponds to the polymer backbone and carbazole-based host molecules, and semi-oxidation peak

which corresponds to the phenoxazine moiety (electron-donating molecule) of the TADF units. The intensity of this peak increase with increasing the molar ratio of TADF. Th reduction peaks of all designed polymers could not be identified, therefore the LUMO values were calculated from the difference between the optical band gaps and the HOMO values.

4.3 Conclusion

Side chain strategy was applied to prepare a series of yellow-green emitting TADF hyperbranched polymers P5 – P8 through a Suzuki polycondensation approach. The structure of the designed polymers P5-P8 was confirmed using ^{1}H NMR spectroscopy. Polymers P5-P8 were obtained in good yields. A gradual increase of the ratio of TADF monomer in polymers P5-P8 (0%, 5%, 10% and 20%) was confirmed by the observation of a gradual increase in the intensity of signals from the TADF units in their ^{1}H NMR spectra. As a result of their hyperbranched structure, polymers P5-P8 showed great solubility in common organic solvents such as DCM, chloroform, THF and toluene. The designed polymers P6-P8 possessed slightly lower number average molecular weights Mn ranging between 13000 - 14600 Da compared to P5 which possessed the highest Mn of 19000 Da, this is attributed to the high steric hinderance of the carbazole molecules of M2 . The thermal, photophysical and electrochemical behaviour of P6-P8 has been compared with those of polymer P5 which has no TADF repeat units. Thermally, all polymers P5-P8 showed excellent thermal resistance to degradation ranging from 251 – 375 ˚C. All polymers with TADF incorporated repeat units showed higher thermal stability than polymer P5 which has no TADF dye substituents. The polymers are therefore, promising for OLED devices because of their excellent solubility and resistance to thermal degradation during operation.

The photoluminescence spectroscopy indicates the transfer of energy from the polymers' backbones to the TADF substituents once the P6-P8 were grafted with the TADF units. P5, which was synthesised with 0% of the TADF unit, displayed a single emission peak at around 394.5 nm. In contrast, P6-P8, in diluted toluene, displayed dual emission peaks at approximately (413.5 nm, ± 0.09) and (543.5 nm, ± 0.07), which are assigned to the emissions of the polymers' backbone and the TADF moiety, respectively. Furthermore, the intensity of the TADF peak (approximately 543.5 nm, ± 0.03) increased as the molar ratio of the TADF units was increased; this indicates a more efficient transfer of energy from the backbone of the polymer to the TADF moiety. The complete energy transfer from the backbone to the TADF unit occurred in the solid state, as evidenced by the increased intensity of the peak at the tail of spectra (approximately 547.5 nm) and the decreased intensity of the peak at the polymer backbone.

UV-Vis spectroscopy was employed to investigate the optical properties of all designed polymers in both diluted toluene and in thin films. The maximum absorption peaks of all P5-

P8 polymers in solution were found to be in the ultraviolet-visible region between 355 nm and 368 nm). Breaking the conjugation system in the polymer's backbones reduces electronic delocalisation throughout the polymer's chains, leading to a comparatively short wavelength.

The noticed decrease of the optical band gaps of all designed polymers P5-P8 in thin film is attributed to the increase of the aromatic compounds in the polymers, leading to a more conjugated system.

The electrochemical behaviour of all designed polymers P5-P8 was investigated via cyclic voltammetry (CV) under the protection of nitrogen atmosphere. P6-P8 (grafted with TADF moiety with the ratio of 5%-20% respectively) exhibited low HOMO levels and compared to P5 which has no TADF units. This is due to the effect of increasing the TADF ratio in polymers P6-P8. The LUMO values of all designed TADF polymers P5 – P8 were calculated from the difference between the HOMO values and the optical band gaps, as the reduction curves could not be identified appropriately. The electro band gaps were calculated to be 3.28 eV, 3.23 eV, 3.24 eV and 3.21 eV for all designed P5, P6, P7 and P8 respectively.

Chapter 5: Synthesis and Design of TADF Hyperbranched Polymers Based on DPEPO Derivatives for OLED Applications

Abstract

Emitters that possess TADF properties are promising materials for use in solution-processed OLEDs. In this chapter, a sidechain engineering approach is described to design a number of green TADF copolymers. The new hyperbranched polymers main structure was designed using both triplet energy host units (DPEPO moiety) and non-conjugated units (1,3,5-tris((6-phenoxyhexyl)oxy)benzene). Each of the polymers with DPEPO repeat units (P10-P12) were grafted with various ratios of the green-emitting TADF moiety PXZ-TRZ in 5%, 10% and 20% respectively. P9 was synthesised with 0% of the TADF units PXZ-TRZ in order to compare its properties with the other TADF grafted polymers (P10-P12). The successful confirmation of the polymers' structures was undertaken using ^{1}H NMR spectroscopy, with the observation of a gradual increase in the signals from the TADF monomer repeat units with increasing incorporation of the TADF ratio in P10-P12. In terms of solubility, all polymers were completely soluble in a number of organic solvents such as THF, chloroform and DCM. P10-P12 possessed generally a number average molecular weights Mn ranging between 9000 and 11600 Da compared to P9 which has a higher number average molecular weight Mn of 23800 Da. The low molecular weight is attributed to the steric hindrance in P10-P12. All polymers P9-P12 exhibited great thermal stability with the lowest degradation temperature at 257 ^{0}C. In the solid state, PL spectra of P10 and P12 showed complete energy transfer from the polymer backbone to the TADF units approximately at 534 – 539 nm.

5.1 Introduction

Research into OLEDs has made significant advances since the initial report by Tang and Vanslyke in 1987 which has established the way for a great deal of work into the area, with the goal of improving OLED efficiency and lowering their cost for applications such as lighting and visual displays.[272] 75% of all excitons are non-radiative triplets, which are produced in conventional fluorescent emitters as a result of electrical excitation,[238] and this has been an early barrier to device efficiency. Theoretically, this path has a maximum IQE of 63% (even if the annihilation of two triplets can yield one emissive singlet). Phosphorescent emitters with the highest value of IQE can be obtained by harvesting triplet excitons using organometallic compounds, including heavy metal atoms such as iridium and palladium.[273] Optimised layered designs have been utilised in the development of highly efficient grey and white OLEDs, including phosphorescent emitters, which were fabricated by thermal deposition processes conducted under high *vacuum* conditions (chemical vapour deposition).[274-277] Nevertheless, phosphorescent emitters based on heavy metals result in substantial ecological and financial impacts. The aforementioned limitations have prompted scholars to explore more cost-effective and ecologically sustainable solutions. Furthermore, when compared to solution techniques such as spin-coating or printing, *vacuum* deposition methods exhibit a significantly higher energy footprint. Consequently, there is a reason for the scientific and industrial sectors to develop solution-based techniques that utilise metal-free organic materials.[184, 277, 278] In order to meet the requirements of solution-processed technology, substantial financial and time investments are required to develop more efficient TADF materials with these properties.[279-282]

In 2019, Zhuo et al. designed and investigated a series of green TADF copolymers P0-P12 following the sidechain strategy.[126] The TADF moiety namely 10,10′-(((2-(4-(9H-carbazol-9-yl) phenyl) pyrimidine−4,6-diyl) pyrimidine bis (4,1-phenylene) bis (10H-phenoxazine) (PXZ-Pm-MeOCz) has been grafted into each sidechain of the designed copolymers P0-P12 with various molar ratios of 0%, 0.03%, 0.06%, 0.09% and 0.12% respectively as illustrated in scheme 5.1 below. Copolymers' main chains have been designed to include both non-conjugated units (tetraphenyl silicon moiety) and partially conjugated units (carbazole moiety). Utilising only non-conjugated units as a main chain backbone could affect the conductive properties which results in an undesired device's performance. Therefore, an equilibrium (charge balance) can be reached by using both non-conjugated and partially conjugated units.

It is noteworthy that each of the synthesised TADF polymers P0-P9 demonstrated high PLQYs in the solid state, ranging from 0.64 to 0.71. This characteristic makes them applicable to be used in non-doped OLEDs. In addition, the maximum EQE of the non-doped solution-processed OLEDs reached 7.0% once these TADF polymers were utilised as emitting layers.[126]

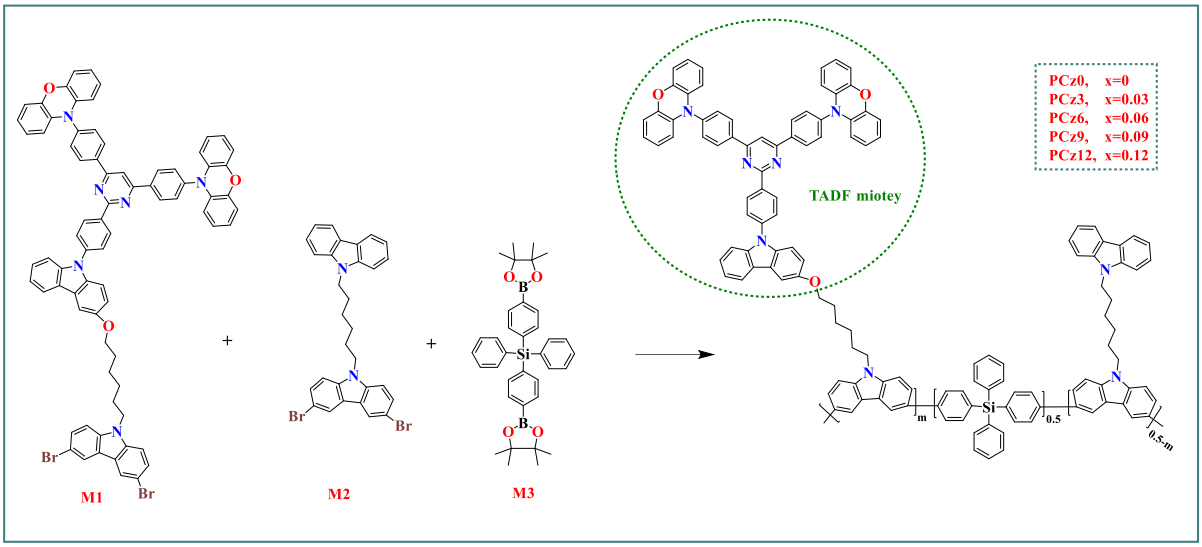

Scheme 5.1 Design of green TADF copolymers by Zhuo et al. Five polymers have been prepared using a polymer sidechain strategy. The polymer sidechains have been grafted with different ratios of the TADF emitter (0%, 0.03%, 0.06%, 0.09% and 0.12%). Grafting the TADF emitter as a sidechain with different ratios was applied to investigate the polymers' properties, such as the thermal, optical and electrochemical properties. Connecting the TADF moiety as sidechains to the polymer backbone via non-conjugated linkages is beneficial. This is to keep the functionalities of the polymer backbone and the TADF sidechains preserved separately.

5.2 Results and Discussion

As a green TADF light emitter in OLED devices, PXZ-TRZ is widely acknowledged for its efficiency. A substrate must undergo evaporation of PXZ-TRZ in order to obtain the active layers, which are necessary for the emitter's implementation in devices. Polymer sidechain engineering was utilised to enable the incorporation of TADF units onto the sidechains of backbone polymers, thereby enabling the use of polymer-based TADF materials in solution-processed devices. Using this strategy, the hyperbranched polymer backbone acts as the host and charge transport channel, while the grafted TADF unit on the polymer sidechain adds functionality and acts as the guest emitter. In this work, a series of yellow to green TADF hyperbranched polymers are designed and synthesised by using a sidechain engineering approach; to achieve equilibrium, their polymeric backbone is composed of repeat units which

include DPEPO moiety which is known as an efficient host material to TADF materials when fabricating devices using vapour evaporation of small molecules.

The selection of DPEPO as one of the main repeat units in the polymers host materials is explained by the many great features of DPEPO such as its high triplet energy (3.3 eV) and excellent electron transporting ability. This is to avoid undesired triplet transfer from the guest TADF emitter to the host material which would reduce EL efficiency. The electronic delocalisation within the polymer backbone, caused by the DPEPO host as repeat units was controlled by 1,3,5-tris((6-phenoxyhexyl)oxy)benzene from M6. Applying M6 as a spacer in the polymeric backbone plays an essential role in terms of modifying the triplet energy (E_T) of the polymer host.

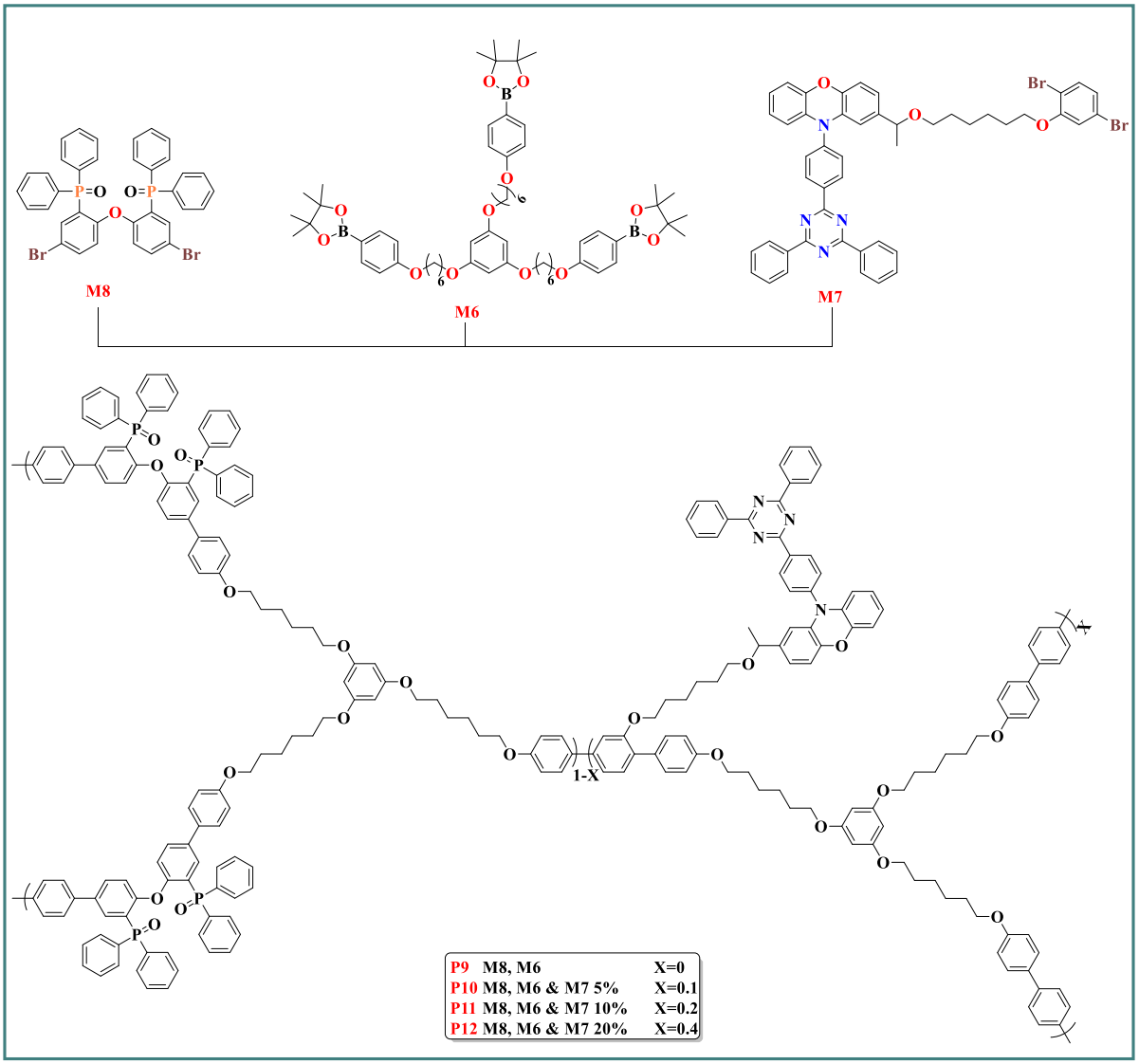

Scheme 5.2 Design of yellow-green TADF hyperbranched polymers P9 – P12. Four hyperbranched polymers were prepared using different molar ratios of M8, M6 and M7. P9 was prepared using the ratio of (50:50, M8:M6), while the polymer from P10 – P12 were prepared using the molar ratio of (45,

50, 5), (40, 50, 10) and (30, 50, 20) of the selected M8, M6 and M7 respectively. Reagents and conditions; THF, Sat.$NaHCO_3$, $Pd(OAc)_2$, $P(o\text{-}tol)_3$, K_2CO_3, 24h, Reflux.

In this chapter, a series of yellow-green light-emitting hyperbranched polymers were designed *via* the Suzuki cross-coupling approach. Various molar ratios of M6, M8 and M7 were incorporated yielding the required polymers P9 – P12 as shown in scheme 5.2 above. M6 and M8 were reacted with the selected ratio of 50:50 to afford P9 with 0% feeding of the TADF (M7). P10 – P12 were synthesised using different molar ratios of M6, M8 and M7 as 50:45:05, 50:40:10 and 50:30:20 respectively. the influence of grafting TADF in P10 – P12 was, investigated and compared with P9 which contains 0% of TADF unit. The structure of all designed polymers P9 – P12 was verified and confirmed via ^1H NMR analysis. Moreover, the solubility behaviour of all polymers was examined in different solvents such as chloroform, DCM, THF and toluene. Furthermore, properties such as molecular weight determination, thermal stability, photophysical properties and electrochemical behaviours were studied and investigated for the designed polymers P9 – P12.

5.2.1 Synthesis of $DPEPOBr_2$ M8

The target monomer (M8) namely 1-bromo-4-[4-bromo-2-(diphenylphosphinoyl)-phenoxy]-5 (diphenylphosphinoyl)-benzene ($DPEPOBr_2$), was prepared through two synthetic steps, by using DPEPOhos as a starting material, resulting in the formation of product (25) namely bis[2-(diphenylphosphino)phenyl] ether oxide (DPEPO). The last step of preparing M8 was achieved upon bis-bromination of DPEPO, obtaining the required product (26) M8 as shown in the scheme 5.3 below.

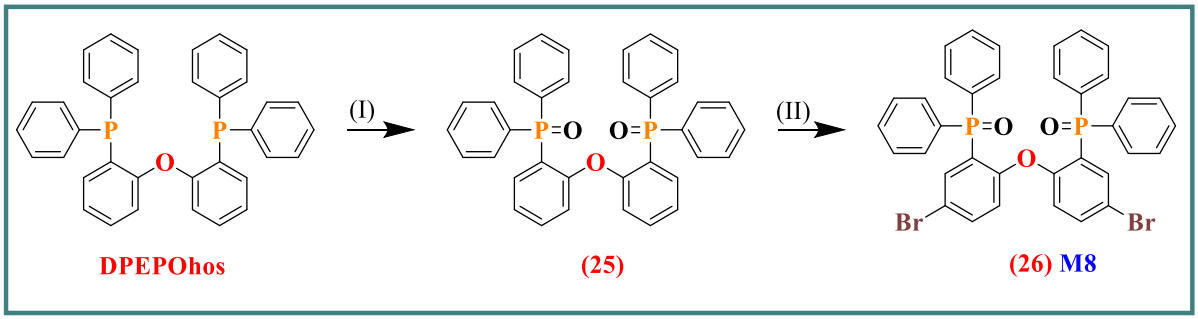

Scheme 5.3 Monomeric steps of synthesis M8. Product (25) was prepared via oxidation of DPEPOhos using hydrogen peroxide as an oxidising agent with respect to other reaction conditions mentioned below. M8 was prepared through the bromination of compound (25) to afford 1-Bromo-4-[4-bromo-2-(diphenylphosphinoyl)-phenoxy]-5 (diphenylphosphinoyl)-benzene. Reagents and conditions; (I) H_2O_2 (30%, aq), DCM, 0 ^0C, 5 h. (II) NBS, glacial acetic acid, H_2SO_4, room temperature, 7.5 h.

Product (25) was prepared according to the synthetic procedure illustrated by Miyata et al.[283] The reaction was conducted under N_2 environment at 0 ^{0}C, using anhydrous DCM as a solvent and hydrogen peroxide (30%, aq) as an oxidising agent. The required product was obtained as a white solid in a high yield of 94.6%. The reaction underwent *via* an oxidation mechanism as illustrated in the scheme 5.5 below. The phosphorus atoms from the starting material (DPEPOhos) acted as a nucleophile, which attacked one of the hydrogen peroxide oxygen atoms, resulting in the intermediate (a) formation of phosphine oxide protonated on the oxygen atom (see scheme 5.5).

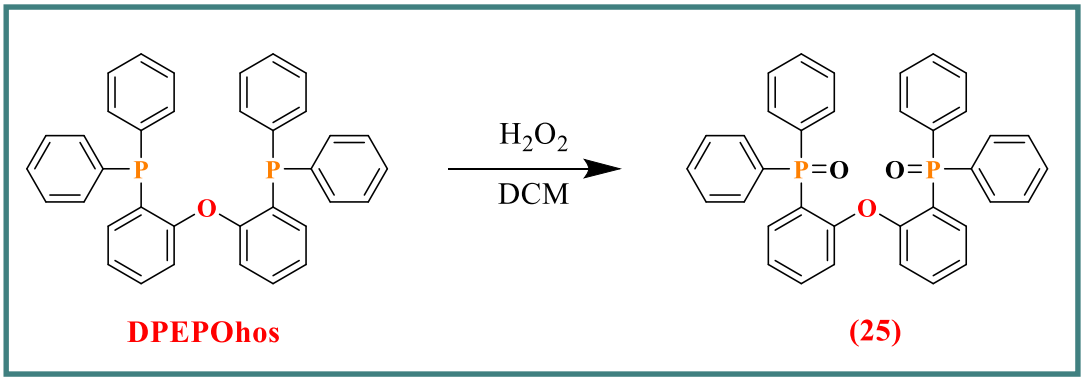

Scheme 5.4 Synthetic conditions of compound (25). Reagents and conditions; (I) H_2O_2 (30%, aq), DCM, 0 ^{0}C, 5 h.

Subsequently, the second phosphine group present in the resultant compound (b) undergoes oxidation, leading to the generation of a tertiary phosphine oxide group. This chemical transformation ultimately yields the required compound (25).

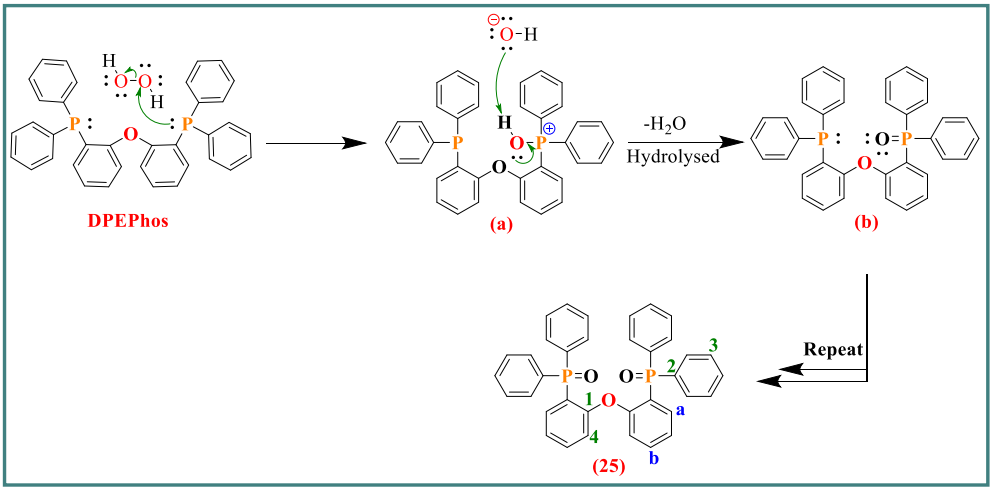

Scheme 5.5 The proposed mechanism for compound (25). The synthesis of Bis[2-(diphenylphosphino)phenyl] ether oxide (DPEPO) was carried out under the protection of N_2, using

DCM as a reaction medium and hydrogen peroxide (30%, aq) as an oxidising agent. The reaction underwent *via* an oxidation mechanism in two synthetic steps; the phosphorus atoms from the starting material (DPEPOhos) acted as a nucleophile, which attacked one of the hydrogen peroxide oxygen atoms, resulting in the intermediate (a) formation of phosphine oxide protonated on the oxygen atom. Next, the second phosphine group present in the resultant compound (b) undergoes oxidation, leading to the generation of a tertiary phosphine oxide group. This chemical transformation ultimately yields the required compound.

The success of the reaction and formation of the target product was confirmed *via* ^{1}H NMR spectroscopy, ^{13}C NMR, elemental analysis and mass spectrometry. ^{1}H NMR characterisation identified a total of 28 protons, assigned to the aromatic protons of the product (25). A quartet was observed at 6.07 ppm, assigned to the two protons located in the *ortho*-position (a) from the chemical structure of compound (25) in scheme 5.5 above; this is attributed to the strong coupling with (P) atom.[284] in addition, a triplet was observed at 7.10 ppm, corresponding to the two protons in the *para*-position (b); this shielding caused by the electron-donating ether group which shifted the triplet to be upfield (see figure 8.18 in the appendix). The analysis of ^{13}C NMR showed a number of carbon peaks, a peak at 158.92 ppm which corresponds to the ether carbon atom (1) (phenyl carbon attached to the oxygen atom). The effect of electronegativity of oxygen caused the deshielding. Further peaks were observed at 143.14 ppm, 128.47 ppm and 123.81 ppm, assigned to the numbered carbon atoms 2, 3 and 4 respectively in the final chemical structure of compound (25) mentioned in the scheme 5.5 above. The analysis of mass spectrometry verified the structure of the required product by giving the value of 571.19. Further verification of the structure of compound (25) was approved by the concordant results from elemental analysis as C, 75.80; H, 4.99 which matched the calculated values C, 75.78; H, 4.95.

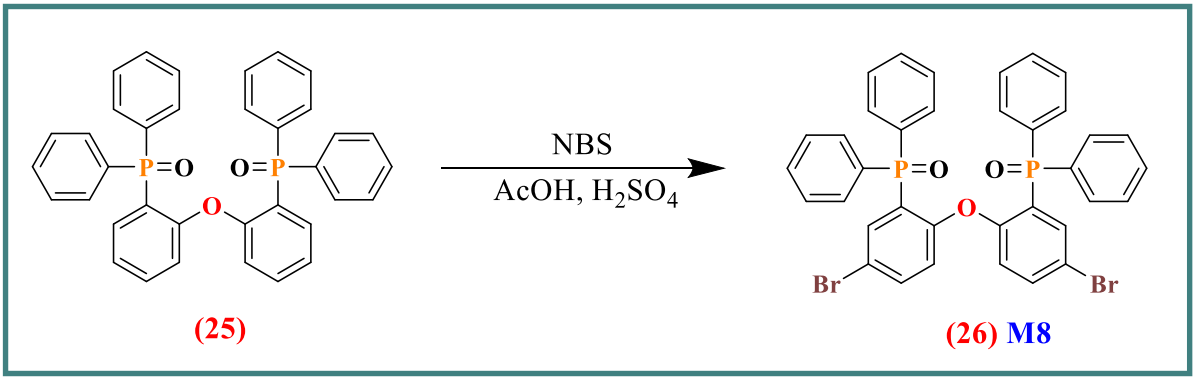

(25) (26) M8

Scheme 5.6 Synthetic conditions of compound (26) M8. Reagents and conditions; NBS, glacial acetic acid, H_2SO_4, room temperature, 7.5 h. In a dark environment.

The synthesis of product (26), namely DPEPOBr$_2$ M8 was carried out following a modified synthetic procedure by Han et al.[285] The reaction was conducted under dark conditions using N-Bromosuccinimide (NBS) as a brominating agent, H_2SO_4 as a catalyst and glacial acetic acid as a reaction medium as illustrated in the scheme 5.6 above. The crude product showed two spots in the TLC plate, which after purification *via* column chromatography using the eluent of (PE/EA, 14:1), afforded the pure target monomer as a white powder in a yield of 68%. The reaction mechanism consisted of an electrophilic aromatic substitution, which was already explained in chapter (2) as mechanism to prepare compound (2).

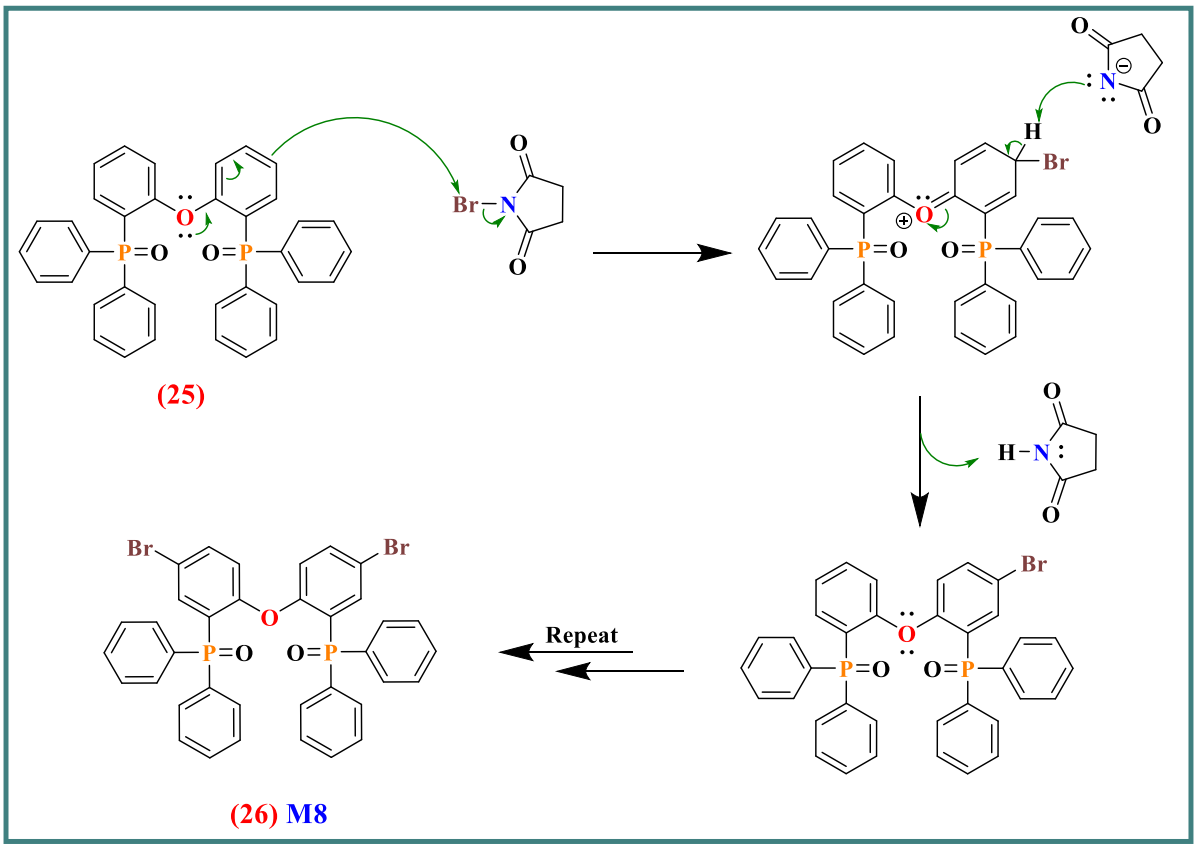

Scheme 5.7 The proposed mechanism for the preparation of compound (26) M8. The bromination of compound (25)was carried out under the protection of N_2, in the dark environment using NBS as a brominating agent and glacial acetic acid as a reaction medium. The electrophilic aromatic substitution was applied to be the reaction mechanism to afford 1-bromo-4-[4-bromo-2-(diphenylphosphinoyl)-phenoxy]-5 (diphenylphosphinoyl)-benzene (DPEPOBr$_2$) M8.

The identification of compound (26) M8 was verified *via* ^{1}H NMR, ^{13}C NMR and elemental analysis. The characterisation *via* ^{1}H NMR confirmed the bis-bromination of (25) at the *para*-positions of the oxygen atom and the formation of M8. The ^{1}H NMR analysis revealed a doublet of doublet at 7.83 ppm, multiplet at 7.77 ppm and quartet at 5.88 ppm, corresponding

to the two protons in position (a), twenty-two protons in position (b) and the last two protons in position (c). Moreover, the analysis of ^{13}C showed a new signal at 117.45 ppm, assigned to the two carbons bonded covalently to the new bromine substituents. Furthermore, characterisation by elemental analysis confirmed the successful preparation of M8 with concordant results between measured and calculated elemental percentages as C, 59.37; H, 3.60; Br, 21.94 and C, 59.39; H, 3.57; Br, 21.91 respectively.

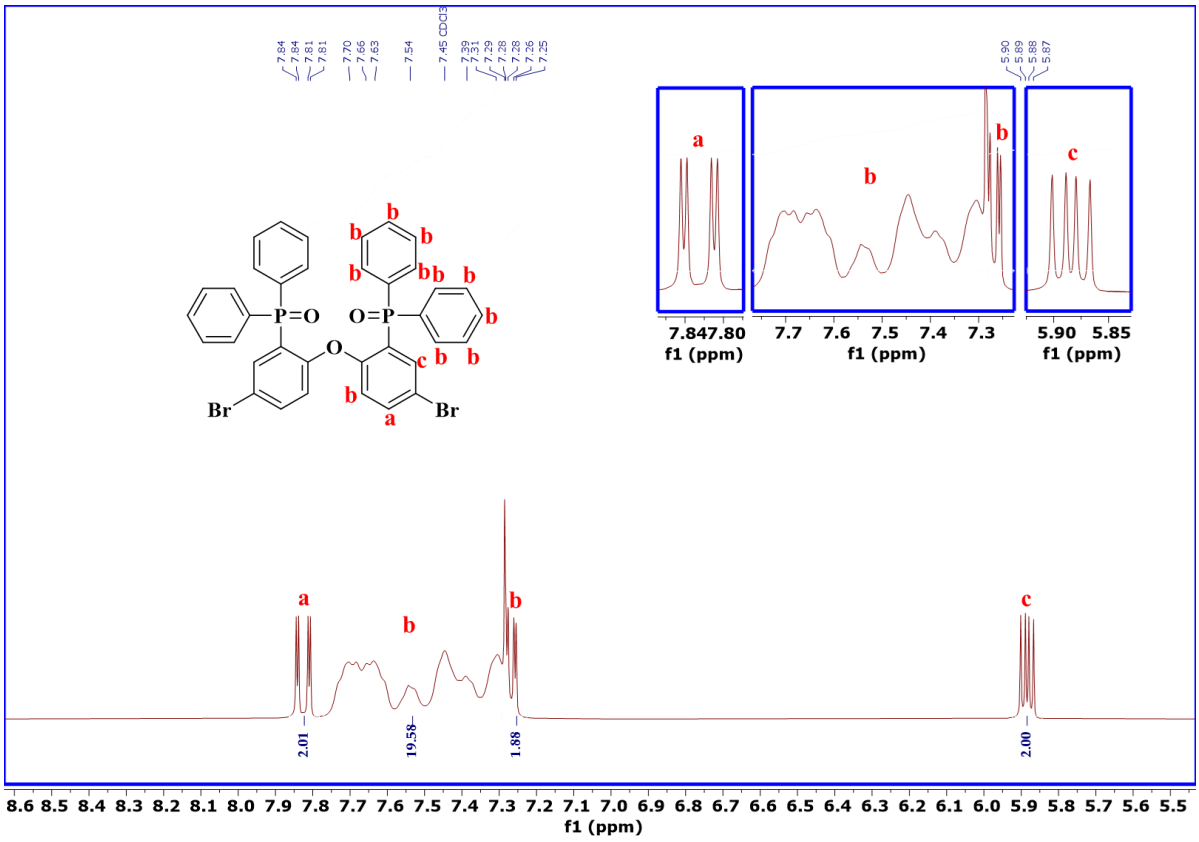

Figure 5.1 ^{1}H NMR spectrum of M8 in $CDCl_3$; 7.83 (dd, J = 12.7, 2.5 Hz, 2H), 7.77 – 7.58 (m, 8H), 7.54 (s, 2H), 7.39 (s, 6H), 7.31 (s, 3H), 7.28 – 7.27 (m, 1H), 7.26 (d, J = 2.5 Hz, 1H), 5.88 (q, J = 5.1 Hz, 2H).

5.2.2 Design and Synthesis of polymers P9, P10, P11 and P12

The designed polymers P9, P10, P11 and P12 were synthesised *via* Suzuki coupling reactions, with similar conditions to those detailed in the chapter 4. M8, M6 and TADF (M7) were selected to be polymerised with different molar ratios, affording the designed polymers. M8 and M7 were reacted within the molar ratio of 50:50 with 0% incorporation of TADF (M7) in order to obtain P9, whilst P10, P11 and P12 were designed in different molar ratios of the monomers as 45:50:5, 40:50:10 and 30:50:20 respectively. The reaction conditions were

similar to the reaction conditions applied to prepare the designed polymers in the previous chapter. The polymerisation reactions took 24 hours. This was followed by end-capping of the polymers *via* the subsequent addition of bromobenzene and then phenylboronic acid to improve the polymers' stability once applied in the OLED devices.

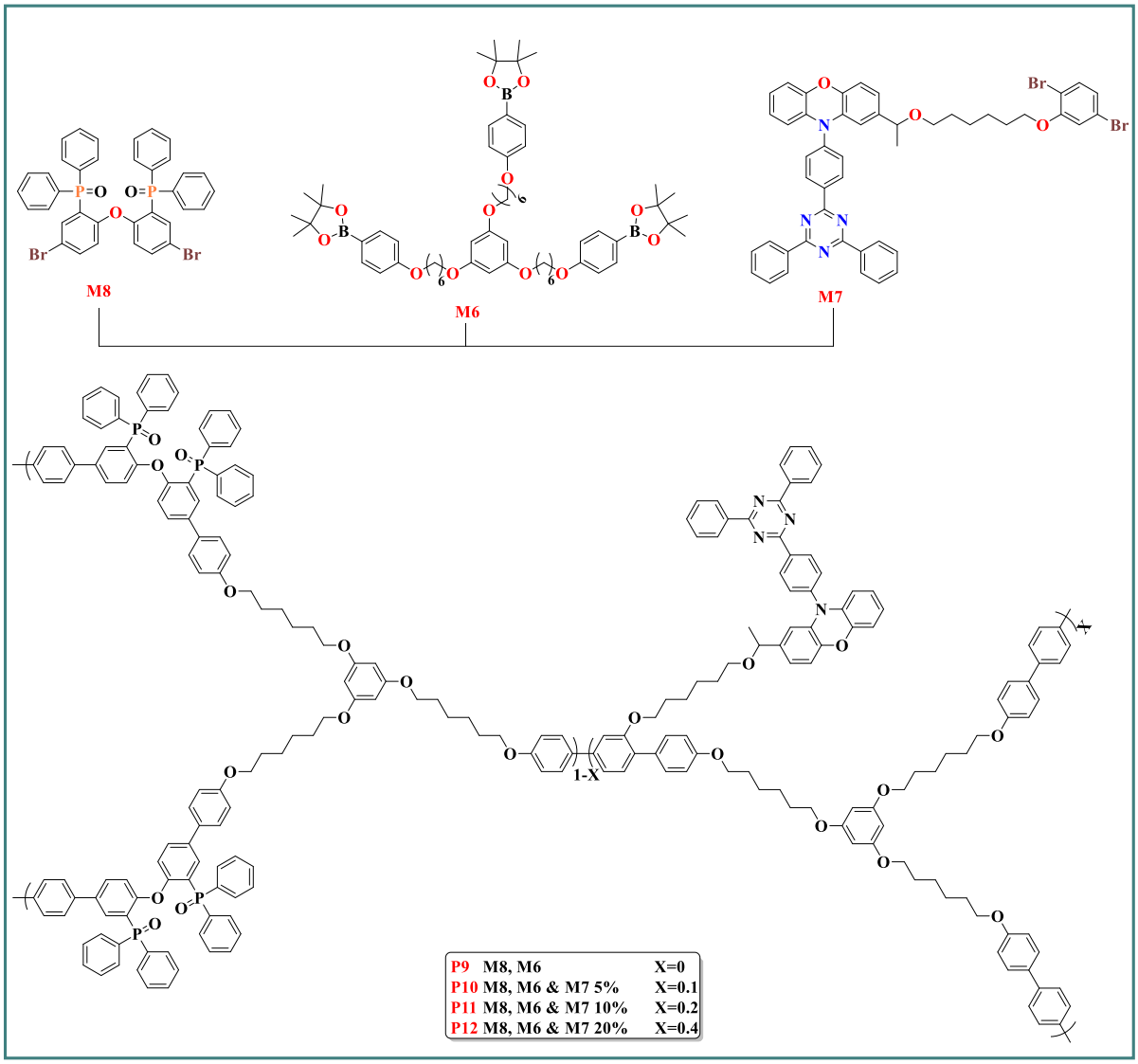

Scheme 5.8 The design of P9 – P12 with different ratios of TADF monomer M7. Four hyperbranched polymers were prepared using different molar ratios of M8, M6 and M7. P9 was prepared using the ratio of (50:50, M8:M6), while the polymer from P10 – P12 were prepared using the molar ratio of (45, 50, 5), (40, 50, 10) and (30, 50, 20) of the selected M8, M6 and M7 respectively. Reagents and conditions; THF, Sat.$NaHCO_3$, $Pd(OAc)_2$, $P(o\text{-}tol)_3$, K_2CO_3, 24h, Reflux.

The purification of the designed polymers was undertaken in three steps, initially by eliminating the excess catalysts *via* the addition of chloroform at the end of polymerisation and reaction with a solution of ammonium hydroxide to remove palladium catalyst residues,

followed by washing the organic layers with water to remove the ammonium hydroxide. The organic layers were reduced to a minimum amount of solvent followed by precipitation of the polymers with methanol, to obtain the designed polymers P9, P10, P11 and P12 in yields of 53%, 56%, 55% and 65% respectively. All polymers P9 – P12 exhibited excellent solubility in common organic solvents such as (chloroform, DCM, toluene and THF). The structural confirmation of the structures of all polymers P9 – P12 has been verified using ^{1}H NMR analysis as illustrated in figure 5.2 below.

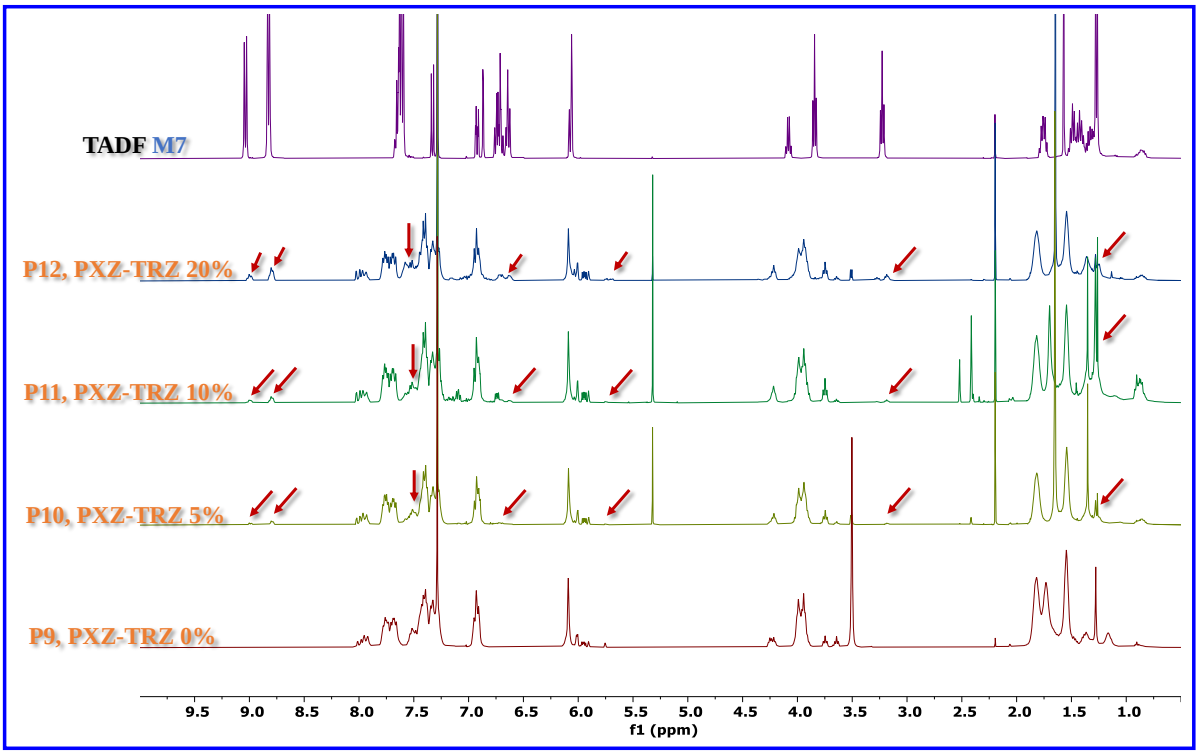

Figure 5.2 ^{1}H NMR spectra of the designed polymers P9 – P12 and TADF M7 in $CDCl_3$. The five NMR spectra for TADF M7, P12, P11, P10, and P9 were stacked, respectively (from top to bottom). These spectra showed the comparison among all TADF hyperbranched polymers grafted with TADF (M7) in different mole ratios. In P9, the TADF units were not grafted into the polymer's sidechain; therefore, no TADF spectra were observed in the polymer. However, in the polymers 10, 11, and 12, the corresponding TADF spectra increased proportionally with increasing feeding molar ratios from 5% to 20%. The data of all stacked spectra in $CDCl_3$ are as follows; **TADF M7**; 9.04 (d, J = 8.5 Hz, 2H), 8.83 (dd, J = 6.5, 1.4 Hz, 4H), 7.69 – 7.54 (m, 7H), 7.33 (d, J = 8.3 Hz, 1H), 6.92 (dd, J = 8.4, 2.1 Hz, 1H), 6.87 (d, J = 2.2 Hz, 1H), 6.78 – 6.67 (m, 3H), 6.64 (ddd, J = 7.6, 5.8, 1.7 Hz, 2H), 6.13 – 5.97 (m, 2H), 4.08 (q, J = 6.4 Hz, 1H), 3.84 (t, J = 6.4 Hz, 2H), 3.23 (t, J = 6.4 Hz, 2H), 1.76 (m, J = 14.0, 6.7 Hz, 2H), 1.53 – 1.29 (m, 6H), 1.27 (d, J = 6.5 Hz, 3H). **P9**; 8.06 – 7.87 (m, 1H), 7.84 – 7.59 (m, 4H), 7.56 – 7.30 (m, 8H), 7.02 – 6.81 (m, 3H), 6.09 (bs, 2H), 6.03 – 5.86 (m, 1H), 4.29 – 4.16 (m, 1H), 4.08 – 3.86 (m, 4H), 3.76 (bs, 0.36H), 3.66 (bs, 0.38H), 1.73 (bs, 10H), 1.32 (bs, 2H), 1.17 (bs, 1H). 0.89 (bs, 0.33H). **P10**; 9.01 (bs, 0.09H), 8.80 (bs, 0.14H), 8.06 – 7.85 (m, 1H), 7.84 – 7.61 (m, 3H), 7.60 – 7.32 (m, 5H), 7.01 – 6.82 (m, 2H), 6.14 – 6.05 (m, 1H), 6.04 – 5.86 (m, 1H), 4.22 (s, 1H), 4.07 – 3.86 (m, 3H), 3.81 – 3.68 (m, 1H), 1.82 (bs, 3H), 1.65 (bs, 4H), 1.54 (bs, 4H), 1.44 – 1.18 (m, 3H), 0.87 (bs, 1H). **P11**; 9.02 (bs, 0.27H), 8.82 (bs, 0.43), 8.06 – 7.87 (m, 1H), 7.84 – 7.62 (m, 5H), 7.59 – 7.36 (m,

7H), 7.03 – 6.81 (m, 4H), 6.80 – 6.66 (m, 1H), 6.15 – 6.04 (m, 2H), 6.03 – 5.85 (m, 1H), 4.22 (bs, 1H), 4.07 – 3.84 (m, 5H), 3.82 – 3.69 (m, 1H), 1.82 (bs, 6H), 1.70 (bs, 5H), 1.54 (bs, 6H), 1.42 – 1.33 (m, 3H), 1.31 – 1.22 (m, 5H), 0.94 – 0.83 (m, 2H). **P12**; 9.00 (s, 0.51H), 8.79 (s, 0.76H), 8.05 – 7.89 (m, 1H), 7.83 – 7.63 (m, 4H), 7.62 – 7.47 (m, 3H), 7.47 – 7.30 (m, 8H), 7.00 – 6.83 (m, 3H), 6.76 – 6.57 (m, 1H), 6.14 – 5.98 (m, 2H), 5.97 – 5.87 (m, 1H), 4.22 (s, 1H), 4.08 – 3.84 (m, 5H), 3.75 (s, 1H), 1.82 (s, 5H), 1.65 (s, 6H), 1.54 (s, 6H), 1.43 – 1.19 (m, 4H), 0.87 (s, 1H).

P9 with 0% molar ratio feeding of TADF revealed a broad multiplet at 8.02 ppm, which is assigned to some the aromatic protons in M8. Furthermore, a broad multiplet was observed at 7.77 ppm, corresponding to the terminal aromatic phenyl rings in M6. In addition, the peak of the alkoxy protons present in M6 have been observed as a broad multiplet at 3.99 ppm. Hence, the synthesis of P9 has been verified successfully based on the ^{1}H NMR analysis. Polymers P10 – P12 confirmed the incorporation of the TADF (M7) in their polymeric side chains, as they show a number of peaks at 8.99 ppm, 8.79 ppm, 7.5 ppm, 3.28 ppm and 1.28 ppm which correspond to the TADF (M7) protons. It can be seen from the ^{1}H NMR spectra of P10 – P12, how the intensity of the incorporated TADF (M7) monomer peaks increased with the increase of its molar ratio in the final polymers. The actual molar ratios of the incorporated TADF (M7) units was determined and calculated from the ^{1}H NMR spectra for the polymers P10 – P12 to be 4.6, 7.16 and 15.5 respectively as revealed in the table 5.1 below.

Table 5.1 The ratio of TADF (M7) in the polymeric side chains of P9 - P12

Polymers	Feed Molar Ratio %	Actual Molar Ratio %
P9 0% TRZ-PXZ	0	0
P10 5% TRZ-PXZ	5	4.6
P11 10% TRZ-PXZ	10	7.16
P12 20% TRZ-PXZ	20	15.2

P9 was prepared with 0% molar ratio of M7 in comparison with P10, P11 and P12, which were prepared using molar ratios of 5%, 10% and 20% respectively. The calculated molar ratio of M7 in P10 – P12 using the integrated NMR spectra showed values of 4.6 %, 7.16 % and 15.2 % respectively.

5.2.3 Molecular Weight of P9, P10, P11 and P12

The determination of the number average molecular weight (Mn), weight average molecular weight (Mw), and polydispersity index (PDI) of the synthesised polymers P9-P12 was conducted using gel permeation chromatography (GPC) as illustrated in table 5.2. THF was employed as the eluent, alongside the molecular weight of polystyrene as a standard reference.

Table 5.2 GPC data of the designed polymer P9 – P12

Polymers	Mn(Da)	Mw(Da)	PDI	Yield	Fraction
P9 0% TRZ-PXZ	23800	31000	1.3	53%	Chloroform
P10 5% TRZ-PXZ	10200	19000	1.8	56%	Chloroform
P11 10% TRZ-PXZ	9000	18200	2	55%	Chloroform
P12 20% TRZ-PXZ	11600	23600	2	65%	Chloroform

It can be seen from table 5.2 above, all polymers exhibited Mn and Mw values with a significant gap between those values. This could be attributed to the massive mass of polymers' molecules which result in high values of Mw. P9 had the highest number average molecular weight (Mn = 23800) compared to TADF polymers P10, P11 and P12 which showed lower molecular weight ranging between 9000 – 11600 Da. This is could attributed to an increase of DPEPO repeat units in the polymeric materials. The lower number average molecular weights of TADF polymers P10 – P12, could be attributed to the increase of the steric hindrance in the polymeric backbone which result in more rigid polymers. The PDI of the designed polymer P9 were calculated to be 1.3. It has been reported that a significant number of hyperbranched polymerisations result in materials exhibiting high polydispersities.[286] However, the precipitation of the polymers in their workup means that there is a certain degree of fractionation which affects the PDI values of the polymers. It is also to be noted that the values of the molecular weights obtained through GPC should be under-estimated as linear polystyrene standards were used in the GPC measurements.

5.2.4 Thermal Properties of P9, P10, P11 and P12

The thermal properties of polymers P9 - P12 were examined using TGA under N_2 atmosphere. The analysis was conducted at a heating rate of 10°C min^{-1}. As depicted in the table 5.3 provided below, the initial thermal degradation temperatures of the proposed polymers P9 – P12 were observed to be 257 °C, 367 °C, 389 °C, and 399 °C, respectively.

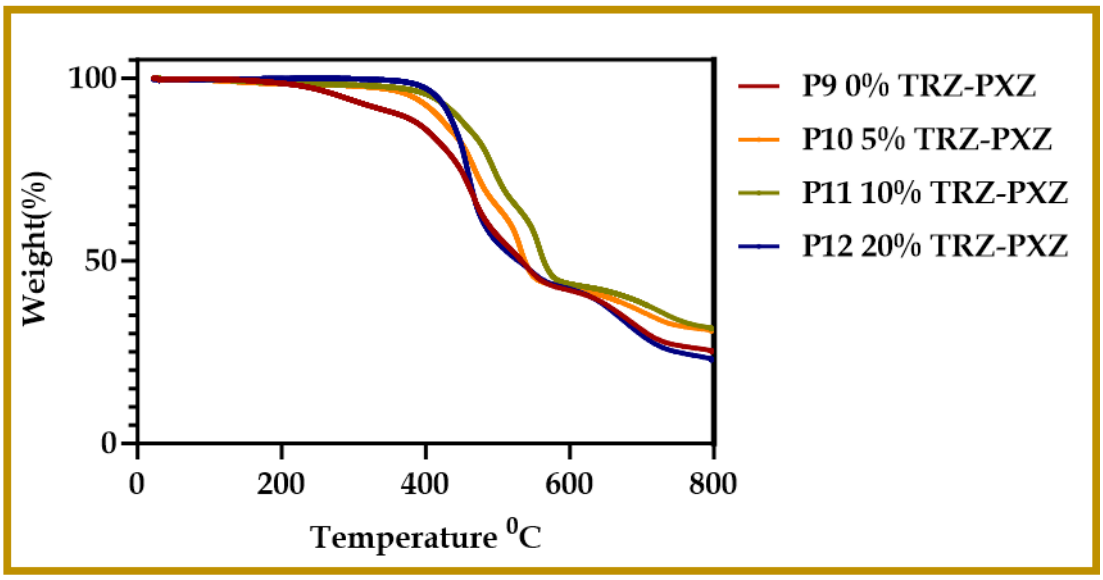

Figure 5.3 TGA analysis of P9 – P12. The thermal stability of all designed polymers 9 – 12 showed a proportional increase with increasing the TADF feeding ratios (0% > 5% > 10% > 20%). The degradation temperatures of all designed polymers were measured from the decomposition curves to be 257 °C, 367 °C, 389 °C and 399 °C respectively.

From the figure above, it is clear that all polymers exhibited excellent thermal stability such as 389 °C and 398 °C, particularly for polymers incorporating different ratios of TADF monomer (PXZ–TRZ) 5% - 20% in their polymeric side chains. P9 which possesses 0% of TADF units in its polymeric structure presented the lowest thermal resistance amongst the designed polymers with a degradation temperature of 257 °C. In comparison, P10 – P12 showed notable increases in the thermal stability from 367 °C - 399 °C proportionally with increasing the TADF moiety in the polymeric side chains. This is attributed to the increase of the steric hindrance in the TADF moiety in the polymeric side chains of P10, P11 and P12, resulting in more rigid polymers. Therefore, higher temperatures are required to promote cleavage in these polymers.

Table 5.3 Thermal data of P9 – P12

Polymers	Td (˚C)
P9 0% TRZ-PXZ	257
P10 5% TRZ-PXZ	367
P11 10% TRZ-PXZ	389
P12 20% TRZ-PXZ	399

Polymers P5 – P8 based one carbazole host molecules in chapter 4 exhibited lower thermal stabilities to those of polymers P9 – P12 based on DPEPO host molecules. This is attributed to the high thermal resistance of DPEPO molecules in the polymeric side chains.

5.2.5 Optical Properties of P9, P10, P11 and P12

Investigation of the photophysical properties of the polymers P9 – P12, which incorporate different molar ratios of TADF (PXZ–TRZ) 0%, 5%, 10% and 20% respectively was carried out *via* UV-vis absorption spectroscopy and photoluminescence (PL) spectroscopy in both toluene solutions and in thin films. In addition, the TADF (PXZ–TRZ) monomer was investigated optically to be compared with polymers P10-P12. The optical band gaps of all polymers P9- P12 were calculated from the polymers' onsets of absorption in thin films. The optical data of all polymers with the TADF monomer are listed in table 5.4 below.

Table 5.4 Optical data for P9 – P12 in (a) solution and in (b) thin film. PL data of P9 – P12 in (c) solution and in (d) thin film. (e) Error in the range at the maximum of the absorbance curve for different extinction coefficients. The optical band gap of P9 – P12.

Polymers/ Compounds	λ_{abs} (a) (nm)	λ_{abs} (b) (nm)	λ_{Onset} Film (nm)	λ_{em} (c) (nm)	λ_{em} (d) (nm)	$E_{g\ opt}$ (eV)
P9 0% TRZ-PXZ	283	285.5	341	347	349	$3.63 \pm 0.07^{(e)}$
P10 5% TRZ-PXZ	284	285.5	339	378.5	530	$3.65 \pm 0.04^{(e)}$
P11 10% TRZ-PXZ	285	287.5	338.5	388.5	534	$3.66 \pm 0.06^{(e)}$
P12 20% TRZ-PXZ	287.5	286.5	341	390	539	$3.63 \pm 0.02^{(e)}$
TRZ-PXZ	435	445	----	546.5	550.5	---

As shown in figure 5.4 (a), P9 showed maximum absorption at 283 ppm, which corresponds to the π-π* transition resulting from the polymer backbone without any further absorptions in solution, compared to the polymers P10 – P12 which observed maximum absorptions between 284 – 287 nm, with a notable weak broad peak from 378 nm to 487 nm. This is due to the ICT process from the phenoxazine (donor) to the triphenyltriazine (acceptor) in the TADF moiety. Confirming the successful incorporation of the TADF units in the polymers' side chains. Increasing the ratio of the TADF moieties in the polymeric structures, led to an increase in the intensity of this peak. The same optical behaviours were observed in thin films of the polymers P9 – P12. The optical band gaps of the designed polymers have been calculated to be 3.63 eV, 3.65 eV, 3.66 eV and 3.63 eV. These polymers' short wavelength absorption is obviously caused by their non-conjugated system, which results in a larger energy gap between the π-π*

transition from repeat units and, thus, a lower absorbance wavelength. In comparison with P5-P8 investigated in the previous chapter, 3,6-functionalised carbazole repeat units improve the electronic delocalisation along the backbone of the polymer by enhancing the conjugation system. Consequently, the carbazole-based polymers demonstrate a greater absorption shift towards longer wavelengths compared to the group of polymers (P9-P12) based DPEPO repeat units described in this chapter.By comparing the optical band gap values of P9-P12 to the P5-P8, it is clear that the last set of polymers possess lower band gap values. This could be attributed to the increase of aromatic compounds in the polymer, which in turn increase the conjugation and the electron delocalisation. Therefore, the low optical gap can be obtained.

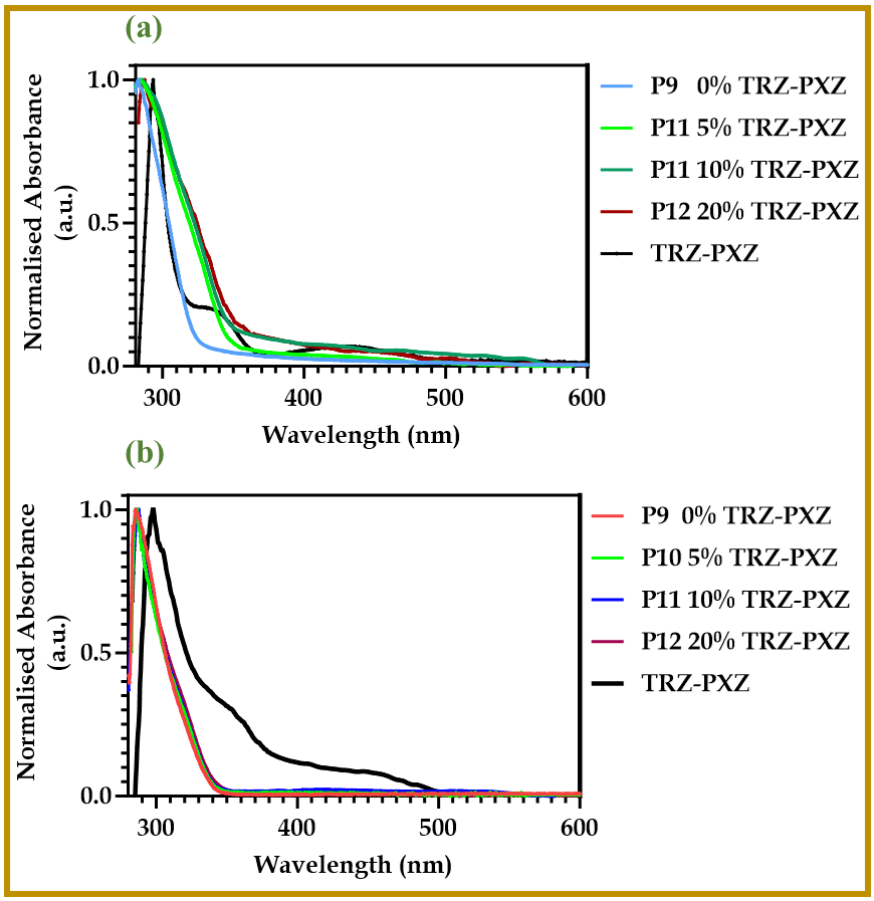

Figure 5.4 (a) Normalised UV vis absorption spectra of P9 – P12 in solution and (b) in thin films. In terms of the UV-vis spectra, all polymers from P9-P12 exhibited blue shifts in solution with notable broad absorptions from 378 – 487 nm in P10, P11 and P12. These weak absorptions are attributed to the ICT process occurring between the donor molecule, phenoxazine, and the acceptor molecule, triphenyltriazine. In the thin film of P9, P10, P11 and P12, redshifts were observed compared to the absorptions of the same polymers in solution. This is attributed to the effect of increasing the intermolecular π-π interaction of DPEPO repeat units in thin films.

The photoluminescence (PL) spectra of the designed polymers P9 – P12 together with TADF (PXZ – TRZ) in both toluene solution and thin films are illustrated in figure 5.5 (c) and figure 5.5 (d) respectively. Polymers P10 – P12 (grafted with different molar ratios of TADF) in solution presented dual emission at approximately 388.5 nm and 548.5 nm compared to P9 which showed only one polymeric emission peak. The dual emission peaks are corresponding respectively to the polymeric side chain and the TADF units respectively. It can be observed in figure 5.5 (c), the intensity of the more red-shifted peak at 546.5 nm increased proportionally once the ratio of TADF increased in the polymeric side chain. This confirms the efficient energy transfer from the polymeric backbone to the TADF (PXZ – TRZ). In the solid state, the PL spectra of the P10 – P12 (grafted with different molar ratios of TADF) showed different behaviours compared to the behaviour of the same polymers in solution. P10 (grafted with 5% moles of TADF) showed weak emission at 375 nm, this can be clearly ascribed to the emission arising from the polymeric backbone, which is likely due to incomplete energy transfer from the polymeric backbone to the TADF units. On the other hand, the PL spectra of P11 and P12, which were grafted with 10% and 20% of the TADF units, showed only one TADF peak at 534 and 539 nm, along with tail residual peaks arising from the main chain's backbone at 368 and 371 nm, respectively. This observation provides clear proof for the entire transfer of interchain and intrachain energy from the polymeric backbone to the TADF units. Furthermore, the PL spectra of P10 – P12 in solid state presented more red-shifted peaks from 531 nm, this due to the increase of aggregation in the polymeric side chain which caused by increasing the TADF concentration in the polymer. Hence, the emission profile is notably more influenced by the TADF unit in comparison to the copolymers, as indicated by the red-shifted emission which similar to the PL spectra of P6 – P8 in solid state in chapter 4.

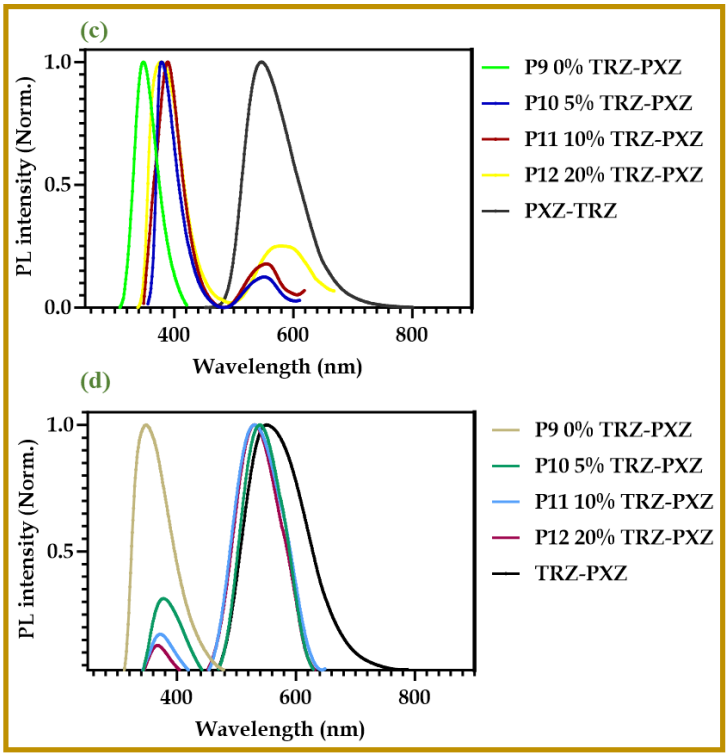

Figure 5.5 (c) Normalised PL emission spectra of P9 – P12 in solution and (d) in thin film. In solution, P9 showed only one polymeric emission in comparison with the grafted P10, P11 and P12 with different molar ratios of TADF, which exhibited dual emissions corresponding to the polymer (at short wavelength) and the TADF sidechain (at long wavelength). The intensity of TADF sidechain emissions increases proportionally with increasing the molar ratios of the TADF, indicating that energy is transferred more effectively from the polymeric backbone to the TADF units. In the thin film, P9 exhibited the same behaviour in solution by showing one polymeric peak with more red shifting. P10 (grafted with 5% of TADF) in comparison with P11 and P12, showed one small polymeric peak ~ 375 nm. This means incomplete energy transfer from the polymeric backbone to the TADF (PXZ – TRZ) units. However, both P11 and P12 exhibited only one TADF emission at ~ 531 nm, confirming the complete and efficient energy transfer from the polymers' main chain to the TADF sidechains.

5.2.6 Electrochemical Properties of P9, P10, P11 and P12

The designed polymers P9 – P12 (grafted with different molar ratios of TADF 0% - 20% respectively), were investigated electrochemically via cyclic voltammetry (CV). The analysis was conducted to determine the HOMO and LUMO levels values, which can be used to calculate the electrochemical band gaps of the designed polymers P9 – P12. The HOMO level values were calculated through the oxidation's onset of the polymer, while the LUMO level values could not be determined easily from the onset of reductions as the reduction waves of films could not easily be observed using cyclic voltammetry. This could be attributed to the larger sidechains of polymers that could impede the diffusion of the bulky BuN+ cation into

the polymer film, resulting in the unobserved reductions of all polymers P5–P8. Because of this, charge balance would be impossible, leading to a huge overpotential and a change in the reduction to occur outside of the solvent window.[270] Therefore, the LUMO level values were therefore calculated by subtracting the optical band gap values from the HOMO levels. data is summarised in table 5.5 below.

Table 5.5 CV data of P9 – P12, (a) HOMO and (b) LUMO level values, (c) The electrochemical band gaps.

Polymers	HOMO (eV)	LUMO (eV)	$E_{g\ elect}$ (eV)©
P9 0% TRZ-PXZ	-5.31	-1.68	3.63
P10 5% TRZ-PXZ	-5.09	-1.44	3.65
P11 10% TRZ-PXZ	-5.05	-1.39	3.66
P12 20% TRZ-PXZ	- 4.99	-1.36	3.63

As can be noticed in the figure 5.6, polymers P10 – P12 (possess different molar ratios of TADF 5% - 20% respectively), showed two oxidation peaks compared to P9 which presented one oxidation peak. The first semi-oxidation peak in P10 – P12 is attributed to the presence of phenoxazine (electron donor) and the second oxidation peak corresponds to the polymer backbone respectively. It has been reported that once the TADF ratio in the polymer side chain increased, shallower HOMO levels can be obtained.[267] The deepest HOMO level value was obtained in P9 as -5.31. This is due to the effect of increasing the non-conjugation system in the polymer. The electro band gaps of all designed P9, P10, P11 and P12 were calculated to be 3.63 eV, 3.65 eV, 3.66 eV and 3.63 eV respectively.

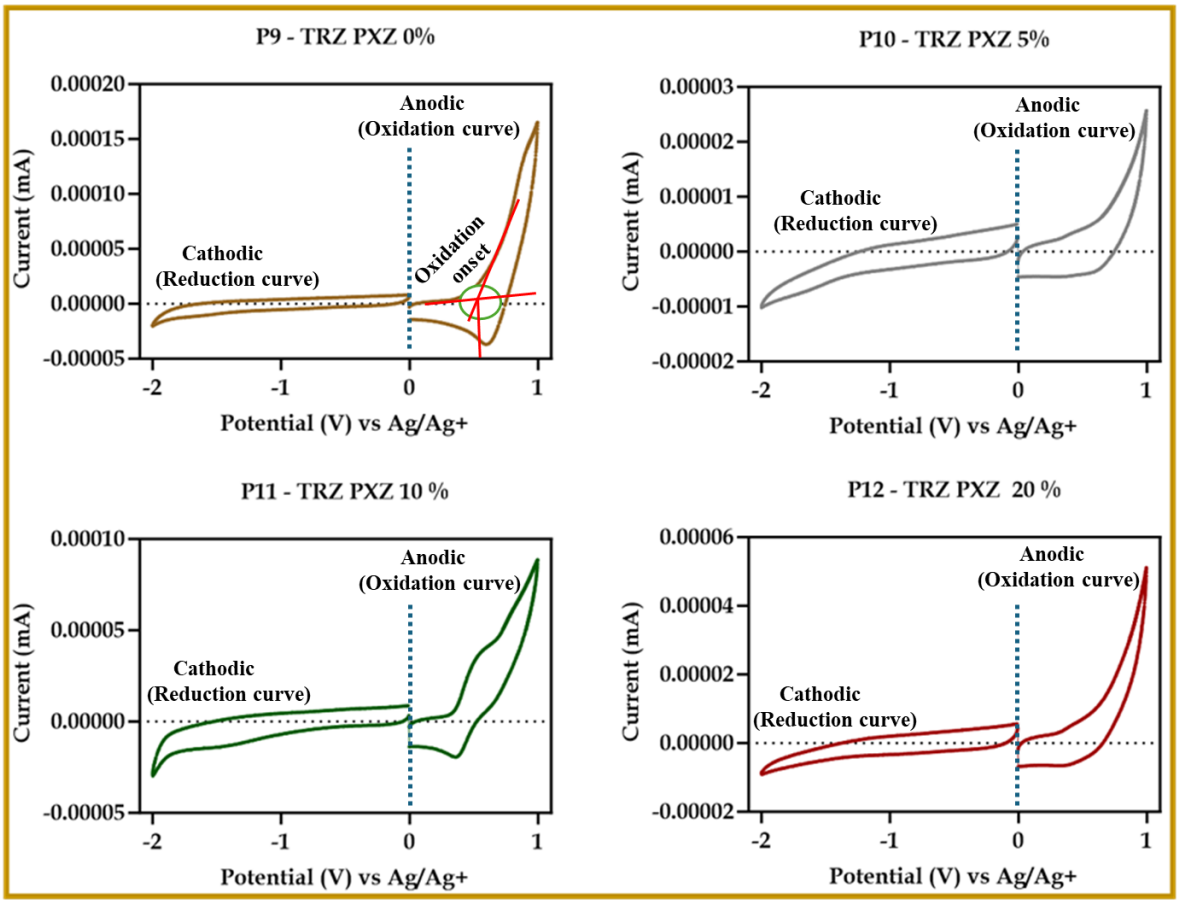

Figure 5.6 The CV analysis of P9 – P12. Polymer 9 (containing 0% of the TADF) exhibited only one oxidation and reduction peak. Polymers from P10-P12, which grafted with different molar ratios of the TADF (5%, 10% and 20% respectively) exhibited two peaks of oxidations; the first oxidation peak which corresponds to the polymer backbone, and the semi-oxidation peak which corresponds to the phenoxazine moiety (electron-donating molecule) of the TADF units. The intensity of this peak increases with increasing the molar ratio of TADF. The reduction peaks of all designed polymers could not be identified, therefore the LUMO values were calculated from the difference between the optical band gaps and the HOMO values.

5.3 Conclusion

Side-chain engineering has been shown as a highly practical and efficient approach to provide efficient solution processable emitting materials, for the synthesis of TADF-based polymers, due to the ability of the polymer to obtain the characteristics of the TADF units positioned across its side chain. Furthermore, the electroluminescent (EL) device performance can be improved if the polymer backbones possess both a high triplet energy level and desirable charge transporting characteristics.[287-289]

In order to enhance the OLEDs emitting layer properties using TADF materials, a series of yellow-green light emitting TADF polymers P9-P12 have been synthesised and investigated following the above strategy. P9 which contains 0% TADF units was synthesised in order to compare its properties to those with TADF grafted polymers P10-P12 which have different ratios of TADF units 5%, 10% and 20% respectively. The chemical structure of the designed polymers were confirmed *via* ^{1}H NMR. P10-P12 showed gradual increases in the intensities of peaks at 8.99 nm, 8.79 nm and 3.28 nm from TADF units. This confirmed the successful incorporation of the TADF units into the polymers side chains. Furthermore, the actual ratios of incorporated TADF units in P10, P11 and P12 were calculated from the integrated NMR spectra to be 4.6%, 7.16% and 15.2% respectively.

GPC was used to determine the polymers' molecular weights together with polydispersity (PDI). P9 possessed the highest molecular weight value of 23800 Da compared to other TADF polymers P10-P12 which possessed lower molecular weight values, this is attributed to the excess of aromatic DPEPO molecules in the polymer backbone. The lower molecular weight values of 10200 Da, 9000 Da and 11600 Da owned by P10, P11 and P12, was attributed to the increase of steric hinderance in the polymer backbone which leads to more rigid structures.

All designed polymers exhibited high solubility in common organic solvents such as DCM, Chloroform, Toluene and THF once they examined. In terms of thermal stability, the designed polymers showed increase in thermal resistance from 257 °C – 399 °C proportionally with increasing the ratio of TADF units. These features indicated a good potential of these polymers to be used as good candidates for emitting layer in solution processible OLEDs.

The UV-vis spectra of all designed polymers were conducted in solution and in thin films to investigate the optical properties. In solution, all polymers P9-P12 showed maximum absorption from 283 – 287 nm, with notable weak broad absorption between 378 – 487 nm in P10 - P12. This is attributed to ICT process from the phenoxazine to the triphenyltriazine in

the TADF moieties attached to the polymers. The optical band gaps of all designed polymers were determined in thin films, P9 and P12 owned the lowest optical band gaps 3.63 eV compared to P10 and P11. This could be due to the higher conjugation and electron delocalization caused by an excess of aromatic compounds in the polymer. As a result, a narrow optical gap can be achieved.

The PL spectra revealed the energy transfer from the polymer backbone to the TADF units incorporated in the polymers. In toluene solutions, dual emission was observed at approximately 388 nm and 548 nm for P10-P12, in contrast to P9, which exhibited a single peak of polymeric emission. The short wavelength peak in P10-P12 attributed to the polymer backbone while the long wavelength peak assigned to the TADF unit. The TADF emission peak at ~548.5 increased gradually with increasing the TADF ratio in P10-P12, confirming the efficient energy transfer from the polymer backbone to the TADF side chain. In solid state, the entire transfer of energy from the polymer backbone to the TADF unit was confirmed in P11 and P12 by observing only one TADF emission at 534 and 539 nm respectively.

The electrochemical behaviour of all polymers was conducted under N_2 atmosphere using cyclic voltammetry (CV). P10-P12 presented shallower HOMO and deeper LUMO levels. This is due to the effect of increasing the TADF ratio in the designed polymers P10 - P12. The LUMO values of all designed TADF polymers P5 – P8 were calculated from the difference between the HOMO values and the optical band gaps, as the reduction curves could not be identified appropriately. The electro band gaps were calculated to be 3.63 eV, 3.65 eV, 3.66 eV and 3.63 eV for all designed P9, P10, P11 and P12 respectively.

Chapter 6: Conclusion and Future Work

6.1 Introduction

The rapid rise of research efforts in organic emissive materials has been driven by an increased interest in industries that utilise OLEDs as next-generation displays and lighting sources. Fluorescent materials were initially used to rapidly achieve the evolution of primarily organic emissive materials in OLEDs. Subsequently, phosphorescent based on heavy metal complexes were introduced, and ultimately, materials based on TADF properties were developed. The ability to convert triplet excitons into singlet excitons allows for an energy utilisation efficiency (EUE) of about 100% (25% of singlet excitons plus 75% of triplet excitons via the RISC) in the latest materials possessing TADF properties, without any requirement for any heavy metal materials. In recent years, there has been substantial progress in the advancement of cutting-edge OLEDs that utilise materials with TADF properties. Although there have been advancements in efficiency, the use of evaporation techniques for their deposition requires complex structures, a high cost, and precise control. As a result, this strategy is unaffordable and infeasible for large-scale device manufacture. Compared to other manufacturing methods, solution processing is a more straightforward, cost-effective, and easily manageable option for facilitating mass production. Nevertheless, most of the TADF dopants that have been identified are small molecules which in fact unsuitable to be used in solution processing. Hence, developing organic emissive materials based on a solution processing technology that possesses TADF properties is significant.

The main objective of this study has been accomplished, which is the preparation and design of solution processable TADF hyperbranched polymers. The introduction of hyperbranched polymers in the OLED emitting layer effectively disperses the TADF emitting material and inhibits aggregation-caused quenching (ACQ) and exciton annihilation effects. Moreover, the presence of branches enhances the material's solubility, which makes the solution process the favoured way of processing. This approach enables the straightforward adjustment of host-guest ratios to simplify performance comparisons and reduce manufacturing expenses, thus encouraging the growth of the OLED sector.

Chapter 2 describes the preparation and design of two hyperbranched polymers P1 and P2 that have been prepared using a single monomer *via* the AB_2 method of polycondensation in the absence and the presence of core (4-nitrophenyl acetate). The final structures of both polymers have been confirmed *via* ^1H NMR, showing the reduction in the intensity of acetoxy group spectra around ~ 2.40 ppm. this confirmed the consumption of acetoxy methyl groups during

the polymerisation. Both polymers exhibited poor solubility in the commonly used organic solvents such as chloroform, DCM and THF. Therefore, low yields, low molecular weights and low thermal stability of both polymers were obtained. These undesired properties could be attributed to the occurrence of internal cyclisation reactions during the early polymeric steps, which in turn prevents the growth of the polymer's branch and results in a rigid structure. The optical properties, including the optical band gaps of both hyperbranched polymers, were studied and investigated in both solution and films, showing more redshift values in the film, and this is due to the higher degree of planarity in the thin film as a result of increasing the intermolecular π-π interaction. In addition, the electrochemical behaviour of both polymers has been investigated in terms of determining the HOMO and LUMO values.

Chapter 3 reported the synthesis of two hyperbranched polymers P3 and P4 that have been synthesised and investigated using the A_2B_3 polycondensation approach. Carbazole was used as a host material to enhance the hole-transporting properties in both polymers. Furthermore, the central aliphatic branches in B_3 played a crucial role in enhancing the solubility of polymers. The ^{1}H NMR spectra confirmed the final structure of both polymers, while the GPC analysis was used to determine the molecular weights and the PDI of both polymers. Great behaviour of high solubility was observed once both polymers were examined in the common organic solvents such as DCM, chloroform, toluene and THF. In terms of thermal stability, P3 showed better thermal stability in comparison with P4, this is due to the increase of carbazole rings in the polymer P3. The optical properties of both polymers, including UV-vis absorptions and PL spectra, have been measured in both solution and film. Furthermore, the optical band gaps of both polymers P3 and P4 have been calculated and investigated to be 3.08 eV and 2.95 eV respectively. In addition, the electrochemical behaviour of both polymers has been investigated in terms of determining the HOMO, LUMO values.

Chapter 4 described the side-chain engineering strategy which was proposed to design the targeted TADF hyperbranched polymers P5 – P8. In this strategy, the main chain's polymer included both partially conjugated and non-conjugated units. While the grafted side chain included the TADF units. Including both partially conjugated and non-conjugated units in the main chain of the polymer has a positive impact in terms of charge transport characteristics and device performance. The four TADF hyperbranched polymers P5 – P8 were synthesised via Suzuki polycondensation using partially conjugated carbazole units as host material with high triplet energy which is higher than the guest TADF's (E_T). Utilising carbazole as host material has a role in enhancing the hole-transporting properties and restraining the concentration

quenching caused by the TADF moieties. In addition, introducing the non-conjugated branched structure 1,3,5-tris((6-phenoxyhexyl)oxy)benzene of M6 in the polymer's main chain as a spacer has a role in reducing the conjugation along the main chain and therefore enhancing the solubility of the target TADF hyperbranched polymers. The TADF moieties of the side chain consist of PXZ (donor) and TRZ (acceptor). These generate the charge transfer within the TADF structure and result in the production of the green-yellow TADF dye, which in turn enhances colour properties in the emitting layer of the OLED device. The target TADF hyperbranched polymers P5 – P8 have been synthesised and designed successfully. Various ratios of the TADF moieties were incorporated into the polymer's main chain to study the effect of TADF minorities on the P6 – P8 in comparison with P5, which was synthesised without TADF units. The four designed TADF hyperbranched polymers showed remarkable solubility in the common organic solvents. The characterisation of ^{1}H NMR confirmed the final structures of all designed polymers P5 – P8. Moreover, the molecular weight and the PDI values were determined using the GPC. Their molecular weight values range from 13000 to 19000 Da. In terms of thermal stability, all designed polymers exhibited great thermal stability ranging from 251 to 375 °C. it has been observed that the thermal resistance of the designed polymers P5 – P8 increases proportionally with increasing the ratio of TADF moieties in the polymer's side chain. The optical properties, including the UV-vis absorptions and the PL spectra, have been investigated in both solution and film. The incorporation of TADF in the designed polymers P6 – P8 has been observed as a broad weak absorption between 375 – 493 nm in the UV, confirming the presence of the TADF moieties in the polymers' side chain of P6 – P8. In the PL spectra, the transfer of energy either partially (observed in the dual emission peaks of P6) or completely (observed in the dual emission peaks of P7 and P8) from the polymer's backbone to the polymer's side chain (TADF units) has been noticed and confirmed. Furthermore, the optical band gaps of the designed polymers P5 – P8 were calculated to be 3.28 eV, 3.23 eV, 3.24 eV and 3.21 eV respectively. Additionally, the electrochemical behaviour of the designed TADF polymers P5 – P8 has been investigated in terms of determining the HOMO, LUMO and electro band gaps values. Shallower HOMO and deeper LUMO values were noticed in the designed polymers P6 – P8. These due to the increase of the TADF ratio in the designed polymers from 5% to 20 %, which in turn increases the PXZ and TRZ units. The HOMO and LUMO levels can be affected by either increasing or reducing the donor and acceptor units, respectively.

Chapter 5 reported the same strategy used in Chapter 4 that was applied to design the TADF hyperbranched polymers P9 – P12. In this chapter, the polymer's main chain consisted of DPEPO units as a partially conjugated host material with high triplet energy ~ 3 eV and the non-conjugated branched structure 1,3,5-tris((6-phenoxyhexyl)oxy)benzene of M6 as a spacer. While the TADF moieties were grafted into the polymer's side chain. The DPEPO was employed to facilitate the electron transport properties with respect to other functionalities mentioned in the summary of Chapter 4 above. While the non-conjugated branched structure 1,3,5-tris((6-phenoxyhexyl)oxy)benzene of M6 was introduced in the polymer's main chain to reduce the conjugation along the polymers' backbone. The function of TADF moieties as a side-chain polymer has been mentioned in the summary of Chapter 4 above. The designed TADF hyperbranched polymers P9 – P12 have been successfully confirmed and investigated. ^{1}H NMR analysis was utilised to confirm the chemical structure of all designed polymers P9 – P12. The molecular weights, together with the PDI of all designed polymers P9 – P12, were determined via the GPC, showing their molecular weight values in the range of 9000 – 23800 Da. Great thermal stabilities were revealed by the designed polymers P9 – P12, with the lowest degradation temperature of 257 °C for P9 which contains 0% of the TADF. In polymers P10 – P12, the thermal stability increased proportionally with increasing the TADF ratios, showing degradation temperatures in the range of 367 – 399 °C (by increasing the aromatic rings of the PXZ and TRZ units in the side chains of the designed polymers P10, P11 and P12, the thermal stability of the polymers will be indeed increased). In addition, the optical properties of the designed polymers P9 – P12 including the UV-vis absorptions and the PL spectra, have been investigated in both solution and film. The complete or partial energy transfer from the polymer backbone to the TADF side chain was observed in the thin film of the PL spectra around 546 nm. Furthermore, the electrochemical properties of the TADF polymers P9 – P12 have been examined to determine the values of HOMO, LUMO levels. The polymers P10 – P12 exhibited shallower HOMO levels and deeper LUMO levels, resulting in reduced electro-band gap values. The TADF ratio in the proposed polymers has been increased from 5% to 20%, resulting in an increase in the PXZ and TRZ units. Both the HOMO and LUMO levels can be influenced by either raising or reducing the donor and acceptor units, respectively. To be more clear, increasing PXZ units (donor molecules) in the polymer's side chains leads to shallower HOMO values**.** In contrast, increasing TRZ units (acceptor molecules) in the polymer's side chains leads to deeper HOMO values**.**

6.2 Future Work

In this thesis, a series of solution-processable hyperbranched polymers were designed using different strategies and investigated *via* various analytical methods. Carbazole and DPEPO derivatives were applied to be used as host materials, as they featured high triplet energy levels and worked basically as hole and electron transporting carriers respectively in the OLED devices. More investigations are required to explore the potential of specific hyperbranched polymers synthesised and examined in this thesis as active layers for OLEDs, taking into account their optical and electrochemical properties exhibited at different ratios of TADF units. This research involved the synthesis of an effective TADF-small unit (PXZ-TRZ) which was grafted into the side chain of the host polymers' backbone. This resulted in a range of non-conjugated polymers with varying molar ratios of TADF units. The resulting hyperbranched polymers effectively obtained the TADF characteristics from the small molecule connected to them, known as PXZ-TRZ. It would be important to examine the charge mobility and thin-film characteristics of the designed polymers. Consequently, it is necessary to conduct additional investigations of the electroluminescence properties of such polymers in collaboration with the Department of Physics.

Through the preparation of polymers P1 and P2 in the first chapter, undesired results were obtained, such as low solubilities in the commonly used solvents, low yields, low thermal stabilities with increasing heating rates, and low molecular weights. These factors affect and limit the use of these materials as emissive layers for fabricating OLED devices using solution processing. To overcome these in the future, firstly, monomers are required to be well prepared, designed, and purified, as polymerisation can be disrupted by the monomers or solvent impurities (a side reaction could be produced that prevents the polymerisation from being completed); therefore, purification is a very essential step. Furthermore, introducing some solubilising groups could assist in terms of increasing the solubility of targeted polymers. Secondly, the polymerisation should be monitored in terms of the given time with continuous observation of the polymerisation behaviour, such as some changes in colour, viscosity, and forming precipitation, which indicates the end of the polymerisation. Thirdly, the polymerisation should be end-capped using end-capping groups to prevent the polymer’s aggregation or overgrowth. The extreme temperature could affect the polymerisation, hence, the polymerisation should be conducted at a controlled temperature in the future. We recommend incorporating various core (4-nitrophenyl acetate) ratios in P2 to observe the potential influence of these differences on P2 properties.

Measuring hyperbranched polymers' molecular weight using GPC with linear polystyrene as standard is not appropriate and the obtained results can not be accurate. Therefore, we can conduct further analyses using different GPC standards to accurately and appropriately measure the molecular weights of the hyperbranched polymers. Another analysis using Matrix-Assisted Laser Desorption/Ionization Time of Flight (MALDI) mass spectrometry should be used to measure the designed polymers' molecular weight as this analysis could measure the molecular weight of polymers below 11000 Da.

Once the previous issues of P1 and P2 are sorted out, it is strongly recommended that the TADF moiety, which was grafted with different molar ratios in P6-P9 and P10-P12 in chapters 4 and 5, respectively, could be attached to the four polymers reported in chapters 2 (P1 and P2) and 3 (P3 and P4). The attachment of TADF units as a side chain to the polymers' main chain in chapters 2 and 3 can greatly influence their properties, such as the obtained molecular weight, the optical properties (including the UV-vis and the PL), the thermal stabilities, and the electrochemical behaviours (which can be influenced by increasing the PXZ (donor molecules) and TRZ (accepter molecules). Incorporating the TADF units with different molar ratios in chapters 4 and 5 showed great features in terms of thermal stability, high solubility materials, and efficient energy transfer from the polymers' backbone to the TADF side chains in PL.

In the CV, the measurement of the reduction of all designed polymers in chapters 2, 3, 4 and 5 failed. All designed polymers were measured in acetonitrile solutions of tetrabutylammonium perchlorate. Therefore, during the reduction process, the larger sidechains of polymers may have impeded the diffusion of the bulky BuN+ cation into the polymer film, resulting in the unobserved reductions of all polymers. Because of this, charge balance would be impossible, leading to a huge overpotential and a change in the reduction occurring outside of the solvent window. The same issue was reported by Schwiderski and Rasmussen,[270] they could not measure the reduction of one of their designed polymers. So, when KPF_6 is applied as an alternative electrolyte instead of tetrabutylammonium perchlorate, the reduction of the polymer is measured and observed. Therefore, KPF_6 as an electrolyte is recommended to be used in the CV for measuring the reduction of whole-designed polymers in this thesis.

Chapter 7: Experimental Section

7.1 Chemicals and Solvents

Unless otherwise, all chemicals and reagents were obtained from commercial sources and used in unaltered forms. Synthesis of selected compounds was performed in an inert argon environment using anhydrous solvents obtained from the University of Sheffield's Chemistry Department using the Grubbs solvent purification method.

7.2 Instruments and Analytical Techniques

7.2.1 Nuclear Magnetic Resonance (NMR)

Purcell and Bloch discovered the phenomena of nuclear magnetic resonance in 1946. It relies on the fact that magnetic fields interact with the magnetic moments of different atoms' nuclei. A nuclear spin, a kind of angular momentum, is connected with the magnetic moment of nuclei. A spin number specifies the value of nuclear spin. Nucleus characteristics and spin number determine the nuclear magnetic moment corresponding to the nuclear spin. Nuclei with an even number of protons and neutrons have a nuclear spin and magnetic moment equal to zero, but those with an odd number of protons or neutrons have a non-zero spin and magnetic moment. Within the group of nuclei that have an odd number of protons or neutrons, certain nuclei, including ^{1}H, ^{31}P, ^{13}C, and ^{15}N, possess a spin number of ½. This particular spin number is advantageous for practical uses of magnetic resonance. When the nuclei's spin state is measured separately in the magnetic field, two spin states are observed: one corresponding to a magnetic quantum number of ½ and the other corresponding to a magnetic quantum number of e½. One of these states represents the alignment of nuclei in the same direction as the magnetic field, while the other represents their alignment in the opposite direction. The energies of these two spin states are distinct.[290] It should be noted that, according to quantum physics, the nuclei in an object are not always in pure quantum states of ½ and e½. Within a static magnetic field, nuclei possessing a magnetic moment that is not zero tend to adopt the orientation that entails a minimal amount of energy. However, thermal energy disrupts this orientation. Nuclear moments in a magnetic field are thus likely to be virtually randomly oriented in space, with a little higher probability of being in the direction of the field (i.e., with lower energy).[291]

Bruker Avance AV 3HD 400 (400 MHz) and Bruker Avance 100 (100 MHz) spectrometers were utilised to obtain ^{1}H and ^{13}C NMR spectra of the monomers and polymers using deuterated solvents including deuterium oxide D_2O, chloroform-d, acetone-d_6, and DMSO-d_6 at room temperature. All deuterated solvents were purchased from various commercial sources (*Thermo Fisher* Scientific and Merck) and used in their purported form. Internal Standard

tetramethylsilane (TMS) was used to calibrate the chemical shifts (δ). NMR spectra were recorded in Hz for the coupling constant (J), and ppm for the spectral measurement. Splitting patterns in nuclear magnetic resonance (NMR) are typically abbreviated as s (singlet), d (doublet), dd (doublet of doublet), t (triplet), qt (quartet), m (multiplet), bs (broad singlet), bd (broad doublet), and bm (broad multiplet). NMR spectral analysis was performed using MestreNova software.

7.2.2 Mass Spectrometry (MS)

Mass spectrometry (MS) is a precise and very sensitive analytical technique employed in several scientific fields such as environmental, pharmaceutical, medical, forensic, and food sciences. It allows for accurate quantification and detection of substances. This approach entails the extraction of gaseous ions from samples in either a liquid or solid condition. Once converted into a gaseous form, these substances are then sorted according to their mobility in an electric and magnetic field.[292] The ions that have been detected or separated are examined in a mass spectrum. A mass spectrum is a graphical representation that displays the distribution of ions based on their mass in a given sample. MS exhibits the highest abundance and a high m/z (mass/charge) value when a purified substance is present in the sample.[293] When coupled with gas-liquid chromatography (GLC) or high-performance liquid chromatography (HPLC), the mass spectrometer operates as a strong detector, facilitating the identification of even tiny particles of a specific substance within a given sample.[294, 295] The structural elucidations of organic, bio-organic, and organometallic compounds are another application of MS. Additionally, it is utilised to determine the molecular mass of an atom and is a burgeoning instrument in the scientific field of proteomics, which is a subfield of biochemistry devoted to the structural investigation of proteins.[296]

In terms of MS working principles, high vapour pressure (heating) is applied to the sample undergoing analysis in a mass spectrometer; this induces ion fragmentation and ionisation. Voltage is used to accelerate the ionised ions in the sample, causing them to move in a mass analyser in accordance with their mass. The velocity at which the ions carrying opposite charges travel in the mass analyser is equivalent. The detector subsequently induces these ions to move through a magnetic force, resulting in the perpendicular or circular motion of ions with comparable velocities. When subjected to a magnetic field, the charged ions follow a path that is perpendicular to the field. This occurs because the magnetic force creates a centripetal force, which is directed towards the centre. Subsequently, ions possessing identical magnetic and

electric charges are directed through the system without any deviation, ultimately reaching the data system where they are recorded. The mass spectrum acquired from this method facilitates the subsequent analysis of substances present in the sample.[297]

Relating to sample analysis, Perkin Elmer Turbomass with autosampler and autosystem XL Gas Chromatography was used to analyse product mass spectrometry. Electron ionisation (EI) and chemical ionisation (CI) methods were utilised to generate mass spectra.

7.2.3 Elemental Analysis (EA)

Elemental analysis (EA) is a chemical analytical technique used to evaluate the elemental structure of chemical compounds and their composites. This method allows for the identification of the elements present in a substance and the calculation of the percentage by mass of each chemical element. This information is used to determine the empirical formula. Once the total molecular weight of the chemical being examined is determined, the analysis result allows for the establishment of the molecular formula. However, it is not possible to determine the structure or the specific manner in which atoms are linked together by chemical bonds. Elemental analysis relies on the controlled and dynamic combustion of materials in a reactor, followed by the measurement of the quantity of the related oxides. The samples are combusted in a temperature-controlled column containing an oxidizing-reducing catalytic chamber. The analyser, which is mainly a simplified version of the gas chromatograph, is where the evolved gases are normally directed. A detector such as a thermally conductive detector (TCD) is utilised to detect all gases, including H_2O, CO, CO_2, and N_xO_y, which have been separated by chromatographic columns. CHNS or CHN analysis is another term for elemental analysis, which involves the measurement of carbon (C), hydrogen (H), nitrogen (N), and sulphur (S). Oxygen is frequently calculated as the discrepancy between the sum of the amounts of CHNS obtained and the overall percentage. However, it should be identified in a separate analysis where the pyrolysis process occurs for excellent practices. Typically, in the CHNS + O technique, the samples are placed into the apparatus using vessels made of tin or silver. A non-reactive environment, consisting of helium (He) or argon (Ar), is employed. However, for the purpose of combustion during CHN analysis, oxygen is introduced. The catalytic bed often consists of CuO or WO_3, which facilitate the production of N_2, N_xO_y, CO_2, H_2O, SO_2, and SO_3 gases. Hence, the inclusion of a reduction column is required to remove an excess of oxygen and ultimately yield N_2, CO_2, H_2O, and SO_2. Subsequently, the quantities of N, C, H, and S are calculated accordingly. The amount of oxygen is determined by analysing the CO peak

during the pyrolysis process. It is also possible to determine the chlorine concentration using certain setups of elemental analysers. The high temperature is frequently used in elemental analysis. Since temperatures in the region of 1800 °C are achieved, the EA technique can measure a wide variety of samples. In terms of accuracy, the elemental analysis provides an accurate sample determination.[298]

The Perkin Elmer 2400 series II analyser was used for carbon, hydrogen, and phosphorus elemental analyses, while the Schoniger oxygen flask combustion method was used for halide anions analysis. The chemical compounds sampled weighed approximately 7 mg for CHP analysis and 10 to 15 mg for anion analysis.

7.2.4 Gel Permeation Chromatography (GPC)

Gel permeation chromatography (GPC) or size-exclusion chromatography (SEC) is a highly preferred method for analysing polymers and oligomeric substances. GPC separates molecules in the mobile phase based on their effective size. Generally, there is a direct correlation between molecular size and molecular mass. The column(s) used for analysing organic compounds is filled with a densely interconnected spherical matrix made of polystyrene and divinylbenzene. This matrix has a well-regulated pore size. Sample molecules of small size can diffuse through the pores, while those exceedingly large are effectively excluded. Consequently, bigger molecules are eluted faster than smaller molecules. The nature of the separation is therefore particularly mechanical, as opposed to chemical as in alternative chromatographic methods. Any molecules with a retention time equal to or greater than the pores elute initially. The column's exclusion limit is defined by the smallest molecule that unable to permeate the pore. All molecules below a specific size have an equal chance of passing through the pores, causing them to elute at the dead volume or total permeation volume. The separation of molecules occurs according to their molecular sizes between these two extremes. [299]

To begin analysing a sample with an unknown molecular mass or dispersion of molecular masses, a calibration plot is first generated using a set of narrow disperse standards with known molecular masses. This plot shows the sample's molecular mass (log Mr) against the elution volume or time. To analyse the sample, it is first common practice to determine which calibration function provides the greatest fit to the plot. Subsequently, it is possible to determine the polydispersity (Mw (the mass average molecular mass /Mn (the number average molecular mass)) and the peak molecular mass (Mp) using this method. The calibration via polystyrene standards is commonly utilised to determine the molecular masses of polymers

with varying chemical structures. The reported molecular masses are expressed in relation to polystyrene.

Molecular range/distribution characterisation of the various organic polymers and co-polymers utilised as thickeners in anaerobic, radiation-curable, and acrylic adhesives is another application where GPC proves to be an exceptionally valuable technique. Solubility is the main limiting factor; however, the implementation of potent solvents such as tetrahydrofuran expands the range of applications that can be achieved with this method. Additionally, solubility issues can be resolved by using high temperatures. To ensure efficient high-temperature GPC, temperature control is essential for all components, including the injector, columns, and detector. There are commercial systems that incorporate these concepts.[299]

Using the GPCmax VE2001 GPC solvent/sample module and the Waters 410 Differential Refractometer with a RI-detection method, the number and weight average molecular weight of the whole designed polymers were calculated. The GPC curve was calibrated using a series of standard polystyrene samples. Tetrahydrofuran (THF) was used as both a solvent to dissolve the prepared sample and as a reference with some drops of toluene.

Polydispersity for the whole polymers was calculated via the following equation.

PDI=Mn/Mw

Where **Mn** refers to the number average molecular weight and **Mw** refers to the weight average molecular weight.

7.2.5 Ultraviolet Visible Absorption Spectroscopy (UV-vis)

UV-vis spectrophotometer is an analytical instrument that analyses the absorption of light by molecules in the UV-visible spectrum. When an atom or molecule absorbs a photon or particle, the energy of the photon is transferred to the electron of the atom or molecule. Consequently, the energy level of the electron increases, and UV-Vis spectroscopy analyses this increase in energy. The ultraviolet-visible (UV-Vis) spectrophotometer works by illuminating a light source on a sample that covers the visible range of wavelengths which is usually from 190 to 900 nm. The instruments then measure how much light each wavelength's wavelength is absorbed, passed through, or reflected by the sample. For some spectrophotometers, wavelengths up to 3200 nm can be measured. Through the utilisation of a wide range of accessories and sample holders, a UV-Vis spectrophotometer can perform a range of different measurements. The purpose of these accessories is to provide a variety of measuring abilities

and sample features, such as differentiating between liquids and solids, and they are designed to support a wide range of measurement circumstances. Determining the molecular structure of a solid or liquid sample, the concentration of a particular molecule in a solution, the wavelengths at which a material transmits or absorbs light, the colour of a material, and the reflectance properties of a surface are all ways of finding out about its chemical and physical properties. UV–Vis spectrophotometry is extensively utilised for identifying and measuring of organic materials,[300] such as polymers.

The working principle of the UV-vis spectrophotometer can be summarised simply as follows;

- Materials can absorb, reflect, or transmit light.
- The spectrophotometer is used to determine the light intensity that is absorbed in the ultraviolet and visible areas.
- Light transmission through a sample can be compared to an incident light source reference measurement.
- The determination of analyte concentration in a sample via the spectrophotometer is possible through the utilisation of Beer-Lambert Law $A=\varepsilon bc$, (Where the symbols A, ε, b, and c refer to the absorbance, molar absorption coefficient, liquid sample thickness, and solution concentration, respectively). This law states that the quantity of light absorbed is directly proportional to both the sample concentration and the length of the path.

All synthesised polymers had their UV-vis optical characteristics analysed using a Hitachi U-2010 Double Beam UV/Visible Spectrophotometer. First, around 1.2 mg of the sample dissolved in chloroform ($CHCl_3$) was placed into quartz cuvettes with a minimal length (1cm) to determine the polymer absorbance in the solution. Subsequently, in the solid state, the polymer's absorbance was determined via controllable drop-cast thin films on quartz substrates.

7.2.6 Thermogravimetric Analysis (TGA)

Thermogravimetric analysis (TGA) is a highly effective method for determining the heat stability of various materials, such as polymers. This method involves measuring the variations in the weight of the sample when its temperature is increased. The TGA technique can be used to measure the sample moisture and volatile contents. The equipment comprises a remarkably responsive scale for measuring changes in weight and an automated furnace for controlling the heat of the sample. The balance is positioned above the furnace and is isolated thermally from the heat. A highly accurate hang-down wire is suspended from the balance and extends into the

furnace. The sample pan is located at the end of the hanging wire, and its position must be continuously replicable. To achieve the highest levels of sensitivity and accuracy in weighing, it is necessary to maintain the balance away from any thermal influences, such as in a thermostatic chamber. Introducing an infrared spectrometer into TGA enables the analysis and identify all gases produced during the decomposition of the sample. Rapid-cooling microfurnace is incorporated into the TGA apparatus. The heating element is composed of platinum, which can resist temperatures up to 1,000 °C. A furnace located outside of the main system, equipped with a heating component composed of platinum and 30% rhodium, has the ability to increase the temperature range up to 1,500°C. A contemporary device typically includes a computing system to calculate the fraction or percentage of weight loss. The commonly used TGA has a temperature range exceeding 1,000°C, a balance sensitivity of 0.1 µg, and the ability to change the heat-up rate while operating in an air or alternative gas environment (such as under N_2 atmosphere). The heating rate capacity of TGA can range from 0.1°C to 200°C per minute.[301]

All obtained polymers have been thermally analysed under an inert nitrogen atmosphere, TGA curves were collected using the Perkin Elmer Pyris 1 Thermogravimetric Analyser at a scan rate of 10 °C minute^{-1}. Approximately, 6-8 mg of each polymer was required, and platinum trays were utilised as sample holders.

7.2.7 Cyclic Voltammetry (CV)

Cyclic voltammetry (CV) is a fundamental electrochemical technique used to evaluate the properties of materials. In this method, the current is measured by oscillating the potential between positive and negative values within certain limits. The data extracted from the CV can be utilised to get information about the electrochemical characteristics of the material. The material exhibits reduction and oxidation peaks, which can be used to predict the capacitive behaviour of the electrode. Thus, it is possible to determine the potential at which the substance undergoes oxidation and reduction. CV is supplied with a ramp signal as an input. A positive ramp signal with a positive slope is supplied for the forward scan. However, the voltage switches for the second half-cycle, resulting in a reverse cyclic voltammogram. This voltage shift occurs after the initial half-cycle. As the system utilises redox reactions to reach equilibrium, its ultimate goal is to restore its initial position. The system exhibits a cyclical pattern that provides details about the changes which it has experienced. It is possible to conduct the CV experiment using a single cycle or several possible cycles. The scan rate is

the slope of the ramp signal, measured in volts per unit of time. In this range, the scan rate can be at any point from a few hundred to a few thousand millivolts per second. The system's scan rate can be adjusted to gain a better understanding of the cell's electrochemistry. Therefore, the scan rate significantly influences the voltammetric characteristics of the sample undergoing analysis. Reduction and oxidation peak currents, in addition to peak potentials, may undergo some variation depending on the scan rate. If the peak current (also known as faradaic current) increases as the scan rate increases, it indicates a high rate capability and improved pseudocapacitive behaviour of the electrode material.[302] A higher scan rate leads to an increased occurrence of redox reactions because of the presence of electroactive substances on the surface of the working electrode. However, when the scan rate is decreased, there is a potential for the forward or reverse scan peak to be missed. This is due to the extended time that the products of the reduction or oxidation have to undergo a chemical reaction, during which they may not be electrically active. CV also facilitated the determination of the electron transfer coefficient, which represents the quantity of electrons transported in a reaction. Additionally, CV can identify the rate-limiting factor, which is the component that limits the reaction rate, as well as the reaction rate constant. The disparity between the two maximum potentials observed in the CV provides information about the impact of the analytes' diffusion rates. Furthermore, the ratio of the anodic and cathodic peak currents can be utilised to determine whether the system is reversible, irreversible, or quasireversible.

CV can accurately predict the electrochemical behaviour of polymers by measuring the electrochemical band gaps, electron affinities, and work functions of the polymers.[303] Therefore, CV is employed to investigate the compound's chemical and electrochemical behaviour. Additionally, CV can assist in the functionalisation of materials by carrying out a variety of redox reactions through the use of several scans.

The electrochemical behaviour of the obtained polymers was recorded on a Princeton Applied Research Model 263A Potentiostat/Galvanostat. All CV measurements were performed in 0.1 M tetrabutylammonium perchlorate electrolyte solutions in acetonitrile (CH_3CN). The system comprises of three distinct electrodes: (i) an Ag/Ag^+-based referencing electrode, (ii) a platinum disc-based working electrode, and (iii) a platinum wire-based counter electrode. All electrodes were immersed in the electrolyte after saturation with N_2 under the following of N_2 during the measurement. Ferrocene was used as the redox system reference in accordance with IUPAC recommendations.

7.2.8 Photoluminescence Spectroscopy (PL)

Photoluminescence (PL) is a quantum mechanical process that involves the transmission of photon energy to an electron in its ground state once it is absorbed by the material, which is subsequently exited to an excited state within a femtosecond time. In the case of organic molecules with multiple excited states, electrons that are excited to higher energy levels instantly undergo nonradiative relaxation to the lowest excited states. This relaxation process occurs through the excitation of molecular vibrations in molecules or the emission of phonons in solids, and it takes place within picoseconds. This phenomenon is known as thermalisation or, more specifically, internal conversion, which involves transitions between states with the same spin multiplicity. Following that, the electrons combine repeatedly in a process known as radiative recombination, releasing photons and resulting in what is referred to as PL. Thermalisation-induced radiative transitions are limited and challenging to occur and are referred to as hot luminescence. Hence, the photons that are absorbed typically possess greater energy compared to the photons that are emitted. This energy is referred to as the Stokes' shift. It should be noted that in addition to absorption, some of the incident light is reflected while other is scattered. There are two types of scattering: Rayleigh scattering is characterised by its elastic nature, as it does not involve the annihilation or generation of excitations in the form of phonons. On the other hand, Raman scattering is inelastic and occurs when combined with either the annihilation of phonon (anti-Stokes Raman) or the generation of phonon (Stokes Raman). Although the quantum efficiency (QE) of the Raman scattering is low, typically 10^{-8} to 10^{-6}, it contains details regarding the molecular vibrations or phonons and solid crystallinity. In Raman scattering, two photons are absorbed and then released through a virtual middle state called an intragap. The scattered light is then reemitted within picoseconds. PL has separate one-photon processes compared to Raman scattering, starting with the absorption of photon and then being completed by photon emission with a transition period of over 0.1 ns.[304]

The PL spectra for the whole prepared polymers were measured via a Hitachi F-4500 Fluorescence Spectrophotometer with Hamamatsu Photonics R928F Photomultiplier Tube (PMT). 2 mg of each polymer was dissolved in dry toluene (2 ml), and then emissions were determined utilising a Quartz Glass Fluorescence Cuvette (light path length = 1 cm) at room temperature. Subsequently, the polymer's emission was determined via controllable drop-cast thin films on quartz substrates in the solid state.

7.3 Synthesis of Monomers

7.3.1 3,6-Dibromo-9H-carbazole[193] (1)

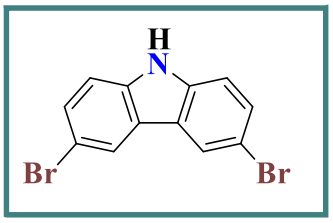

Carbazole (10 g, 59 mmol) was placed into a two-neck round bottom flask and dissolved using dry toluene (50 mL) under an atmosphere of argon. NBS (22.05 g, 123 mmol) was placed into a two-neck bottomed round flask, and then dry DMF (130 mL) was used to dissolve the sample under an inert atmosphere. Next, the carbazole mixture was placed in an ice bath, and the NBS solution was then added dropwise in a dark environment and left to stir overnight at RT. The resulting mixture was poured into ice water and left for 7 hours to precipitate. The precipitate formed was filtered, washed with water, collected and finally recrystallised using EtOH to obtain a white powder (15.88 g, 97%).

^{1}H NMR (400 MHz, DMSO-d6) δ 11.60 (s, br, 1H), 8.44 (s, 2H), 7.58 – 7.45 (m, 4H). **^{13}C NMR (101 MHz, DMSO-d6) δ** 139.26, 129.18, 123.85, 123.78, 113.66, 111.45. **EIMS (m/s):** $[M]^+$,$[M+2]^+$,$[M+4]^+$ 323.90, 324.89, 326. **E.A. calculated for $C_{12}H_7Br_2N$:** C 44.35, H 2.17, N 4.31, Br 49.17; found C 44.54, H 2.69, N 4.13, Br 46.0.

7.3.2 3,6-Dimethoxy-9H-carbazole[194] (2)

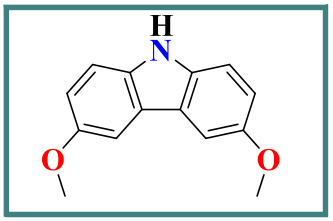

3,6-Dibromo-9H-Carbazole (10 g, 30 mmol) and copper iodide (22.50 g, 118 mmol) were charged into a two neck round bottom flask and degassed. Dry DMF (330 mL) was added in the presence of argon. Sodium metal (10 g, 434 mmoL) was dissolved in MeOH (180 mL) in an ice bath under an inert atmosphere of argon to form sodium methoxide (CH_3ONa). The sodium methoxide solution was then added to the 3,6-dibromo-9H- carbazole mixture under an argon atmosphere using a double tipped needle, then the reaction temperature was raised to

110 ^{0}C and left to stir overnight. Once the mixture cooled to RT, ionised water and ethyl acetate were used for the extraction. The organic layers were collected, dried over $MgSO_4$, filtered and then solvent reduced via rotary evaporation to obtain the product as a white solid (5.66 g, 80 %).

^{1}H NMR (400 MHz, $CDCl_3$) δ 11.59 (s, br, 1H), 7.53 (s, 2H), 7.33 (d, *J* = 8.8 Hz, 2H), 7.08 (dd, *J* = 8.8, 2.5 Hz, 2H), 3.96 (s, 6H). **^{13}C NMR (101 MHz, $CDCl_3$) δ** 153.68, 123.75, 115.24, 111.54, 102.90, 56.10,. **EIMS (m/s):** $[M]^+$ 228.1. **E.A. calculated for $C_{14}H_{13}NO_2$:** C 73.99, H 5.77, N 6.16; found C 73.97, H 5.79, N 6.18.

7.3.3 Methyl 4-(3,6-Dimethoxy-9H-carbazole-9-yl)benzoate[195] (3)

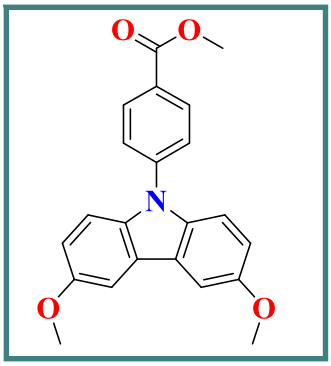

3,6-Dimethoxy-9H-carbazole (4.37 g, 19 mmol) and NaH (0.461 g, 19 mmol) were placed into a two neck round bottom flask under argon. Dry DMF (69 mL) was used to dissolve the mixture. One hour later, 4-fluorobenzoic acid methyl ester (2.66 g, 1.7 mL, 17 mmol) was added to the mixture. After complete addition, the system was degassed, refilled with argon and the temperature heated up to 70 ^{0}C, then the reaction was left to stir for 72 h. The mixture was extracted using deionized water and ethyl acetate (3 times) with ratio (1:1). The organic layer collected was dried over $MgSO_4$, filtered and the solvent was concentrated under reduced pressure. The resulting solid was recrystallized from hot MeOH to obtain white crystals (5.33 g, 77 %).

^{1}H NMR (400 MHz, $CDCl_3$) δ 8.28 (d, *J* = 8.7 Hz, 2H), 7.67 (d, *J* = 8.7 Hz, 2H), 7.57 (s, 2H), 7.43 (d, *J* = 8.9 Hz, 2H), 7.07 (dd, *J* = 8.9, 2.5 Hz, 2H), 4.01 (s, 3H), 3.98 (s, 6H). **^{13}C NMR (101 MHz, $CDCl_3$) δ** 166.31, 154.22, 142.39, 135.26, 131.34, 125.73, 115.31, 110.78, 103.05, 56.10, 52.31. **EIMS (m/s):** $[M]^+$ 362.1. **E.A. calculated for $C_{22}H_{19}NO_4$:** C 73.12, H 5.30, N 3.88; found C 73.29, H 5.54, N 4.08.

7.3.4 4-(3,6-Dimethoxy-9H-carbazol-9'-yl)benzoic acid[196] (4)

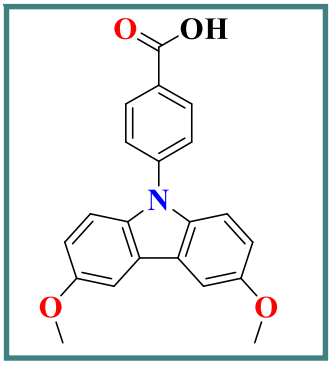

Methyl 4-(3,6-dimethoxy-9H-carbazol-9'-yl)benzoate (2.30g, 6 mmol) was dissolved in a mixture of MeOH (100mL) and 1M NaOH (100 mL). The reaction was heated to reflux for 6 h. MeOH was evaporated using a rotary evaporator, then the aqueous mixture was tested using pH paper to confirm that the pH > 10. After confirmation of pH, the aqueous layer was extracted with Et_2O and the extract washed with 1M NaOH (3 times). The combined aqueous layer was then acidified using conc HCl, then extracted with DCM (3 times). The organic phase was collected, dried over $MgSO_4$ and filtered, the filtrate was collected and the solvent was concentrated using a rotary evaporator to obtain the product as a white powder (1.9 g, 86 %).

^{1}H NMR (400 MHz, $CDCl_3$) δ 13.08 (s, br, 1H), 8.37 (d, *J* = 7.9 Hz, 2H), 7.73 (d, *J* = 8.9 Hz, 2H), 7.58 (s, 2H), 7.47 (d, *J* = 8.1 Hz, 2H), 7.09 (dd, *J* = 8.9, 2.5 Hz, 2H), 3.99 (s, 6H). **^{13}C NMR (101 MHz, $CDCl_3$) δ** 171.2, 154.5, 143.3, 135.5, 132.1, 126.7, 125.6, 124.5, 115.4, 110.7, 103.1, 56.2 **EIMS (m/s):** $[M]^+$ 348.1. **E.A. calculated for $C_{21}H_{17}NO_4$:** C 72.61, H 4.93, N 4.03; found C 72.59, H 4.90, N 4.02.

7.3.5 4-(3',6'-Dihydroxy-9H-carbazol-9'-yl) benzoic acid[197] (5)

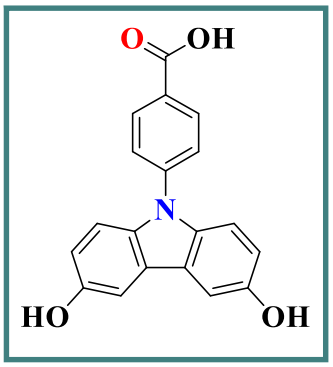

In a degassed one neck round bottom flask, a mixture of 4-(3',6'-dimethoxy-9H-carbazol-9'-yl)benzoic acid (1.5 g, 4 mmol) and pyridinium chloride (7.5 g, 64 mmol) was heated to 160 ^{0}C for 60 min. The mixture was allowed to cool down, then cold deionized water (150 mL) was added, and the aqueous layer was extracted with ethyl acetate (3 x 150 mL). The organic phase was collected, dried over Na_2SO_4 and filtered. The solvent was concentrated to obtain a creamy solid. The resultant was washed with $CHCl_3$ to obtain a white powder (1.2 g, 87%).

^{1}H NMR (400 MHz, DMSO-d6) δ 13.00 (s, br, 1H), 8.32 (d, *J* = 8.0 Hz, 2H), 7.70 (d, *J* = 8.7 Hz, 2H), 7.55 (s, 2H), 7.44 (d, *J* = 8.1 Hz, 2H), 7.03 (dd, *J* = 8.8, 2.4 Hz, 2H), 4.6 (s, br, 2H).^{13}C **NMR (101 MHz, DMSO) δ** 171.0, 154.5, 142.9, 135.4, 132.0, 125.6, 125.5, 124.3, 115.3, 110.8, 103.1 **EIMS (m/s):** $[M]^{+}$ 320.1. **E.A. calculated for $C_{19}H_{13}NO_4$:** C 71.47, H 4.10, N 4.39; found C 71.50, H 4.12, N 4.41.

7.3.6 4-(3,6-Diacetoxy-9H-carbazol-9-yl) benzoic acid[198] (6) M1

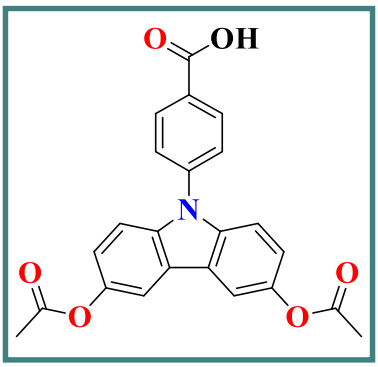

4-(3',6'-Dihydroxy-9H-carbazol-9'-yl)benzoic acid (0.490g, 1.5 mmol) and triethylamine (0.5 g, 3.5 mmol) were charged in a two neck round bottom flask under an argon atmosphere, and

anhydrous DMF (10 mL) was added. After 30 minutes, acetyl chloride (1.2 mL, 16 mmol) was added to the mixture and the reaction left to stir overnight at RT. The resulting mixture was extracted using deionized water/ DCM (3 times) with ratio of (1:1). The organic phase was collected, dried over Na_2SO_4 and filtered, then the solvent was reduced using a rotary evaporator to obtain a yellow oil. The resulting oil was added slowly as drops to 100 mL of petroleum ether in ice bath to form a brown precipitate. The resulting precipitate was purified via column chromatography using petroleum ether and ethyl acetate (3:1) as an eluent to afford a white solid (0.300 g, 74 %).

^{1}H NMR (400 MHz, $CDCl_3$) δ 13.11 (br,s, 1H) 8.34 (d, *J* = 8.5 Hz, 2H), 8.22 (d, *J* = 1.9 Hz, 2H), 7.69 (d, *J* = 8.5 Hz, 2H), 7.55 (dd, *J* = 8.7, 2.0 Hz, 2H), 7.35 (d, *J* = 8.7 Hz, 2H), 2.46 (s, 6H). **^{13}C NMR (101 MHz, $CDCl_3$) δ** 170.2, 167.1, 145.0, 141.0, 138.3, 131.8, 126.8, 123.5, 121.5, 114.2, 111.0, , 21.3. **EIMS (m/s):** $[M]^+$ 404.1 **E.A. calculated for $C_{23}H_{17}NO_6$:** C 68.48, H 4.25, N 3.47; found C 68.46, H 4.22, N 3.46.

7.3.7 3,6-Dibromo-9-ethyl-carbazole[217] (7) M2

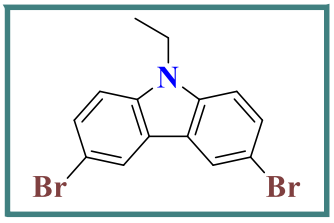

Under an argon atmosphere, (3.00 g, 53 mmol) of KOH was charged in a 250 ml round bottom flask, and DMF (35 ml) was added as a dropwise. Mixture was left under stirring at RT for 10 minutes. Furthermore, 3,6-dibromo-9H-carbazole (1.5 g, 4.2 mmol) was added. The mixture left to be stirred at RT for 30 minutes. Bromoethane (1.515 g, 1.03 ml, 13.9 mmol) was gently added to the mixture. After complete addition, the reaction was left under stirring overnight at RT. 350 ml of deionised water was added to the resulting components, then extracted with DCM (350 ml) thrice. The organic phase was collected, dried over Na_2SO_4, and reduced under vacuum pressure to obtain the final product as white solid (1.25 g, 77 %).

^{1}H NMR (400 MHz, DMSO-d6) δ 8.48 (s, 2H), 7.67 – 7.55 (m, 4H), 4.44 (q, *J* = 7.1 Hz, 2H), 1.29 (t, *J* = 7.1 Hz, 3H). **^{13}C NMR (101 MHz, DMSO-d6) δ** 139.10, 129.35, 124.04, 123.54, 112.22, 111.75, 37.81, 14,09. **EIMS (m/s):** $[M]^+$,$[M+2]^+$,$[M+4]^+$, 351.93 352.93, 354.93.

E.A. calculated for $C_{14}H_{11}Br_2N$: C, 47.63; H, 3.14; Br, 45.26; N, 3.97 ; found C 47.80; H, 3.19; Br, 45.30; N, 3.99.

7.3.8 3,6-Dimethoxy-9-ethyl-carbazole[194] (8)

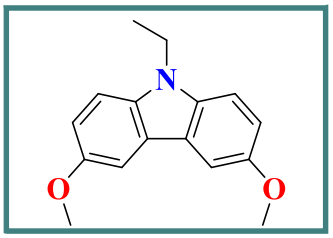

In 250 ml round bottom flask, sodium (3.5 g, 152 mmol) was dissolved in dry MeOH (37 ml). This was added to another 250 ml round bottom flask, containing 3,6-dibromo-9-ethyl-carbazole (3.5 g, 13.7 mmol) and CuI (7.93 g, 41 mmol), which already were dissolved in DMF (70 ml). The reaction mixture was heated gradually up to 120 ^{0}C and left under stirring for 48 hours. The resulting mixture was cooled down to RT, then ethyl acetate (200 ml) was added. The mixture was then filtered through a silica gel pad, and washed with water (200 ml) three times. The organic phase was collected, dried over $MgSO_4$ and solvent reduced under vacuum pressure. The obtained crude material was purified via silica gel column chromatography using ethyl acetate/petroleum ether, 1:6, obtaining the product as pale-yellow solid (2 g , 79 %).

^{1}H NMR (400 MHz, $CDCl_3$) δ 7.57 (s, 2H), 7.31 (d, *J* = 8.8 Hz, 2H), 7.13 (dd, *J* = 8.8, 2.5 Hz, 2H), 4.33 (q, *J* = 7.2 Hz, 2H), 3.96 (s, 6H), 1.42 (t, *J* = 7.2 Hz, 3H). **^{13}C NMR (101 MHz, $CDCl_3$) δ** 153.19, 135.61, 122.91, 115.00, 109.29, 103.19, 56.20, 37.72, 13.95. **EIMS (m/s):** $[M]^+$ calculated 353.05 found 354.04. **E.A. calculated for $C_{16}H_{17}NO_2$:** C, 47.63; H, 3.14; N, 3.97 ; found C 47.64; H, 3.16; N, 3.99

3,6-Dihydroxy -9-ethyl-carbazole[218] (9) M3

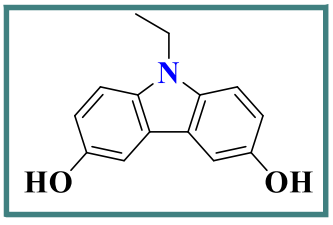

3,6-Dimethoxy-9-ethyl-carbazole (1.00 g, 4.4 mmol) was added to double neck round bottom flask under nitrogen, then degassed. Anhydrous DCM (15 ml) was added to the flask gently. After 10 minutes, the mixture was placed in an ice bath to cool down at 0 ^{0}C. BBr_3, 1M soln.

in CH_2Cl_2 (19.71 g, 13.5 ml, 78 mmol) was added dropwise to the mixture over 15 minutes. After complete addition, the mixture was stirred for 15 minutes more at 0 ^{0}C and allowed to warm up to RT. The reaction was left under stirring overnight at RT. The resulting mixture was quenched and adjusted to pH of 7 with saturated $NaHCO_3$, following by the extraction with DCM (150 ml) three times. The organic layers were collected, dried over Na_2SO_4 and reduced under vacuum to obtain the target product as pale-green (0.860 g, 86 %).

^{1}H NMR (400 MHz, DMSO-d6) δ 8.87 (s, br, 2H), 7.35 – 7.27 (m, 4H), 6.90 (dd, *J* = 8.7, 2.4 Hz, 2H), 4.27 (q, *J* = 7.1 Hz, 2H), 1.23 (t, *J* = 7.1 Hz, 3H). **^{13}C NMR (101 MHz, DMSO-d6) δ** 150.47, 134.86, 122.92, 115.33, 109.78, 105.49, 37.38, 14.16. **EIMS (m/s):** $[M]^+$ 228.25. **E.A. calculated for $C_{14}H_{13}NO_2$:** C, 73.99; H, 5.77; N, 6.16 ; found C, 74.05; H, 5.80; N, 6.20.

7.3.9 3,6-Dimethoxy-9-phenyl-9H-carbazole[219] (10)

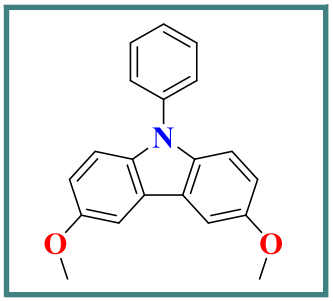

Dry CH_3CN (65 ml) was added to 3,6-dimethoxy- 9H-carbazole (2.2 g, 9.6 mmol) with iodobenzene (2.22 g, 10 mmol) under nitrogen. Then, copper powder (363 mg, 5.7 mmol) and Cs_2CO_3 (5.9 g, 18 mmol) were carefully added to the solution. The reaction heated up to 90 ^{0}C and left under stirring for 48 hours. TLC was used to monitor the progress of reaction (EA/PE, 1:20). After complete conversion, the resulting components were filtered, extracted using deionised water/EA (1:2) three times, and the organic phase was collected. The combined organic layers were dried over Na_2SO_4, filtered and the solvent reduced via rotary evaporator to obtain the residue. The crude product was purified through column chromatography using eluent (EA/PE, 1:20), following by recrystallisation from EtOH to obtain the final product as white crystals (2.5 g, 85.3 %).

^{1}H NMR (400 MHz, $CDCl_3$) δ 7.61 (dd, *J* = 8.2, 1.7 Hz, 2H), 7.55 (dd, *J* = 7.2, 1.4 Hz, 2H), 7.47 – 7.37 (m, 3H), 7.21 (d, *J* = 8.7 Hz, 2H), 6.89 (dd, *J* = 8.8, 2.4 Hz, 2H), 3.96 (s, 6H). **^{13}C NMR (101 MHz, $CDCl_3$) δ** 154.01, 138.19, 136.31, 129.81, 126.95, 126.71, 123.58, 115.20,

110.72, 102.86, 56.15,. **EIMS (m/s):** $[M]^+$ 304.34. **E.A. calculated for $C_{20}H_{17}NO_2$:** C, 79.19; H, 5.65; N, 4.62; found C, 79.25; H, 5.70; N, 4.60.

7.3.10 3,6-Dihydroxy-9-phenyl-9H-carbazole[218] (11) M4

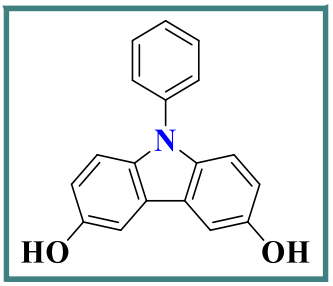

The same experimental conditions as used to prepare M2. 3,6-Dimethoxy-9-phenyl-9H-carbazole (0.950 g, 3.4 mmol), anhydrous DCM (12 ml), BBr_3, 1M soln. in CH_2Cl_2 (18.25g, 12.5 ml, 72.8 mmol), Saturated solution $NaHCO_3$. The final product was obtained as a pale gray (0.640 g, 74.24 %).

^{1}H NMR (400 MHz, DMSO-d6) δ 9.08 (s, 2H), 7.63 (dd, *J* = 8.2, 2.2 Hz, 2H), 7.55 (dd, *J* = 7.2, 1.4 Hz, 2H), 7.47 – 7.37 (m, 3H), 7.21 (d, *J* = 8.7 Hz, 2H), 6.89 (dd, *J* = 8.8, 2.4 Hz, 2H). **^{13}C NMR (101 MHz, DMSO-d6) δ** 151.61, 138.33, 135.04, 130.46, 127.06, 126.41, 123.86, 115.74, 110.56, 105.54, 60.23. **EIMS (m/s):** $[M]^+$ 276.28. **E.A. calculated for $C_{18}H_{13}NO_2$:** C, 78.53; H, 4.76; N, 5.09; found C, 78.56; H, 4.75; N, 5.11.

7.3.11 2-ethyl-2-((tosyloxy)methyl)propane-1,3-diyl bis(4-methylbenzenesulfonate)[222] (12) M5

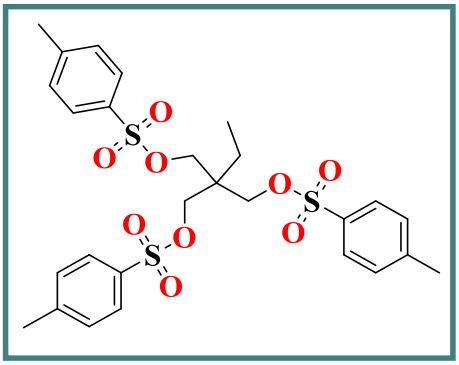

Into a 500 ml double neck round bottom flask under nitrrogen, 1,1,1-Tris(hydroxymethyl)propane (10 g , 74.5 mmol) was charged, and dissolved in a solution of DCM (164 ml) and Et_3N (67.53 g, 667 mmol). TsCl (51.19 g, 268 mmol) was added dropwise to the solution at 0 ^{0}C. After complete addition, the mixture was left under stirring at RT for 72 hours. Solvents were reduced under vacuum to obtain the residue as a black oil, which was precipitated in a mixed solvent of 0.25 M HCl aq. (1400 ml) and MeOH (250 ml). The resulting solid was collected, washed several times by water following by MeOH, and then dried. The target product was obtained after drying as a white solid (37.54 g, 84.41 %).

^{1}H NMR (400 MHz, $CDCl_3$) δ 7.74 (d, *J* = 8.6 Hz, 6H), 7.38 (d, *J* = 7.8 Hz, 6H), 3.79 (s, 6H), 2.49 (s, 9H), 1.38 (q, *J* = 7.6 Hz, 2H), 0.67 (t, *J* = 7.6 Hz, 3H).**^{13}C NMR (101 MHz, $CDCl_3$) δ** 145.40, 131.87, 130.11, 127.97, 67.68, 41.93, 21.72, 21.60, 6.59. **EIMS (m/s):** $[M]^+$ 597.73. **E.A. calculated for $C_{27}H_{32}O_9S_3$:** C, 54.34; H, 5.41; S, 16.12; found C, 54.37; H, 5.44; S, 16.15.

7.3.12 1,3,5-tris(6-bromohexyloxy)benzene[250] (13)

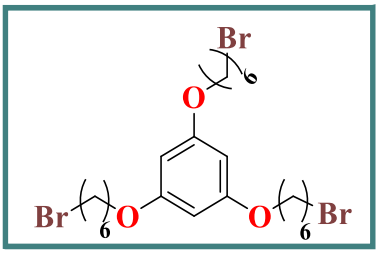

A mixture of 1,6-dibromohexane (17.7 g, 72.5 mmol), benzene-1,3,5-triol (2.7 g, 21.4 mmol), and cesium carbonate (24 g, 73.6 mmol) were charged in a 250 ml double neck round bottom flask. DMF (75 ml) was added to the mixture under an argon atmosphere to dissolve the reactants. Next, the reaction was left under stirring at RT for 72 hours. The reaction was monitored using TLC with eluent of (PE/EA, 9:1). Upon conversion, deionised water (50 ml) was added, and the resulting aqueous phase was extracted with DCM (50 ml) three times. The separated organic layers were collected, dried over $MgSO_4$, filtered and solvent was reduced under vacuum pressure to obtain the residue. Column chromatography (PE/EA, 9:1) was used to purify the crude, giving the final product as dense pale yellow oil (8.74 g, 66.36 %).

^{1}H NMR (400 MHz, $CDCl_3$) δ 6.08 (s, 3H), 3.94 (t, *J* = 6.4 Hz, 6H), 3.45 (t, *J* = 6.8 Hz, 6H), 1.97 – 1.85 (m, 6H), 1.85 – 1.73 (m, 6H), 1.56 – 1.45 (m, 12H). **^{13}C NMR (101 MHz, $CDCl_3$) δ** δ 161.68, 97.69, 68.79, 34.93, 30.00, 29.43, 28.54, 25.33.**EIMS (m/s):** $[M]^+$,$[M+2]^+$,$[M+4]^+$

613.05, 614.05, 616.04. **E.A. calculated for $C_{24}H_{39}Br_3O_3$:** C, 46.85; H, 6.39; Br, 38.96; found C, 46.55; H, 6.25; Br, 38.69

7.3.13 1,3,5-Tris[[6'-(4"-bromophenoxy)hexyl]oxy]benzene[251] (14)

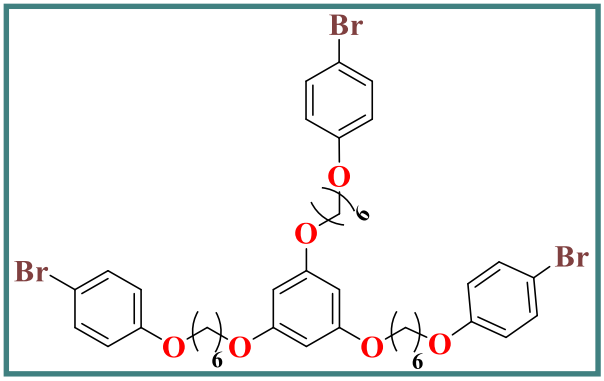

A solution of 1,3,5-tris(6-bromohexyloxy)benzene (1.8 g, 2.9 mmol), K_2CO_3 (1.4556 g, 10.5 mmol), 18-Crown-6 (0.180 g, 0.68 mmol), 4-bromophenol (1.8228 g, 10.5 mmol) and 2-butanone (60 mL) were charged in a 100 ml round bottom flask. The mixture was degassed and left under N_2 with stirring at 90 ^{0}C for 48 hours. After monitoring reaction using TLC, the mixture allowed to cool down to RT, the mixture was filtered and the solvent removed using a rotary evaporator. After removing solvent, the residue was dissolved in DCM and washed with brine (3 x 150 mL). The organic layer was dried over $MgSO_4$, filtered and solvent reduced under vacuum. Next, the resulting crude was purified via column chromatography using an eluent of hexane/ethyl acetate(15:1) to obtain a white solid, which was recrystallised from EtOH to produce the final product as a white crystals (2.45 g, 94.23%).

^{1}H NMR (400 MHz, $CDCl_3$) δ 7.38 (d, *J* = 8.6 Hz, 6H), 6.79 (d, *J* = 9.3 Hz, 6H), 6.08 (s, 3H), 3.94 (m, 12H), 1.88 – 1.76 (m, 12H), 1.57 – 1.48 (m, 12H). **^{13}C NMR (101 MHz, $CDCl_3$) δ** 160.93, 158.20, 132.22, 116.31, 112.64, 93.81, 68.09, 67.81, 29.18, 29.11, 25.88, 25.82. **EIMS (m/s):** $[M]^+$,$[M+2]^+$,$[M+4]^+$ 889.12, 891.56, 893.13. **E.A. calculated for $C_{42}H_{51}Br_3O_6$:** C, 56.58; H, 5.77; Br, 26.89; found C, 56.40; H, 5.40; Br, 26.75.

7.3.14 1,3,5-tris((6-(4-(4,4,5,5-tetramethyl-1,3,2-dioxaborolan-2-yl)phenoxy)hexyl)oxy) benzene[252] (15) M6

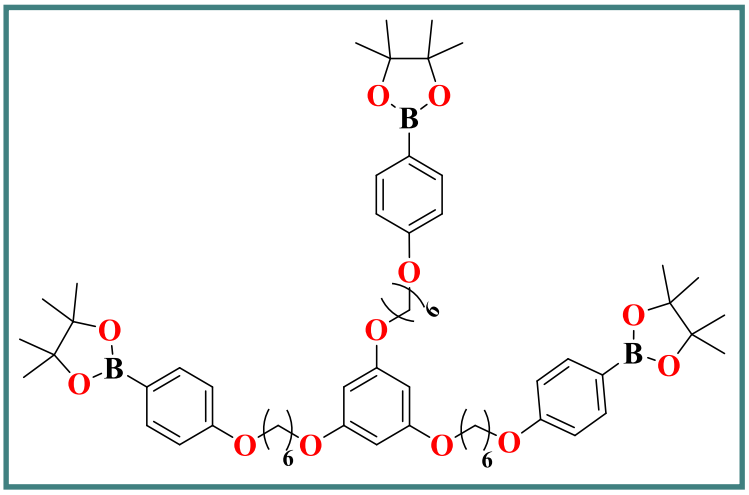

A mixture of 1,3,5-tris[[6'-(4"-bromophenoxy)hexyl]oxy]benzene (1.75 g, 1.9 mmol), potassium acetate (1.128 g, 11.4 mmol), bis(pinacolato)diboron (1.7045 g, 6.71 mmol) and $Pd(dppf)Cl_2$ (0.0816 g, 0.11 mmol) were charged under argon in a 100 ml two neck round bottom flask. Next, the mixture was degassed, then anhydrous DMF (15 ml) was added to dissolve the mixture. After complete addition, the reaction temperature was raised up to 100 ^0C, and the mixture left under stirring for 48 hours. After monitoring the reaction using TLC, the reaction temperature was allowed to cool down to RT and 250 ml of deionized water was added. The resulting aqueous solution was extracted with diethyl ether (3×130 ml), then the organic layers were collected, dried over $MgSO_4$, filtered and solvent was reduced under vacuum pressure giving the crude material. Silica gel column chromatography with the selective ratio of (hex/EA, 3:1) was used to purify the crude, affording the final product after the precipitation from MeOH as a white solid (1.65 g, 81 %).

^{1}H NMR (400 MHz, $CDCl_3$) δ 7.76 (d, J = 9.0 Hz, 6H), 6.91 (d, J = 8.2 Hz, 6H), 6.08 (s, 3H), 4.01 (t, J = 6.5 Hz, 6H), 3.94 (t, J = 6.4 Hz, 6H), 1.89 – 1.76 (m, 12H), 1.58 – 1.49 (m, 12H), 1.35 (s, 36H). **^{13}C NMR (101 MHz, $CDCl_3$) δ** 161.71, 160.93, 136.50, 113.87, 93.81, 83.52, 67.84, 67.63, 29.20, 29.17, 25.91, 25.87, 24.87. **EIMS (m/s):** $[M]^+$ 1033.91. **E.A. calculated for $C_{60}H_{87}B_3O_{12}$:** C, 69.78; H, 8.49; found C, 69.70; H, 8.55.

7.3.15 10- Acetylphenoxazine[254] (16)

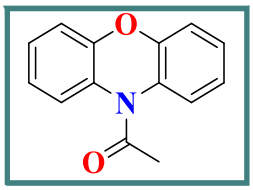

An anhydrous DCM (6 ml) was added under N_2 atmosphere to dissolve acetyl chloride (0.9 g, 0.81 ml, 11.4 mmol). At 0 ^{0}C, the previous solution was added dropwise to the solution of 10*H*-phenoxazine (1.5 g, 8.1 mmol) and triethylamine (1.245g, 1.71 mL, 12.3 mmol) in dry DCM (14 mL). The mixture was left under stirring for 4 hours. Later, 0.125 M HCl aq. (60 ml) was used to quench the reaction. The resulting aqueous phase was extracted with DCM thrice (60 ml), and the collected organic phases dried over $MgSO_4$, filtered and the solvent was reduced under vacuum pressure giving the residue. This was purified using silica gel column chromatography (PE/EA: 5:1) to afford the product as a pale green solid (1.69 g, 90%).

^{1}H NMR (400 MHz, $CDCl_3$) δ 7.51 (dd, *J* = 8.2, 1.7 Hz, 2H), 7.25 – 7.19 (m, 2H), 7.16 (m, 4H), 2.36 (s, 3H). **^{13}C NMR (101 MHz, $CDCl_3$) δ** 169.33, 151.08, 129.53, 126.92, 125.19, 123.38, 116.92, , 23.02. **EIMS (m/s):** $[M]^+$ 226.12. **E.A. calculated for $C_{14}H_{11}NO_2$:** C, 74.65; H, 4.92; N, 6.22: C, 69.78; H, 8.49; B, 3.14 found C, 74.70; H, 4.98; N, 6.15.

7.3.16 2- Acetylphenoxazine[255] (17)

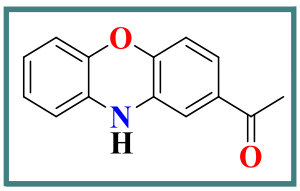

In 250 ml double neck round bottom flask, 10-acetylphenoxazine

(4.42g, 19.6 mmol) was charged, and carbon disulphide (78 ml) was added. The prepared solution was added dropwise to aluminium chloride (7.85 g, 58 mmol) at reflux temperature over 1.5 hours. After complete addition, the reaction mixture was cooled down to RT, and acetyl chloride (2.30 g , 29.3mmol) was added gently to the mixture. Next, the reaction was heated up to reflux and left under stirring for 3 hours. The reaction mixture was allowed to cool down, and mashed ice with 13 M HCl (90 ml) was added, forming a crude solid. This was filtered, washed and refluxed in a mixture of concentrated HCl and glacial acetic acid (1:4) for 30 minutes. The resulting precipitate was filtered, washed with H_2O, and then dried. The dried

precipitate was dissolved in ethyl acetate (100 ml) and extracted with water three times. The organic layers were collected, dried over $MgSO_4$ and solvent was evaporated via rotary evaporator to afford the target product as yellowish green crystals (4.10 g, 92.7 %).

^{1}H NMR (400 MHz, DMSO-d6) δ 8.42 (s, br, 1H), 7.25 (dd, *J* = 8.3, 2.1 Hz, 1H), 6.96 (d, *J* = 2.1 Hz, 1H), 6.76 (td, *J* = 7.5, 1.6 Hz, 1H), 6.69 (d, *J* = 8.2 Hz, 1H), 6.66 – 6.54 (m, 2H), 6.45 (dd, *J* = 7.7, 1.5 Hz, 1H), 2.44 (s, 3H). **^{13}C NMR (101 MHz, DMSO-d6) δ** 196.54, 147.48, 142.60, 133.47, 133.02, 132.08, 125.04, 122.89, 121.11, 115.76, 115.28, 113.91, 112.40, 26.74. **EIMS (m/s):** $[M]^+$ 226.09. **E.A. calculated for $C_{14}H_{11}NO_2$:** C, 74.65; H, 4.92; N, 6.22 found C, 74.70; H, 4.90; N, 6.15.

7.3.17 2-Chloro-4,6-diphenyl-1,3,5-triazine[256] (18)

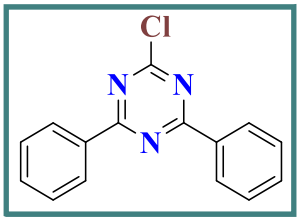

In a dry atmosphere free of oxygen, a solution of iodine activated, Mg (0.49 g, 20 mmol) in dry THF (14 ml) was prepared and stirred. To the prepared mixture, bromobenzene (2.44 g, 15.5 mmol) was dissolved in dry THF (20 ml) was added dropwise over the course of 15 minutes forming a Grignard reagent. This was added dropwise to a solution of cyanuric chloride (0.95 g , 5.1 mmol) in dry THF (30 ml) at 0 ^{0}C. After complete addition, the reaction temperature was raised up to 60 ^{0}C and left stirring overnight. The conversion of reaction was monitored via TLC (PE/DCM, 3:1). Upon completion, the resulting mixture was cooled down to RT, then an aqueous solution of HCl (14%, 60 ml) was poured into the mixture. The resulting residue was extracted with DCM thrice, and then the organic layers were collected, dried over Na_2SO_4, and solvent was reduced under vacuum pressure obtaining the crude material. Silica gel column chromatography (eluent PE/DCM, 3:1) was used to purify the crude to give the target product as a white solid (1.1 g, 80 %).

^{1}H NMR (400 MHz, DMSO-d6) δ 8.69 (dd, *J* = 7.6, 1.6 Hz, 4H), 7.68 (t, *J* = 8.1 Hz, 2H), 7.60 (t, *J* = 8.1 Hz, 4H).**^{13}C NMR (101 MHz, DMSO-d6) δ** 173.4, 172.6, 134.4, 133.6, 129.8, 128.6. **EIMS (m/s):** $[M]^+$ 268.09 **E.A. calculated for $C_{15}H_{10}ClN_3$:** C, 67.30; H, 3.77; Cl, 13.24; N, 15.70 Found C, 67.39; H, 3.88; Cl, 13.30; N, 15.55.

7.3.18 2-(4'-Aminophenyl)-4,6-diphenyl-1,3,5-triazine[257] (19)

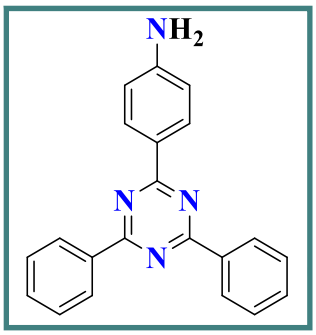

To a mixture of 2-chloro-4,6-diphenyl-1,3,5-triazine (5 g, 18.6 mmol), 4-(4',4',5',5' tetramethyl 1,3,2-dioxaborolan-2'-yl) aniline (4.50 g, 20.5 mmol) and $Pd(PPh_3)_4$ (1.08 g, 0.938 mmol) in anhydrous THF (100 ml), was added an aqueous solution of potassium carbonate (5.17 g, 37.4 mmol) under N_2. After complete addition, the reaction was left under stirring at reflux for 72 hours. After allowing the mixture to cool down, a mixture of ethyl acetate and deionised water was used to extract the resulting mixture. The extracted organic layers were collected, dried over $MgSO_4$ and the solvent was evaporated via a rotary evaporator giving the crude, which was precipitated from chloroform (80 ml) resulting in a brown solid. The obtained solid was washed three times with chloroform which after drying, formed the final product as a white powder (4.80 g, 79.3 %).

^{1}H NMR (400 MHz, DMSO-d6) δ 8.72 (dd, *J* = 7.4, 2.4 Hz, 4H), 8.46 (d, *J* = 8.4 Hz, 2H), 7.70 – 7.60 (m, 6H), 6.74 (d, *J* = 8.4 Hz, 2H), 4.18 (s, br, 2H). **^{13}C NMR (101 MHz, DMSO-d6) δ** 171.7, 170.6, 135.9, 135.1, 132,4, 131.7, 130.3, 128.5, 128.4, 127.3. **EIMS (m/s):** $[M]^+$ 325.15. **E.A. calculated for $C_{21}H_{16}N_4$:** C, 77.76; H, 4.97; N, 17.27. Found: C, 77.85; H, 5.10; N, 17.20.

7.3.19 2-(4'-Bromophenyl)-4,6-diphenyl-1,3,5-triazine[257] (20)

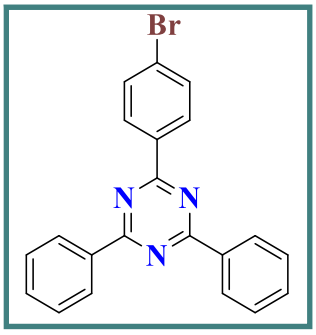

A solution of 2-(4'-aminophenyl)-4,6-diphenyl-1,3,5-triazine (4.32 g, 13.3 mmol) in hydrobromic acid (47%, 19.5 ml) was prepared at 0 ^{0}C, and left under stirring for half an hour. To the stirred mixture, a cold solution of sodium nitrite (1.16 g, 13.6 mmol) in deionised water (27 ml), which was stirred previously for half an hour, was added gently. After complete addition, the reaction mixture was kept at cold environment and left under stirring for an hour and half. To the previous stirred mixture, CuBr (1.15 g, 8 mmol) in HBr (8 ml) was added, then the reaction left stirring for 20 minutes at RT. After 20 minutes of stirring, the mixture was heated up to reflux and left for 24 hours. TLC (eluent of (hex/$CHCl_3$) was used to monitor the conversion of reaction. After complete conversion, the mixture was placed in an ice bath and the pH was adjusted to 7 by adding a solution of $NaHCO_3$. The aqueous resulting mixture was extracted with $CHCL_3$ thrice, then the extracted organic layers were collected, dried over $MgSO_4$, and solvent reduced under vacuum. The resulting residue was purified via silica gel column chromatography using (hex/$CHCl_3$, 4:1) as an eluent to afford the final product as a white powder (3.50 g, 67.7 %).

^{1}H NMR (400 MHz, $CDCl_3$) δ 8.78 (dd, *J* = 6.5, 1.3 Hz, 4H), 8.66 (d, *J* = 8.6 Hz, 2H), 7.72 (d, *J* = 8.6 Hz, 2H), 7.68 – 7.56 (m, 6H). **^{13}C NMR (101 MHz, $CDCl_3$) δ** 171.71, 170.81, 136.03, 135.19, 132.65, 131.90, 130.47, 128.99, 128.67, 127.48. **EIMS (m/s):** $[M]^+$,$[M+2]^+$,$[M+4]^+$ 388.04, 389.04, 391.04. **E.A. calculated for $C_{21}H_{14}BrN_3$:** C, 64.85; H, 3.72; Br, 20.50; N, 10.75. Found: C, 64.84; H, 3.71; Br, 20.48; N, 10.73.

7.3.20 10-(4'-(4",6"-diphenyl-1,3,5-triazin-2"-yl)phenyl)-10*H*-phenoxazin-2-yl)ethan-1-one[258] (21)

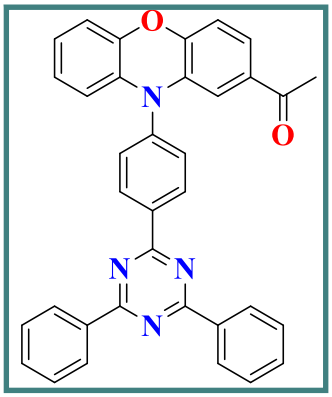

To the stirred solution under N_2 of 2-(4-bromophenyl)-4,6-diphenyl-1,3,5-triazine (1.05 g, 2.70 mmol), 2-acetylphenoxazine (0.500 g, 2.21 mmol) and K_2CO_3 (1.71 g, 12.3 mmol) in dry toluene (40 ml), was added dropwise a solution of $Pd(OAc)_2$ (27.79 mg , 0.123 mmol) and tri-tert-butylphosphine (91.98 mg, 0.454 mmol) in dry toluene over 10 minutes. The reaction

mixture was refluxed under stirring for 24 hours. Next, when the reaction was allowed to cool down to RT, a green brown precipitate was formed. Subsequently, the resulting precipitate was dissolved in DCM (100 ml) and washed three times with water (100 ml). The collected organic layer was dried over $MgSO_4$ and solvent was reduced. The crude was then purified via silica gel column chromatography (eluent of DCM/PE, 1:2, 1:1) to afford the final product as a yellow solid (0.950 g, 80.5 %).

^{1}H NMR (400 MHz, $CDCl_3$) δ 9.05 (d, *J* = 8.5 Hz, 2H), 8.84 (dd, *J* = 8.0, 1.4 Hz, 4H), 7.71 – 7.55 (m, 8H), 7.33 (dd, *J* = 8.3, 2.0 Hz, 1H), 6.80 – 6.63 (m, 5H), 6.06 (dd, *J* = 7.8, 1.6 Hz, 1H), 2.38 (s, 3H). **^{13}C NMR (101 MHz, $CDCl_3$) δ** 196.28, 171.89, 170.78, 148.25, 143.27, 142.11, 136.77, 136.04, 134.15, 133.40, 132.98, 132.74, 132.05, 130.78, 129.05, 128.94, 128.73, 128.55, 124.07, 123.56, 121.94, 115.80, 26.18. **EIMS (m/s):** $[M]^+$ 533.20. **E.A. calculated for $C_{35}H_{24}N_4O_2$:** C, 78.93; H, 4.54; N, 10.52 . Found: C, 78.85; H, 4.80; N, 10.77.

7.3.21 10-(4'-(4",6"-diphenyl-1,3,5-triazin-2"-yl)phenyl)-10*H*-phenoxazin-2-yl)ethan-1-ol[259] (22)

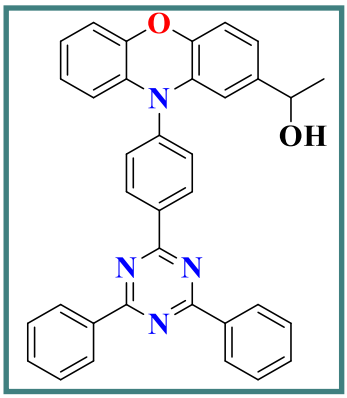

A solution of sodium borohydride (0.241 g, 6.3 mmol) dissolved in EtOH (8 ml) was added to the prepared solution of 10-(4'-(4",6"-diphenyl-1,3,5-triazin-2"-yl)phenyl)-10*H*-phenoxazin-2-yl)ethan-1-one(0.900 g, 1.6 mmol) in 1,4-dioxane (26 ml). The resulting mixture was left under stirring for 3 hours at RT, and the reaction heated up to 60 ^{0}C for a further 1 hour. Upon completion, the reaction temperature allowed to reached RT, then concentrated HCl was added to decompose the excess of borohydride. The resulting mixture was extracted with DCM (100 ml) and the extract washed several times with water (each 100 ml). The extracted organic layer was dried over $MgSO_4$ and the solvent was reduced under vacuum pressure giving the crude material, which was recrystallised from co-solvents (toluene-petroleum ether) to afford the final product as golden orange crystals (0.680 g, 75.3 %).

^{1}H NMR (400 MHz, $CDCl_3$) δ 9.03 (d, *J* = 8.4 Hz, 2H), 8.84 (dd, *J* = 6.5, 1.3 Hz, 4H), 7.72 – 7.56 (m, 8H), 6.78 – 6.68 (m, 4H), 6.64 (td, *J* = 7.6, 1.8 Hz, 1H), 6.13 – 6.01 (m, 2H), 4.59 (q, *J* = 6.4 Hz, 1H), 4.19 (bs, 1H), 1.33 (d, *J* = 6.5 Hz, 3H). **^{13}C NMR (101 MHz, $CDCl_3$) δ** 171.9, 170.6, 144.1, 143.1, 142.6, 141.22, 136.7, 136.39, 133.7, 133.6, 132.5, 131.6, 131.2, 129.1, 128.6, 123.2, 121.9, 118.5, 115.8, 115.2, 113.3, 110.8, 69.7, 24.8. **EIMS (m/s):** $[M]^+$ 535.31. **E.A. calculated for $C_{35}H_{26}N_4O_2$:** C, 78.63; H, 4.90; N, 10.48. Found: C, 78.90; H, 5.10; N, 10.55.

7.3.22 1,4-Dibromo-2-(6'-bromohexyloxy)benzene[260] (23)

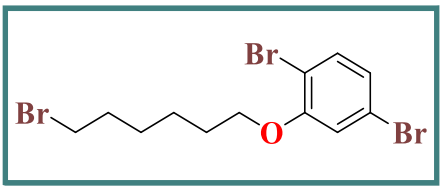

Under N_2 atmosphere, 1,6-dibromohexane (0.61 mL, 970 mg, 3.9 mmol), 2,5-dibromophenol (500 mg, 1.9 mmol) and KOH (450 mg, 8 mmol) were dissolved in anhydrous DMSO (17 ml). Then, the reaction mixture was left under stirring overnight. The resulting mixture was dissolved in DCM (150 ml) and extracted with deionised water (150 ml) thrice. The extracted organic layers were collected, dried over $MgSO_4$ and solvent was removed via rotary evaporator. The residue was then purified using silica gel column chromatography (DCM/PE, 1:10), obtaining the final product as a colourless crystals (0.790 g, 96 %).

^{1}H NMR (400 MHz, $CDCl_3$) δ 7.40 (d, *J* = 8.3 Hz, 1H), 7.02 (d, *J* = 2.1 Hz, 1H), 6.98 (dd, *J* = 8.3, 2.2 Hz, 1H), 4.03 (t, *J* = 6.3 Hz, 2H), 3.46 (t, *J* = 6.8 Hz, 2H), 2.00 – 1.83 (m, 4H), 1.64 – 1.50 (m, 4H). **^{13}C NMR (101 MHz, $CDCl_3$) δ** 156.06, 134.10, 124.64, 121.49, 116.47, 111.06, 69.20, 33.78, 30.96, 28.77, 27.82, 25.21. **EIMS (m/s):** $[M]^+$,$[M+2]^+$,$[M+4]^+$ 412, 414, 416. **E.A. calculated for $C_{12}H_{15}Br_3O$:** C, 34.73; H, 3.64; Br, 57.77. Found C, 34.65; H, 3.80; Br, 57.85.

7.3.23 2-(1-((6‴-(2,5-dibromophenoxy)hexyl)oxy)ethyl)-10-(4′-(4″,6″-diphenyl-1,3,5-triazin-2-yl)phenyl)-10*H*-phenoxazine[261] (24) M7

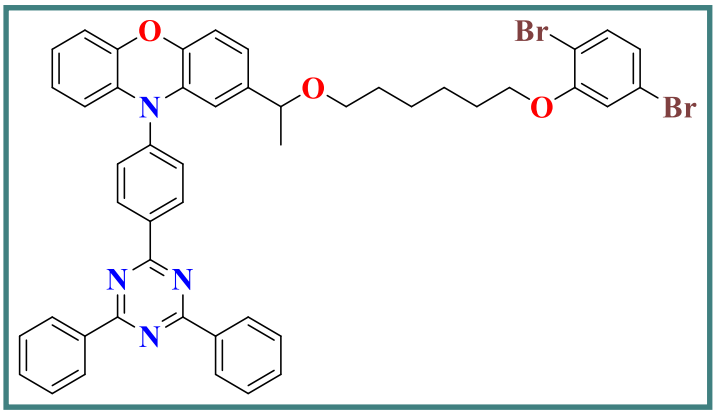

In anhydrous DMF (8 ml), a mixture of 1-(10-(4-(4,6-diphenyl-1,3,5-triazin-2-yl)phenyl)-10*H*-phenoxazin-2-yl)ethanol (0.830 g, 1.5 mmol) and KOH powder (0.875 g, 15.6 mmol) were dissolved and stirred for 3 hours at RT. To the stirred solution, a solution of 1,4-dibromo-2-(6-bromohexyloxy)benzene (0.965 g, 2.3 mmol) in anhydrous DMF (5 ml) was added dropwise. The reaction mixture was stirred at 55 ^{0}C for 24 hours. Upon completion, deionised water was added to quench the reaction and the aqueous resulting mixture was extracted with DCM (130 ml) three times. The extracted organic layers were collected, dried over $MgSO_4$ and solvent was removed under reduced pressure. the crude was purified via silica gel column chromatography using (DCM/PE, 1:1) to afford the product after the recrystallisation of MeOH as yellow solids (1 g, 74.1 %).

^{1}H NMR (400 MHz, $CDCl_3$) δ 9.04 (d, *J* = 8.5 Hz, 2H), 8.83 (dd, *J* = 6.5, 1.4 Hz, 4H), 7.69 – 7.54 (m, 7H), 7.33 (d, *J* = 8.3 Hz, 1H), 6.92 (dd, *J* = 8.4, 2.1 Hz, 1H), 6.87 (d, *J* = 2.2 Hz, 1H), 6.78 – 6.67 (m, 3H), 6.64 (ddd, *J* = 7.6, 5.8, 1.7 Hz, 2H), 6.13 – 5.97 (m, 2H), 4.08 (q, *J* = 6.4 Hz, 1H), 3.84 (t, *J* = 6.4 Hz, 2H), 3.23 (t, *J* = 6.4 Hz, 2H), 1.76 (m, *J* = 14.0, 6.7 Hz, 2H), 1.53 – 1.29 (m, 6H), 1.27 (d, *J* = 6.5 Hz, 3H). **^{13}C NMR (101 MHz, $CDCl_3$) δ** 171.84, 170.86, 156.31, 144.68, 144.56, 144.06, 138.54, 136.37, 134.30, 134.29, 133.70, 131.92, 131.22, 130.97, 128.80, 128.69, 126.42, 123.67, 123.22, 121.87, 121.20, 120.48, 118.91, 118.37, 118.15, 116.49, 115.53, 112.19, 78.25, 68.80, 68.01, 29.80, 29.63, 26.13, 25.30, 22.95. **EIMS (m/s):** $[M]^+$,$[M+2]^+$,$[M+4]^+$ 866.90, 868.85, 870.75. **E.A. calculated for $C_{47}H_{40}Br_2N_4O_3$ (%):** C, 64.99; H, 4.64; Br, 18.40; N, 6.45. Found C, 65.15; H, 4.55; Br, 18.50; N, 6.40.

7.3.24 Bis[2-(diphenylphosphino)phenyl]ether dioxide (DPEPO)[283] (25)

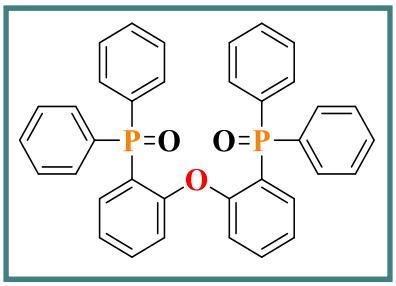

In dry environment free of oxygen, DPEPhos (3 g, 5.5 mmol) was charged in a two neck round bottom flask, then dissolved completely by anhydrous DCM (60 ml) at 0 ^{0}C. To the previous solution, 30% hydrogen peroxide aq. (13.8 ml, 111.6 mmol) was added, and the reaction left under stirring for 5 hours at 0 ^{0}C. Distilled water (60 ml) was added to quench the reaction mixture. The aqueous phase was extracted with DCM (110 ml) thrice, then the organic phases were collected, and dried over $MgSO_4$. After drying, the solvent was reduced in a rotary evaporator to obtain the residue, which was finally precipitated from hexane, providing the pure product as a white solid (3 g, 94.6 %).

^{1}H NMR (400 MHz, $CDCl_3$) δ 7.77 – 7.59 (m, 10H), 7.50 (d, *J* = 7.8 Hz, 2H), 7.43 (d, *J* = 8.0 Hz, 4H), 7.33 (s, 2H), 7.26 (s, 4H), 7.18 (tdd, *J* = 8.2, 1.9, 0.9 Hz, 2H), 7.10 (t, *J* = 7.5, 2H), 6.07 (q, *J* = 8.3 Hz, 2H). **^{13}C NMR (101 MHz, $CDCl_3$) δ** 158.92, 134.13, 133.82, 132.09, 131.90, 131.43, 128.47, 128.35, 128.12, 123.81, 123.70, 120.15. **EIMS (m/s):** $[M]^+$ 571.19. **E.A. calculated for $C_{36}H_{28}O_3P_2$:** C, 75.78; H, 4.95; found C, 75.80; H, 4.99.

7.3.25 1-Bromo-4-[4-bromo-2-(diphenylphosphinoyl)-phenoxy]-5 (diphenylphosphinoyl)-benzene (DPEPOBr2)[285] (26) M8

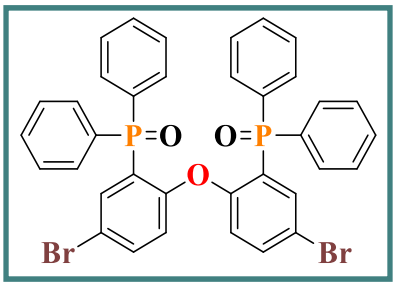

NBS (1.26 g ,7 mmol) was added in portions to the solution of DPEPO (2 g, 2.74 mmol) in H_2SO_4 (3.50 ml) and glacial acetic acid (10.52 ml) at RT. After complete addition, the reaction left was under stirring for 7.5 hours. The reaction was monitored by TLC (eluent ofPE/EA,

1:14). After complete conversion, deionised water was added to quench the reaction, and the aqueous layer then extracted with DCM (3 x 150 ml). The collected organic layers were dried over $MgSO_4$, then filtered and solvent was reduced under vacuum. The residue was purified via column chromatography (PE/EA, 14:1) obtaining the final product as a white powder (1.7 g, 68 %).

^{1}H NMR (400 MHz, $CDCl_3$) δ 7.83 (dd, *J* = 12.7, 2.5 Hz, 2H), 7.77 – 7.58 (m, 8H), 7.53-7.18 (m, 14H), 5.88 (q, *J* = 8.1 Hz, *J* = 5.5 Hz, 2H). **^{13}C NMR (101 MHz, $CDCl_3$) δ** 157.42, 157.40, 136.73, 136.71, 136.52, 136.45, 128.54, 127.39, 126.43, 121.71, 117.45. **EIMS (m/s):):** $[M]^+$,$[M+2]^+$,$[M+4]^+$, 726.98, 728.35, 730.97 **E.A. calculated for $C_{36}H_{26}Br_2O_3P_2$:** C, 59.37; H, 3.60; Br, 21.94; found C, 59.39; H, 3.57; Br, 21.91.

7.4 Synthesis of polymers:

7.4.1 General synthetic procedures of P1 & P2

P1 & **P2** were prepared via step growth polycondensation (AB_2) of M1 in the absence and the presence of core respectively according to the synthetic procedure reported in the literature[199]. **M1** was copolymerised under the protection of argon in different ratios with diphenyl ether as a solvent. The polymerisation occurred in two stages. Initially, by reacting the mixture in a dry round bottom flask and heating it up to 225 ^{0}C for 50 minutes, then cooled it down to 180 ^{0}C and left it under reduced vacuum for further 4 hours. Upon completion, the resulting crude was dissolved in hot THF and precipitated in iced cold methanol. Thereafter, the precipitate was filtered, washed with methanol several times, and then dried in the vacuum oven to afford the target polymers.

7.4.1.1 Synthesis of Polymer P1 (No core incorporated)

P1 was prepared following the general synthetic procedure above. **M1** (170 mg, 0.42 mmol) and diphenyl ether (170 mg, 0.99 mmol) were charged and copolymerised with respect to other polymerisation conditions, yielding (25%).

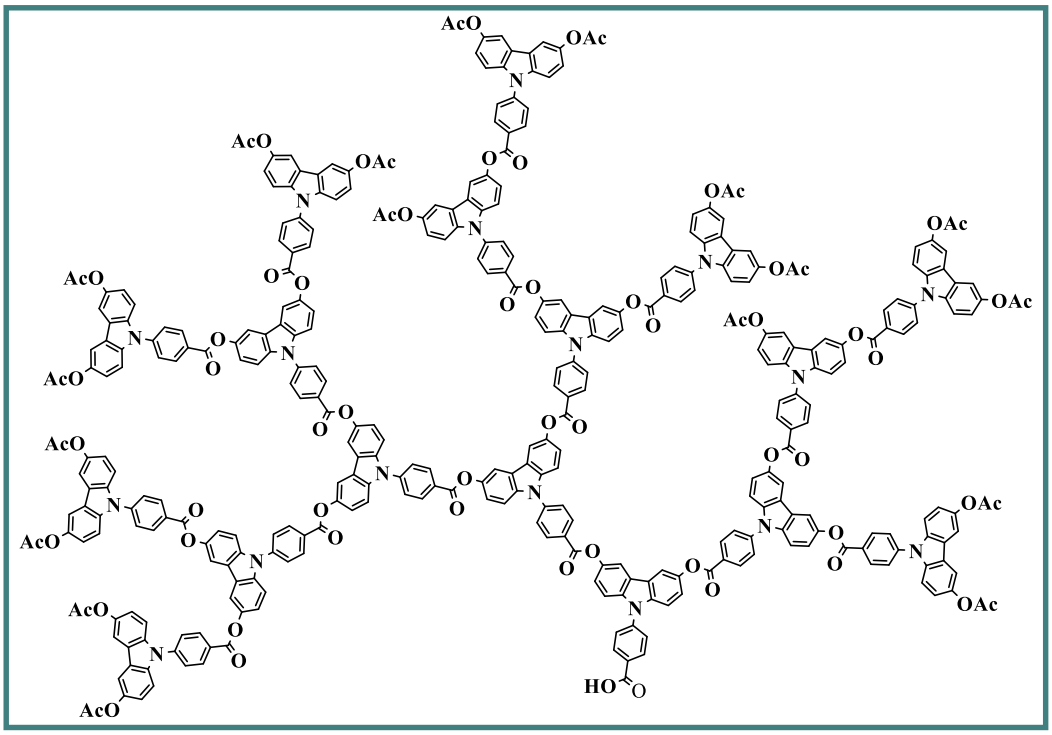

^{1}H NMR (400 MHz, $CDCl_3$) δ 8.51 – 8.45 (m, 2H), 8.28 – 8.20 (m, 3H), 7.82 – 7.74 (m, 2H), 7.62 – 7.54 (m, 3H), 7.41 (s, 1H), 7.40 – 7.32 (m, 13H), 7.16 – 7.08 (m, 6H), 7.07 – 7.00 (m, 11H), 2.41 (s, 0.67H).

IR: 3307 cm^{-1}, 2970 – 2875 cm^{-1}, 1733 cm^{-1}.

7.4.1.2 Synthesis of polymer P2 with the incorporation of 4-nitrophenyl acetate core (20:1)

P2 was prepared following the general synthetic procedure above. **M1** (260 mg, 0.64 mmol), diphenyl ether (280 mg, 1.6 mmol) and 4-nitrophenyl acetate (40 mg, 0.22 mmol) were charged and copolymerised with respect to other polymerisation conditions, yielding (28 %).

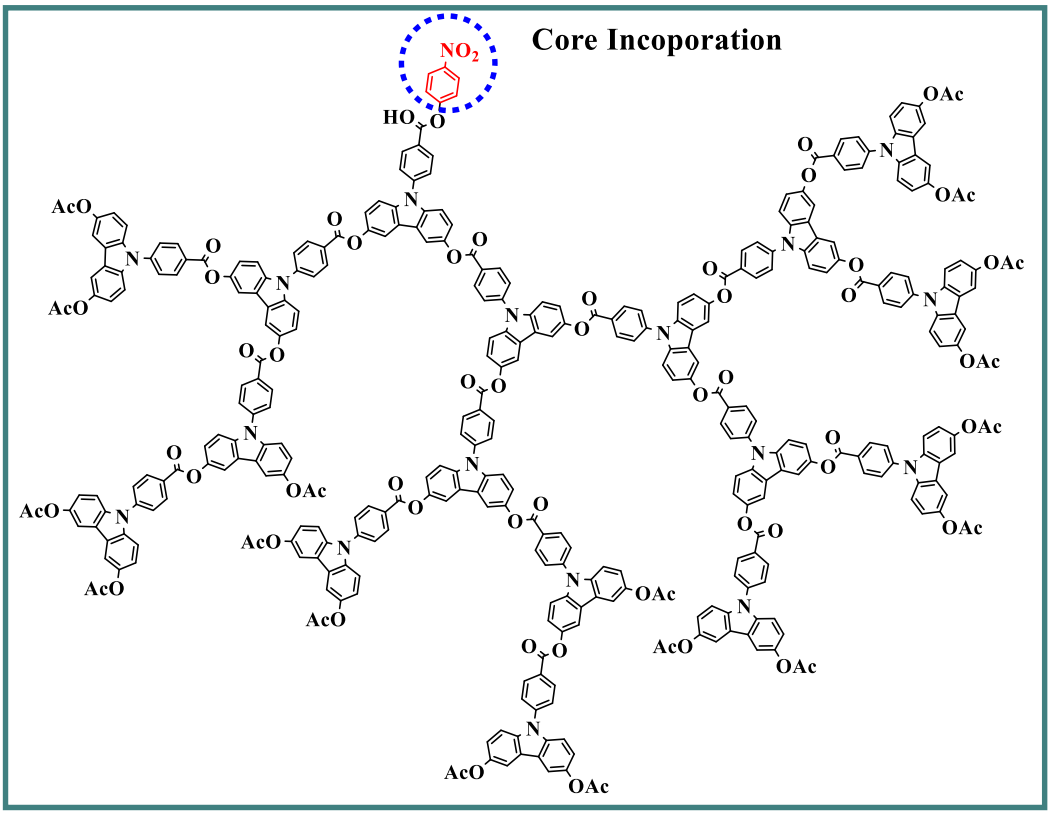

^{1}H NMR (400 MHz, $CDCl_3$) δ 8.55 – 8.44 (m, 6H), 8.42 – 8.35 (m, 2H), 8.28 – 8.20 (m, 7H), 7.85 – 7.66 (m, 9H), 7.65 – 7.47 (m, 10H), 7.46 – 7.31 (m, 9H), 7.26 – 7.20 (m, 1H), 7.16 – 7.09 (m, 1H), 7.07 – 7.01 (m, 1H), 2.41 (s, 2H).

IR: 3314 cm^{-1}, 2970 – 2872 cm^{-1}, 1737 cm^{-1}.

7.4.2 General Synthetic Procedures of P3 & P4

P3 & P4 were prepared via polycondensation polymerisation of (A_2B_3) of two different functionalised monomers according to the synthetic procedure reported in the literature[216]. M3 and M4 (bifunctionalised monomers, 1.5 eq) were copolymerised with M5 (trifunctionalised monomer, 1 eq) under N_2 atmosphere. An anhydrous DMF was used as a solvent along with potassium carbonate (30 eq). The reaction was left under stirring for 73 hours at 120 ^{0}C, and then allowed to cool down to RT. The resulting mixture was precipitated in deionised water and subsequently filtered. the precipitate was washed three times with water and left to dry in the vacuum oven overnight. The dried solid was then dissolved in $CHCl_3$ and precipitated with MeOH to afford the final polymers after drying.

7.4.2.1 Preparation of P3

M3 (107 mg, 0.470 mmol), M5 (189 mg, 0.316 mmol), K_2CO_3 (1.32 g, 9.59 mmol) and DMF (8 ml). Yield (70%).

^{1}H NMR (400 MHz, $CDCl_3$) δ 7.95 – 7.31 (m, 6H), 7.16 (s, 13H), 4.57 – 3.54 (m, 18H), 2.36 (s, 1H), 1.97 (s, 2H), 1.44 – 0.59 (m, 25H).

7.4.2.2 Preparation of P4

M4 (122 mg, 0.445 mmol), M5 (176 mg, 0.294 mmol), K_2CO_3 (1.23 g, 8.93 mmol) and DMF (6 ml). Yield (72%).

^{1}H NMR (400 MHz, $CDCl_3$) δ 8.18 (s, 7H), 7.95 – 7.31 (m, 41H), 7.25 – 6.53 (m, 28H), 5.82 (s, 3H), 4.72 – 4.00 (m, 19H), 3.92 (s, 6H), 1.91 (s, 22H), 1.24 – 0.34 (m, 18H).

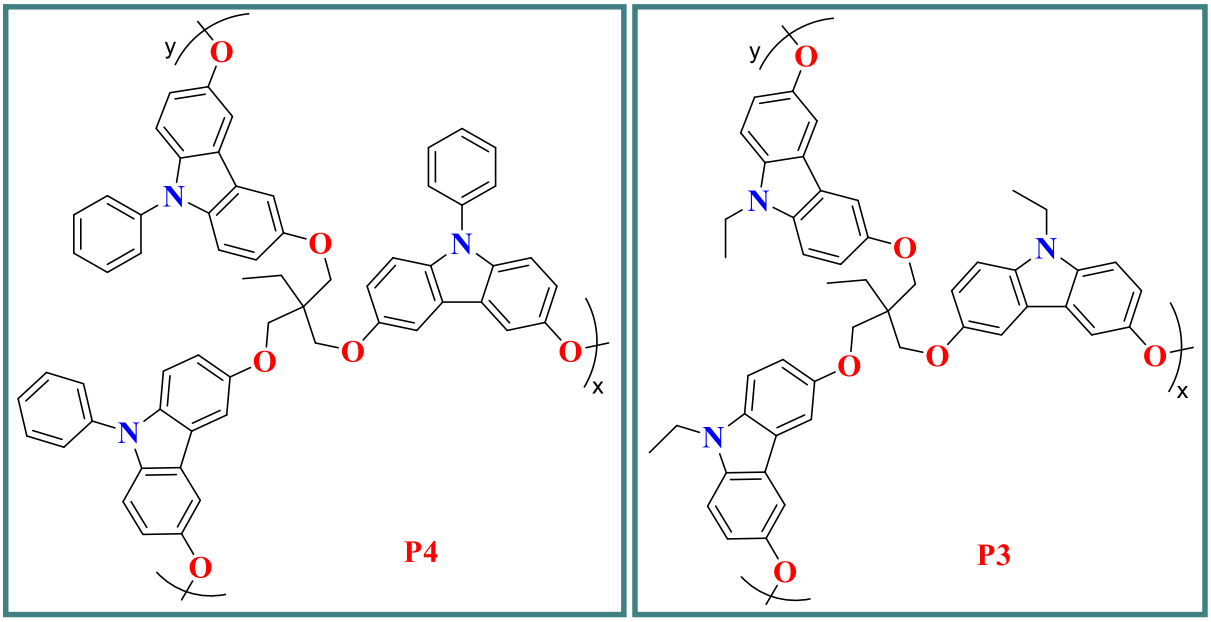

7.4.3 The Proposed Synthetic Procedures to Prepare Polymers (P5-P12)

The whole target polymers from P5 to P12 were synthesised via Suzuki coupling reaction according to the preparation method illustrated in the literature[181]. Different ratios of the synthesised monomer M2, M6, M7 and M8 were incorporated in the synthesis of the target polymers affording the (P5 0%, P6 5%, P7 10%, P8 20%) and (P9 0%, P10 5%, P11 10%, P12 20%). Bis-functionalised monomers M2 and M8 (various equivalences) were polymerised under N_2 with tris-functionalised monomer M6 (various equivalences), incorporating M7 with various ratio as well. To the prepared mixture, tri*(*o-tolyl*)*-phosphine (0.26 eq) and $Pd(OAc)_2$ (0.13 eq) was added and then degassed. Pre-degassed and bubbling with N_2 for 4 hours saturated $NaHCO_3$ (1.5 - 4 ml) was added to the mixture, and left under stirring for 10 minutes at RT. An anhydrous THF (2.5-5.5) was added, then mixture, then degassed and reaction temperature was heated up to 80 ^{0}C. At reflux, reaction mixture was left under stirring for 24 hours. Precipitates were formed, and reaction temperature cooled down to RT, then (100 µml of bromobenzene, 12.6 eq) was added, mixture degassed and heated up to reflux for 2 hours. Next, mixture allowed to cool down to RT, phenylboronic acid (120 mg, 13.06 eq) was added to the mixture, following by the degassing and heated it up to reflux for 3 hours. Upon completion, reaction cooled down, then chloroform (250 ml) and an ammonium hydroxide (40 ml, 30-33 wt. % in H_2O) were added to the reaction mixture and left under stirring at 70 ^{0}C for 4 hours. The resulting mixture was extracted with water and chloroform three times and the extracted organic layer were dried over $MgSO_4$, filtered and solvent reduced to about 25 ml via rotary evaporator. The crude was precipitated in MeOH (200 ml), then collected and dried in vacuum oven to obtain the target polymer as solids.

7.4.3.1 Preparation of The Target Polymers (P5-P8)

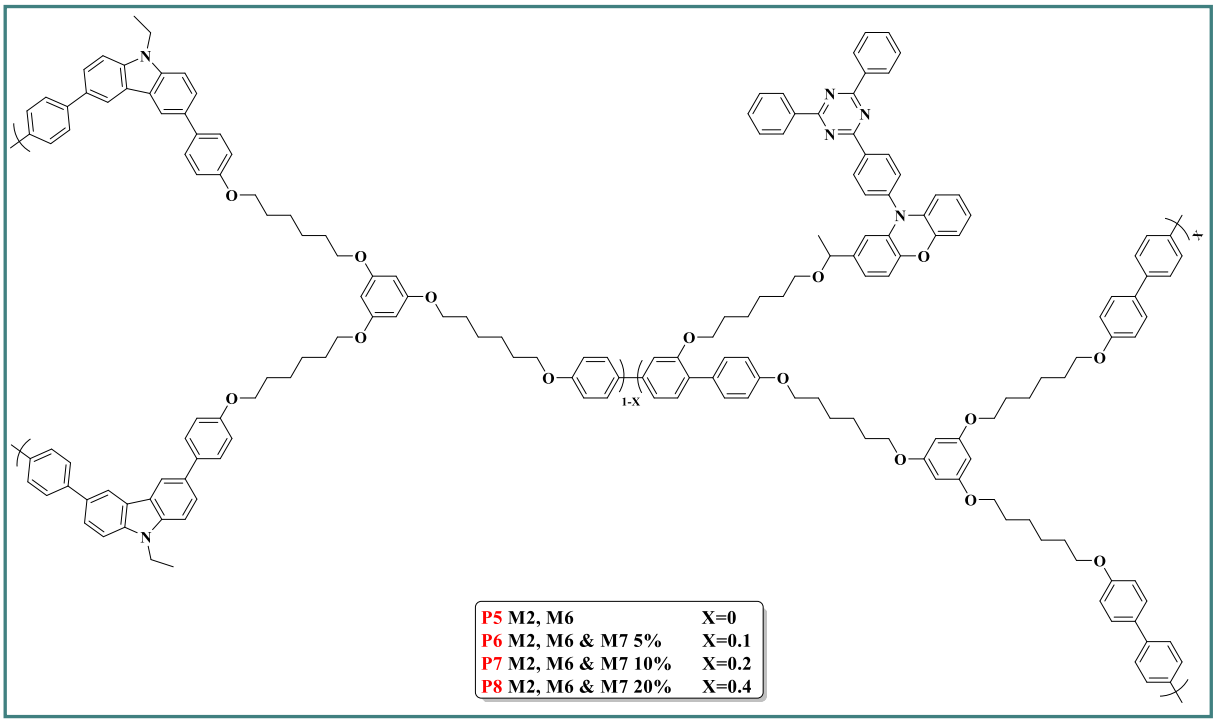

P5 M2, M6, M7 0%

Following a general synthetic procedure, M2 (44 mg, 0.126 mmol), M6 (88 mg, 0.085 mmol), tri(o-tolyl)-phosphine (6.7 mg, 0.02 mmol), $Pd(OAc)_2$ (2.4 mg, 0.01 mmol), saturated $NaHCO_3$ (3 ml) and anhydrous THF (3.5 ml). Yield (58%).

^1H NMR (400 MHz, $CDCl_3$) δ 8.33 – 8.23 (m, 4H), 8.23 – 8.15 (m, 1H), 7.81 – 7.71 (m, 4H), 7.66 – 7.55 (m, 10H), 7.55 – 7.43 (m, 9H), 7.41 – 7.29 (m, 8H), 7.01 (s, 11H), 6.11 (s, 3H), 4.52 – 4.29 (m, 7H), 4.28 – 4.15 (m, 3H), 4.10 – 3.86 (m, 15H), 3.64 (s, 2H), 1.83 (s, 17H), 1.66 – 1.34 (m, 41H).

P6 M2, M6, M7 5%

Following a general synthetic procedure, M2 (42 mg, 0.118 mmol), M6 (88 mg, 0.085 mmol), M7 (5.5 mg, 0.0063 mmol), tri(o-tolyl)-phosphine (6.7 mg, 0.02 mmol), $Pd(OAc)_2$ (2.4 mg, 0.01 mmol), saturated $NaHCO_3$ (3 ml) and anhydrous THF (3.5 ml). Yield (55%).

^1H NMR (400 MHz, $CDCl_3$) δ 9.02 (bs, 0.09H), 8.81 (bs, 0.1H), 8.30 (m, 1H), 7.85 – 7.31 (m, 2H), 7.14 – 6.52 (m, 1H), 6.11 (bs, 1H), 4.58 – 3.56 (m, 3H), 1.82 (bs, 2H), 1.52 (bs, 4H), 1.28 (s, 1H), 0.97 – 0.64 (m, 0.31H).

P7 M2, M6, M7 10%

Following a general synthetic procedure, M2 (40 mg, 0.113 mmol), M6 (88 mg, 0.085 mmol), M7 (11.1 mg, 0.012 mmol), tri*(*o-tolyl*)*-phosphine (6.7 mg, 0.02 mmol), $Pd(OAc)_2$ (2.4 mg, 0.01 mmol), saturated $NaHCO_3$ (3 ml) and anhydrous THF (3.5 ml). Yield (52%).

^1H NMR (400 MHz, $CDCl_3$) δ 9.01 (bs, 0.20H), 8.82 (bs, 0.38H), 8.34 – 8.04 (m, 1.08H), 7.75 – 7.39 (m, 5H), 7.12 – 6.83 (m, 3H), 6.77 – 6.55 (m, 0.59H), 6.17 – 5.97 (m, 1.38H), 4.52 – 4.12 (m, 2H), 4.11 – 3.79 (m, 4H), 1.82 (s, 5H), 1.68 – 1.38 (m, 9.41H), 1.28 (s, 2H), 0.87 (s, 1H).

P8 M2, M6, M7 20%

Following a general synthetic procedure, M2 (35.8 mg, 0.101 mmol), M6 (88 mg, 0.085 mmol), M7 (22.2 mg, 0.0255 mmol), tri*(*o-tolyl*)*-phosphine (6.7 mg, 0.02 mmol), $Pd(OAc)_2$ (2.4 mg, 0.01 mmol), saturated $NaHCO_3$ (3 ml) and anhydrous THF (3.5 ml). Yield (60%).

^1H NMR (400 MHz, $CDCl_3$) δ 9.02 (bs, 0.40H), 8.80 (s, 0.63H), 8.36 – 8.14 (m, 1H), 7.73 – 7.52 (m, 4H), 7.51 – 7.38 (m, 2H), 7.37 – 7.30 (m, 1H), 7.28 – 7.06 (m, 3H), 7.05 – 6.83 (m, 3H), 6.78 – 6.59 (m, 1H), 6.17 – 5.96 (m, 2H), 4.20 (s, 2H), 4.11 – 3.74 (m, 5H), 3.34 – 3.11 (m, 1H), 1.83 (s, 5H), 1.70 – 1.39 (m, 10H), 1.38 – 1.01 (m, 8H), 0.89 (s, 2H).

7.4.3.2 Preparation of The Target Polymers (P9-P12)

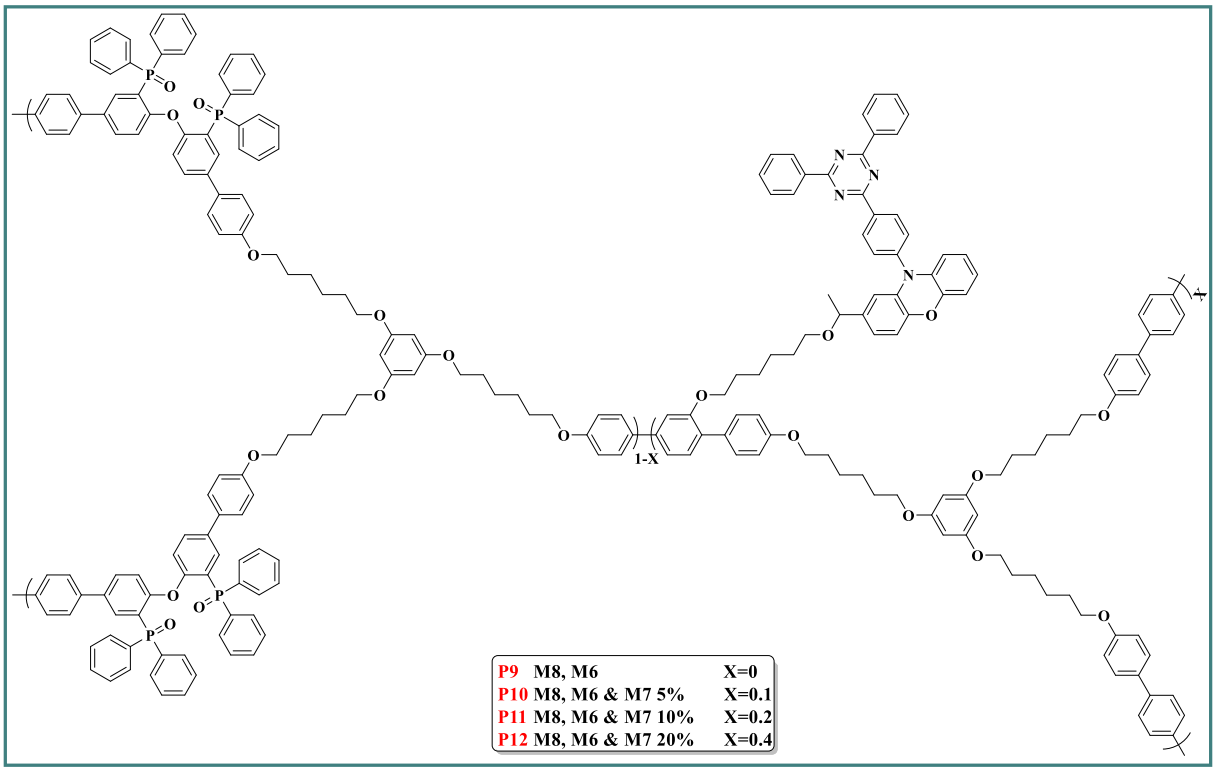

P9 M8, M, M8 0%

Following a general synthetic procedure, M8 (87.2 mg, 0.119 mmol), M6 (83 mg, 0.081 mmol), tri(o-tolyl)-phosphine (6.3 mg, 0.02 mmol), $Pd(OAc)_2$ (2.3 mg, 0.01 mmol), saturated $NaHCO_3$ (3 ml) and anhydrous THF (3.5 ml). Yield (53%).

^{1}H NMR (400 MHz, $CDCl_3$) δ 8.06 – 7.87 (m, 1H), 7.84 – 7.59 (m, 4H), 7.56 – 7.30 (m, 8H), 7.02 – 6.81 (m, 3H), 6.09 (bs, 2H), 6.03 – 5.86 (m, 1H), 4.29 – 4.16 (m, 1H), 4.08 – 3.86 (m, 4H), 3.76 (bs, 0.36H), 3.66 (bs, 0.38H), 1.73 (bs, 10H), 1.32 (bs, 2H), 1.17 (bs, 1H). 0.89 (bs, 0.33H).

P10 M8, M6, M7 5%

Following a general synthetic procedure M8 (83.4 mg, 0.114 mmol), M6 (83 mg, 0.081 mmol), M7 (5.23 mg, 0.0060 mmol), tri(o-tolyl)-phosphine (6.3 mg, 0.02 mmol), $Pd(OAc)_2$ (2.3 mg, 0.01 mmol), saturated $NaHCO_3$ (3 ml) and anhydrous THF (3.5 ml). Yield (56%).

^{1}H NMR (400 MHz, $CDCl_3$) δ 9.01 (bs, 0.09H), 8.80 (bs, 0.14H), 8.06 – 7.85 (m, 1H), 7.84 – 7.61 (m, 3H), 7.60 – 7.32 (m, 5H), 7.01 – 6.82 (m, 2H), 6.14 – 6.05 (m, 1H), 6.04 – 5.86 (m,

1H), 4.22 (s, 1H), 4.07 – 3.86 (m, 3H), 3.81 – 3.68 (m, 1H), 1.82 (bs, 3H), 1.65 (bs, 4H), 1.54 (bs, 4H), 1.44 – 1.18 (m, 3H), 0.87 (bs, 1H).

P11 M8, M6, M7 10%

Following a general synthetic procedure M8 (78.6 mg, 0.107 mmol), M6 (83 mg, 0.081 mmol), M7 (10.47 mg, 0.012 mmol), tri*(*o-tolyl*)*-phosphine (6.3 mg, 0.02 mmol), $Pd(OAc)_2$ (2.3 mg, 0.01 mmol), saturated $NaHCO_3$ (3 ml) and anhydrous THF (3.5 ml). Yield (55%).

^1H NMR (400 MHz, $CDCl_3$) δ 9.02 (bs, 0.27H), 8.82 (bs, 0.43), 8.06 – 7.87 (m, 1H), 7.84 – 7.62 (m, 5H), 7.59 – 7.36 (m, 7H), 7.03 – 6.81 (m, 4H), 6.80 – 6.66 (m, 1H), 6.15 – 6.04 (m, 2H), 6.03 – 5.85 (m, 1H), 4.22 (bs, 1H), 4.07 – 3.84 (m, 5H), 3.82 – 3.69 (m, 1H), 1.82 (bs, 6H), 1.70 (bs, 5H), 1.54 (bs, 6H), 1.42 – 1.33 (m, 3H), 1.31 – 1.22 (m, 5H), 0.94 – 0.83 (m, 2H).

P12 M8, M6, M7 20%

Following a general synthetic procedure M8 (69.8 mg, 0.095 mmol), M6 (83 mg, 0.081 mmol), M7 (20.94 mg, 0.024 mmol), tri*(*o-tolyl*)*-phosphine (6.3 mg, 0.02 mmol), $Pd(OAc)_2$ (2.3 mg, 0.01 mmol), saturated $NaHCO_3$ (3 ml) and anhydrous THF (3.5 ml). Yield (65%).

^1H NMR (400 MHz, $CDCl_3$) δ 9.00 (s, 0.51H), 8.79 (s, 0.76H), 8.05 – 7.89 (m, 1H), 7.83 – 7.63 (m, 4H), 7.62 – 7.47 (m, 3H), 7.47 – 7.30 (m, 8H), 7.00 – 6.83 (m, 3H), 6.76 – 6.57 (m, 1H), 6.14 – 5.98 (m, 2H), 5.97 – 5.87 (m, 1H), 4.22 (s, 1H), 4.08 – 3.84 (m, 5H), 3.75 (s, 1H), 1.82 (s, 5H), 1.65 (s, 6H), 1.54 (s, 6H), 1.43 – 1.19 (m, 4H), 0.87 (s, 1H).

Chapter 8: References and Supplementary Section

8.1 References

1. G. Horowitz, D. Fichou, X. Peng, Z. Xu and F. Garnier, *Solid State Communications*, 1989, **72**, 381-384.
2. M. Koden, *History of OLEDs* 2017.
3. S. Kunić and Z. Šego, 2012.
4. J. Van Der Holst, F. Van Oost, R. Coehoorn and P. Bobbert, *Physical Review B*, 2009, **80**, 235202.
5. M. Moral, L. Muccioli, W.-J. Son, Y. Olivier and J.-C. Sancho-Garcia, *Journal of Chemical Theory and Computation*, 2015, **11**, 168-177.
6. S. Kappaun, C. Slugovc and E. J. List, *International Journal of Molecular Sciences*, 2008, **9**, 1527-1547.
7. H. Uoyama, K. Goushi, K. Shizu, H. Nomura and C. Adachi, *Nature*, 2012, **492**, 234-238.
8. X.-K. Chen, D. Kim and J.-L. Brédas, *Accounts of Chemical Research*, 2018, **51**, 2215-2224.
9. I. Lyskov and C. M. Marian, *The Journal of Physical Chemistry C*, 2017, **121**, 21145-21153.
10. T. Yamada, *Advanced Display Technology: Next Generation Self-Emitting Displays*, 2021, 83-106.
11. C. G. Camara, J. V. Escobar, J. R. Hird and S. J. Putterman, *Nature*, 2008, **455**, 1089-1092.
12. X. Y. Wei, X. Wang, S. Y. Kuang, L. Su, H. Y. Li, Y. Wang, C. Pan, Z. L. Wang and G. Zhu, *Advanced Materials*, 2016, **28**, 6656-6664.
13. E. Ducrot, Y. Chen, M. Bulters, R. P. Sijbesma and C. Creton, *Science*, 2014, **344**, 186-189.
14. X.-H. Zhu, J. Peng, Y. Cao and J. Roncali, *Chemical Society Reviews*, 2011, **40**, 3509-3524.
15. H. Yersin, *Highly Efficient OLEDs: Materials Based on Thermally Activated Delayed Fluorescence*, John Wiley & Sons, 2019.
16. M. Cinquino, C. T. Prontera, M. Pugliese, R. Giannuzzi, D. Taurino, G. Gigli and V. Maiorano, *Micromachines*, 2021, **12**, 652.
17. U. Giovanella, M. Pasini and C. Botta, *Applied Photochemistry: When Light Meets Molecules*, 2016, 145-196.

18. T.-H. Han, W. Song and T.-W. Lee, *ACS Applied Materials & Interfaces*, 2015, **7**, 3117-3125.
19. X. Zhou, M. Pfeiffer, J. Blochwitz, A. Werner, A. Nollau, T. Fritz and K. Leo, *Applied Physics Letters*, 2001, **78**, 410-412.
20. M. T. Greiner and Z.-H. Lu, *NPG Asia Materials*, 2013, **5**, e55-e55.
21. M. Kröger, S. Hamwi, J. Meyer, T. Riedl, W. Kowalsky and A. Kahn, *Applied physics letters*, 2009, **95**.
22. M. Vasilopoulou, G. Papadimitropoulos, L. C. Palilis, D. G. Georgiadou, P. Argitis, S. Kennou, I. Kostis, N. Vourdas, N. A. Stathopoulos and D. Davazoglou, *Organic Electronics*, 2012, **13**, 796-806.
23. J.-H. Lee, D.-S. Leem and J.-J. Kim, *Organic Electronics*, 2008, **9**, 805-808.
24. J. Kim, M. Kim, J. Won Kim, Y. Yi and H. Kang, *Journal of Applied Physics*, 2010, **108**.
25. M. Strukelj, F. Papadimitrakopoulos, T. M. Miller and L. J. Rothberg, *Science*, 1995, **267**, 1969-1972.
26. B. Minaev, G. Baryshnikov and H. Agren, *Physical Chemistry Chemical Physics*, 2014, **16**, 1719-1758.
27. L. Akcelrud, *Progress in Polymer Science*, 2003, **28**, 875-962.
28. L. N. Viana, A. P. S. Soares, D. L. Guimarães, W. J. S. Rojano and T. D. Saint'Pierre, *Journal of Environmental Chemical Engineering*, 2022, **10**, 108915.
29. Y. Huang, E.-L. Hsiang, M.-Y. Deng and S.-T. Wu, *Light: Science & Applications*, 2020, **9**, 105.
30. D. Zhang, T. Huang and L. Duan, *Advanced Materials*, 2020, **32**, 1902391.
31. C. Zhang, C. Ji, Y. B. Park and L. J. Guo, *Advanced Optical Materials*, 2021, **9**, 2001298.
32. M. Fröbel, T. Schwab, M. Kliem, S. Hofmann, K. Leo and M. C. Gather, *Light: Science & Applications*, 2015, **4**, e247-e247.
33. C. Adachi, M. A. Baldo, M. E. Thompson and S. R. Forrest, *Journal of Applied Physics*, 2001, **90**, 5048-5051.
34. Z. Wang, M. Helander, J. Qiu, D. Puzzo, M. Greiner, Z. Hudson, S. Wang, Z. Liu and Z. Lu, *Nature Photonics*, 2011, **5**, 753-757.
35. M. Baldo, S. Lamansky, P. Burrows, M. Thompson and S. Forrest, *Applied Physics Letters*, 1999, **75**, 4-6.
36. P. Langevin, *Annals of Chemistry and Physics*, 1903, **28**, 289-384.

37. C. Murawski, K. Leo and M. C. Gather, *Advanced Materials*, 2013, **25**, 6801-6827.
38. D. Beljonne, Z. Shuai, A. Ye and J. L. Brédas, *Journal of the Society for Information Display*, 2005, **13**, 419-427.
39. C. Adachi, *Japanese Journal of Applied Physics*, 2014, **53**, 060101.
40. H. Yersin, R. Czerwieniec and A. Hupfer, *Organic Photonics V,* 2012.
41. D. Volz, Y. Cheng, R. Liu, M. Wallesch, D. Zink, J. Göttlicher, R. Steininger, H. Flügge, C. Fléchon and J. Navarro, *Adv. Mater*, 2015, **27**, 2538-2543.
42. Y. Tao, C. Yang and J. Qin, *Chemical Society Reviews*, 2011, **40**, 2943-2970.
43. A. Endo, M. Ogasawara, A. Takahashi, D. Yokoyama, Y. Kato and C. Adachi, *Advanced Materials*, 2009, **21**, 4802-4806.
44. M. N. Berberan-Santos and J. M. Garcia, *Journal of the American Chemical Society*, 1996, **118**, 9391-9394.
45. G. Blasse and D. R. McMillin, *Chemical Physics Letters*, 1980, **70**, 1-3.
46. C. Adachi, S. Tokito, T. Tsutsui and S. Saito, *Japanese Journal of Applied Physics*, 1988, **27**, L269.
47. D. Guo-Zhang, L. Hong-Jian, P. Yan-Zhi, D. Xiao-Yu and X. Qiang, *Chinese Physics*, 2005, **14**, 2590.
48. L. Hung and C. Chen, *Materials Science and Engineering: R: Reports*, 2002, **39**, 143-222.
49. L. J. Rothberg and A. J. Lovinger, *Journal of Materials Research*, 1996, **11**, 3174-3187.
50. J. Eng and T. J. Penfold, *The Chemical Record*, 2020, **20**, 831-856.
51. B. Valeur and M. N. Berberan-Santos, *Molecular Fluorescence: Principles and Applications*, John Wiley & Sons, 2012.
52. B. R. Masters*, Adaptive Optics for Biological Imaging.,* 2013.
53. A. C.-A. Chen, J. U. Wallace, S. K.-H. Wei, L. Zeng, S. H. Chen and T. N. Blanton, *Chemistry of Materials*, 2006, **18**, 204-213.
54. D. Y. Kondakov, *Journal of The Society for Information Display*, 2009, **17**, 137-144.
55. Q. Peng, W. Li, S. Zhang, P. Chen, F. Li and Y. Ma, *Advanced Optical Materials*, 2013, **1**, 362-366.
56. L. Canham, *Faraday Discussions*, 2020, **222**, 10-81.
57. S. Hirata, Y. Sakai, K. Masui, H. Tanaka, S. Y. Lee, H. Nomura, N. Nakamura, M. Yasumatsu, H. Nakanotani and Q. Zhang, *Nature Materials*, 2015, **14**, 330-336.
58. Y. Im, M. Kim, Y. J. Cho, J.-A. Seo, K. S. Yook and J. Y. Lee, *Chemistry of Materials*, 2017, **29**, 1946-1963.

59. Q. Zhang, B. Li, S. Huang, H. Nomura, H. Tanaka and C. Adachi, *Nature Photonics*, 2014, **8**, 326-332.
60. Y. Wu, Y. Zhu, Z. Zhang, C. Zhao, J. He, C. Yan and H. Meng, *Molecules*, 2022, **27**, 348.
61. I. Lee and J. Y. Lee, *Organic Electronics*, 2016, **29**, 160-164.
62. Q. Zhang, D. Tsang, H. Kuwabara, Y. Hatae, B. Li, T. Takahashi, S. Y. Lee, T. Yasuda and C. Adachi, *Advanced Materials*, 2015, **27**, 2096-2100.
63. W. Song, I. Lee and J. Y. Lee, *Advanced Materials*, 2015, **27**, 4358-4363.
64. I. HoáLee and J. YeobáLee, *Journal of Materials Chemistry C*, 2015, **3**, 8834-8838.
65. M. Numata, T. Yasuda and C. Adachi, *Chemical Communications*, 2015, **51**, 9443-9446.
66. T. Serevičius, T. Nakagawa, M.-C. Kuo, S.-H. Cheng, K.-T. Wong, C.-H. Chang, R. C. Kwong, S. Xia and C. Adachi, *Physical Chemistry Chemical Physics*, 2013, **15**, 15850-15855.
67. C. Mayr, S. Y. Lee, T. D. Schmidt, T. Yasuda, C. Adachi and W. Brütting, *Advanced Functional Materials*, 2014, **24**, 5232-5239.
68. S. Youn Lee, T. Yasuda, H. Nomura and C. Adachi, *Applied Physics Letters*, 2012, **101**.
69. K. Sato, K. Shizu, K. Yoshimura, A. Kawada, H. Miyazaki and C. Adachi, *Physical Review Letters*, 2013, **110**, 247401.
70. A. Endo, K. Sato, K. Yoshimura, T. Kai, A. Kawada, H. Miyazaki and C. Adachi, *Applied Physics Letters*, 2011, **98**.
71. O. Y. Kim, B. S. Kim and J. Y. Lee, *Synthetic Metals*, 2015, **201**, 49-53.
72. J. W. Sun, J. H. Lee, C. K. Moon, K. H. Kim, H. Shin and J. J. Kim, *Advanced Materials*, 2014, **26**, 5684-5688.
73. B. S. Kim and J. Y. Lee, *Advanced Functional Materials*, 2014, **24**, 3970-3977.
74. D. R. Lee, B. S. Kim, C. W. Lee, Y. Im, K. S. Yook, S.-H. Hwang and J. Y. Lee, *ACS Applied Materials &Interfaces*, 2015, **7**, 9625-9629.
75. J. Li, T. Nakagawa, J. MacDonald, Q. Zhang, H. Nomura, H. Miyazaki and C. Adachi, *Solid-State and Organic Lighting,* 2013.
76. W.-L. Tsai, M.-H. Huang, W.-K. Lee, Y.-J. Hsu, K.-C. Pan, Y.-H. Huang, H.-C. Ting, M. Sarma, Y.-Y. Ho and H.-C. Hu, *Chemical Communications*, 2015, **51**, 13662-13665.
77. T. A. Lin, T. Chatterjee, W. L. Tsai, W. K. Lee, M. J. Wu, M. Jiao, K. C. Pan, C. L. Yi, C. L. Chung and K. T. Wong, *Advanced Materials*, 2016, **28**, 6976-6983.
78. Y. Wada, K. Shizu, S. Kubo, K. Suzuki, H. Tanaka, C. Adachi and H. Kaji, *Applied Physics Letters*, 2015, **107**.

79. K. Shizu, H. Tanaka, M. Uejima, T. Sato, K. Tanaka, H. Kaji and C. Adachi, *The Journal of Physical Chemistry C*, 2015, **119**, 1291-1297.
80. D. R. Lee, S.-H. Hwang, S. K. Jeon, C. W. Lee and J. Y. Lee, *Chemical Communications*, 2015, **51**, 8105-8107.
81. K. Shizu, M. Uejima, H. Nomura, T. Sato, K. Tanaka, H. Kaji and C. Adachi, *Physical Review Applied*, 2015, **3**, 014001.
82. J. H. Burroughes, D. D. Bradley, A. Brown, R. Marks, K. Mackay, R. H. Friend, P. L. Burns and A. B. Holmes, *Nature*, 1990, **347**, 539-541.
83. Y. J. Cho, K. S. Yook and J. Y. Lee, *Scientific Reports*, 2015, **5**, 7859.
84. Y. J. Cho, S. K. Jeon and J. Y. Lee, *Advanced Optical Materials*, 2016, **4**, 688-693.
85. S.-H. Hwang, *Advanced Materials*, 2015, **27**, 2515-2520.
86. M. Kim, S. K. Jeon, S.-H. Hwang, S.-S. Lee, E. Yu and J. Y. Lee, *The Journal of Physical Chemistry C*, 2016, **120**, 2485-2493.
87. H. M. Kim, J. M. Choi and J. Y. Lee, *RSC Advances*, 2016, **6**, 64133-64139.
88. B. Li, H. Nomura, H. Miyazaki, Q. Zhang, K. Yoshida, Y. Suzuma, A. Orita, J. Otera and C. Adachi, *Chemistry Letters*, 2014, **43**, 319-321.
89. H. Kaji, H. Suzuki, T. Fukushima, K. Shizu, K. Suzuki, S. Kubo, T. Komino, H. Oiwa, F. Suzuki and A. Wakamiya, *Nature Communications*, 2015, **6**, 8476.
90. Y. J. Cho, S. K. Jeon, B. D. Chin, E. Yu and J. Y. Lee, *Angewandte Chemie International Edition*, 2015, **54**, 5201-5204.
91. M. Kim, S. K. Jeon, S.-H. Hwang, S.-s. Lee, E. Yu and J. Y. Lee, *Chemical Communications*, 2016, **52**, 339-342.
92. S. Sudheendran Swayamprabha, D. K. Dubey, Shahnawaz, R. A. K. Yadav, M. R. Nagar, A. Sharma, F. C. Tung and J. H. Jou, *Advanced Science*, 2021, **8**, 2002254.
93. J.-H. Lee, C.-H. Chen, P.-H. Lee, H.-Y. Lin, M.-k. Leung, T.-L. Chiu and C.-F. Lin, *Journal of Materials Chemistry C*, 2019, **7**, 5874-5888.
94. D. Wang, C. Cheng, T. Tsuboi and Q. Zhang, *CCS Chemistry*, 2020, **2**, 1278-1296.
95. J. Lee, *Journal of Information Display*, 2023, **24**, 57-70.
96. A. Monkman, *ACS Applied Materials & Interfaces*, 2021, **14**, 20463-20467.
97. W. Song, W. Lee, K. K. Kim and J. Y. Lee, *Organic Electronics*, 2016, **37**, 252-256.
98. Y. J. Cho, K. S. Yook and J. Y. Lee, *Advanced Materials*, 2014, **26**, 4050-4055.
99. H. Nakanotani, K. Masui, J. Nishide, T. Shibata and C. Adachi, *Scientific Reports*, 2013, **3**, 2127.
100. D. P.-K. Tsang, T. Matsushima and C. Adachi, *Scientific Reports*, 2016, **6**, 22463.

101. Y. Zou, S. Gong, G. Xie and C. Yang, *Advanced Optical Materials*, 2018, **6**, 1800568.
102. Y. Suzuki, Q. Zhang and C. Adachi, *Journal of Materials Chemistry C*, 2015, **3**, 1700-1706.
103. M. Fischer and F. Vögtle, *Angewandte Chemie International Edition*, 1999, **38**, 884-905.
104. D. Astruc, E. Boisselier and C. Ornelas, *Chemical Reviews*, 2010, **110**, 1857-1959.
105. S. M. Grayson and J. M. Frechet, *Chemical Reviews*, 2001, **101**, 3819-3868.
106. G. R. Newkome and C. Shreiner, *Chemical Reviews*, 2010, **110**, 6338-6442.
107. B. Wex and B. R. Kaafarani, *Journal of Materials Chemistry C*, 2017, **5**, 8622-8653.
108. J. Li and D. Liu, *Journal of Materials Chemistry*, 2009, **19**, 7584-7591.
109. L. Wang, Y. Jiang, J. Luo, Y. Zhou, J. Zhou, J. Wang, J. Pei and Y. Cao, *Advanced Materials*, 2009, **21**, 4854-4858.
110. C. Liu, Q. Fu, Y. Zou, C. Yang, D. Ma and J. Qin, *Chemistry of Materials*, 2014, **26**, 3074-3083.
111. Y. Wang, Y. Lu, B. Gao, S. Wang, J. Ding, L. Wang, X. Jing and F. Wang, *Chemical Communications*, 2016, **52**, 11508-11511.
112. K. Brunner, A. Van Dijken, H. Börner, J. J. Bastiaansen, N. M. Kiggen and B. M. Langeveld, *Journal of the American Chemical Society*, 2004, **126**, 6035-6042.
113. W.-C. Chen, C.-S. Lee and Q.-X. Tong, *Journal of Materials Chemistry C*, 2015, **3**, 10957-10963.
114. L. Chen, S. Wang, Z. Yan, J. Ding and L. Wang, *Journal of Materials Chemistry C*, 2017, **5**, 5749-5756.
115. S. C. Lo, R. N. Bera, R. E. Harding, P. L. Burn and I. D. Samuel, *Advanced Functional Materials*, 2008, **18**, 3080-3090.
116. D. Xia, B. Wang, B. Chen, S. Wang, B. Zhang, J. Ding, L. Wang, X. Jing and F. Wang, *Angewandte Chemie International Edition*, 2014, **126**, 1066-1070.
117. Y. Wang, S. Wang, J. Ding, L. Wang, X. Jing and F. Wang, *Chemical Communications*, 2017, **53**, 180-183.
118. W. Shi, M. Sun, X. Hu, B. Ren, J. Cheng, C. Li, X. Duan, X. Fu, J. Zhang and H. Chen, *Advanced Materials*, 2017, **29**, 1701089.
119. N. Van der Vaart, H. Lifka, F. Budzelaar, J. Rubingh, J. Hoppenbrouwers, J. Dijksman, R. Verbeek, R. Van Woudenberg, F. Vossen and M. Hiddink, *Journal of the Society for Information Display*, 2005, **13**, 9-16.
120. G. Gustaffason, *Nature*, 1922, **357**, 477.

121. A. E. Nikolaenko, M. Cass, F. Bourcet, D. Mohamad and M. Roberts, *Advanced Materials*, 2015, **27**, 7236-7240.
122. Y. Zhang, C. Zuniga, S.-J. Kim, D. Cai, S. Barlow, S. Salman, V. Coropceanu, J.-L. Brédas, B. Kippelen and S. Marder, *Chemistry of Materials*, 2011, **23**, 4002-4015.
123. X. Yin, Y. He, X. Wang, Z. Wu, E. Pang, J. Xu and J.-a. Wang, *Frontiers in Chemistry*, 2020, **8**, 725.
124. J. Luo, G. Xie, S. Gong, T. Chen and C. Yang, *Chemical Communications*, 2016, **52**, 2292-2295.
125. X. Lin, Y. Zhu, B. Zhang, X. Zhao, B. Yao, Y. Cheng, Z. Li, Y. Qu and Z. Xie, *ACS applied materials & interfaces*, 2018, **10**, 47-52.
126. X. Zhou, M. Huang, X. Zeng, T. Chen, G. Xie, X. Yin and C. Yang, *Polymer Chemistry*, 2019, **10**, 4201-4208.
127. G. Méhes, K. Goushi, W. J. Potscavage Jr and C. Adachi, *Organic Electronics*, 2014, **15**, 2027-2037.
128. W. Song and J. Y. Lee, *Advanced Optical Materials*, 2017, **5**, 1600901.
129. D. Zhang, M. Cai, Z. Bin, Y. Zhang, D. Zhang and L. Duan, *Chemical Science*, 2016, **7**, 3355-3363.
130. D. H. Lee, H. W. Son, T. N. Le, E. Y. Park, J. H. Kim and M. C. Suh, *Journal of Industrial and Engineering Chemistry*, 2023, **117**, 140-148.
131. S. A. Bagnich, A. Rudnick, P. Schroegel, P. Strohriegl and A. Köhler, *Philosophical Transactions of the Royal Society A: Mathematical, Physical and Engineering Sciences*, 2015, **373**, 20140446.
132. P. Strohriegl, D. Wagner, P. Schrögel, S. T. Hoffmann, A. Köhler, U. Heinemeyer and I. Münster, *Organic Light Emitting Materials and Devices XVII,* 2013.
133. T. Oshiyama, N. Yasukawa, H. Kita, T. Matsui, M. Sumita and K. Morihashi, *Bulletin of the Chemical Society of Japan*, 2017, **90**, 195-204.
134. E. Varathan, D. Vijay, P. S. V. Kumar and V. Subramanian, *Journal of Materials Chemistry C*, 2013, **1**, 4261-4274.
135. K. L. Woon, Z. A. Hasan, B. K. Ong, A. Ariffin, R. Griniene, S. Grigalevicius and S.-A. Chen, *RSC Advances*, 2015, **5**, 59960-59969.
136. C. Han, Y. Zhao, H. Xu, J. Chen, Z. Deng, D. Ma, Q. Li and P. Yan, *Chemistry–A European Journal*, 2011, **17**, 5800-5803.
137. S. G. Ihn, N. Lee, S. O. Jeon, M. Sim, H. Kang, Y. Jung, D. H. Huh, Y. M. Son, S. Y. Lee and M. Numata, *Advanced Science*, 2017, **4**, 1600502.

138. M. Y. Wong and E. Zysman-Colman, *Advanced Materials*, 2017, **29**, 1605444.
139. D. Chen, S.-J. Su and Y. Cao, *Journal of Materials Chemistry C*, 2014, **2**, 9565-9578.
140. Y. Wu, X. Hao, J. Wu, J. Jin and X. Ba, *Macromolecules*, 2010, **43**, 731-738.
141. K. Shizu, J. Lee, H. Tanaka, H. Nomura, T. Yasuda, H. Kaji and C. Adachi, *Pure and Applied Chemistry*, 2015, **87**, 627-638.
142. S. Beaupré and M. Leclerc, *Journal of Materials Chemistry A*, 2013, **1**, 11097-11105.
143. T. Nishimoto, T. Yasuda, S. Y. Lee, R. Kondo and C. Adachi, *Materials Horizons*, 2014, **1**, 264-269.
144. N. Blouin and M. Leclerc, *Accounts Chemical Research*, 2008, **41**, 1110-1119.
145. N. D. McClenaghan, R. Passalacqua, F. Loiseau, S. Campagna, B. Verheyde, A. Hameurlaine and W. Dehaen, *Journal of the American Chemical Society*, 2003, **125**, 5356-5365.
146. P. Moonsin, N. Prachumrak, R. Rattanawan, T. Keawin, S. Jungsuttiwong, T. Sudyoadsuk and V. Promarak, *Chemical Communications*, 2012, **48**, 3382-3384.
147. K. Albrecht, Y. Kasai, A. Kimoto and K. Yamamoto, *Macromolecules*, 2008, **41**, 3793-3800.
148. W. Jiang, L. Duan, J. Qiao, G. Dong, D. Zhang, L. Wang and Y. Qiu, *Journal of Materials Chemistry*, 2011, **21**, 4918-4926.
149. B. Zhang, G. Tan, C. S. Lam, B. Yao, C. L. Ho, L. Liu, Z. Xie, W. Y. Wong, J. Ding and L. Wang, *Advanced Materials*, 2012, **24**, 1873-1877.
150. J. Li, T. Zhang, Y. Liang and R. Yang, *Advanced Functional Materials*, 2013, **23**, 619-628.
151. P. Moonsin, N. Prachumrak, S. Namuangruk, S. Jungsuttiwong, T. Keawin, T. Sudyoadsuk and V. Promarak, *Chemical Communications*, 2013, **49**, 6388-6390.
152. A. Kimoto, J. S. Cho, K. Ito, D. Aoki, T. Miyake and K. Yamamoto, *Macromolecular Rapid Communications*, 2005, **26**, 597-601.
153. J. Zhang, D. Ding, Y. Wei and H. Xu, *Chemical Science*, 2016, **7**, 2870-2882.
154. C. Han, F. Zhao, Z. Zhang, L. Zhu, H. Xu, J. Li, D. Ma and P. Yan, *Chemistry of Materials*, 2013, **25**, 4966-4976.
155. N. Lin, J. Qiao, L. Duan, L. Wang and Y. Qiu, *The Journal of Physical Chemistry C*, 2014, **118**, 7569-7578.
156. M. Kim and J. Y. Lee, *Advanced Functional Materials*, 2014, **24**, 4164-4169.

157. S. Gong, Y.-L. Chang, K. Wu, R. White, Z.-H. Lu, D. Song and C. Yang, *Chemistry of Materials*, 2014, **26**, 1463-1470.
158. K. Masui, H. Nakanotani and C. Adachi, *Organic Electronics*, 2013, **14**, 2721-2726.
159. P. J. Flory, *Journal of the American Chemical Society*, 1952, **74**, 2718-2723.
160. Y. H. Kim and O. W. Webster, *Macromolecules*, 1992, **25**, 5561-5572.
161. Y. Zheng, S. Li, Z. Weng and C. Gao, *Chemical Society Reviews*, 2015, **44**, 4091-4130.
162. B. I. Voit, *Comptes Rendus Chimie*, 2003, **6**, 821-832.
163. C. Schlenk, A. W. Kleij, H. Frey and G. van Koten, *Angewandte Chemie International Edition*, 2000, **39**, 3445-3447.
164. B. Voit, *Journal of Polymer Science Part A: Polymer Chemistry*, 2000, **38**, 2505-2525.
165. T. Guo, R. Guan, J. Zou, J. Liu, L. Ying, W. Yang, H. Wu and Y. Cao, *Polymer Chemistry*, 2011, **2**, 2193-2203.
166. J. Kim, J. Park, S.-H. Jin and T. S. Lee, *Polymer Chemistry*, 2015, **6**, 5062-5069.
167. D.-F. Tang, G.-A. Wen, X.-Y. Qi, H.-Y. Wang, B. Peng, W. Wei and W. Huang, *Polymer*, 2007, **48**, 4412-4418.
168. A. K. Palai, S. P. Mishra, A. Kumar, R. Srivastava, M. N. Kamalasanan and M. Patri, *Journal of Polymer Science Part A: Polymer Chemistry*, 2011, **49**, 832-841.
169. W. Lai, D. Liu and W. Huang, *Science China Chemistry*, 2010, **53**, 2472-2480.
170. H. Wang, Y. Sun, Z. Qi, F. Kong, Y. Ha, S. Yin and S. Lin, *Macromolecules*, 2008, **41**, 3537-3542.
171. S. I. Bhat, Y. Ahmadi and S. Ahmad, *Industrial & Engineering Chemistry Research*, 2018, **57**, 10754-10785.
172. T. Emrick, H.-T. Chang and J. M. Frechet, *Macromolecules*, 1999, **32**, 6380-6382.
173. M. Liu, N. Vladimirov and J. J. Frechet, *Macromolecules*, 1999, **32**, 6881-6884.
174. M. Trollsås, B. Atthoff, H. Claesson and J. L. Hedrick, *Macromolecules*, 1998, **31**, 3439-3445.
175. F. Wurm, J. Nieberle and H. Frey, *Macromolecules*, 2008, **41**, 1184-1188.
176. H. Chen and J. Kong, *Polymer Chemistry*, 2016, **7**, 3643-3663.
177. Q. Wei, J. Wang, X. Shen, X. A. Zhang, J. Z. Sun, A. Qin and B. Z. Tang, *Scientific Reports*, 2013, **3**, 1093.
178. M. Jikei, S.-H. Chon, M.-a. Kakimoto, S. Kawauchi, T. Imase and J. Watanebe, *Macromolecules*, 1999, **32**, 2061-2064.
179. Y. Miura, H. Oka and M. Morita, *Macromolecules*, 1998, **31**, 2041-2046.

180. A. F. Littke, C. Dai and G. C. Fu, *Journal of the American Chemical Society*, 2000, **122**, 4020-4028.
181. N. Miyaura and A. Suzuki, *Chemical Reviews*, 1995, **95**, 2457-2483.
182. A. Suzuki, *Pure and Applied Chemistry*, 1985, **57**, 1749-1758.
183. J. K. Bin, N. S. Cho and J. I. Hong, *Advanced Materials*, 2012, **24**, 2911-2915.
184. H. Zheng, Y. Zheng, N. Liu, N. Ai, Q. Wang, S. Wu, J. Zhou, D. Hu, S. Yu and S. Han, *Nature Communications*, 2013, **4**, 1971.
185. H. Wu, L. Ying, W. Yang and Y. Cao, *Chemical Society Reviews*, 2009, **38**, 3391-3400.
186. S. Gong, C. Yang and J. Qin, *Chemical Society Reviews*, 2012, **41**, 4797-4807.
187. Y. Xin, G.-A. Wen, W.-J. Zeng, L. Zhao, X.-R. Zhu, Q.-L. Fan, J.-C. Feng and L.-H. Wang, *Macromolecules*, 2005, **38**, 6755-6758.
188. W.-L. Yu, B. Liu, J. Pei, G. Zeng and W. Huang, *Chinese Journal of Polymer Science*, 2001, **19**, 603-614.
189. G.-x. Jiang, C.-l. Bian, J.-q. Ding and L.-x. Wang, *Chinese Journal of Polymer Science*, 2013, **31**, 787-797.
190. X. Wang, L. Zhao, S. Shao, J. Ding, L. Wang, X. Jing and F. Wang, *Macromolecules*, 2014, **47**, 2907-2914.
191. Z. Zhou, N. Luo, X. Shao, H. L. Zhang and Z. Liu, *ChemPlusChem*, 2023, **88**, e202300261.
192. Y. Xie, Y. Gong, M. Han, F. Zhang, Q. Peng, G. Xie and Z. Li, *Macromolecules*, 2019, **52**, 896-903.
193. M. Ludwiczak, M. Majchrzak, M. Bayda, B. Marciniak, M. Kubicki and B. Marciniec, *Journal of Organometallic Chemistry*, 2014, **750**, 150-161.
194. M. L. Louillat, A. Biafora, F. Legros and F. W. Patureau, *Angewandte Chemie International Edition*, 2014, **53**, 3505-3509.
195. M. Zhang, C. Yang, A. K. Mishra, W. Pisula, G. Zhou, B. Schmaltz, M. Baumgarten and K. Müllen, *Chemical Communications*, 2007, 1704-1706.
196. R. Matsubara, T. Shimada, Y. Kobori, T. Yabuta, T. Osakai and M. Hayashi, *Chemistry–An Asian Journal*, 2016, **11**, 2006-2010.
197. J.-B. Harle, S. Mine, T. Kamegawa, V. T. Nguyen, T. Maeda, H. Nakazumi and H. Fujiwara, *The Journal of Physical Chemistry C*, 2017, **121**, 15049-15062.
198. T. M. Milzarek and T. A. Gulder, *Organic Letters*, 2020, **23**, 102-106.
199. P. J. Flory, *Principles of Polymer Chemistry*, Cornell University Press, 1953.

200. H. Chen, K. Lin, H. Liang, J. Tan, D. Zhou, X. Zhang, F. Liu and Y. Wang, *Synthetic Metals*, 2022, **291**, 117200.
201. T. Sudyoadsuk, P. Moonsin, N. Prachumrak, S. Namuangruk, S. Jungsuttiwong, T. Keawin and V. Promarak, *Polymer Chemistry*, 2014, **5**, 3982-3993.
202. J. Xu, F. Yan, X. Sun and Z. Wang, *Journal of Photochemistry and Photobiology A: Chemistry*, 2019, **382**, 111938.
203. A. A. Adeniyi, T. L. Ngake and J. Conradie, *Electroanalysis*, 2020, **32**, 2659-2668.
204. Z. T. Liu, Y. M. He, B. L. Li, J. Liu and Q. H. Fan, *Macromolecular rapid communications*, 2007, **28**, 2249-2255.
205. Z. T. Liu, Y. M. He, Z. J. Wang, Y. Feng and Q. H. Fan, *Journal of Polymer Science Part A: Polymer Chemistry*, 2008, **46**, 886-896.
206. M. Wang, X. Wei, W. Zhang, H. Zhao, Y. Wu, Y. Miao, H. Wang and B. Xu, *Journal of Solid State Chemistry*, 2021, **298**, 122122.
207. A. B. Cook, R. Barbey, J. A. Burns and S. Perrier, *Macromolecules*, 2016, **49**, 1296-1304.
208. K. Wooley, C. Hawker, R. Lee and J. Fréchet, *Polymer Journal*, 1994, **26**, 187-197.
209. L. Hobson and W. JamesáFeast, *Chemical Communications*, 1997, 2067-2068.
210. J. Hao, M. Jikei and M.-A. Kakimoto, *Macromolecules*, 2002, **35**, 5372-5381.
211. H. Wang, Q. Wang, Z. Huang and W. Shi, *Polymer Degradation and Stability*, 2007, **92**, 1788-1794.
212. S. Barua, P. Chattopadhyay and N. Karak, *Journal of Materials Chemistry B*, 2015, **3**, 5877-5885.
213. S. Pramanik, R. Konwarh, K. Sagar, B. K. Konwar and N. Karak, *Progress in Organic Coatings*, 2013, **76**, 689-697.
214. D. Zhou, L. Pierucci, Y. Gao, J. O'Keeffe Ahern, X. Huang, A. Sigen and W. Wang, *ACS Applied Materials & Interfaces*, 2017, **9**, 5793-5802.
215. B. Das, M. Mandal, A. Upadhyay, P. Chattopadhyay and N. Karak, *Biomedical Materials*, 2013, **8**, 035003.
216. C. Lu, H. Wang, X. Wang, Y. Li, T. Oiu, L. He and X. Li, *Journal of Applied Polymer Science*, 2010, **117**, 517-523.
217. L. Guo, C. Li, H. Shang, R. Zhang, X. Li, Q. Lu, X. Cheng, Z. Liu, J. Z. Sun and X. Yu, *Chemical Science*, 2020, **11**, 661-670.
218. M. B. Hillyer, H. Gan and B. C. Gibb, *ChemPhysChem*, 2018, **19**, 2285-2289.

219. Z. Teng, H. Lv, Y. Zhang, Y. Zhang, J. Guan and W. Chengyin, *Journal of Chromatographic Science*, 2016, **54**, 1743-1751.
220. R. Rabie, M. M. Hammouda and K. M. Elattar, *Research on Chemical Intermediates*, 2017, **43**, 1979-2015.
221. A. Steinmetz, *Catalysts Cesium from Acros Organics*, 2011, 3-11.
222. H. Matsukizono and T. Endo, *Journal of the American Chemical Society*, 2018, **140**, 884-887.
223. Y. Lu, T. Nemoto, M. Tosaka and S. Yamago, *Nature Communications*, 2017, **8**, 1863.
224. S. Habibu, N. M. Sarih, N. A. Sairi and M. Zulkifli, *Royal Society Open Science*, 2019, **6**, 190869.
225. T.-T. Zhang, J.-F. Jia and H.-S. Wu, *The Journal of Physical Chemistry A*, 2010, **114**, 12251-12257.
226. K. Dogan, A. Gulkaya, M. Forough and O. z. l. Persil Çetinkol, *ACS Omega*, 2020, **5**, 22874-22882.
227. E. Polikarpov and A. B. Padmaperuma, *Material Matters*, 2012, **7**, 2-6.
228. Y. Tao, K. Yuan, T. Chen, P. Xu, H. Li, R. Chen, C. Zheng, L. Zhang and W. Huang, *Advanced Materials*, 2014, **26**, 7931-7958.
229. Y. Chi and P.-T. Chou, *Chemical Society Reviews*, 2010, **39**, 638-655.
230. M. Zhu and C. Yang, *Chemical Society Reviews*, 2013, **42**, 4963-4976.
231. T. Itoh, *Chemical Reviews*, 2012, **112**, 4541-4568.
232. F. B. Dias, K. N. Bourdakos, V. Jankus, K. C. Moss, K. T. Kamtekar, V. Bhalla, J. Santos, M. R. Bryce and A. P. Monkman, *Advanced Materials*, 2013, **25**, 3707-3714.
233. R. Ishimatsu, S. Matsunami, T. Kasahara, J. Mizuno, T. Edura, C. Adachi, K. Nakano and T. Imato, *Angewandte Chemie International Edition,* 2014, **126**, 7113-7116.
234. Q. Zhang, H. Kuwabara, W. J. Potscavage Jr, S. Huang, Y. Hatae, T. Shibata and C. Adachi, *Journal of the American Chemical Society*, 2014, **136**, 18070-18081.
235. K. Albrecht, K. Matsuoka, K. Fujita and K. Yamamoto, *Angewandte Chemie International Edition*, 2015, **54**, 5677-5682.
236. Y. J. Cho, K. S. Yook and J. Y. Lee, *Advanced Materials*, 2014, **26**, 6642-6646.
237. S. Shao, J. Ding, L. Wang, X. Jing and F. Wang, *Journal of the American Chemical Society*, 2012, **134**, 15189-15192.
238. M. Segal, M. Baldo, R. Holmes, S. Forrest and Z. Soos, *Physical Review B*, 2003, **68**, 075211.
239. Y. Cao, I. D. Parker, G. Yu, C. Zhang and A. J. Heeger, *Nature*, 1999, **397**, 414-417.

240. J. S. Wilson, A. Dhoot, A. Seeley, M. S. Khan, A. Köhler and R. H. Friend, *Nature*, 2001, **413**, 828-831.
241. M. Reufer, M. J. Walter, P. G. Lagoudakis, A. B. Hummel, J. S. Kolb, H. G. Roskos, U. Scherf and J. M. Lupton, *Nature Materials*, 2005, **4**, 340-346.
242. S. Jegadesan, S. Sindhu, R. C. Advincula and S. Valiyaveettil, *Langmuir*, 2006, **22**, 780-786.
243. Y. Tao, Q. Wang, C. Yang, Q. Wang, Z. Zhang, T. Zou, J. Qin and D. Ma, *Angewandte Chemie International Edition*, 2008, **47**, 8104-8107.
244. V. Promarak, M. Ichikawa, D. Meunmart, T. Sudyoadsuk, S. Saengsuwan and T. Keawin, *Tetrahedron Letters*, 2006, **47**, 8949-8952.
245. S. Bettington, M. Tavasli, M. R. Bryce, A. Beeby, H. Al-Attar and A. P. Monkman, *Chemistry–A European Journal*, 2007, **13**, 1423-1431.
246. V. Barlier, V. Bounor-Legaré, G. Boiteux, J. Davenas, A. Slazak, A. Rybak and J. Jung, *Synthetic Metals*, 2009, **159**, 508-512.
247. J. Shinar and V. Savvateev, in *Organic Light-Emitting Devices: A Survey*, Springer, 2004, pp. 1-41.
248. R. J. Martín-Palma and A. Lakhtakia, in *Engineered Biomimicry*, Elsevier Inc., 2013, pp. 383-398.
249. B. Kumar, B. K. Kaushik and Y. S. Negi, *Polymer Reviews*, 2014, **54**, 33-111.
250. D. Shi, Y. Wang, Y. Liu, Z. Zhang, J. Luo, J. He, Q. Chen, G. Lei and W. Zhu, *Chemistry–An Asian Journal*, 2012, **7**, 2096-2101.
251. J. Nithyanandhan and N. Jayaraman, *Tetrahedron*, 2006, **62**, 6228-6235.
252. T. Ishiyama, M. Murata and N. Miyaura, *Journal of Organic Chemistry*, 1995, **60**, 7508-7510.
253. E. K. Reeves, O. R. Bauman, G. B. Mitchem and S. R. Neufeldt, *Israel Journal of Chemistry*, 2020, **60**, 406-409.
254. H. Vanderhaeghe, *Journal of Organic Chemistry*, 1960, **25**, 747-753.
255. P. MÜLLER, N. P. Buu-Hoi and R. Rips, *Journal of Organic Chemistry*, 1959, **24**, 37-39.
256. H. Zhong, E. Xu, D. Zeng, J. Du, J. Sun, S. Ren, B. Jiang and Q. Fang, *Organic Letters*, 2008, **10**, 709-712.
257. H. Tanaka, K. Shizu, H. Miyazaki and C. Adachi, *Chemical Communications*, 2012, **48**, 11392-11394.

258. Y. K. Moon, H. J. Jang, S. Hwang, S. Kang, S. Kim, J. Oh, S. Lee, D. Kim, J. Y. Lee and Y. You, *Advanced Materials*, 2021, **33**, 2003832.
259. H. Kamogawa, Y. Todo and M. Nanasawa, *Journal of Polymer Science: Polymer Chemistry Edition*, 1981, **19**, 2571-2579.
260. C.-H. Hsieh, W.-C. Chen, S.-H. Yang, Y.-C. Chao, H.-C. Lee, C.-L. Chiang and C.-Y. Lin, *AIMS Materials Science*, 2017, **4**, 878-893.
261. X. Luo, X. Ma, F. Lebreux, I. E. Markó and K. Lam, *Chemical Communications*, 2018, **54**, 9969-9972.
262. F. C. Krebs, R. B. Nyberg and M. Jørgensen, *Chemistry of Materials*, 2004, **16**, 1313-1318.
263. K. T. Nielsen, K. Bechgaard and F. C. Krebs, *Macromolecules*, 2005, **38**, 658-659.
264. Y.-Y. Liu, J.-H. Cao, Y. Li, Y.-K. Wang and D.-Y. Wu, *European Polymer Journal*, 2023, **200**, 112528.
265. Z. Yao, W. Zong, K. Wang, P. Yuan, Y. Liu, S. Xu and S. Cao, *Reactive and Functional Polymers*, 2021, **163**, 104898.
266. C. Zhao, Y. Li, Y. Liu, H. Xie and W. Yu, *Advanced Composites and Hybrid Materials*, 2023, **6**, 27.
267. W. Zong, W. Qiu, P. Yuan, F. Wang, Y. Liu, S. Xu, S.-J. Su and S. Cao, *Polymer*, 2022, **240**, 124468.
268. J. C. Costa, R. J. Taveira, C. F. Lima, A. Mendes and L. M. Santos, *Optical Materials*, 2016, **58**, 51-60.
269. G. Xie, J. Luo, M. Huang, T. Chen, K. Wu, S. Gong and C. Yang, *Adv. Mater*, 2017, **29**, 1604223.
270. R. L. Schwiderski and S. C. Rasmussen, *Synthetic Metals*, 2014, **193**, 58-63.
271. Y. Wang, K. Bai, S. Wang, J. Ding and L. Wang, *ACS Applied Materials & Interfaces*, 2018, **10**, 32365-32372.
272. Y. Ooyama and Y. Harima, *European Journal of Organic Chemistry*, 2009, **2009**, 2903-2934.
273. M. Thompson, *Mrs Bulletin*, *Cambridge University Press,* 2007, **32**, 694-701.
274. S. Reineke, F. Lindner, G. Schwartz, N. Seidler, K. Walzer, B. Lüssem and K. Leo, *Nature*, 2009, **459**, 234-238.
275. Y. Li, X. Gao, L. Wang and G. Tu, *RSC Advances*, 2017, **7**, 40533-40538.
276. S. Reineke, M. Thomschke, B. Lüssem and K. Leo, *Reviews of Modern Physics*, 2013, **85**, 1245.

277. Y. Li, Q. Wei, L. Cao, F. Fries, M. Cucchi, Z. Wu, R. Scholz, S. Lenk, B. Voit and Z. Ge, *Frontiers in Chemistry*, 2019, **7**, 688.
278. Q. Wei, N. Fei, A. Islam, T. Lei, L. Hong, R. Peng, X. Fan, L. Chen, P. Gao and Z. Ge, *Advanced Optical Materials*, 2018, **6**, 1800512.
279. X. Ban, A. Zhu, T. Zhang, Z. Tong, W. Jiang and Y. Sun, *ACS Applied Materials & Interfaces*, 2017, **9**, 21900-21908.
280. X. Ban, A. Zhu, T. Zhang, Z. Tong, W. Jiang and Y. Sun, *Chemical Communications*, 2017, **53**, 11834-11837.
281. Y. Wada, S. Kubo and H. Kaji, *Advanced Materials*, 2018, **30**, 1705641.
282. X. Cai, D. Chen, K. Gao, L. Gan, Q. Yin, Z. Qiao, Z. Chen, X. Jiang and S. J. Su, *Advanced Functional Materials*, 2018, **28**, 1704927.
283. K. Miyata, T. Nakagawa, R. Kawakami, Y. Kita, K. Sugimoto, T. Nakashima, T. Harada, T. Kawai and Y. Hasegawa, *Chemistry–A European Journal*, 2011, **17**, 521-528.
284. H. Xu, L.-H. Wang, X.-H. Zhu, K. Yin, G.-Y. Zhong, X.-Y. Hou and W. Huang, *The Journal of Physical Chemistry B*, 2006, **110**, 3023-3029.
285. C. Han, Z. Zhang, H. Xu, G. Xie, J. Li, Y. Zhao, Z. Deng, S. Liu and P. Yan, *Chemistry–A European Journal*, 2013, **19**, 141-154.
286. F. Wurm and H. Frey, in *Polymer Science: A Comprehensive Reference, 10 Volume Set*, Elsevier, 2012, pp. 177-198.
287. S. Shao, J. Ding, T. Ye, Z. Xie, L. Wang, X. Jing and F. Wang, *Advanced Materials*, 2011, **23**, 3570-3574.
288. S. Shao, J. Ding, L. Wang, X. Jing and F. Wang, *Journal of American Chemical Society*, 2012, **134**, 20290-20293.
289. C. Li, Y. Wang, D. Sun, H. Li, X. Sun, D. Ma, Z. Ren and S. Yan, *ACS Applied Materials & Interfaces*, 2018, **10**, 5731-5739.
290. V. Mlynárik, *Analytical Biochemistry*, 2017, **529**, 4-9.
291. L. G. Hanson, *Concepts in Magnetic Resonance Part A: An Educational Journal*, 2008, **32**, 329-340.
292. H. H. Willard, L. L. Merritt Jr, J. A. Dean and F. A. Settle Jr, 1988.
293. O. D. Sparkman, *Journal of the American Society for Mass Spectrometry*, 2000, **12**, 1144.
294. J. Barker, *Mass Spectrometry: Analytical Chemistry by Open Learning*, John Wiley & Sons, 1999.

295. J. T. Watson and O. D. Sparkman, *Introduction to Mass Spectrometry: Instrumentation, Applications, and Strategies for Data Interpretation*, John Wiley & Sons, 2007.
296. E. De Hoffmann and V. Stroobant, *Mass Spectrometry: Principles and Applications*, John Wiley & Sons, 2007.
297. F. G. Strathmann and A. N. Hoofnagle, *American Journal of Clinical Pathology*, 2011, **136**, 609-616.
298. E. Frąckowiak, A. Płatek-Mielczarek, J. Piwek and K. Fic, in *Advances in Inorganic Chemistry*, Elsevier, 2022, vol. 79, pp. 151-207.
299. R. Leonard and K. Quigley, 2005.
300. M. L. Passos, M. C. Sarraguça, M. L. M. Saraiva, T. P. Rao and V. Biju, 2019.
301. S. Ebnesajjad, in *Handbook of Adhesives and Surface Preparation*, Elsevier, 2011, pp. 31-48.
302. T. Kim, A. Ramadoss, B. Saravanakumar, G. K. Veerasubramani and S. J. Kim, *Applied Surface Science*, 2016, **370**, 452-458.
303. A. Kamath, S. Raghu and H. Devendrappa, *Optical Materials*, 2016, **51**, 213-222.
304. T. Aoki, *Characterization of Materials*, 2002, 1-12.

8.2 Supplementary Section

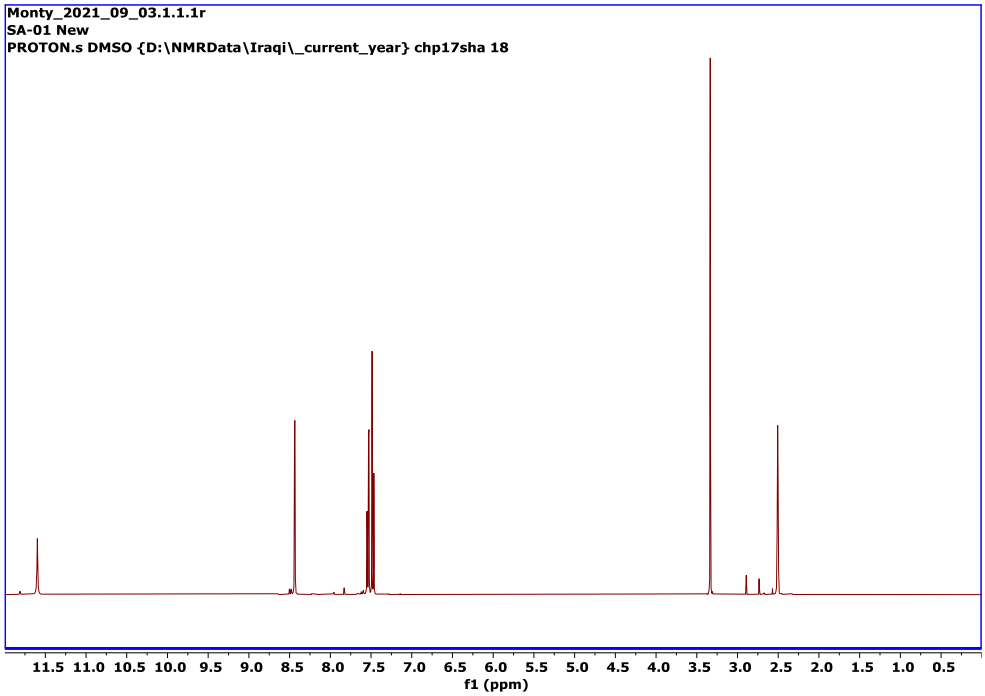

Figure 8.1 ^{1}H NMR spectrum of compound (1) in DMSO-d6; 11.60 (s, br, 1H), 8.44 (s, 2H), 7.58 – 7.45 (m, 4H).

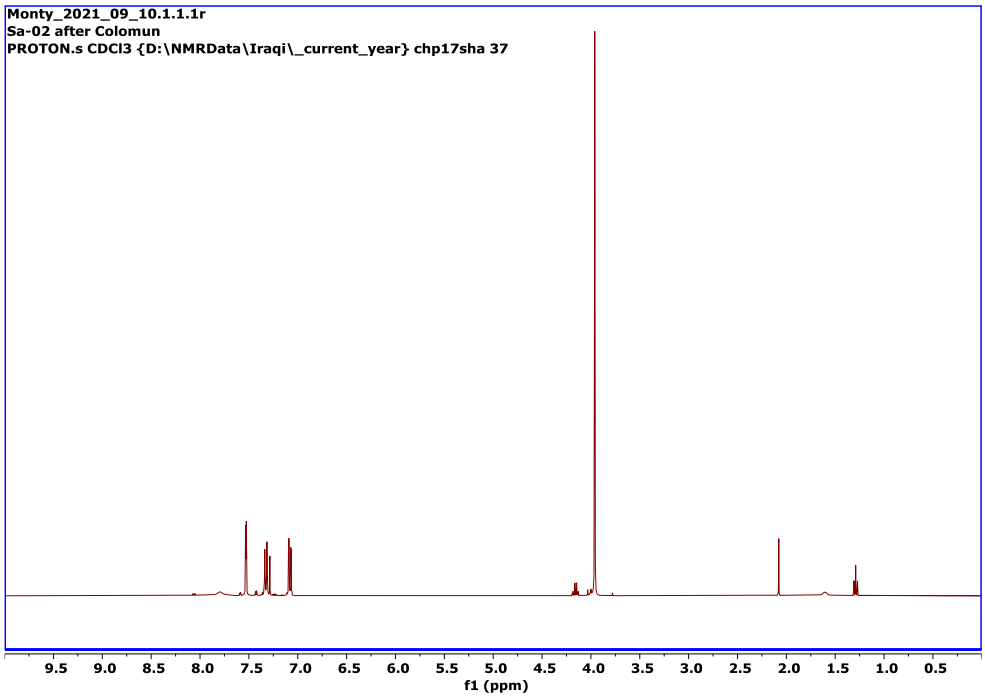

Figure 8.2 ^{1}H NMR spectrum of compound (2) in $CDCl_3$; 11.59 (s, br, 1H), 7.53 (s, 2H), 7.33 (d, *J* = 8.8 Hz, 2H), 7.08 (dd, *J* = 8.8, 2.5 Hz, 2H), 3.96 (s, 6H).

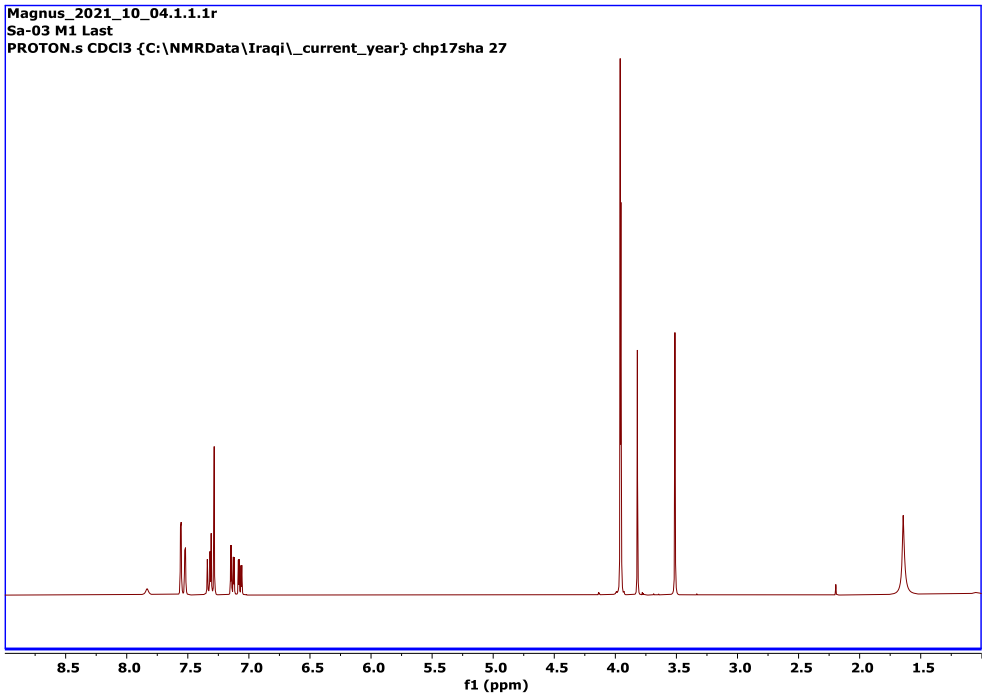

Figure 8.3 ^{1}H NMR spectrum of compound (3) in $CDCl_3$; 8.28 (d, *J* = 8.7 Hz, 2H), 7.67 (d, *J* = 8.7 Hz, 2H), 7.57 (s, 2H), 7.43 (d, *J* = 8.9 Hz, 2H), 7.07 (dd, *J* = 8.9, 2.5 Hz, 2H), 4.01 (s, 3H), 3.98 (s, 6H).

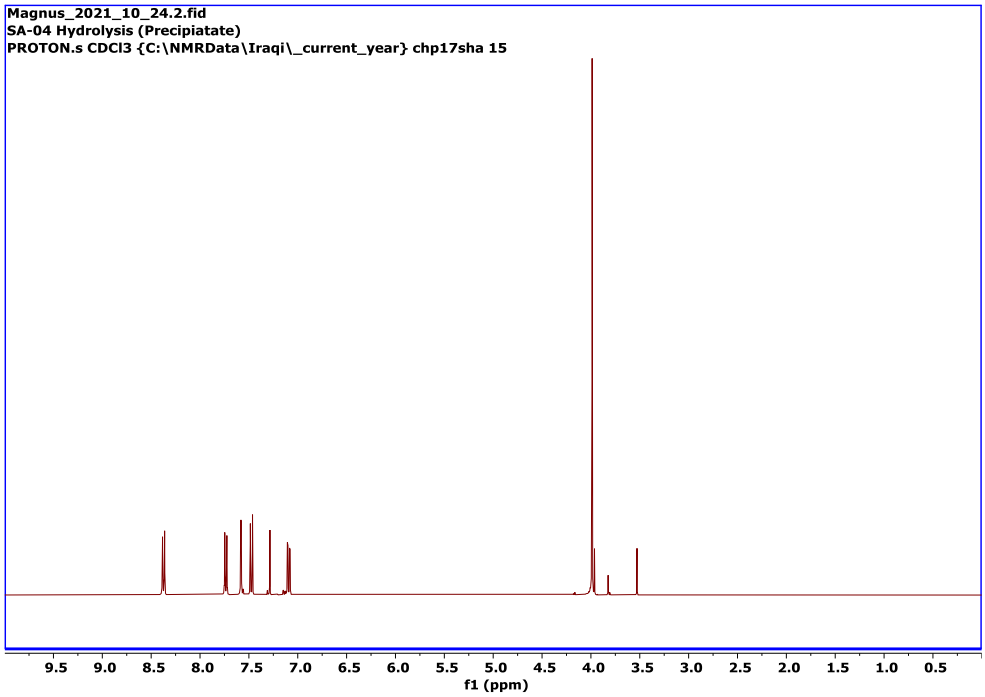

Figure 8.4 ^{1}H NMR spectrum of compound (4) in $CDCl_3$; 13.08 (s, br, 1H), 8.37 (d, *J* = 7.9 Hz, 2H), 7.73 (d, *J* = 8.9 Hz, 2H), 7.58 (s, 2H), 7.47 (d, *J* = 8.1 Hz, 2H), 7.09 (dd, *J* = 8.9, 2.5 Hz, 2H), 3.99 (s, 6H).

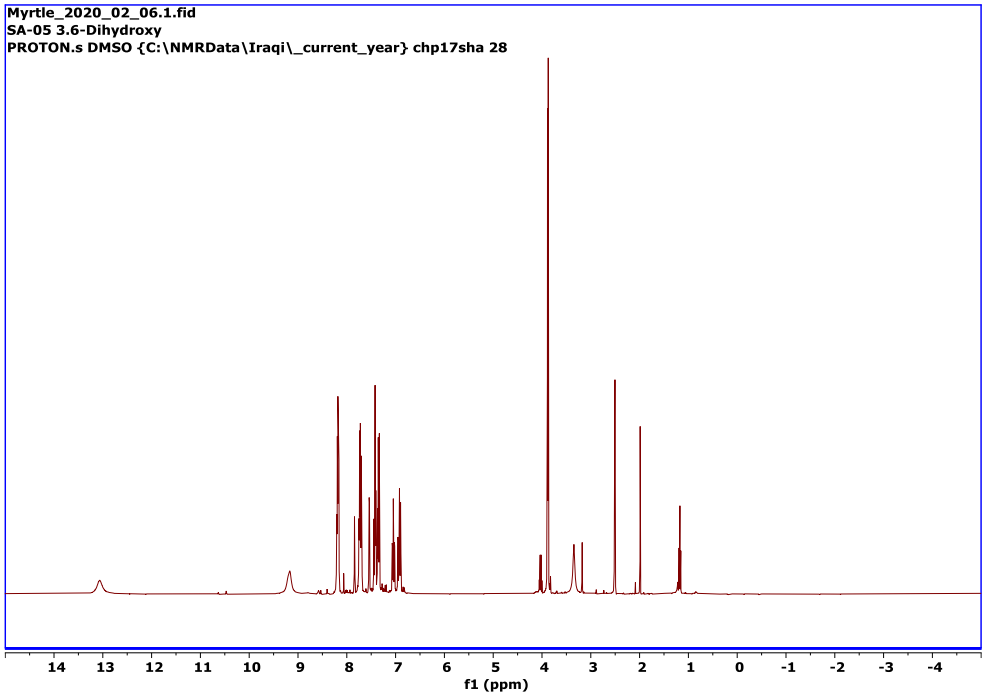

Figure 8.5 ^{1}H NMR spectrum of compound (5) in DMSO-d6; 13.00 (s, br, 1H), 8.32 (d, J = 8.0 Hz, 2H), 7.70 (d, J = 8.7 Hz, 2H), 7.55 (s, 2H), 7.44 (d, J = 8.1 Hz, 2H), 7.03 (dd, J = 8.8, 2.4 Hz, 2H), 4.6 (s, br, 2H).

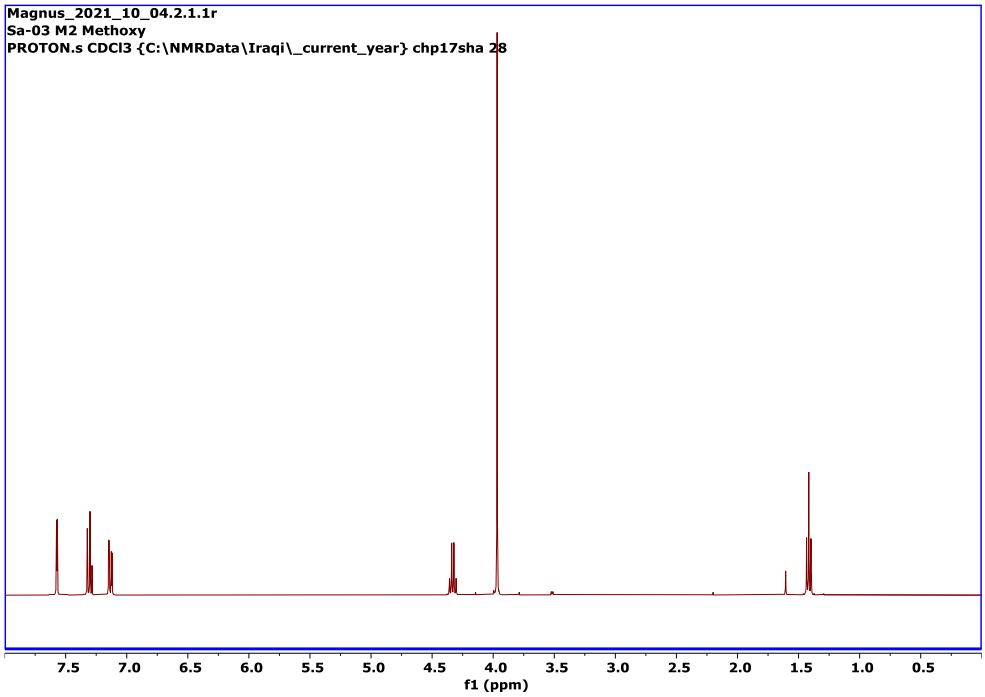

Figure 8.6 ^{1}H NMR spectrum of compound (8) in $CDCl_3$; 7.57 (s, 2H), 7.31 (d, J = 8.8 Hz, 2H), 7.13 (dd, J = 8.8, 2.5 Hz, 2H), 4.33 (q, J = 7.2 Hz, 2H), 3.96 (s, 6H), 1.42 (t, J = 7.2 Hz, 3H).

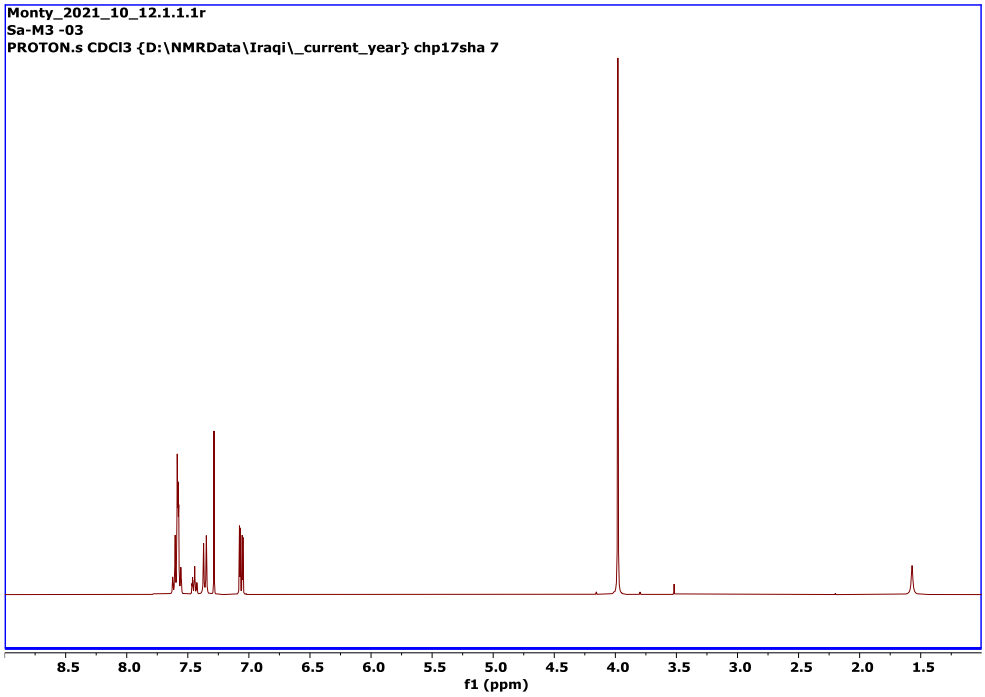

Figure 8.7 ^{1}H NMR spectrum of compound (10) in $CDCl_3$; 7.61 (dd, *J* = 8.2, 1.7 Hz, 2H), 7.55 (dd, *J* = 7.2, 1.4 Hz, 2H), 7.47 – 7.37 (m, 3H), 7.21 (d, *J* = 8.7 Hz, 2H), 6.89 (dd, *J* = 8.8, 2.4 Hz, 2H), 3.96 (s, 6H).

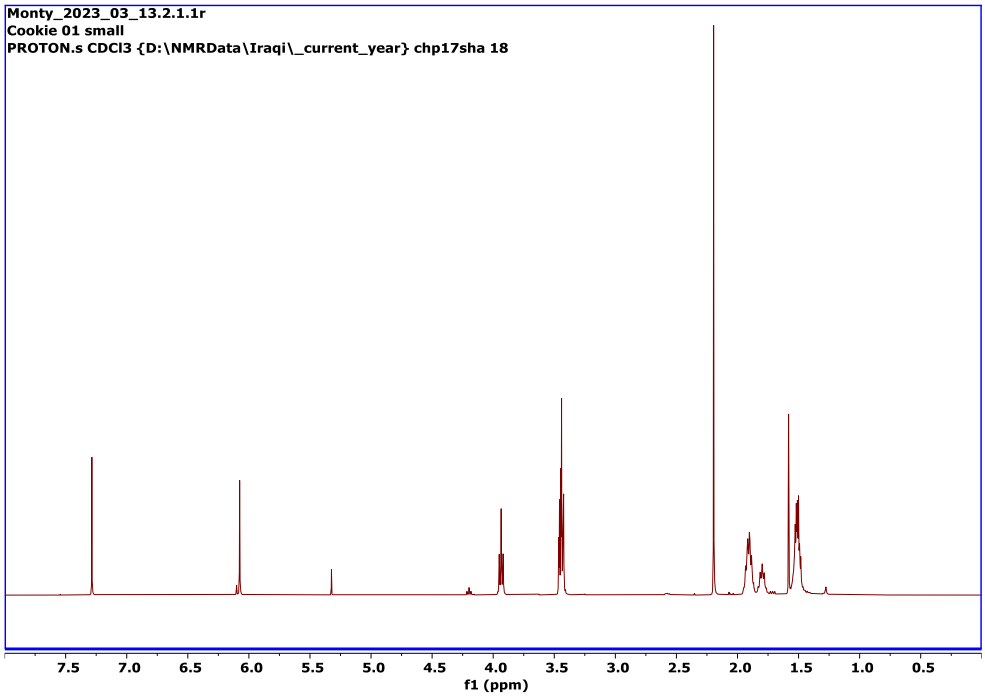

Figure 8.8 ^{1}H NMR spectrum of compound (13) in $CDCl_3$; 6.08 (s, 3H), 3.94 (t, *J* = 6.4 Hz, 6H), 3.45 (t, *J* = 6.8 Hz, 6H), 1.97 – 1.85 (m, 6H), 1.85 – 1.73 (m, 6H), 1.56 – 1.45 (m, 12H).

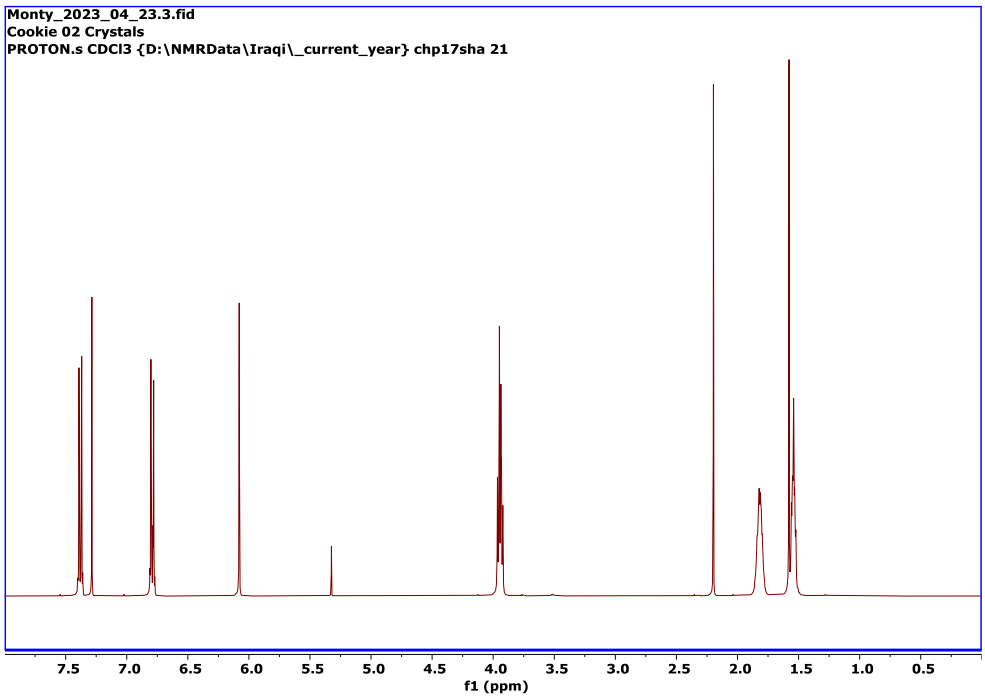

Figure 8.9 ^{1}H NMR spectrum of compound (14) in $CDCl_3$; 7.38 (d, *J* = 8.6 Hz, 6H), 6.79 (d, *J* = 9.3 Hz, 6H), 6.08 (s, 3H), 3.94 (m, 12H), 1.88 – 1.76 (m, 12H), 1.57 – 1.48 (m, 12H).

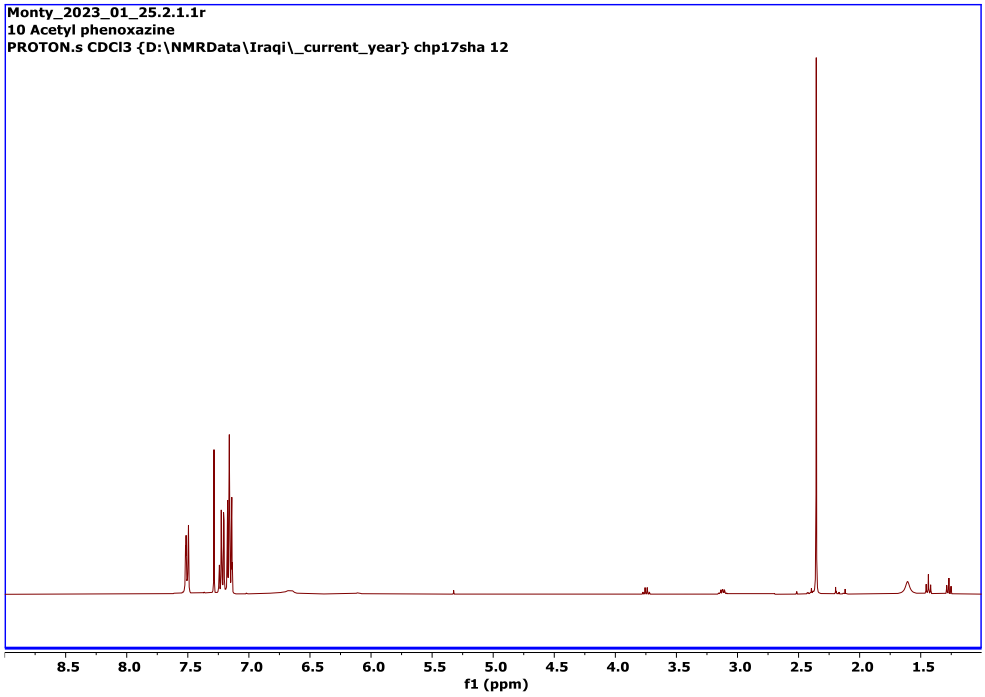

Figure 8.10 ^{1}H NMR spectrum of compound (16) in $CDCl_3$; 7.51 (dd, *J* = 8.2, 1.7 Hz, 2H), 7.25 – 7.19 (m, 2H), 7.16 (m, 4H), 2.36 (s, 3H).

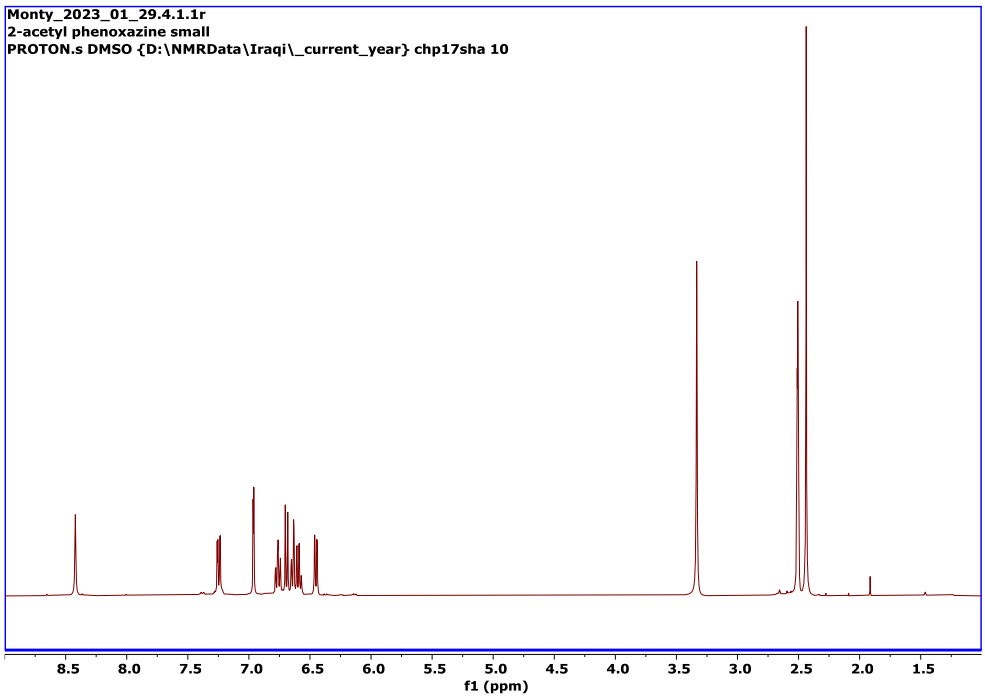

Figure 8.11 ^{1}H NMR spectrum of compound (17) in DMSO-d6; 8.42 (s, br, 1H), 7.25 (dd, J = 8.3, 2.1 Hz, 1H), 6.96 (d, J = 2.1 Hz, 1H), 6.76 (td, J = 7.5, 1.6 Hz, 1H), 6.69 (d, J = 8.2 Hz, 1H), 6.66 – 6.54 (m, 2H), 6.45 (dd, J = 7.7, 1.5 Hz, 1H), 2.44 (s, 3H).

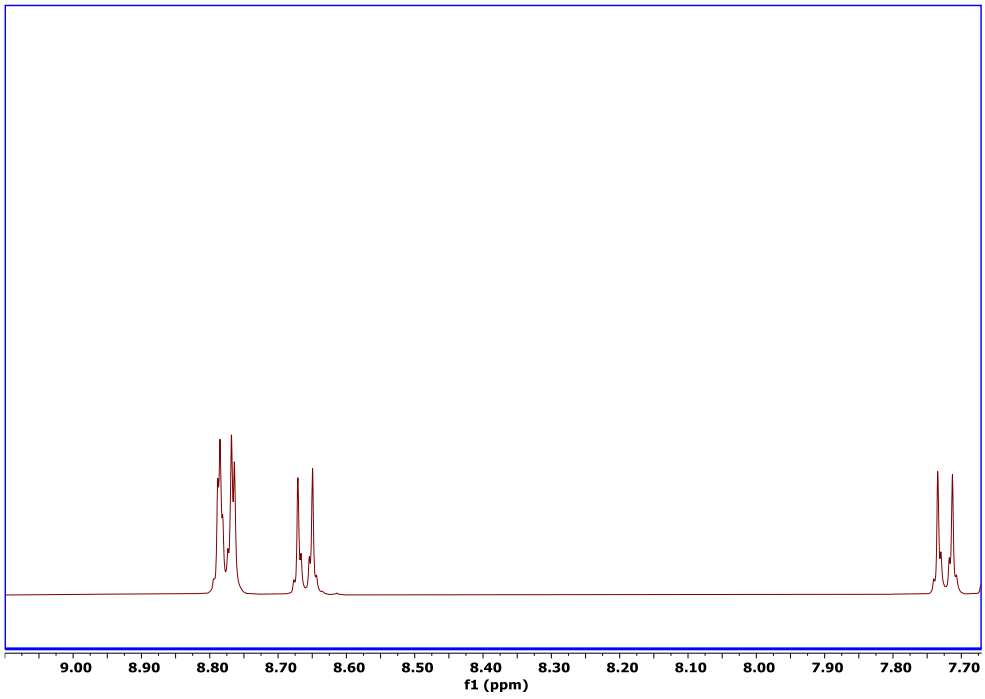

Figure 8.12 ^{1}H NMR spectrum of compound (18) in DMSO-d6; 8.69 (dd, J = 7.6, 1.6 Hz, 4H), 7.68 (t, J = 8.1 Hz, 2H), 7.60 (t, J = 8.1 Hz, 4H).

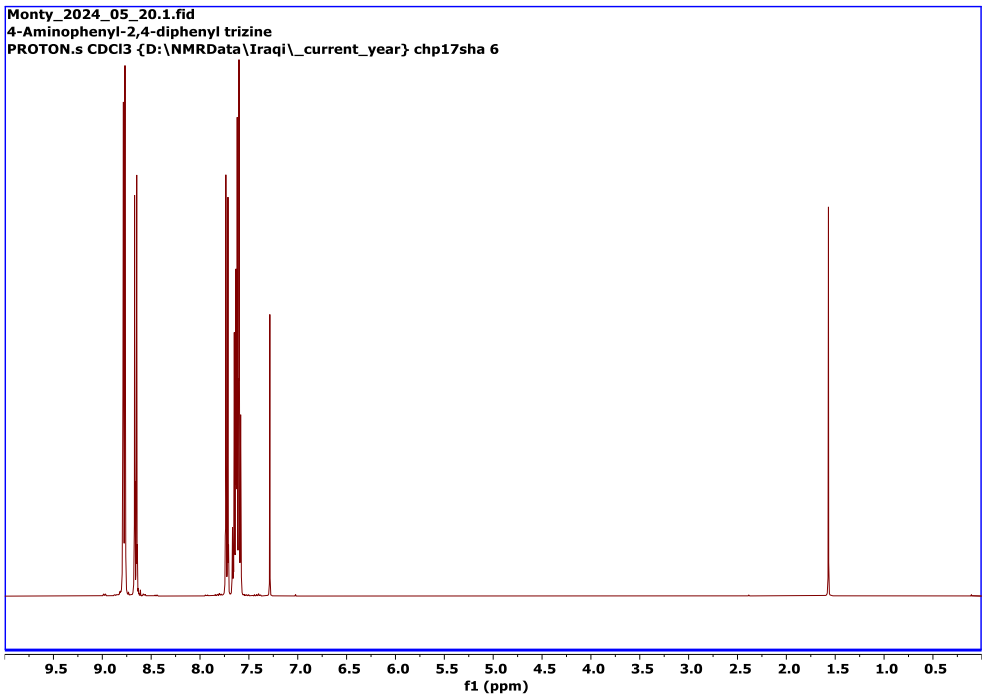

Figure 8.13 ^{1}H NMR spectrum of compound (19) in DMSO-d6; 8.72 (dd, *J* = 7.4, 2.4 Hz, 4H), 8.46 (d, *J* = 8.4 Hz, 2H), 7.70 – 7.60 (m, 6H), 6.74 (d, *J* = 8.4 Hz, 2H), 4.18 (s, br, 2H).

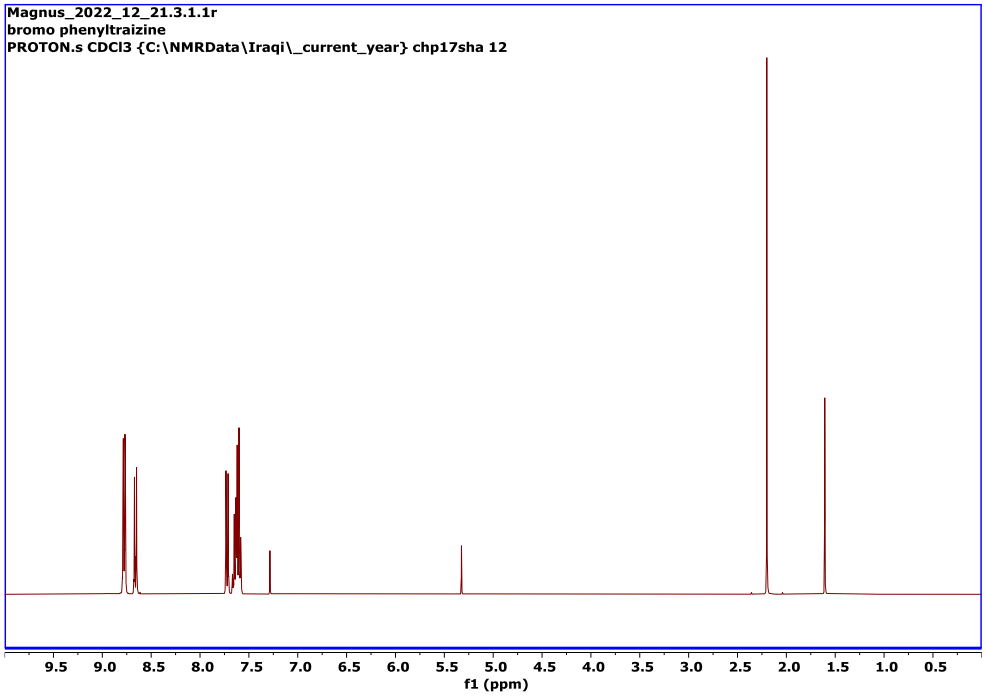

Figure 8.14 ^{1}H NMR spectrum of compound (20) in $CDCl_3$; 8.78 (dd, *J* = 6.5, 1.3 Hz, 4H), 8.66 (d, *J* = 8.6 Hz, 2H), 7.72 (d, *J* = 8.6 Hz, 2H), 7.68 – 7.56 (m, 6H).

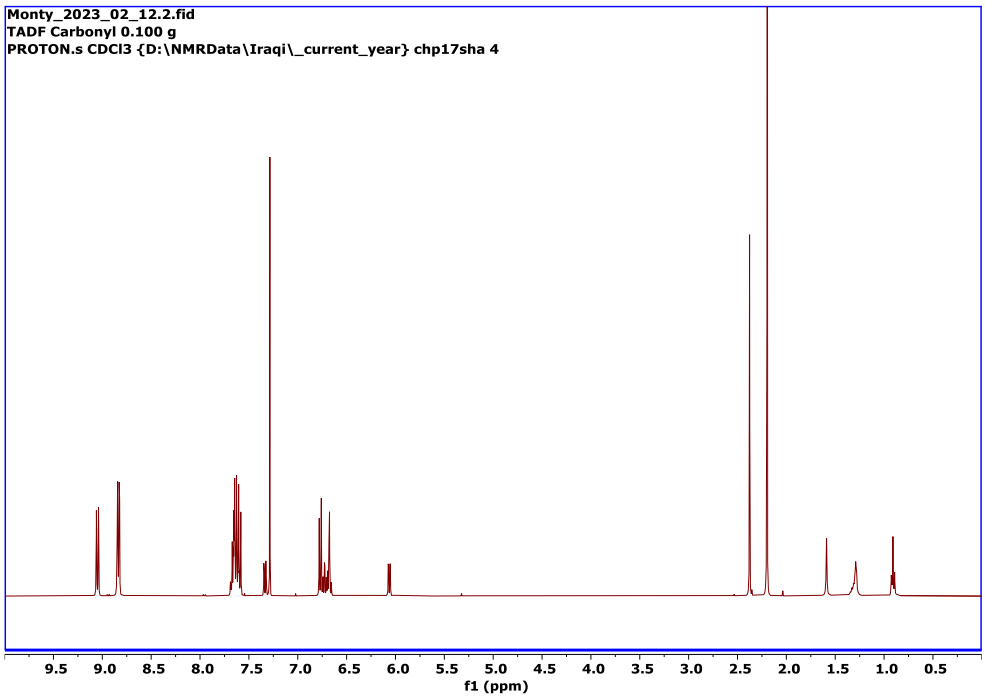

Figure 8.15 ^{1}H NMR spectrum of compound (21) in $CDCl_3$; 9.05 (d, *J* = 8.5 Hz, 2H), 8.84 (dd, *J* = 8.0, 1.4 Hz, 4H), 7.71 – 7.55 (m, 8H), 7.33 (dd, *J* = 8.3, 2.0 Hz, 1H), 6.80 – 6.63 (m, 5H), 6.06 (dd, *J* = 7.8, 1.6 Hz, 1H), 2.38 (s, 3H).

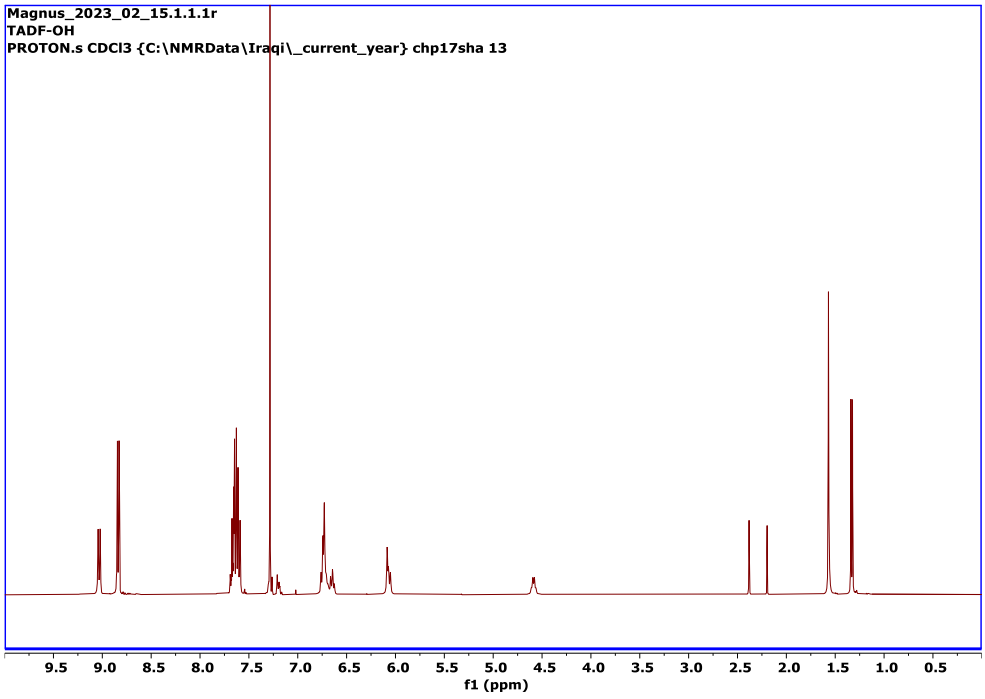

Figure 8.16 ^{1}H NMR spectrum of compound (22) in $CDCl_3$; 9.03 (d, *J* = 8.4 Hz, 2H), 8.84 (dd, *J* = 6.5, 1.3 Hz, 4H), 7.72 – 7.56 (m, 8H), 6.78 – 6.68 (m, 4H), 6.64 (td, *J* = 7.6, 1.8 Hz, 1H), 6.13 – 6.01 (m, 2H), 4.59 (q, *J* = 6.4 Hz, 1H), 4.19 (bs, 1H), 1.33 (d, *J* = 6.5 Hz, 3H).

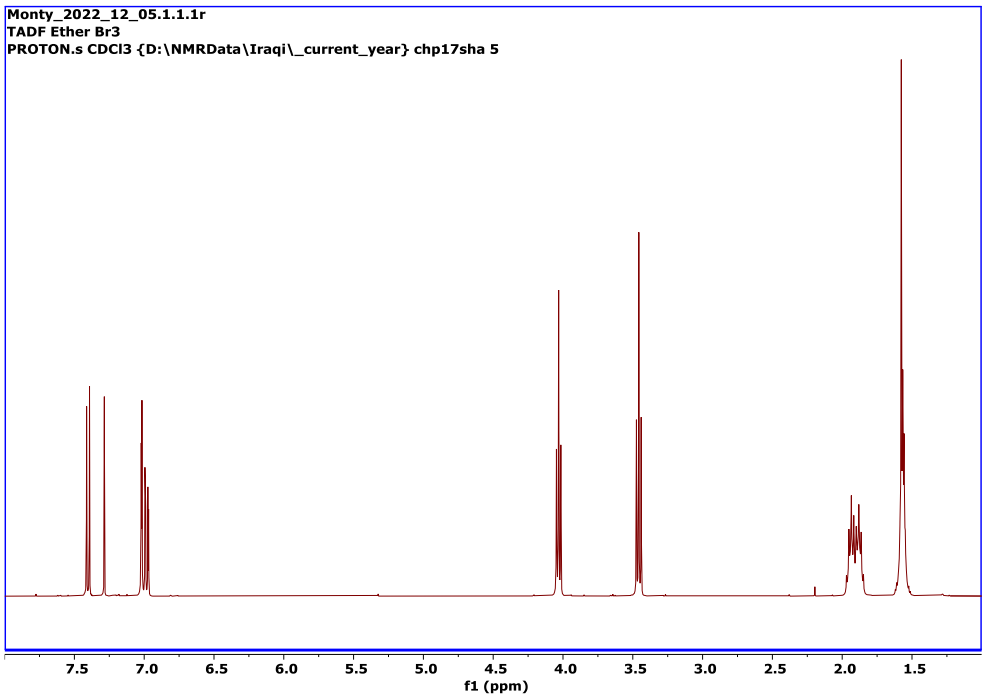

Figure 8.17 ^{1}H NMR spectrum of compound (23) in $CDCl_3$; 7.40 (d, *J* = 8.3 Hz, 1H), 7.02 (d, *J* = 2.1 Hz, 1H), 6.98 (dd, *J* = 8.3, 2.2 Hz, 1H), 4.03 (t, *J* = 6.3 Hz, 2H), 3.46 (t, *J* = 6.8 Hz, 2H), 2.00 – 1.83 (m, 4H), 1.64 – 1.50 (m, 4H).

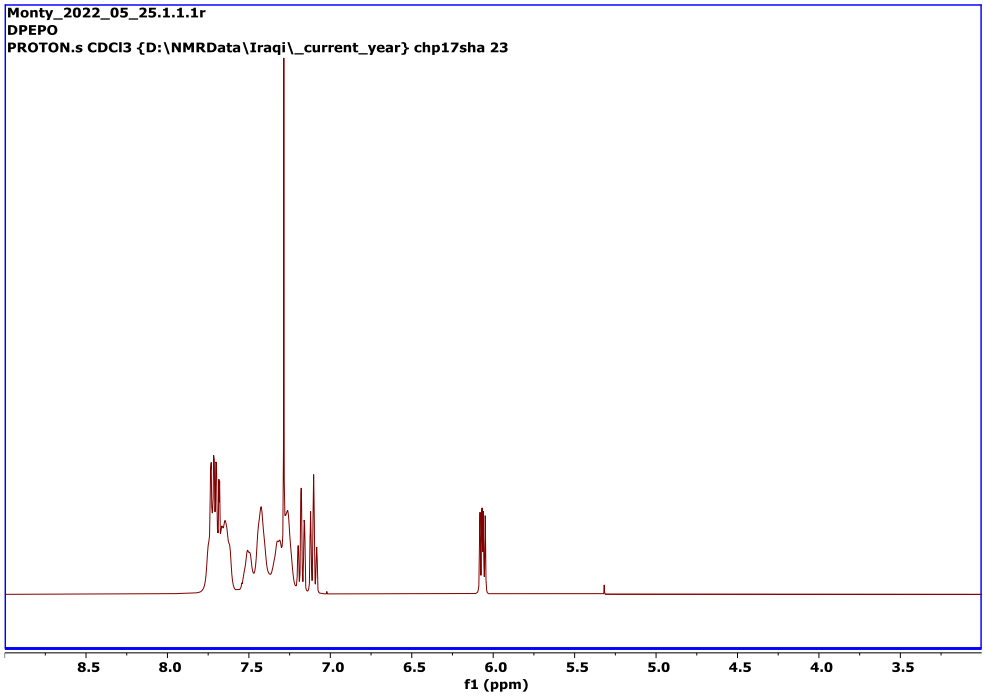

Figure 8.18 ^{1}H NMR spectrum of compound (25) in $CDCl_3$; 7.77 – 7.59 (m, 10H), 7.50 (d, *J* = 7.8 Hz, 2H), 7.43 (d, *J* = 8.0 Hz, 4H), 7.33 (s, 2H), 7.26 (s, 4H), 7.18 (tdd, *J* = 8.2, 1.9, 0.9 Hz, 2H), 7.10 (t, *J* = 7.5, 2H), 6.07 (q, *J* = 8.3 Hz, 2H).

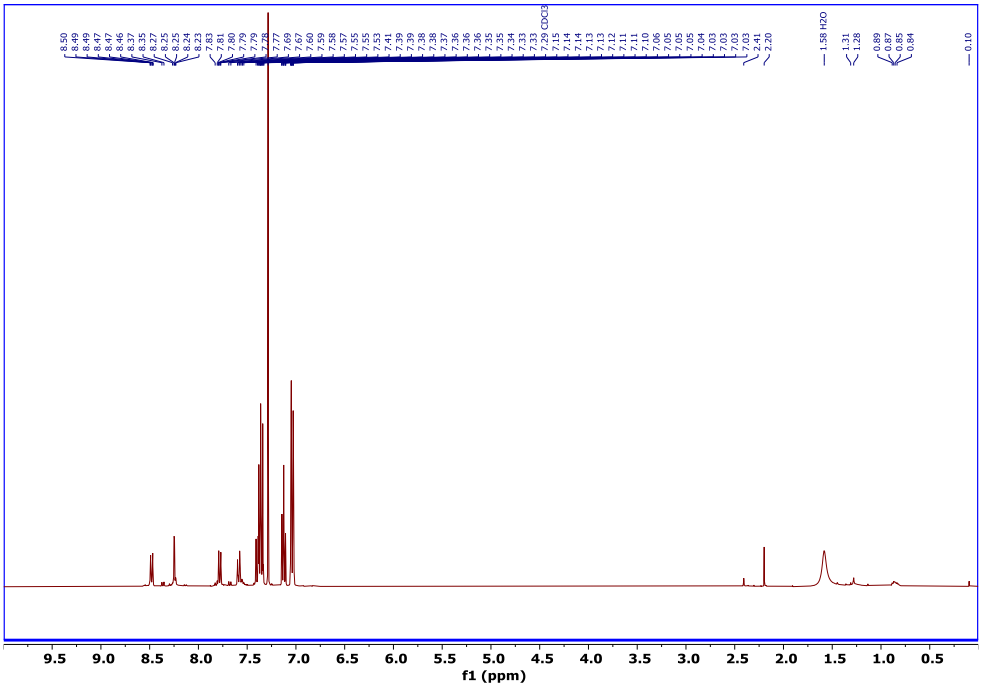

Figure 8.19 ^{1}H NMR spectrum of P1 in $CDCl_3$; 8.51 – 8.45 (m, 2H), 8.28 – 8.20 (m, 3H), 7.82 – 7.74 (m, 2H), 7.62 – 7.54 (m, 3H), 7.41 (s, 1H), 7.40 – 7.32 (m, 13H), 7.16 – 7.08 (m, 6H), 7.07 – 7.00 (m, 11H), 2.41 (s, 0.67H).

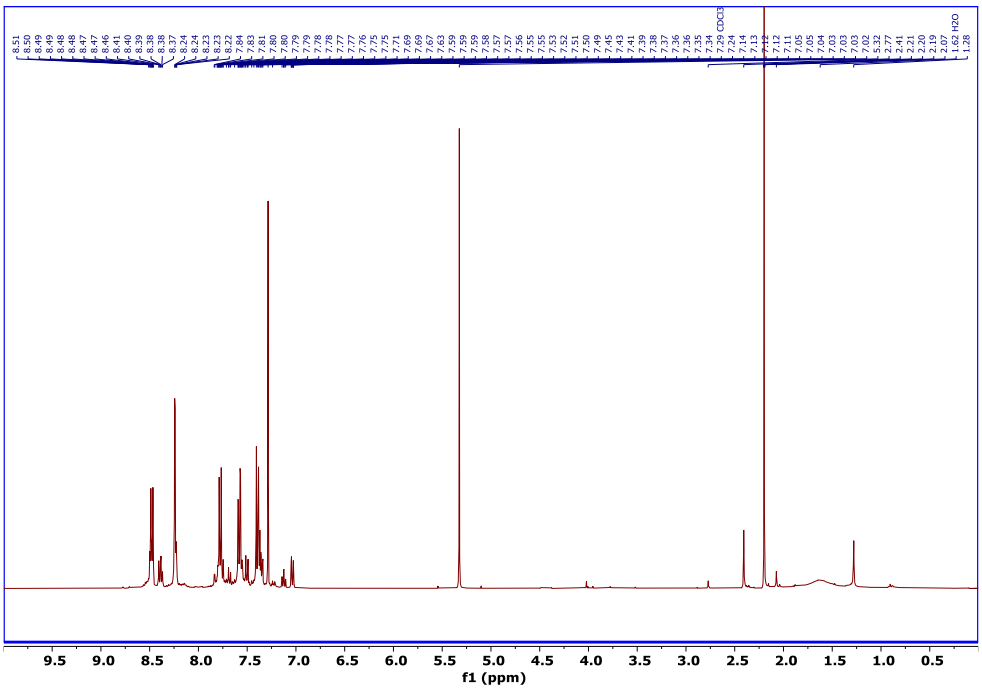

Figure 8.20 ^{1}H NMR spectrum of P2 in $CDCl_3$; 8.55 – 8.44 (m, 6H), 8.42 – 8.35 (m, 2H), 8.28 – 8.20 (m, 7H), 7.85 – 7.66 (m, 9H), 7.65 – 7.47 (m, 10H), 7.46 – 7.31 (m, 9H), 7.26 – 7.20 (m, 1H), 7.16 – 7.09 (m, 1H), 7.07 – 7.01 (m, 1H), 2.41 (s, 2H).

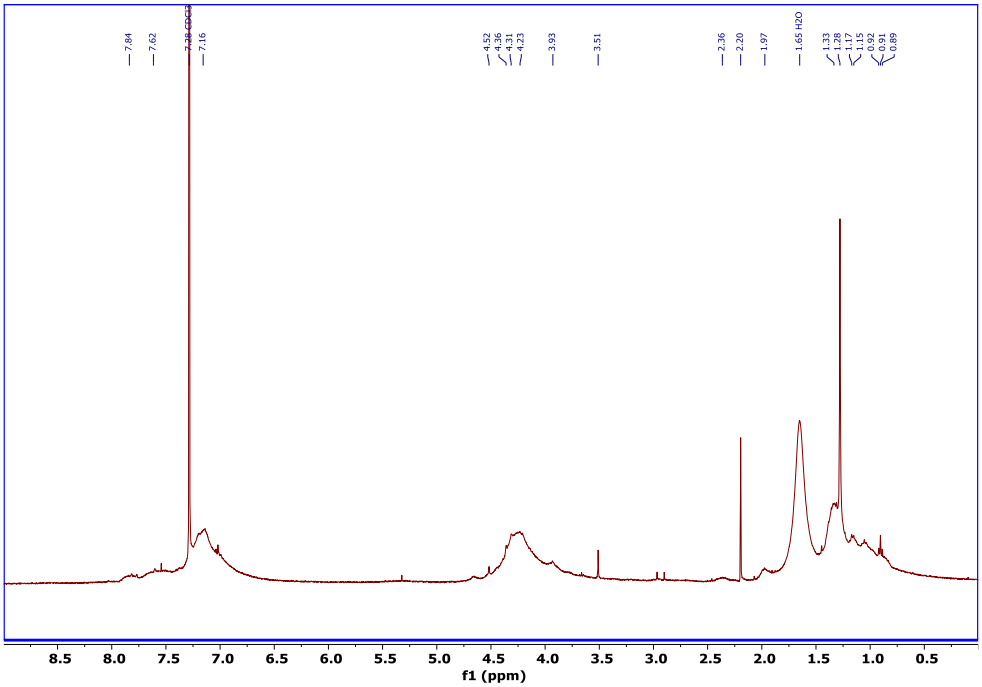

Figure 8.21 ^{1}H NMR spectrum of P3 in $CDCl_3$; 7.95 – 7.31 (m, 6H), 7.16 (s, 13H), 4.57 – 3.54 (m, 18H), 2.36 (s, 1H), 1.97 (s, 2H), 1.44 – 0.59 (m, 25H).

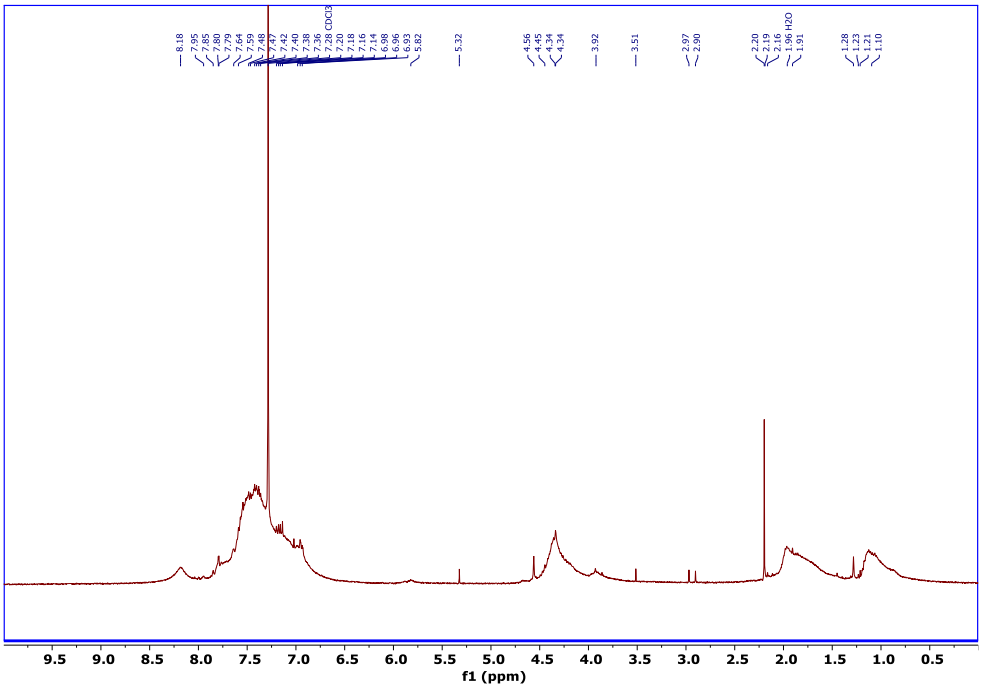

Figure 8.22 ^{1}H NMR spectrum of P4 in $CDCl_3$; 8.18 (s, 7H), 7.95 – 7.31 (m, 41H), 7.25 – 6.53 (m, 28H), 5.82 (s, 3H), 4.72 – 4.00 (m, 19H), 3.92 (s, 6H), 1.91 (s, 22H), 1.24 – 0.34 (m, 18H).

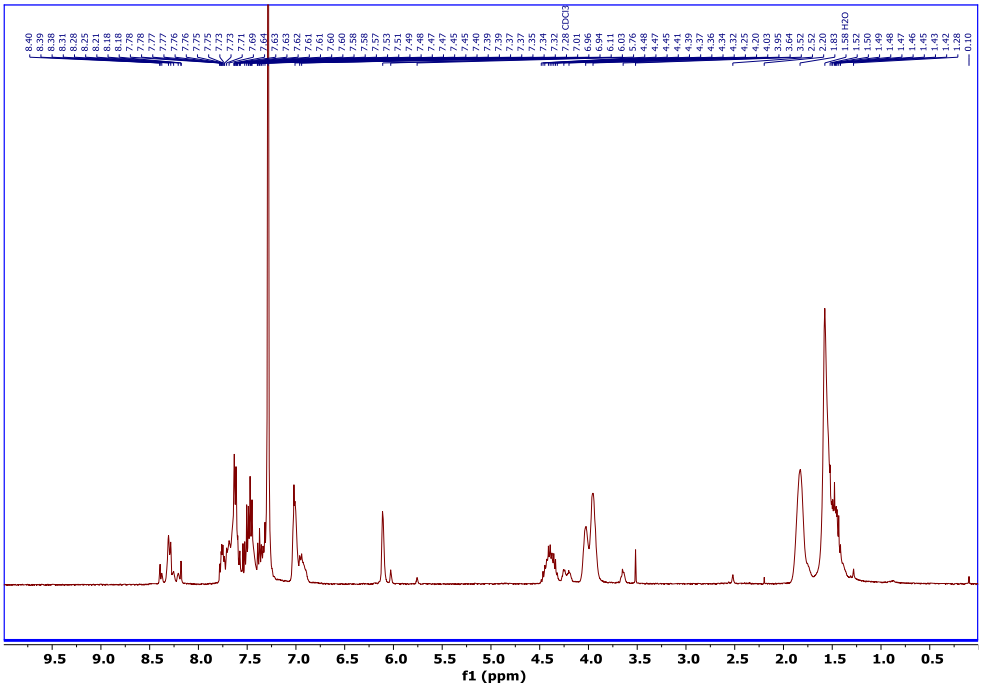

Figure 8.23 ^{1}H NMR spectrum of P5 in $CDCl_3$; 8.33 – 8.23 (m, 4H), 8.23 – 8.15 (m, 1H), 7.81 – 7.71 (m, 4H), 7.66 – 7.55 (m, 10H), 7.55 – 7.43 (m, 9H), 7.41 – 7.29 (m, 8H), 7.01 (s, 11H), 6.11 (s, 3H), 4.52 – 4.29 (m, 7H), 4.28 – 4.15 (m, 3H), 4.10 – 3.86 (m, 15H), 3.64 (s, 2H), 1.83 (s, 17H), 1.66 – 1.34 (m, 41H).

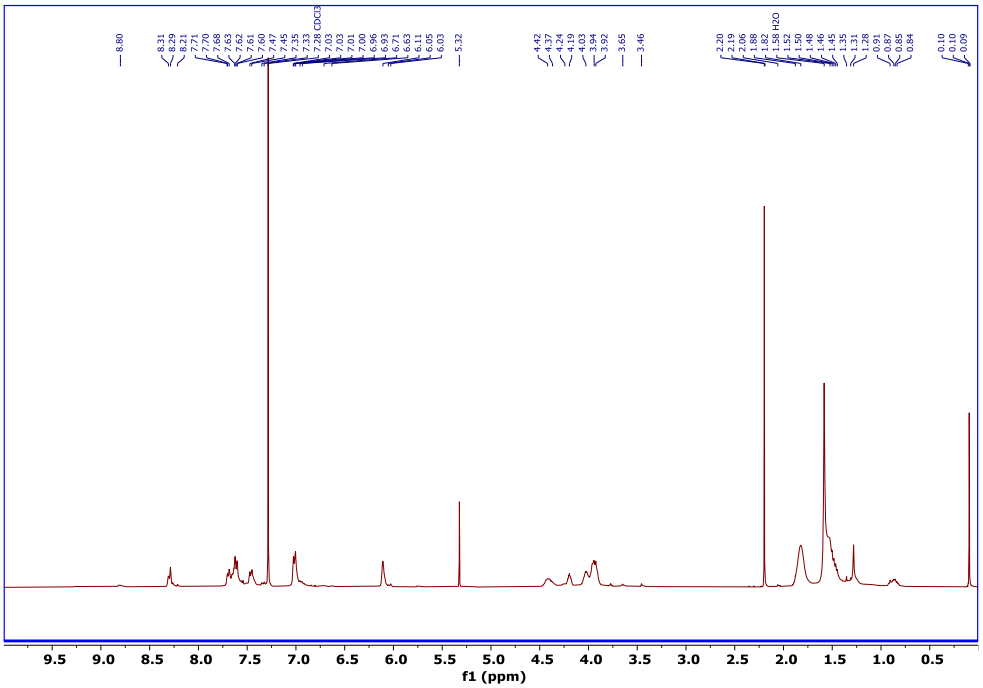

Figure 8.24 ^{1}H NMR spectrum of P6 in $CDCl_3$; 9.02 (bs, 0.09H), 8.81 (bs, 0.1H), 8.30 (m, 1H), 7.85 – 7.31 (m, 2H), 7.14 – 6.52 (m, 1H), 6.11 (bs, 1H), 4.58 – 3.56 (m, 3H), 1.82 (bs, 2H), 1.52 (bs, 4H), 1.28 (s, 1H), 0.97 – 0.64 (m, 0.31H).

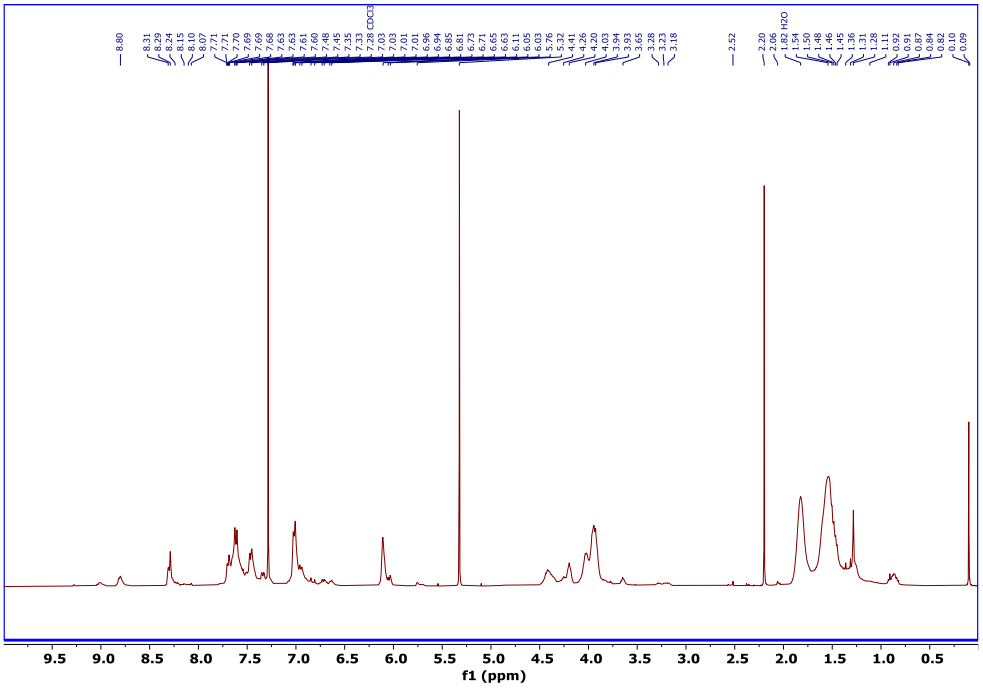

Figure 8.25 ^{1}H NMR spectrum of P7 in $CDCl_3$; 9.01 (bs, 0.20H), 8.82 (bs, 0.38H), 8.34 – 8.04 (m, 1.08H), 7.75 – 7.39 (m, 5H), 7.12 – 6.83 (m, 3H), 6.77 – 6.55 (m, 0.59H), 6.17 – 5.97 (m, 1.38H), 4.52 – 4.12 (m, 2H), 4.11 – 3.79 (m, 4H), 1.82 (s, 5H), 1.68 – 1.38 (m, 9.41H), 1.28 (s, 2H), 0.87 (s, 1H).

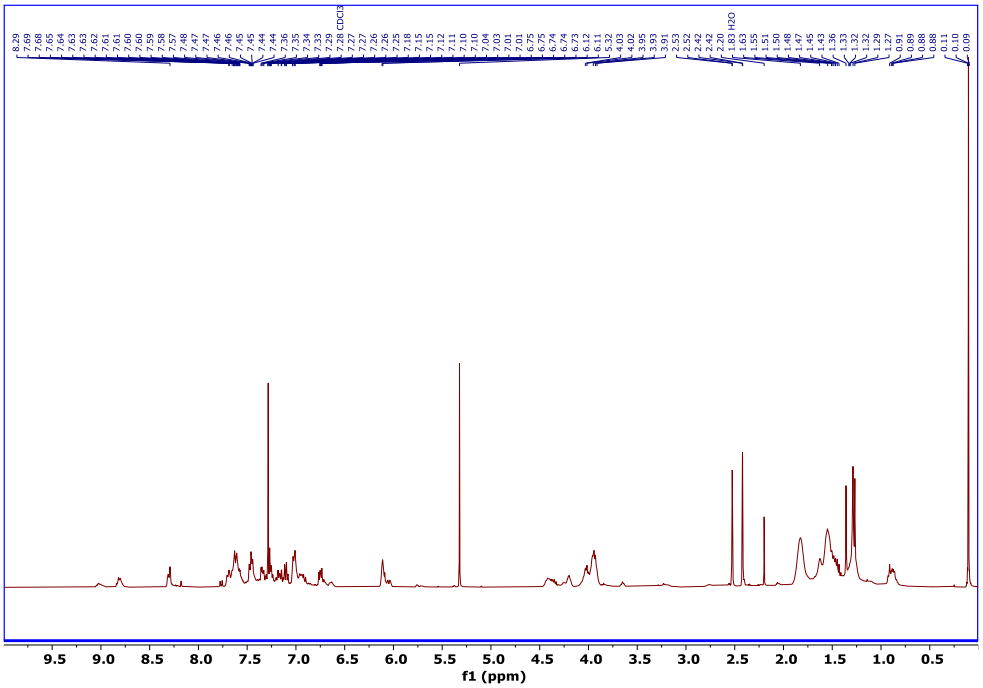

Figure 8.26 ^{1}H NMR spectrum of P8 in $CDCl_3$; 9.02 (bs, 0.40H), 8.80 (s, 0.63H), 8.36 – 8.14 (m, 1H), 7.73 – 7.52 (m, 4H), 7.51 – 7.38 (m, 2H), 7.37 – 7.30 (m, 1H), 7.28 – 7.06 (m, 3H), 7.05 – 6.83 (m, 3H), 6.78 – 6.59 (m, 1H), 6.17 – 5.96 (m, 2H), 4.20 (s, 2H), 4.11 – 3.74 (m, 5H), 3.34 – 3.11 (m, 1H), 1.83 (s, 5H), 1.70 – 1.39 (m, 10H), 1.38 – 1.01 (m, 8H), 0.89 (s, 2H).

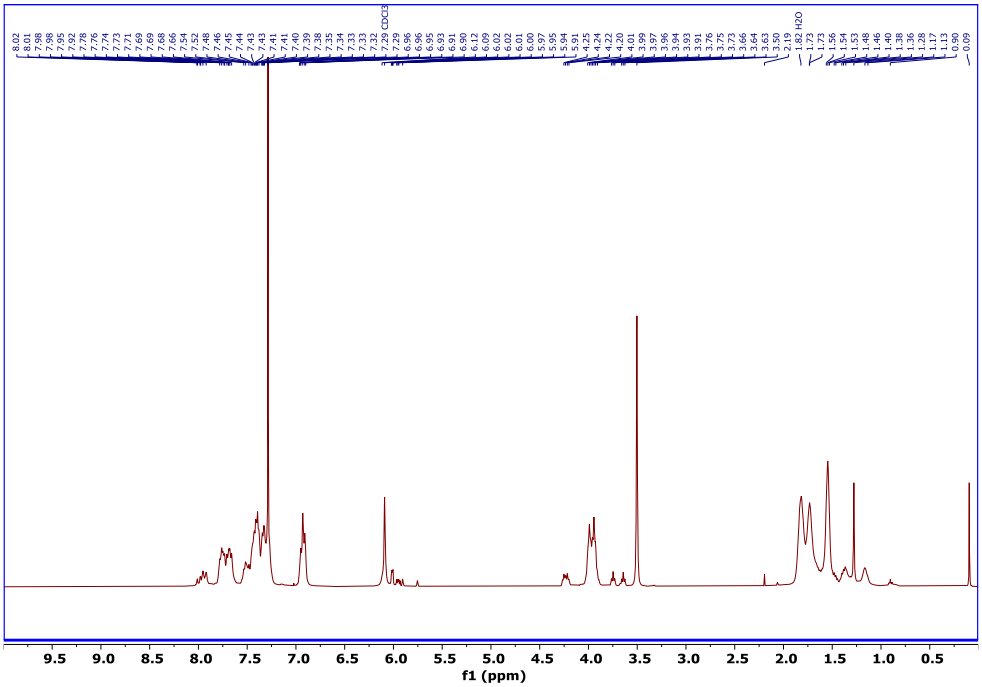

Figure 8.27 ^{1}H NMR spectrum of P9 in $CDCl_3$; 8.06 – 7.87 (m, 1H), 7.84 – 7.59 (m, 4H), 7.56 – 7.30 (m, 8H), 7.02 – 6.81 (m, 3H), 6.09 (bs, 2H), 6.03 – 5.86 (m, 1H), 4.29 – 4.16 (m, 1H), 4.08 – 3.86 (m, 4H), 3.76 (bs, 0.36H), 3.66 (bs, 0.38H), 1.73 (bs, 10H), 1.32 (bs, 2H), 1.17 (bs, 1H). 0.89 (bs, 0.33H).

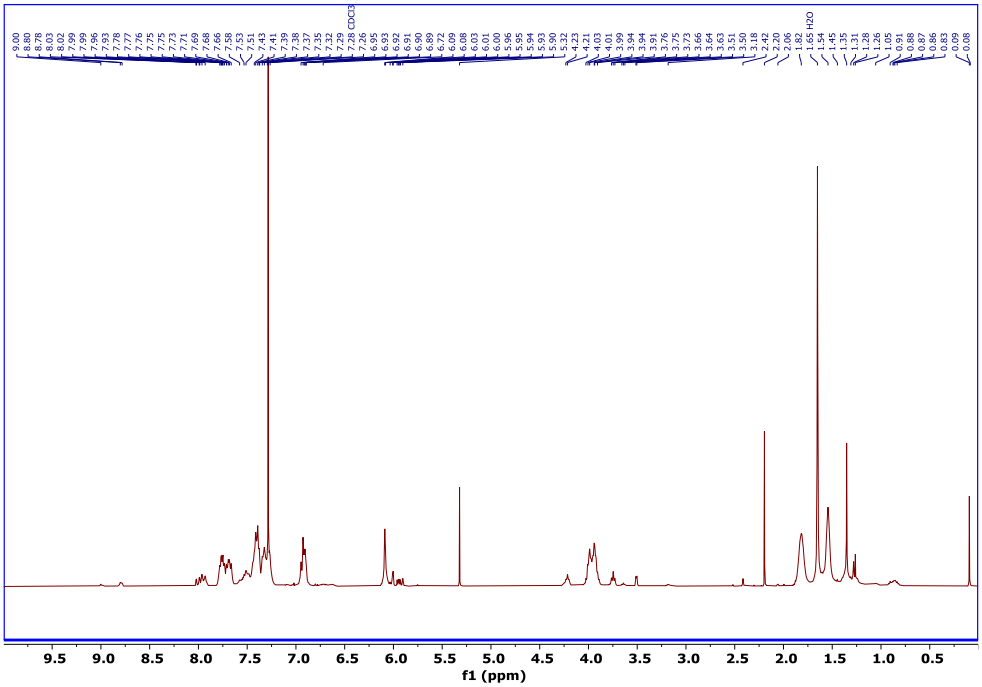

Figure 8.28 ^{1}H NMR spectrum of P10 in $CDCl_3$; 9.01 (bs, 0.09H), 8.80 (bs, 0.14H), 8.06 – 7.85 (m, 1H), 7.84 – 7.61 (m, 3H), 7.60 – 7.32 (m, 5H), 7.01 – 6.82 (m, 2H), 6.14 – 6.05 (m, 1H), 6.04 – 5.86 (m, 1H), 4.22 (s, 1H), 4.07 – 3.86 (m, 3H), 3.81 – 3.68 (m, 1H), 1.82 (bs, 3H), 1.65 (bs, 4H), 1.54 (bs, 4H), 1.44 – 1.18 (m, 3H), 0.87 (bs, 1H).

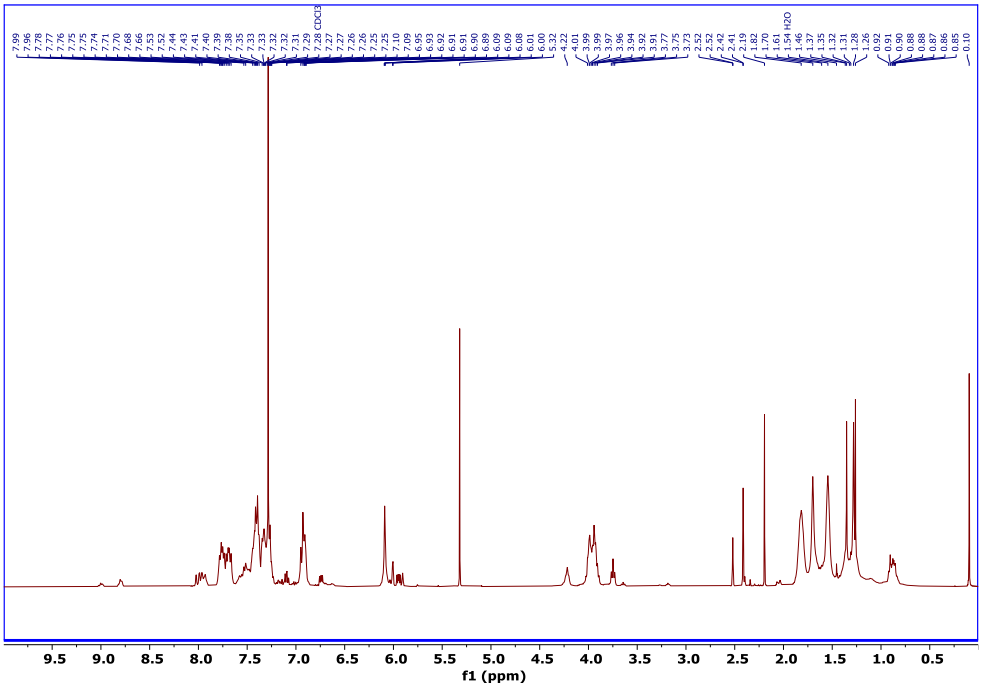

Figure 8.29 ^{1}H NMR spectrum of P11 in $CDCl_3$; 9.02 (bs, 0.27H), 8.82 (bs, 0.43), 8.06 – 7.87 (m, 1H), 7.84 – 7.62 (m, 5H), 7.59 – 7.36 (m, 7H), 7.03 – 6.81 (m, 4H), 6.80 – 6.66 (m, 1H), 6.15 – 6.04 (m, 2H), 6.03 – 5.85 (m, 1H), 4.22 (bs, 1H), 4.07 – 3.84 (m, 5H), 3.82 – 3.69 (m, 1H), 1.82 (bs, 6H), 1.70 (bs, 5H), 1.54 (bs, 6H), 1.42 – 1.33 (m, 3H), 1.31 – 1.22 (m, 5H), 0.94 – 0.83 (m, 2H).

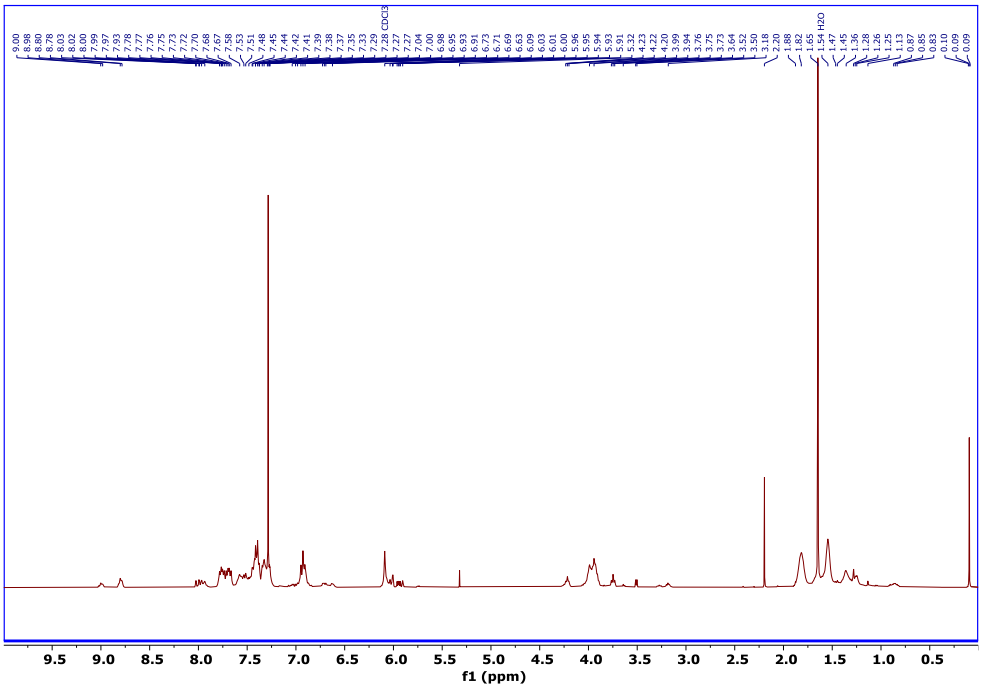

Figure 8.30 ^{1}H NMR spectrum of P12 in $CDCl_3$; 9.00 (s, 0.51H), 8.79 (s, 0.76H), 8.05 – 7.89 (m, 1H), 7.83 – 7.63 (m, 4H), 7.62 – 7.47 (m, 3H), 7.47 – 7.30 (m, 8H), 7.00 – 6.83 (m, 3H), 6.76 – 6.57 (m, 1H), 6.14 – 5.98 (m, 2H), 5.97 – 5.87 (m, 1H), 4.22 (s, 1H), 4.08 – 3.84 (m, 5H), 3.75 (s, 1H), 1.82 (s, 5H), 1.65 (s, 6H), 1.54 (s, 6H), 1.43 – 1.19 (m, 4H), 0.87 (s, 1H).